

FL

DESIGN AND TEST OF A COMPUTER STABILIZED
UNICYCLE

A DISSERTATION
SUBMITTED TO THE DEPARTMENT OF AERONAUTICS AND ASTRONAUTICS
AND THE COMMITTEE ON GRADUATE STUDIES
OF STANFORD UNIVERSITY
IN PARTIAL FULFILLMENT OF THE REQUIREMENTS
FOR THE DEGREE OF
DOCTOR OF PHILOSOPHY

By
Arnoldus Schoonwinkel
December, 1987

© Copyright 1988
by
Arnoldus Schoonwinkel

This is an authorized facsimile, made from the microfilm master copy of the original dissertation or master thesis published by UMI.

The bibliographic information for this thesis is contained in UMI's Dissertation Abstracts database, the only central source for accessing almost every doctoral dissertation accepted in North America since 1861.

UMI Dissertation
Services

A Bell & Howell Company

300 North Zeeb Road
P.O. Box 1346
Ann Arbor, Michigan 48106-1346

1-800-521-0600 734-761-4700
<http://www.umi.com>

Printed in 1999 by digital xerographic process
on acid-free paper

DPBT

09

INFORMATION TO USERS

The most advanced technology has been used to photograph and reproduce this manuscript from the microfilm master. UMI films the original text directly from the copy submitted. Thus, some dissertation copies are in typewriter face, while others may be from a computer printer.

In the unlikely event that the author did not send UMI a complete manuscript and there are missing pages, these will be noted. Also, if unauthorized copyrighted material had to be removed, a note will indicate the deletion.

Oversize materials (e.g., maps, drawings, charts) are reproduced by sectioning the original, beginning at the upper left-hand corner and continuing from left to right in equal sections with small overlaps. Each oversize page is available as one exposure on a standard 35 mm slide or as a 17" x 23" black and white photographic print for an additional charge.

Photographs included in the original manuscript have been reproduced xerographically in this copy. 35 mm slides or 6" x 9" black and white photographic prints are available for any photographs or illustrations appearing in this copy for an additional charge. Contact UMI directly to order.



300 North Zeeb Road, Ann Arbor, MI 48106-1346 USA

Order Number 8808416

Design and test of a computer stabilized unicycle

Schoonwinkel, Arnoldus, Ph.D.

Stanford University, 1988

Copyright ©1988 by Schoonwinkel, Arnoldus. All rights reserved.

U·M·I

300 N. Zeeb Rd.
Ann Arbor, MI 48106

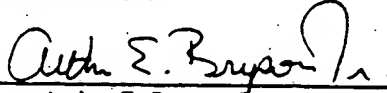
PLEASE NOTE:

In all cases this material has been filmed in the best possible way from the available copy. Problems encountered with this document have been identified here with a check mark ☒.

1. Glossy photographs or pages _____
2. Colored illustrations, paper or print _____
3. Photographs with dark background _____
4. Illustrations are poor copy _____
5. Pages with black marks, not original copy _____
6. Print shows through as there is text on both sides of page _____
7. Indistinct, broken or small print on several pages _____
8. Print exceeds margin requirements _____
9. Tightly bound copy with print lost in spine _____
10. Computer printout pages with indistinct print _____
11. Page(s) _____ lacking when material received, and not available from school or author.
12. Page(s) _____ seem to be missing in numbering only as text follows.
13. Two pages numbered _____. Text follows.
14. Curling and wrinkled pages _____
15. Dissertation contains pages with print at a slant, filmed as received ☒
16. Other _____

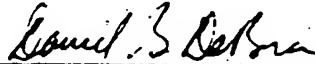
U·M·I

I certify that I have read this thesis and that in my opinion
it is fully adequate, in scope and in quality, as a dissertation
for the degree of Doctor of Philosophy.



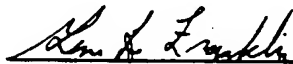
Arthur E. Bryson, Jr.
(Principal Adviser)

I certify that I have read this thesis and that in my opinion
it is fully adequate, in scope and in quality, as a dissertation
for the degree of Doctor of Philosophy.



Daniel B. DeBra
Department of Aeronautics and Astronautics

I certify that I have read this thesis and that in my opinion
it is fully adequate, in scope and in quality, as a dissertation
for the degree of Doctor of Philosophy.



Gene F. Franklin
Department of Electrical Engineering

Approved for the University Committee on Graduate Studies:



Dean of Graduate Studies & Research

To my wife, Tilda and our parents

Acknowledgements

We are not competent to claim anything for ourselves, but our competence comes from God. Praise be to Him, the Father of our Lord Jesus Christ!

II Corinthians 3:5 ; 1:3 N.I.V.

It has been a great privilege to perform this research under the supervision of Professor Arthur E. Bryson. His direction and enthusiasm for this study has been a continuous source of encouragement.

I have also received invaluable practical advice from Professor Daniel B. DeBra, who contributed much to my control system knowledge.

The interest expressed and the suggestions offered by Professors Gene F. Franklin and John V. Breakwell are sincerely appreciated.

I am indebted to Professor David Beach and to the personnel at the student mechanical workshop for coaching me in using the equipment and for advising me during the construction of the test vehicle.

I would like to express my appreciation to several companies that have furnished equipment for this project as a donation or that have offered it at a substantially reduced price : Infranor Inc. (DC Motors), Gespac Inc. (microprocessor hardware), Palo

Alto Shipping Co. (computer software), National (electronics) and Siemens (optical electronics). I would also like to thank Peter Lindener who has loaned several components for the robot to get the project started.

The many productive discussions with my colleagues in the Aerospace Robotics Laboratory, have contributed much to the success of this research project. In this respect Mike Hollars, Sandy Alexander and Grant Wong offered advice from their practical experience, that produced leaps in the progress of my work.

Words seem quite insufficient to express my appreciation towards my loving wife, Tilda, who so graciously provided her moral support to our children, Johan and Tilianna, and to me during our stay at Stanford. She shared in the joys of the successes and in the prayers during the difficult times. She patiently listened to control system theories and also mastered the type setting intricacies to produce this manuscript.

This work is also a tribute to the support, encouragement and sacrifice of our parents who have always been the respected examples in our lives.

Abstract

Active stabilization of unstable flight vehicles is an important research area at present. It is rarely possible for graduate students to become involved in these research efforts, other than on a largely theoretical basis. For this reason we chose to build a land vehicle with interesting unstable dynamics. A unicycle robot has been constructed at a reasonable cost, which facilitates the evaluation of the control strategies in a laboratory environment.

This research investigates the stabilization of a one wheeled vehicle by means of active feedback control. The control methods of a human riding a unicycle are investigated first and a dynamic model which closely emulates the process is derived. A one wheeled robot with mass and inertia properties similar to those of a young child was constructed and used as an experimental vehicle for testing various control algorithms. The research addresses aspects in the fields of robotics, artificial intelligence and modern digital control, but rather than specializing in any of these fields, it strives to combine these disciplines in a unique application where the interaction of these fields can be studied. An underlying approach of this research was to not only design but also evaluate control system performance in a laboratory environment without incurring large financial expenses. The robot has all its electrical and computational power on board, with the ability to receive commands from a radio transmitter to change its direction and forward speed. A linearized model was derived and optimal control systems to stabilize the vehicle were designed and simulated.

An investigation into using accelerometers for detection of the deviation from vertical by measuring the specific force on the robot frame, was conducted. We found that this resulted in unacceptable closed loop system robustness. Theoretical and physical explanations for this phenomenon are presented as well as experimental results to confirm the extreme sensitivity of the design to these sensors.

We show that accurate sensor information on the unicycle's orientation with respect to vertical facilitates the design of closed loop control systems with good stability and robustness characteristics. Such a control system for the longitudinal dynamics of the unicycle robot was demonstrated experimentally.

The sensing, actuation and control abilities of a person riding a unicycle are compared with those of a computerized robot performing a similar task. We propose that this research and the test vehicle form the basis for theoretical and experimental studies into the application of nonlinear, robust and adaptive control systems techniques for unstable systems.

List of Symbols

ψ	=	yaw angle.
ϕ	=	roll angle.
θ	=	pitch angle.
$\bar{\eta}$	=	$\eta_0 + \eta$ = total angular velocity of the rotary turntable T relative to the frame F.
η_0	=	constant component of turntable angular velocity.
η	=	small perturbation of turntable angular velocity.
$\bar{\Omega}$	=	total wheel angular velocity about the axle of the wheel.
Ω_0	=	constant component of wheel angular velocity.
Ω	=	small perturbation of wheel angular velocity.
ρ	=	angle of longitudinal sensor pendulum relative to the frame F.
σ	=	angle of lateral sensor pendulum relative to the frame F.

Wheel mechanical parameters:

m_W	=	mass of the wheel W.
r_W	=	radius of the wheel.
I_1^W, I_2^W, I_3^W	=	moments of inertia of the wheel about 3 mutually perpendicular axes originating at the center of mass of the wheel. I_2^W is the inertia about the axis along

the wheel axle.

Unicycle frame mechanical parameters:

- m_F = mass of the frame, F, of the unicycle.
- r_F = distance from the wheel axle to the center of mass, F^* , of the unicycle frame.
- r_1 = distance the center of mass F^* is located in front of the center line of the frame.
- r_2 = distance the center of mass F^* is located to the side of the center line.
- I_1^F, I_2^F, I_3^F = moments of inertia of the frame about 3 mutually perpendicular axes originating at the center of mass of the frame. I_3^F is the inertia about a vertical axis, and I_1^F about an axis pointing in the direction of normal forward motion of the frame.

Turntable mechanical parameters:

- m_T = mass of the rotary turntable T on top of the unicycle.
- r_T = distance from the wheel axle to the center of mass, T^* , of the turntable.
- I_1^T, I_2^T, I_3^T = moments of inertia of the turntable about 3 mutually perpendicular axes originating at the center of mass of the turntable. I_3^T is the inertia about a nominally vertical axis along the axle of the turntable.

Sensor pendulum mechanical parameters:

- m_p = mass of a sensor pendulum.
- r_p = distance between the hinge point of a sensor pendulum, and its center of mass.
- k_p = spring constant of coil spring attached around the pendulum hinge point.
- f_p = viscous damping coefficient of the sensor pendulum.

- $I_1^S = I_2^R =$ moment of inertia of a sensor pendulum about an axis passing through its center of mass, and perpendicular to the pendulum's plane of oscillation.
- $r_{S3} =$ distance from the wheel axle to the hinge point of the lateral motion sensor pendulum.
- $r_{S1} =$ distance from the center of mass of the lateral pendulum is located in front of the center line of the frame of the unicycle.
- $r_{R3} =$ distance from the wheel axle to the hinge point of the longitudinal motion sensor pendulum.
- $r_{R2} =$ distance from the center of mass of the longitudinal pendulum is located to the side of the center line of the frame of the unicycle.

Other parameters and symbols:

- $f_G =$ viscous friction coefficient at contact point of the rubber tire to the ground.
- $f_W =$ viscous friction coefficient at the wheel axle where it is attached to the unicycle frame.
- $f_T =$ viscous friction coefficient at the rotary turntable axle where it is attached to the frame.
- $g =$ gravity acceleration constant.
- $R_1^W =$ component of the internal reaction force along the \hat{w}_1 unit vector. The W superscript indicates that the reaction force is between the wheel, W, and the unicycle frame. The subscript indicates along which unit vector the reaction force is specified.
- $Q_2^T =$ component of the internal reaction moment along the \hat{f}_2 unit vector. The meaning of the sub- and superscripts are similar to the definition given for reaction forces.
- $Q_W =$ control torque applied to the wheel and unicycle frame

$Q_T =$ by the wheel drive motor.
control torque applied to the rotary turntable and
unicycle frame by the turntable drive motor.

Contents

Acknowledgements	vii
Abstract	ix
List of Symbols	ix
List of Figures	xxi
1 Introduction	1
1.1 Research topic	1
1.2 Organization of the thesis	3
2 Dynamic Model for the Unicycle Robot	5
2.1 Dynamics of a human riding a unicycle	5
2.2 Mechanical design of the unicycle robot	8
2.3 Dynamics of the unicycle robot	10
2.4 Selection of actuators and the drive system	12
2.5 Selection and construction of sensors	14
3 Longitudinal System with Accelerometer Sensor	17
3.1 Introduction	17
3.2 Longitudinal system characteristics	18
3.3 Compensator design by successive loop closure	22
3.3.1 Nominal design	22

3.3.2	Robustness of the longitudinal controller	23
3.3.3	Experimental Results	25
3.4	Longitudinal system LQG design	27
3.4.1	Motivation for using an LQG compensator	27
3.4.2	LQG design method	28
3.4.3	Experimental results and conclusions	29
4	Longitudinal System with Vertical Sensor	39
4.1	Introduction	39
4.2	Control system design with pitch sensor	39
4.3	Experimental tests of the control system	40
4.4	Conclusion	42
5	Lateral Control System	48
5.1	Introduction	46
5.2	Lateral System Characteristics	46
5.3	Lateral system LQG design	51
6	Summary of Contributions and Recommendations	59
6.1	Contributions	59
6.2	Recommendations for future research	63
6.3	Conclusion	64
A	EOMs by Newton-Euler Mechanics	68
A.1	Definition of variables	66
A.2	Translational equations of motion of wheel	67
A.2.1	Linear acceleration of point O	67
A.2.2	Forces acting on W	68
A.2.3	Translational equations of motion of wheel	68
A.3	Rotational equations of motion of wheel	69
A.3.1	Applied moments about O	69
A.3.2	Absolute angular velocity of the \hat{w} -frame	69

A.3.3	Angular momentum of the wheel	70
A.3.4	Rotational equations of motion of the wheel	70
A.4	Translational equations of motion of frame	72
A.4.1	Forces acting on F	72
A.4.2	Absolute translational acceleration of F^*	72
A.4.3	Translational equations of motion of frame F	73
A.5	Rotational equations of motion of frame F	74
A.5.1	Applied moments about F^*	74
A.5.2	Rotational equations of motion for F	75
A.5.3	Rotational equations of motion of frame F	75
A.6	Translational equations of motion of turntable	77
A.6.1	Forces acting on T	77
A.6.2	Absolute acceleration of T^*	77
A.6.3	Translational equations of motion of T	77
A.7	Rotational equations of motion of turntable	78
A.7.1	Angular momentum of turntable T	78
A.7.2	Applied moments to T	78
A.7.3	Rotational equations of motion of T	79
A.8	Translational EOMs of longit. sensor pendulum	80
A.8.1	Absolute angular velocity of the \hat{f} -frame	80
A.8.2	Absolute translational acceleration of R^*	80
A.8.3	Forces acting on R	81
A.8.4	Translational equations of motion of R	81
A.9	Rotational EOMs of longit. sensor pendulum	82
A.9.1	Applied moments about R^*	82
A.9.2	Rotational equations of motion of R	82
A.10	Translational EOMs of lateral sensor pendulum	83
A.10.1	Absolute angular velocity of the \hat{s} -frame	83
A.10.2	Absolute translational acceleration of S^*	83
A.10.3	Forces acting on S	84

A.10.4 Translational equations of motion of S	34
A.11 Rotational EOMs of lateral sensor pendulum	35
A.11.1 Applied moments about S^*	85
A.11.2 Rotational equations of motion of S	85
A.12 Summary of the system dynamic equations	86
A.12.1 Lateral system	86
A.12.2 Longitudinal system	87
B EOMs by using Lagrange's Method	97
B.1 Wheel	98
B.2 Frame	99
B.3 Turntable	100
B.3.1 The Lagrangian and Lagrange's equation	102
B.4 Summary of unicycle dynamic equations	110
B.4.1 Lateral system dynamic equations	110
B.4.2 Longitudinal system dynamic equations	111
C EOMs by using D'Alembert's Principle	112
C.1 Procedure	112
C.2 Lateral equations of motion	115
C.3 Longitudinal equations of motion	115
D State Space Form of the EOMs	117
E Attitude by Means of a Sensor Pendulum	122
E.1 Dynamic equations of motion	122
E.2 Observability matrix	126
E.3 Physical explanation for modal unobservability	128
E.4 Unobservability by pole-zero cancellation	129
E.5 Unobservability by inspection of the F matrix	130

F Unicycle Robot Steered by Sideways Leaning	134
F.1 Dynamic Equations	134
F.2 Lateral equations of motion	137
F.3 Longitudinal equations of motion	137
F.4 Lateral system characteristics	138
F.4.1 Lateral system analysis	141
G Gear Ratio for Maximum Yaw Acceleration	145
G.1 Motivation for the optimal gear ratio	145
G.2 Yaw dynamics with a geared drive system	146
G.3 Yaw acceleration as a function of gear ratio	149
H Servo Accelerometer Design	152
H.1 Introduction	152
H.2 Mechanical design of servo accelerometer	152
H.3 Feedback control system design	153
H.4 Optical pick-off considerations	153
H.5 Detector electronics and servo amplifier design	155
H.6 Openloop frequency response and plant model	155
H.7 Compensation design	156
H.8 ITAE compensator calculation program	158
H.9 Servo accelerometer calibration	161
H.10 Hall-effect frame angle sensor design	163
I Position Encoder and Servo Amplifier Interface	181
I.1 Introduction	181
I.2 Position encoder interface	181
I.3 Operation of the logic circuitry	182
I.4 Selection of the interface clock frequencies	183
I.5 Servo amplifier interface	184

J Analog-to-Digital, Radio and FPP Interface	191
J.1 Analog-to-Digital interface design	191
J.1.1 Hardware design	191
J.1.2 Software for controlling the ADC interface	191
J.1.3 Binary values of the analog input voltage	192
J.1.4 FORTH Program to drive the ADC converter	193
J.2 Radio receiver interface design	195
J.2.1 Hardware design	195
J.2.2 Software interface	195
J.2.3 Program to drive the radio receiver interface	196
J.3 Floating point processor (FPP) interface	199
J.4 Electrical and electronic wiring diagram	199
K Gear Ratio for Maximum Wheel Acceleration	206
K.1 Introduction	206
K.2 Optimal gear ratio for wheel drive system	206
L Unicycle Mechanical Design	214
L.1 Introduction	214
L.2 Effect of center of mass height	216
L.3 Design of the gear drive systems	217
M Mechanical Parameter Measurements	222
M.1 Inertia measurement method	222
M.2 Center of mass measurement method	223
M.3 Friction measurements	223
M.3.1 Longitudinal system friction coefficients	223
M.3.2 Lateral system friction measurements	226
M.4 Measured mechanical parameters	227
M.5 D.C.motor and gear drive system parameters	228

N	Continuous Time Longitudinal Control System	232
N.1	Longitudinal equations of motion	232
N.2	Longitudinal sensors	234
N.3	Longitudinal system characteristics	235
N.3.1	Longit. system characteristics calculation	236
N.3.2	Experimental confirmation transfer functions	239
N.3.3	Upside down unicycle transfer functions	243
N.4	Longitudinal control system design	246
N.4.1	Optimal continuous time regulator design	247
N.5	Process and measurement noise models	249
N.6	Optimal continuous time estimator design	252
N.6.1	LQE gain calculation program	256
O	Discrete Time Longitudinal Control System	272
O.1	Sampling rate selection	272
O.2	Equivalent discrete LQG compensator	273
O.2.1	Discrete time regulator	273
O.2.2	Discrete time estimator	275
O.2.3	Optimal regulator and estimator gains	278
O.3	Modal decomposition of LQG compensator	287
O.4	Pole-zero compensator with accelerometer sensor	290
O.4.1	Successive loop closure compensator parameters	293
O.5	Pole-zero compensator with vertical sensor	298
O.5.1	Pitch feedback compensator calculation	299
P	FORTH Codes for Longitudinal Control	317
P.1	Successive Loop Closure and Accelerometer	317
P.2	LQG Compensator with Accelerometer Sensor	327
P.3	Successive Loop Closure and Pitch Sensor	345

Q Lateral Control System	355
Q.1 Lateral equations of motion	355
Q.2 Lateral sensors	357
Q.3 Lateral system characteristics	358
Q.3.1 Lateral system characteristics calculation	359
Q.4 LQG control system design	363
Q.4.1 Calculation of LQG gains	365

List of Figures

2.1	Unicycle Robot Drawing	16
3.1	Longitudinal System Balance Recovery to an Initial Pitch Angle Error	31
3.2	Locus of the Zeros of the Transfer Function to the Accelerometer Output as a Function of the Accelerometer Height above the Wheel Axle	32
3.3	Longitudinal Accelerometer Feedback Loop Rootlocus when the Accelerom- eter are placed too Low on the Frame	33
3.4	Rootloci for the Longitudinal System Designed Compensators Designed by Successive Loop Closures	34
3.5	Rootlocus for the Closed Loop Longitudinal System as a Function of the Accelerometer Height above the Wheel Axle	35
3.6	Measured Time History of Longitudinal System Signals during an Exper- imental Stabilization Test	36
3.7	Typical Longitudinal Acceleration Measurement while the Unicycle is Moving at a Wheel Speed of 3 rad/sec.	37
3.8	The Time Responses of the Longitudinal Accelerometer Measurement and its Components during a Simulation of a Balance Recovery Sequence	38
4.1	Mechanical Design of Frame Pitch Angle Sensor	43
4.2	Pitch Angle and Wheel Speed Measurements at Zero Commanded Wheel Speed	44
4.3	Pitch Angle and Wheel Speed Measurements at 3 rad/sec Commanded Wheel Speed	45

5.1	Dependence of the Lateral Plant Eigenvalues on the Wheel Speed, Ω_0	54
5.2	Lateral System Closed Loop Poles as a Function of the Wheel Speed for an LQG compensator designed for 3 rad/sec	55
5.3	Lateral System Optimal Regulator Gains as a Function of the Wheel Speed	56
5.4	Lateral System Optimal Estimator Gains on the Turntable Tachometer Measurement, as a Function of the Wheel Speed	57
5.5	Lateral System Optimal Estimator Gains on the Roll Angle Measurement, as a Function of the Wheel Speed	58
A.1	Unicycle Schematic Diagram	89
A.2	Coordinate Frame Translation Definitions 1	90
A.3	Coordinate Frame Translation Definitions 2	91
A.4	Wheel Free Body Diagram	92
A.5	Turntable Free Body Diagram	93
A.6	Unicycle Frame Free Body Diagram	94
A.7	Longitudinal Sensor Pendulum Frame Free Body Diagram	95
A.8	Lateral Sensor Pendulum Frame Free Body Diagram	96
E.1	Inverted Pendulum Schematic Diagram	132
E.2	Sensor Pendulum Schematic Diagram	132
E.3	Locus of Imaginary Axis Zeros as a Function of Sensor Pendulum Height	133
E.4	Locus of Real Axis Zeros as a Function of Sensor Pendulum Height	133
F.1	Steering by Leaning	144
G.1	Turntable Gear Drive Schematic	150
G.2	Normalized Yaw Acceleration as a Function of the Turntable Drive System Gear Ratio	151
H.1	Mechanical Design of Servo Accelerometer	164
H.2	Feedback Control System Block Diagram	165

H.3 Relationship between Differential Photodiode Output and Light Beam Position	166
H.4 Sensitivity to Process Noise Analysis	167
H.5 Servo Accelerometer Electronics	168
H.6 Opto Electronics Printed Circuit Board Layout	169
H.7 Plant Measured and Theoretical Frequency Response	170
H.8 Second Order Electronic Compensator	171
H.9 Closed Loop System Root Locus versus Overall Loop Gain K	172
H.10 Servo Accelerometer Openloop Frequency Responses	173
H.11 Theoretical, Step Response of the Closed Loop Servo Accelerometer	174
H.12 Differential Output of the Optical Detector as a Function of the Ac- celerometer Tilt Angle	175
H.13 Measured Transfer Function for the Lateral Accelerometer	176
H.14 Measured Transfer Function for the Longitudinal Accelerometer	176
H.15 Hall-effect Transducer Electronic Interface	177
H.16 Measured Transfer Function of the Hall-effect Transducer Pitch Angle Sensor	178
L1 Lateral Encoder Rate Extraction Logic Diagram	186
L2 Longitudinal Encoder Rate Extraction Logic Diagram	187
L3 Position Encoder and Servo Amplifier Interface Card Layout	188
L4 Position Encoder Interface Timing Diagram	189
L5 Digital to Analog Converter Interface to Servo Amplifiers	190
J.1 12 Bit Analog-to-Digital Converter and 8 Channel Multiplexer Interface	200
J.2 8254 Programmable Interval Timer Interface	201
J.3 Radio Receiver Interface Timing Diagram	202
J.4 Floating Point Processor Interface to the G-64 bus and MC68000 CPU	203
J.5 Interface Board Layout	204
J.6 Electrical and Electronic Wiring Diagram	205

K.1 Wheel Drive System	212
K.2 Normalized Wheel Acceleration as a Function of the Wheel Drive System Gear Ratio	213
L.1 Wheel Drive System	219
L.2 Turntable Drive System	220
L.3 Effective Longitudinal System Moment of Inertia as a Function of the Height of the Frame Center of Mass above the Wheel Axle	221
M.1 Schematic Diagram of a Bifilar Pendulum for Measuring the Moment of Inertia of an Object	230
M.2 Tachometer and Accelerometer Responses during Free Oscillation of the Upside Down Unicycle	231
N.1 Longitudinal Accelerometer Measurement	261
N.2 Openloop Frequency Response of $\frac{\theta(s)}{Q_w(s)}$	262
N.3 Typical Time Response During a Transfer Function Identification Test	263
N.4 Theoretical and Measured Frequency Responses for the Upside Down Unicycle	264
N.5 General Feedback Control System Blockdiagram	265
N.6 Symmetric Rootlocus of the Longitudinal Closed Loop System for values of $\frac{g}{g}$ ranging from 0 to 10 000	266
N.7 Step Response of the Longitudinal Closed Loop System with Full State Feedback	267
N.8 Frequency Response of the Longitudinal Closed Loop System with Full State Feedback	268
N.9 Symmetric Root Loci of the Compromise Zeros and Estimator Poles	269
N.10 Response of the Longitudinal System with a Full Order Estimator with $\theta(0) = 0.1$ rad	270
N.11 Step Response of the Closed Loop System with a Full Order Estimator and Measurements Corrupted by Noise	271

O.1 Blockdiagram of a Discrete Time LQG Compensator with Integral Error Feedback	305
O.2 Step Response of the Longitudinal Discrete Time System with Full State Feedback	306
O.3 Response of the Longitudinal System with a Full Order Estimator with $\theta(0) = 0.1$ rad, but $\dot{\theta}(0) = 0$ rad	307
O.4 Rootlocus of the Discrete Time Longitudinal Tachometer Loop with Proportional Feedback of the Tachometer Measurement	308
O.5 Rootlocus of the Accelerometer Loop with a First Order Pole-zero Compensator	309
O.6 Block diagram of the Discrete Longitudinal Successive Loop Closure Control System	310
O.7 Step Response of the Longitudinal Closed Loop System Designed by Successive Loop Closure	311
O.8 Loop Gain and Phase versus Frequency of the Discrete Time Longitudinal Control System Designed by Successive Loop Closure	312
O.9 Root Locus of the Discrete Time Longitudinal Tachometer Loop with Integral Error Feedback of the Tachometer Measurement	313
O.10 Root Locus of the Pitch Angle Feedback Loop with a First Order Compensator	314
O.11 Enlargement of the Pitch Loop Root Locus in the Vicinity of $z = 1$. . .	315
O.12 Step Resonse of the Longitudinal Closed Loop System with Pitch Angle Feedback	316
Q.1 Lateral Accelerometer Measurement	370
Q.2 Step Response of the Lateral System with Full State Feedback	371
Q.3 Frequency Response of the Lateral Closed Loop System with Full State Feedback	372
Q.4 Response of the Lateral System with a Full Order Estimator and an Initial Roll Angle of 2 Degrees	373

2

Chapter 1

Introduction

1.1 Research topic

The word 'robot' was created by the Czech playwright Karel Capek [Capek]. He derived it from the Czech words *robota*, which means statute labor, and *robotnik* which is a serf [Oxford Dictionary]. In Capek's 1923 play *Rossum's Universal Robots*, a factory by this name creates these mechanical devices that can tirelessly and automatically do the work of a man. Since the word was coined by Capek, it has found its way into almost every other language and robots have become an almost essential ingredient of every modern science fiction writing or movie. In fact, intelligence and capabilities superior to those of a human are often attributed to them. As this thesis will demonstrate there is more to emulating in a robot the relatively basic human skill of riding a unicycle, than simply *play-writing*.

An important application for feedback control systems is the stabilization of inherently unstable systems. A human may be regarded as an extraordinary control system possessing an impressive array of sensors, actuators, and computational abilities. A human riding a unicycle not only stabilizes the unicycle but controls its speed and direction. The purpose of this research is to emulate this particular human skill in a robot

CHAPTER 1. INTRODUCTION

and apply the latest microprocessor and control systems technology in a laboratory environment in order to gain insight into the processes involved.

This research investigates the stabilization of a one wheeled vehicle by means of active feedback control. The control methods of a human riding a unicycle are investigated first and a dynamic model which closely emulates the process is derived. A one wheeled robot with mass and inertia properties similar to those of a young child was constructed and used as an experimental vehicle for testing various control algorithms. The research addresses aspects in the fields of robotics, artificial intelligence and modern digital control, but rather than specializing in any of these fields, it strives to combine these disciplines in a unique application where the interaction of these fields can be studied. An underlying approach of this research was to not only design but also evaluate control system performance in a laboratory environment without incurring large financial expenses.

The unicycle problem that was investigated is similar to that of an inverted pendulum with both longitudinal and lateral unstable open loop dynamics. Previous work on active stabilization of a bicycle by sideways leaning of a robot body [Van Zytveld] was undertaken where only lateral instability is present in the open loop dynamic system. An autopilot for a motorbike was designed and demonstrated using a rate gyro sensor and a steering actuator [Nashner]. Research was also undertaken on the control of inverted pendulums on stable wheeled carts [Higdon] and [Schaefer]), but applications did not address the problems associated with stabilizing the pendulum if the cart would traverse inclined surfaces. A significant amount of research into stabilizing legged robots has been performed. The work on the hopping pogo stick robots at Carnegie Mellon University [Raibert] bears some relationship to the stabilization of a one wheeled robot.

The work most closely related to the topic of this thesis was performed by researchers at the mechanical engineering department of Waseda University, Tokyo [Iguchi]. In this case a one wheeled robot was stabilized by means of a fast spinning control moment gyro

mounted on the vehicle. If the unicycle leaned sideways, a torque was applied to the control moment gyro by changing the speed of the wheel that rolls on the ground. These investigations differ from the approach of this thesis where stabilization by means of a control moment gyro was ruled out because it bears no relationship with the method employed by humans in stabilizing a unicycle.

1.2 Organization of the thesis

This research employs techniques found in mechanical engineering, dynamics, control system design, microprocessor technology as well as analog electronics. In order to make clear the conceptual contributions of the thesis, the details of the application of these disciplines in solving the problem at hand are documented in appendices. The main text concentrates on motivating the conceptual principles used in solving the unicycle stabilization problem and draws conclusions from the theoretical and experimental results.

Chapter 2 describes the control methods used by a human riding a unicycle and motivates the choice of a dynamic model that represents a reasonable approximation of the actual situation. It also addresses the issues considered in the mechanical design of the one wheeled robot used in the experiments.

Chapter 3 describes the design of a control system for the longitudinal stabilization of the unicycle robot. The advantages and disadvantages of control algorithms designed by successive loop closure and linear quadratic cost function minimization techniques are discussed. Experimental results are presented and analysed. It concludes with an explanation of why vertical stabilization with accelerometers as the primary sensors cannot be obtained in practice.

Chapter 4 shows that a requirement for stabilization of the pitch instability of the unicycle is a sensor which provides a good vertical reference to which the frame attitude

can be compared. It proceeds to discuss the design of candidate longitudinal controllers assuming that pitch attitude information is known, and shows how robustness is improved. Experimental results which demonstrate how the unicycle robot was stabilized longitudinally, are presented.

Chapter 5 discusses control systems to provide lateral stability for the unicycle. After showing that similar robustness problems exist in the lateral control system if accelerometer sensors are used, stabilization methods using roll attitude information are developed.

Chapter 6 summarizes the main findings of this research and proposes extensions of this work.

Chapter 2

Dynamic Model for the Unicycle Robot

2.1 Dynamics of a human riding a unicycle

The process of a human riding a unicycle is quite complex. Not only does a person use a multitude of sensory inputs to monitor the process, but the control actions themselves are nonlinear. As is the case with most skills learned by a human, many of the control feedback loops are closed at a subconscious level. When we attempt to emulate the process of a human riding a unicycle by a computer stabilized one wheeled robot, we first have to simplify the human's actions into mathematical and mechanical models which can be simulated and implemented in a laboratory.

A person on a unicycle maintains longitudinal stability by pedaling faster or slower, by leaning his torso forward or backward and by moving his arms forward and backward. Lateral stability is obtained by leaning his torso sideways, pulling an arm in or stretching it out and by steering the wheel into the direction that he is falling by twisting motions at the hip joints. Many of these control actions are rather jerky. For example, when a person wants to change direction on a unicycle, he would use his torso and out-stretched arms as a reaction inertia to suddenly twist the lower part of his body and the

unicycle into the desired direction. He uses his knowledge (gained by experience) of the nonlinear friction characteristics of the wheel on the ground to apply the correct torque profile to end up in the desired direction. Simultaneously, the rider would lean into the turn to counteract the effect of the ground reaction force and the inertia of his body, which would tend to let the rider fall towards the direction that he had been travelling. To emulate just one such a control action on a robot obviously would be prohibitively complex. The goal is therefore to identify and emulate only the most important control actions of a human rider.

The first and probably the most important simplification is that we assume that we can model the human riding on a unicycle with a linear process. Thereby we choose to represent the rider and unicycle by a finite number of connected rigid bodies and assume that the relative angular position and rate motions are small. We also assume that the control torques and other kinematic variables are continuous functions of time. The restriction to a linear system analysis can be changed later to include studies of nonlinear control methods, but it is reasoned that for the initial studies, we should deal with a linear system model. This not only gives insight into the basic issues involved in controlling a unicycle, but also gives access to the most powerful mathematical and control systems techniques available at present. The assumption of a linear system is also not so unrealistic, because experienced unicycle riders do not execute large amplitude motions when traveling in a straight line or while turning slowly.

We believe that the most basic configuration that will represent the major parts and motions of a human on a unicycle consists of three rigid bodies. As shown in the schematic diagram of Figure A.1 it consists of a wheel, a frame to present the unicycle frame and lower part of the rider's body and a rotary turntable which presents the rider's twisting torso and arms. The most important way in which a human rider maintains longitudinal stability is by means of the torques exerted on the pedals of the wheel. The forward and backward leaning action of the rider is of lesser importance and was not implemented in the robot in order to simplify the mechanical design.

Observation of a human riding a unicycle shows that lateral stability is obtained largely by continuously twisting the wheel in order to steer towards the direction that he is falling. The ground reaction at the contact point between the wheel and the ground applies a moment to the unicycle which rolls it back to vertical. A turntable mounted on top of the robot with its axis of rotation along the centerline of the unicycle is used to simulate the rider's torso and arms.

We show in Appendix F that the unicycle can be stabilized by sideways leaning actions only, but that the yaw angular momentum is uncontrollable from the lean actuator. We decided to exclude the sideways leaning action from the mechanical robot in order to simplify the construction.

A person uses several sensory systems to monitor the stabilization process while riding a unicycle. The four major sensors used to determine orientation with respect to vertical are the vestibular system, visual system, proprioceptive sensors and tactile sensors [Borah] and [Ormsby]. The vestibular system is the primary orientation system of the human and consists of the semicircular canals (which measure angular velocity of the head) and the otolith organs (which respond to linear accelerations and to changes in orientation with respect to the gravity vector). Proprioceptive cues are obtained from limb position signals and muscle length and tension afferents, from which the brain can infer which dynamic forces are acting on the body, based on the person's experience in coordination. A person can also determine his orientation with respect to vertical from tactile pressure cues on the various parts of his body which are in contact with his environment. Finally eye sight is used, which in combination with a person's experience in deducing the direction of vertical from clues in his environment, gives an indication of his lateral and longitudinal orientation. All these sensory inputs are combined in the human brain to determine the spatial orientation of his body. It is obviously impossible to use sensors on the robot with all the sophistication mentioned above.

2.2 Mechanical design of the unicycle robot

The unicycle robot that was designed, consists of three parts: a wheel, a frame on which the drive motors, sensors and electronics are mounted, and a battery pack on top of the frame which can rotate about the vertical axis.

The robot was specifically designed with mass and dimensional properties similar to those of a human riding on a unicycle. This allowed interesting performance comparisons, since the open-loop time constants in the two cases are similar. Although these dimensions and weight make the robot less transportable, it gives the designer more freedom to select equipment without being too concerned about physical size. Enough batteries could also be mounted on the robot to supply electrical power for extended periods of up to two hours of continuous testing without recharging.

Consider a young person of about 50 kg (110 lb) mass. The mass can be roughly divided equally between the body above and below the hips. The upper part of the body that performs the twisting motions will be approximated by a 25 kg cylinder of 0.2 m radius. The moment of inertia about the vertical axis is therefore approximately

$$I_{torso} = \frac{1}{2}MR^2 = 0.5 \text{ kg} \cdot \text{m}^2$$

This compares well with the turntable (battery pack) inertia of $I_3^T = 0.5028 \text{ kg} \cdot \text{m}^2$.

The rider's legs, which are usually slightly bent when resting on the pedals, are approximated by two 12.5 kg cylinders of $r = 8.5 \text{ cm}$ in radius (r) and spaced a distance (d) of 0.1 m apart. The moment of inertia about the vertical centerline between them is given by

$$I_{legs} = 2\left[\frac{1}{2}mr^2 + md^2\right] = 0.34 \text{ kg} \cdot \text{m}^2$$

This inertia is close to the robot's frame plus electronics inertia of $I_3^F = 0.3635 \text{ kg} \cdot \text{m}^2$.

2.2. MECHANICAL DESIGN OF THE UNICYCLE ROBOT

9

The center of mass for the unicycle robot above the wheel axle is given by

$$r^* = \frac{m_{FF} + m_{TT}}{m_F + m_T} = 0.63 \text{ m}$$

which would be located at approximately hip height for a rider sitting on a unicycle.

The mechanical parameters of the robot and the measurement methods are given in Appendix M. The calculations above do not include all the inertia properties of the unicycle plus rider, and only serve as an indication that during the robot construction an attempt was made to let the mechanical system approximate the real life situation.

The reader may wonder why the heavy battery pack is placed at the top of the unicycle robot. Placing the center of mass high not only emulates the real case of a human on a unicycle, but is also advantageous from a control systems point of view. If we consider the unicycle as a simple inverted pendulum, the higher the center of mass is, the larger is the fall-down time constant of the open-loop system. This permits a slower sampling frequency in the control microprocessor, so that it has more time to complete the calculations of the balance algorithm. Furthermore, during balance recovery actions, the wheel drive torque has to accelerate the wheel until its axle is below the center of mass of the unicycle. As we show in section L.2 the effective inertia that the torque has to accelerate depends on the height of the center of mass of the superstructure (frame and turntable). When the center of mass of the superstructure is just above the wheel axle height, the control torque has to accelerate almost all of the superstructure's as well as the wheel's inertia during stabilization actions. If, on the other hand, the superstructure's center of mass is high above the wheel axle, only the wheel's inertia needs to be accelerated (see equations L.4 and L.5).

The frame of the robot was made out of aluminum. All of the more complicated parts were made on a numerically coded milling machine to provide a light but rigid structure to which the motors, gear systems, servo amplifiers, computer rack, sensor electronics and the rotary battery pack could be mounted. A drawing of the unicycle

robot is shown in Figure 2.1 and more detailed drawings are contained in Appendix L. The microprocessor rack is mounted in the middle of the frame between the two motors and the two servo amplifiers on either side of it on the outside of the frame.

2.3 Dynamics of the unicycle robot

The unicycle robot may be modeled as three interconnected rigid bodies as shown in the schematic diagram of Figure A.1. The various coordinate transformations required to describe the relative angular motions of the three rigid bodies are defined in Figures A.2 and A.3.

In Appendix A the dynamic equations of motion are derived by using Newton-Euler mechanics. Each part of the unicycle is considered as a free rigid body with gravity forces, control torques and reaction forces and torques from adjoining bodies acting on it. It also includes the dynamics of two sensor pendulums R and S mounted to the frame which can freely swing in the longitudinal and lateral directions respectively. The derivations make provision for mounting the sensor pendulums anywhere on the unicycle frame.

The equations are generalized to include the situation where the center of mass of the frame is displaced away from the vertical centerline of the robot. Inclusion of the products of inertia into the dynamic equations of motion would significantly complicate the mathematics. Therefore the robot was designed with its mass distribution as symmetrical as possible about the longitudinal and lateral planes which intersect in the vertical centerline. This would cause the products of inertia to be negligibly small or zero (section 7-2, [Greenwood]). It is assumed that the wheel rolls on the ground without slipping, which places a nonholonomic constraint on the dynamic equations. The dynamic equations are derived for a nonzero nominal turntable speed, which produces coupling between the longitudinal and lateral plant dynamics.

2.3. DYNAMICS OF THE UNICYCLE ROBOT

11

The dynamic equations for the three parts of the unicycle with the two sensor pendulums are obtained after eliminating all the internal reaction forces and moments. It results in an eleventh order system with two forcing functions, the wheel torque and the turntable torque. The equations are summarized in section A.12 and presented in state space form in Appendix D.

As a means of checking the equations of motion, the derivation was repeated by using Lagrange's equations in Appendix B. This method is based on the physical principle that the time rate of change of the scalar generalized momentum p_i is equal to the generalized force Q_i due to the applied forces plus an inertial generalized force due to motion in the other generalized coordinates (section 6-6, [Greenwood]). Often the Q_i 's are derivable from a potential function, which is the potential energy of the unicycle in the gravity field of earth, in the present case. This method avoids the need to eliminate all the reaction forces as in Appendix A. The no-slip condition on the wheel is a nonholonomic constraint equation and is included into Lagrange's equation as shown in section B.3.1.

In the Lagrange's method derivation, we did not include the sensor pendulums and asymmetry of the frame since we only wanted to check the dynamic equations of motion. The summary of the dynamic equations of section B.4 indeed confirms that the previous equations are correct.

A third very useful method for checking the dynamic equations of motion is described in Appendix C. It is based on D'Alembert's principle which states that the laws of static equilibrium apply to a dynamical system if the inertial forces, as well as the actual external forces, are considered as applied forces acting on the system (section 1-5, [Greenwood]). After determining the D'Alembert forces, D'Alembert torques and gravitational forces on the three parts of the unicycle, the following procedure ([Bryson 3]) provides the dynamic equations of motion:

- set the two horizontal components of the moment about the ground contact point

equal to zero for the whole unicycle.

- set the vertical component of the moment about the vertical centerline equal to zero for the whole unicycle and include the applied ground friction torque.
- set the moment about the axle of the wheel equal to zero for the frame plus turntable and include the applied torque Q_w and wheel drive friction torque.
- set the moment about the axle of the turntable equal to zero for the turntable and include the applied torque Q_T and the turntable drive friction torque.

The resulting equations in sections C.2 and C.3 serve as an additional confirmation that the dynamic model for the system is derived correctly.

2.4 Selection of actuators and the drive system

One of the aims of this research project was to build a robot that can stabilize itself without any connections to its environment other than the wheel touching the ground. Therefore both its actuators and power source should be on-board. Direct current motors and batteries offer a convenient solution to this requirement.

The choice between direct drive or geared drive systems was dictated by cost. While the former offers advantages of a simpler mechanical design and none of the nonlinearities associated with geared drive systems, these motors were too expensive for the budget of the project. The direct current servo motors (Infranor) that were selected have low inertia armatures which allows high angular acceleration of the rotor and can run at low speeds with full output torque and no cogging. A 316 watt motor was selected for the wheel drive system because the robot is expected to stabilize itself while continuously running at a forward speed as high as 3 meters per second (10 km/h). A smaller 151 watt motor was selected for the turntable drive system. The maximum speeds for these motors are 7000 and 10 000 revolutions per minute for the large and small motor respectively.

A precision cable and polyurethane chain drive system and aluminum gears were used to reduce the motor speeds and increase the motor torques. This system requires no lubrication and the gear ratios can easily be adjusted by using different belt and gear sizes. An effort was made to select optimum gear ratios for the drive systems. For the wheel drive system it is desirable to select a gear ratio which matches the motor rotor inertia to the effective inertia of the longitudinal system dynamics, so that maximum wheel acceleration can be obtained. This will enable the quickest recovery from longitudinal balance disturbances. Appendix K shows how the wheel acceleration as a function of the gear ratio can be derived from the dynamic equations of motion. For the robot parameters listed in Appendix M, a 24:1 gear reduction is near the optimum value for the wheel drive system.

Lateral system stability is maintained by continuously steering into the direction that the unicycle is falling. The optimal gear ratio for the turntable drive system would therefore be the ratio that gives maximum yaw acceleration. Appendix G uses the lateral system dynamic equations of motion and plant parameters to calculate that the optimal gear ratio would be approximately 72:1. The practical limitations of the three stage gear reduction system that was constructed limited the gear ratio to 60:1, but this results in a maximum yaw acceleration that is 98% of the optimum.

Pulse width modulated amplifiers ([Galil Motion]) were used to drive the servo motors. The particular models that were used modulate the 48 V d.c. supply from the batteries to supply a regulated current to the motors. They can continuously supply 10 A to each motor. The servo amplifier receives a reference voltage from the digital-to-analog interface card in the on-board microprocessor, which commands a torque in the motor. The digital computer interface electronics is described in more detail in Appendix L.

2.5 Selection and construction of sensors

The control system needs information on the angular rates of the wheel and the turntable relative to the frame. The turntable speed can be very low and tachometers give poor results at low angular rates. It was therefore decided to use position encoders on the motor rotor shafts to obtain angular velocity information. This method, which is described in detail in Appendix I, uses a high frequency clock to count the number of clock pulses during each pulse from the position encoder as it rotates. The pulse count can then be inverted in the microprocessor to obtain angular velocity information. This method can provide high resolution angular rate information by the appropriate selection of the counter clock frequency and counter register length.

Several balance sensors were considered. As we will show in a later chapter, the ideal sensors would measure the pitch and roll angles of the unicycle with respect to vertical. Instruments which can indicate vertical in the presence of external accelerations other than gravity on the instrument are quite complex [Wrigley]. Vertical gyros, free gyros and optical vertical reference systems can provide this information, but all of these were too expensive for the budget of the project.

Passive sensor pendulums were considered as a means of obtaining vertical reference. All the modes of the unicycle dynamic system are theoretically available from the measurement of the passive sensor pendulum angles relative to the unicycle frame. Unfortunately the commercial instruments of this type do not have the required resolution and some of their parameters (eg. damping factor) are temperature dependent. Furthermore, it is shown in Appendix E that the inverted pendulum modes can be unobservable if the passive sensor pendulums are mounted at the wrong heights.

Rate gyros can be used to measure roll and pitch rates. The inverted pendulum modes are observable from these measurements, but unfortunately these instruments are also fairly expensive.

Analyses in section N.3 and Q.3 show that the inverted pendulum modes are observable from measurements of accelerometers mounted on the unicycle frame. We decided to use this type of sensor because it would allow the robot to ride on inclined terrain and accelerometers of adequate sensitivity could be constructed at an affordable cost. Simulations have shown (see later chapters) that the maximum lateral and longitudinal accelerations are in the order of 0.1 m/s^2 . Appendix H describes how servo accelerometers with an accuracy of about 0.0033 m/s^2 were constructed by careful mechanical, optical and electronic design.

If we are prepared to do tests on horizontal surfaces only, the unicycle can pull a light carriage with position sensors to measure the roll and pitch angles directly. We constructed such a sensor by means of a small magnet and a Hall effect transistor to measure the unicycle frame's pitch angle relative to a horizontal floor surface. This provided an inexpensive way to demonstrate experimentally that the unicycle robot could be stabilized if the vertical orientation information was available to the control system.

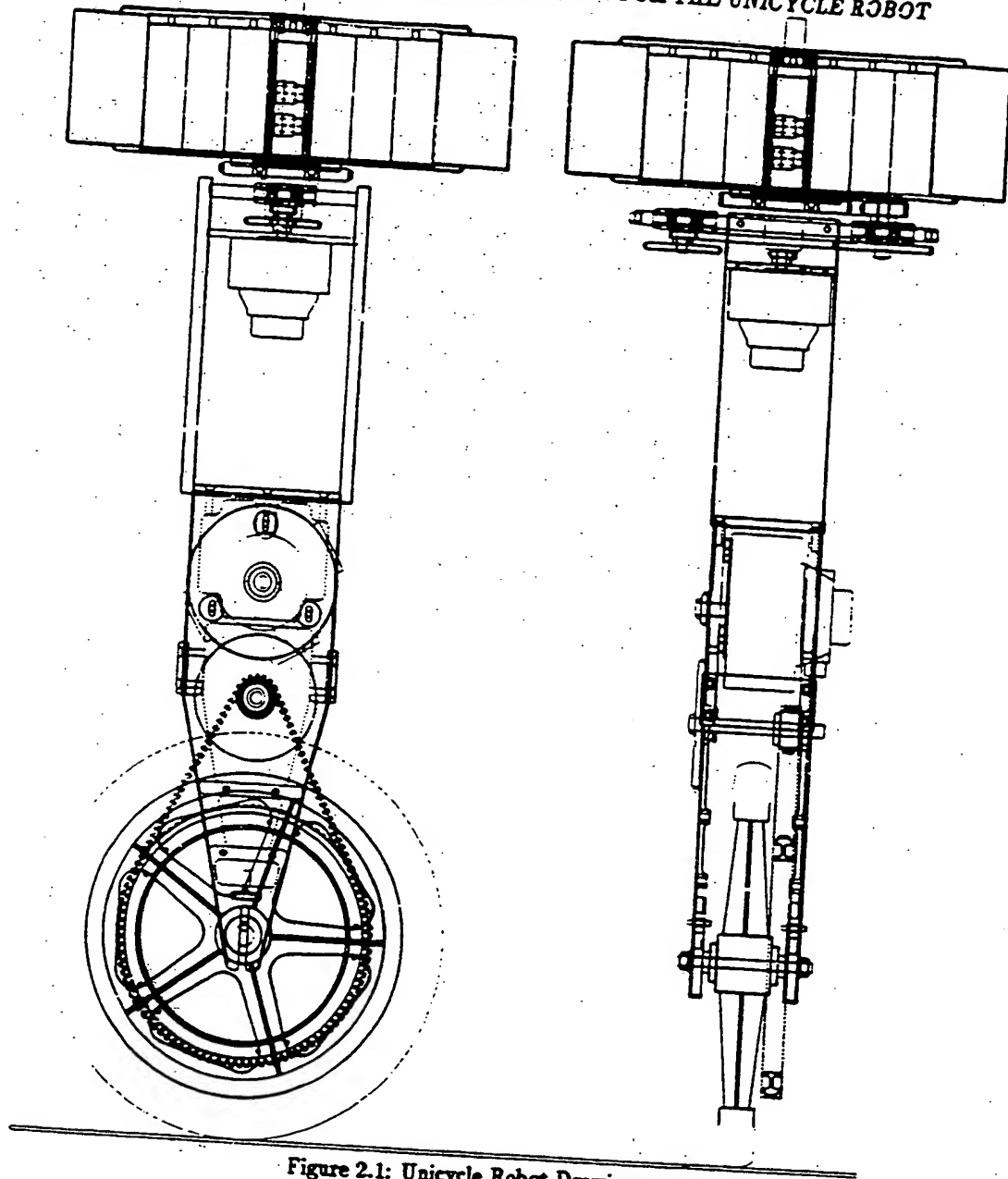


Figure 2.1: Unicycle Robot Drawing

Chapter 3

Longitudinal System with Accelerometer Sensor

3.1 Introduction

A significant simplification of the control system design can be obtained if the lateral and longitudinal system dynamics can be decoupled. Inspection of the system dynamic equations presented at the end of Appendix A, shows that it is indeed possible to decouple the lateral and longitudinal dynamics if the nominal turntable angular rotation speed η_0 is zero and the unicycle frame has left-right symmetry about a vertical plane, i.e. $r_1 = r_2 = 0$. The first requirement implies that the turntable rotation speeds should always be so slow that the gyroscopic effect of this rotating inertia does not significantly couple lateral motions into the longitudinal dynamics. Previous research efforts [Iguchi] have in fact used a fast rotating gyro on the unicycle to slow down the time constants associated with the falling down of the unicycle. Since the purpose of this thesis is to emulate the control method of a human riding a unicycle, where this form of gyroscopic stabilization is absent, the requirement that η_0 must be zero is compatible with the goal of this research.

The second requirement that the center of mass of the unicycle must be on the line

18 CHAPTER 3. LONGITUDINAL SYSTEM WITH ACCELEROMETER SENSOR

of geometric symmetry has been met by the mechanical design and construction of the robot as discussed in the previous chapter.

The dynamic equations of motion for the decoupled longitudinal system are given in Appendix N, equations N.3 and N.4. The pitch angle θ , the wheel perturbation speed $\dot{\Omega}$ and the wheel drive torque Q_w are the variables associated with the longitudinal system dynamics.

3.2 Longitudinal system characteristics

After substituting the measured mechanical parameters into the dynamic equations, we can determine the longitudinal system characteristics. As shown in section N.3 the eigenvalues of the openloop system consist of two poles at approximately plus and minus 7 rad/s in the s-plane. The unstable pole is associated with the inverted pendulum mode of the unicycle, when it falls forward or backward. The third eigenvalue near the origin of the s-plane corresponds to the rigid body horizontal velocity mode for the unicycle as a whole. The fourth mode associated with the wheel's angular position is not shown because we do not intend to control the unicycle's position. Inspection of the modal controllability matrix shows that all modes are controllable from the wheel torque.

A tachometer is mounted on the wheel drive motor shaft. We assume that drive belt elasticity and backlash are negligible so that the tachometer measures the relative speed between the wheel and the unicycle frame. The transfer function from the motor torque to the tachometer measurement has two zeros at approximately plus and minus 2.8 rad/s. The physical meaning of the zero locations can be interpreted after a few calculations:

Simplify equations N.3 and N.4 to

$$I_{11}\ddot{\theta} + I_{12}\dot{\Omega} = J\dot{\theta} - Q_w \quad (3.1)$$

$$I_{12}\ddot{\theta} + I_{22}\dot{\Omega} = Q_w \quad (3.2)$$

The viscous friction constant f_w has been ignored since it has no effect on the zero locations.

Since the tachometer reading is

$$y_t = \Omega - \dot{\theta} \quad (3.3)$$

we can rewrite equations 3.1 and 3.2 to

$$(I_{11} + I_{12})\ddot{\theta} + I_{12}\dot{y}_t = J\dot{\theta} - Q_W \quad (3.4)$$

$$(I_{12} + I_{22})\ddot{\theta} + I_{22}\dot{y}_t = Q_W \quad (3.5)$$

Take the Laplace transform of the above two equations, eliminate $\Theta(s)$ and solve

$$\frac{Y_t(s)}{Q_W(s)} = \frac{(I_{11} + 2I_{12} + I_{22})s^2 - J}{s[(I_{11}I_{22} - I_{12}^2)s^2 - JI_{22}]} \quad (3.6)$$

The zero locations are at

$$\begin{aligned} s &= \pm \sqrt{\frac{J}{I_{11} + 2I_{12} + I_{22}}} \\ &= \pm \sqrt{\frac{(m_F r_F + m_T r_T)g}{I_2^W + m_W r_W^2 + I_2^F + m_F(r_W + r_F)^2 + I_2^T + m_T(r_W + r_T)^2}} \end{aligned} \quad (3.7)$$

If we close a tachometer feedback loop with proportional feedback and command a tachometer speed y_c

$$Q_W = K(y_c - y_t) \quad (3.8)$$

the root loci of two of the closed loop poles approach the zero locations and the other closed loop pole moves to infinity as K becomes large. This implies that with the tightest feedback loop closed on the tachometer measurement, the time constant associated with the instability of the longitudinal system can at best be lengthened to that at the zero locations. With a tight feedback loop a command of $y_c = 0$ implies no relative movement between the wheel and the frame. In this locked wheel situation the unicycle falls over more slowly (longer time constant) than the free wheel condition (shorter time constant associated with the open loop pole positions). Notice that equation 3.7 gives

20 CHAPTER 3. LONGITUDINAL SYSTEM WITH ACCELEROMETER SENSOR

exactly the eigenvalues associated with a unicycle pitching over with a locked wheel.

An accelerometer mounted on the unicycle frame measures the specific force at the point where it is located. Its output is a signal given by equation N.16:

$$y_a(t) = g\theta - r_w\ddot{\Omega} - r_{R3}\ddot{\theta} \quad (3.9)$$

where r_w is the wheel radius and r_{R3} is the height above the wheel axle where the accelerometer is located. The transfer function from the wheel torque to the accelerometer output has an equal number of poles and zeros (3) due to the direct feedthrough term from the wheel torque to the accelerometer measurement (see equation N.16). One of the zeros is at the origin of the s -plane and the locations of the other two zeros vary as a function of the accelerometer height r_{R3} . The locations of these zeros have a significant effect on the closed loop system behaviour and we now proceed to determine these zero locations.

The transfer functions $\frac{\Omega(s)}{Q_w(s)}$ and $\frac{\theta(s)}{Q_w(s)}$ can be calculated from the longitudinal system equations 3.1 and 3.2:

$$\frac{\Omega(s)}{Q_w(s)} = \frac{(I_{11} + I_{12})s^2 - J}{s[(I_{11}I_{22} - I_{12}^2)s^2 - JI_{22}]} \quad (3.10)$$

$$\frac{\theta(s)}{Q_w(s)} = \frac{-(I_{22} + I_{12})s}{s[(I_{11}I_{22} - I_{12}^2)s^2 - JI_{22}]} \quad (3.11)$$

Laplace transform 3.9 and substitute 3.10 and 3.11 into it:

$$\frac{Y_a(s)}{Q_w(s)} = \frac{s\{[(I_{12} + I_{22})r_{R3} - (I_{11} + I_{12})r_w]s^2 + r_wJ - g(I_{12} + I_{22})\}}{s[(I_{11}I_{22} - I_{12}^2)s^2 - JI_{22}]} \quad (3.12)$$

For the case with nonzero friction, the pole will not be exactly at $s = 0$ and thus will not be canceled by the zero at the origin.

The zeros of the accelerometer transfer function are given by

$$s = 0$$

$$\text{and } s = \pm j\sqrt{\frac{g(I_{12} + I_{22}) - r_wJ}{(I_{11} + I_{12})r_w - (I_{12} + I_{22})r_{R3}}} \quad (3.13)$$

By substitution of the parameters from Appendix M into the equation above we see that the pair of zeros are at infinity for the accelerometer mounted at the critical height of

$$\begin{aligned}(r_{R3})_{\infty} &= \frac{(I_{11} + I_{12})r_W}{(I_{12} + I_{22})} \\ &= 0.6675 \text{ m}\end{aligned}\tag{3.14}$$

If an accelerometer were placed at $r_{R3} = (r_{R3})_{\infty}$, it would have zero initial response to an impulse on the wheel torque. With the accelerometer at this height the direct feedthrough term from the control torque Q_W to the accelerometer output y_a becomes zero. It is confirmed by equation N.16 where the coefficient of Q_W , namely $r_{R3}G_1 + r_W G_2$, vanishes when $r_{R3} = (r_{R3})_{\infty}$.

For $r_{R3} < (r_{R3})_{\infty}$ the accelerometer transfer function has a pair of complex zeros and for $r_{R3} > (r_{R3})_{\infty}$ the zeros are on the positive and negative real axis. The location of the zeros is thus very sensitive to small deviations in r_{R3} if r_{R3} is in the vicinity of $(r_{R3})_{\infty}$.

Another undesirable situation occurs when r_{R3} is such that the accelerometer zeros cancel the inverted pendulum poles of the plant. These modes then become unobservable from the accelerometer measurement, which defeats the purpose for which the accelerometer was used in the first place. We can solve for this critical height from equation 3.12:

$$\begin{aligned}(r_{R3})_{unobs} &= \frac{JI_{12}r_W + (I_{11}I_{22} - I_{12}^2)g}{JI_{22}} \\ &= 0.721 \text{ m}\end{aligned}\tag{3.15}$$

The physical explanation for the existence of this point of unobservability is that, if the unicycle was allowed to fall over in the plane of the wheel, this point would move straight down, i.e. it would have no horizontal acceleration. If we think of the spring-mass analogy of the accelerometer, it is clear that such an instrument mounted at this height, with its sensitive axis pointing along the direction of the unicycle travel, will

22 CHAPTER 3. LONGITUDINAL SYSTEM WITH ACCELEROMETER SENSOR

have a zero output. An accelerometer mounted at this point on the unicycle is analogous to the case where an accelerometer is mounted on the bob of a simple pendulum.

A method to identify the longitudinal system dynamic model experimentally is described in section N.3.2. One of the problems of identifying an unstable plant is that its variables do not stay within small perturbation ranges for very long (in the order of one second in this case). The small angles assumption is basic to deriving a valid linearized model for the unicycle dynamics (Appendices A, B and C). A partial identification of the system transfer functions was obtained by hanging the unicycle upside down by its wheel. The dynamic model then changes from an inverted to an ordinary pendulum to which we can apply sinusoidal test signals and measure frequency responses. In section N.3.2 the conclusion is drawn that the actual plant model is acceptably close to the theoretical model because their frequency responses agree to within 2 dB in gain and 10 degrees in phase over the frequency spectrum of signals present in the dynamic system during typical maneuvers.

3.3 Compensator design by successive loop closure

3.3.1 Nominal design

Control systems designed by successive loop closure techniques can produce compensators of low order. This is advantageous when the compensator is implemented in a microprocessor, which takes a finite time to calculate the control command. The shorter this time is, the faster sampling rate can be used, which usually improves the quality of the dynamic response. Several other considerations for the sampling rate selection are discussed in section 0.1.

The longitudinal dynamics are modified to include the delay time between the instant that the measurements are made and the time that the control command is issued (see section N.3.2).

Section 0.4 describes the design of the lowest order compensator that stabilizes the plant. It consists of an inner loop with proportional feedback of the tachometer measurement and an outer loop with a first order compensator on the accelerometer feedback signal. Closing a tight tachometer feedback loop first has the advantage of decreasing the effect of mechanical nonlinearities in the wheel drive system. The major nonlinearity is Coulomb friction which could be removed by means of an offset torque which depends on the sign of the wheel speed. Unfortunately the relatively inexpensive belt and sprocket drive system used in the robot's wheel drive system also causes time varying friction losses which depend on the angular positions of the gears. The most effective way of minimizing the effects of these varying torque losses is by closing a tight (high gain) tachometer feedback loop first.

An integral error feedback compensator on the tachometer feedback signal will increase the low frequency gain in the inner loop and the block diagram of Figure 0.6 shows how this can be incorporated in the design. For the purpose of finding the minimum order compensator, however, proportional feedback only will be used.

The nominal compensator design was obtained through an iterative process and inspection of the root loci and step responses as the loops were closed and the compensator parameters adjusted. The root locus of Figure 0.5 shows that it is theoretically possible to find a compensator which stabilizes the unstable modes of the unicycle by using an accelerometer sensor. The simulation results in Figure 3.1 show that the maximum pitch angle from which the longitudinal control system can recover without exceeding the maximum available motor torque ($(Q_W)_{max} = 15.12 \text{ N} \cdot \text{m}$) is about 5 degrees.

3.3.2 Robustness of the longitudinal controller

We have shown in section 3.2 that the zeros of the transfer function to the accelerometer output change as a function of r_{AS} , the height above the wheel axis where it is mounted. The plot of the zero locations in the z-plane (Figure 3.2) shows large changes of the zero positions for small variations in the accelerometer height, especially in the vicinity of

24 CHAPTER 3. LONGITUDINAL SYSTEM WITH ACCELEROMETER SENSOR

$r_{R3} = (r_{R3})_{\infty}$. For example for r_{R3} changing from only 3.25 cm lower than $(r_{R3})_{\infty}$ (i.e. - 5%) to 3.25 cm higher than $(r_{R3})_{\infty}$ (i.e. + 5%), the zero locations have changed all the way from $z = 1 \pm j0.24$ through $z = \pm\infty$ to $z = 1 \pm 0.24$.

Since these zeros are points to which two of the root locus branches progress, the closed loop system pole locations are also very sensitive to the choice of r_{R3} . Even if r_{R3} is known exactly, equation 3.9 shows that the accelerometer signal is a function of $r_{R3}\bar{\theta}$, so that differences between the real plant and the theoretical model which cause the actual pitch acceleration ($\bar{\theta}$) to differ more than $\pm 5\%$ from the theoretical pitch acceleration, will cause the same dramatic shift in the accelerometer zero locations.

Figure 3.3 illustrates what happens to the root loci if the accelerometer is mounted too low on the frame. In this case where $r_{R3} = 0.5$ m the root loci from the unstable region of the z -plane converge toward the two complex zeros outside the unit circle instead of toward the zero at $z = 1$ and the compensation zero as in the nominal design shown in Figure 0.5. The accelerometer height, r_{R3} , should therefore not be too low because it creates a 'barrier' of zeros which makes it difficult for the root loci from the unstable region of the z -plane to slip through into the unit circle.

If the accelerometer is placed at the nominal design position, $r_{R3} = 0.653$ m the system can be stabilized. Inspection of the root locus of Figure 0.5 shows that although we may stabilize the system, we will not necessarily obtain satisfactory system performance. The damping on the low frequency branches of the root loci becomes better than $\xi = 0.7$ at fairly high loop gains ($K_a > 20$), at which point the damping on the high frequency branches of the rootloci is rapidly decreasing to unacceptably low values.

Placing the accelerometer near $(r_{R3})_{\infty} = 0.6675$ m would not be sensible because of the great sensitivity of the accelerometer zero and closed loop pole positions described earlier. Equation 3.13 shows that for $r_{R3} > (r_{R3})_{\infty}$ the accelerometer zeros are on the

real axis. The unstable pole will therefore always be destabilized as it is attracted to the zero on the positive real axis for increasing loop gain.

A schematic diagram which summarizes the findings of the longitudinal successive loop closure compensator studies is shown in Figure 3.4. Figure 3.5 shows a plot of how the closed loop pole positions change as the accelerometer height deviates from the nominal value of 0.653 m. It shows that the requirement for stability is

$$0.54 < r_{R3} < 0.6707 \text{ m}$$

If the system is expected to be well damped (closed loop poles within the $\xi = 0.5$ curve in the z-plane) the range of acceptable r_{R3} values is actually still more restricted.

3.3.3 Experimental Results

The successive loop closure compensator of section 0.4 was coded in the FORTH computer language and implemented in the on board microprocessor of the unicycle. The computer code is given in section P.1. After executing an algorithm for 5 seconds to bring the unicycle up to a nominal speed of $\Omega_0 = 3.0$ rad/sec while hand holding the robot vertical, the accelerometer feedback loop was closed. Figure 3.6 shows the two measurements during a typical experimental run. The system went unstable when the accelerometer feedback loop was closed and the unicycle released at $t = 5$ seconds. Attempts to adjust the compensator parameters and accelerometer height experimentally to obtain stability were unsuccessful.

Figure 3.7 shows a plot of the accelerometer signal measured during the period between 2.5 and 5.0 seconds of the previous experiment. Noise in the signal can be as high as 0.25 m/s^2 peak to peak from one sample to the next. This noise is caused by high frequency vibrations of the frame due to unevenness in the wheel drive system and the ground surface.

Figure 3.8 shows the theoretical time response of the accelerometer measurement if

26 CHAPTER 3. LONGITUDINAL SYSTEM WITH ACCELEROMETER SENSOR

the unicycle is initially pitched forward at an angle of 5 degrees. The maximum magnitude of the accelerometer signal is just 0.15 m/s^2 . Plots of the components of the accelerometer signal, as expressed in equation 3.9 are also shown. It shows that while some of the components may be reasonably large, they add up in such a way that the measured output of the accelerometer sensor is always small. This causes the pitch attitude information that is essential for the control system to maintain balance to be lost in the noise present in the practical situation.

It seems logical to attempt to low pass filter the accelerometer signal before it is read into the microprocessor. Suppose we add a first order filter on the accelerometer output. This places an additional pole on the positive real z-axis in upper righthand diagram of Figure 3.4. The root locus of the closed loop system now has a branch which moves to $-\infty$ on the real axis. Without repeating the whole design process here, it can be stated that the sensitivity problems discussed in the previous section are aggravated by addition of low pass filtering. Physically it means that the phase lag of a low pass filter causes the attitude information required by the control system, to arrive later in time. In an unstable system it is obviously advantageous to have attitude information available to the controller as soon as possible.

We conclude that, even though accelerometers can in theory be used as attitude sensors, practical applications are unlikely to succeed. The accelerometers measure both the pitch attitude and the frame acceleration at the position where they are mounted. The transfer function to the accelerometer output contains zeros whose locations are not only highly sensitive to parameter variations, but also make it difficult to design low order compensators which will stabilize the unstable eigenvalues of the plant.

Furthermore, the component of the accelerometer signal which contains the attitude information is small (maximum $\cong 0.15 \text{ m/s}^2 = 1.5\%$ of the earth's gravity acceleration). It is therefore required that the accelerometers have high sensitivity, but the sensors then become susceptible to vibrations of the robot frame as it moves along uneven terrain.

3.4 Longitudinal system LQG design

3.4.1 Motivation for using an LQG compensator

Compensators consisting of an optimal regulator and estimator have several attractive properties which we hoped would address some of the problems encountered with stabilizing the longitudinal system. First of all, the design process is highly automated and it usually results in a closed loop system with a good transient response. For the successive loop closure compensator design described in the previous section, an iterative process was required to obtain a closed loop system in which all the modes were reasonably well damped ($\xi < 0.5$). Even with this simple longitudinal plant model, the choice of which loops to close first, the positions of compensator poles, zeros and loop gains is a bit of an art. Compensators designed by minimizing linear quadratic cost functions will make coordinated use of the measurements and can design state feedback gains for closed loop systems that meet reasonable performance requirements. The designer can specify the closed loop performance in terms of a cost function which weights the relative importance of keeping state errors small and using reasonable amounts of control energy.

The state estimator design can be optimized if the statistical nature of the process and measurement noise is known. Even if these characteristics are known only by approximation, the compensators designed by linear quadratic gaussian (LQG) techniques provide good noise filtering as well as phase recovery. This is an important improvement over the successive loop closure design where we would like to filter the noisy accelerometer signal, but have difficulty in compensating for the phase loss associated with it.

Another advantage is that it is easy to solve the problem of long calculation delays in the microprocessor by designing a prediction estimator. It calculates the control command at the end of the current sampling period, based on the measurements at the beginning of the sample period, allowing a full sample period for the microprocessor to perform the calculations.

28 CHAPTER 3. LONGITUDINAL SYSTEM WITH ACCELEROMETER SENSOR

3.4.2 LQG design method

An optimal continuous time regulator was designed first, as described in section N.4. We have included integral error feedback of the wheel speed so that we will be able to accurately control the unicycle speed by means of an external command. The cost function that was minimized to obtain the optimal state feedback gains, contained a single factor for the relative weight between the integral error on the wheel speed and the amount of control energy used. This weighting factor was varied to obtain a ratio which provided good damping on the regulator eigenvalues (Figure N.6) and a step response which reached the commanded speed in approximately 5 seconds (Figure N.7).

Since we did not have an apriori knowledge of the process and measurement noise characteristics, we assumed values for the accelerometer and tachometer measurement noise spectral densities, based on a visual inspection of the relative amount of noise present in these two signals during experiments. The process noise spectral density was then varied until the eigenvalues of the estimator were in the same s-plane region as the regulator eigenvalues. The optimal continuous time estimator gains that were obtained are shown in section N.6 and the theoretical step response of the closed loop system with noise inputs, is shown in Figure N.11.

Using the same sampling period as for the successive loop closure compensator, a discrete equivalent of the continuous time LQG compensator was designed in section O.2. The algorithm by Van Loan [Van Loan] was used to calculate the weighting matrices in the discrete time performance index, which will produce the same performance as the original continuous time system.

The discrete time estimator design was performed by first converting the process noise spectral density to an equivalent process noise covariance matrix for the discrete case, by the duality of the regulator performance index conversion (Appendix D of [Bryson 1]). It is shown in the same reference that a measurement noise spectral

density (R) can be converted to a measurement noise covariance matrix (V) by the relationship

$$R = 2VT_c$$

as long as the measurement noise correlation time T_c is short compared to the shortest time constant of the plant. The shortest time constant for the longitudinal system is about 0.125 sec (from eigenvalue at $s \approx 8 \text{ r/s}$) so that a noise correlation time of $T_c = 0.01 \text{ sec}$ was assumed.

The discrete LQG compensator was designed and the closed loop system simulated. Figure O.3 shows the theoretical time responses of the control torque, wheel speed and pitch angle during a balance recovery maneuver.

3.4.3 Experimental results and conclusions

The LQG control system designed in section O.2 was coded in FORTH after performing a transformation of the compensator matrices to modal form as described in section O.3. Implementing the compensator in modal form reduces the computational load on the on-board microprocessor. The FORTH code is shown in section P.2.

The closed loop system was unstable when tested experimentally. Experimental adjustment of LQG compensator gains in order to stabilize the system is unlikely to succeed because it has four regulator and six estimator gains which can be adjusted.

Studies have shown that LQG controllers have serious defects concerning closed-loop robustness with respect to plant deviations [Doyle 1]. Many techniques are currently suggested to improve system robustness [Doyle 2] and could be applied to the unicycle stabilization problem. However, as we have shown before, the current problems with stabilizing the unicycle reside more with the physical problems present when using an accelerometer, than with the control system design method.

30 CHAPTER 3. LONGITUDINAL SYSTEM WITH ACCELEROMETER SENSOR

Investigations into control methods which can circumvent the problems associated with accelerometer sensors, would be instructional. The approach of this thesis is, however, to first find sensors which will provide the system information that will result in simple, robust compensators.

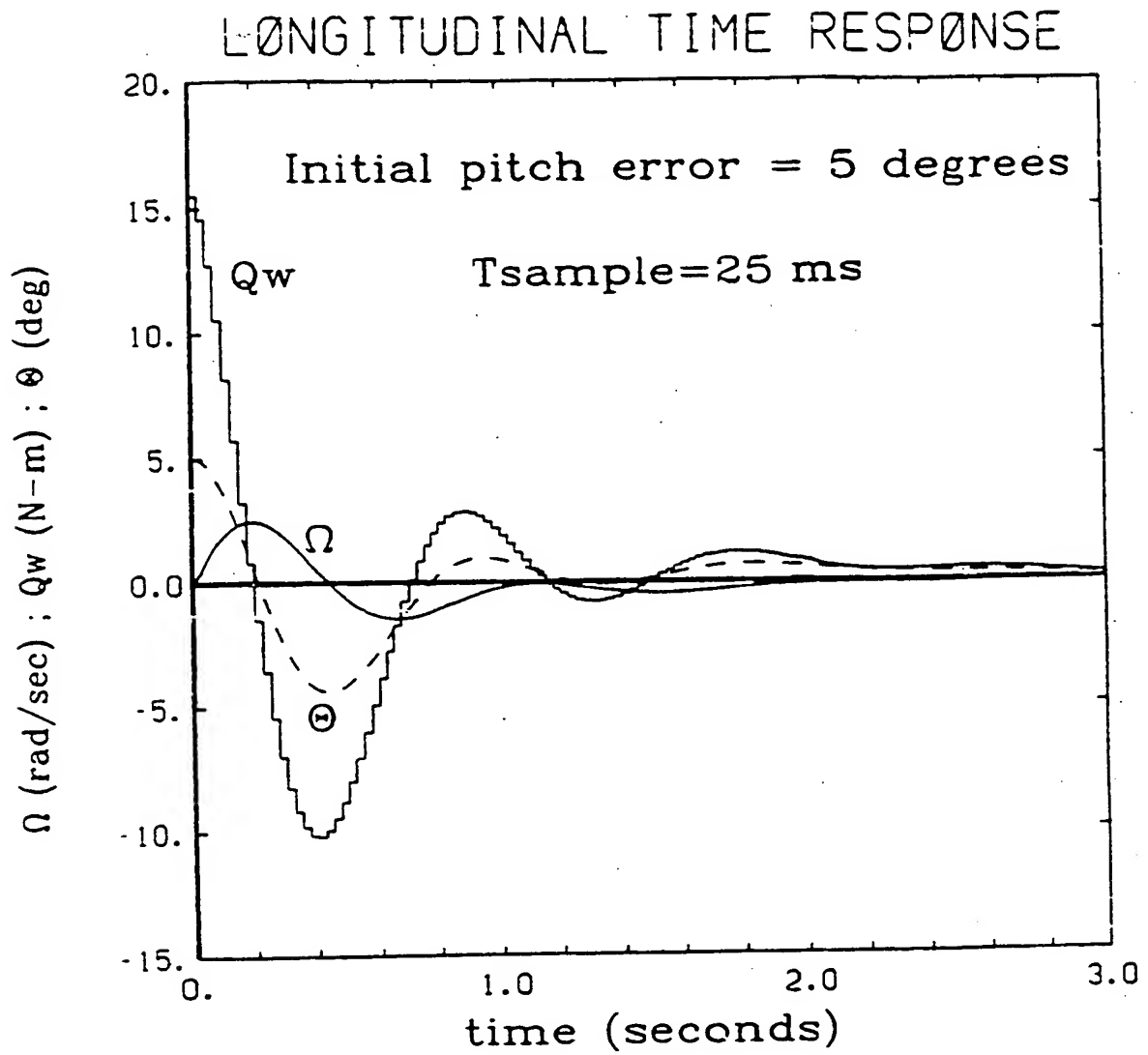


Figure 3.1: Longitudinal System Balance Recovery to an Initial Pitch Angle Error

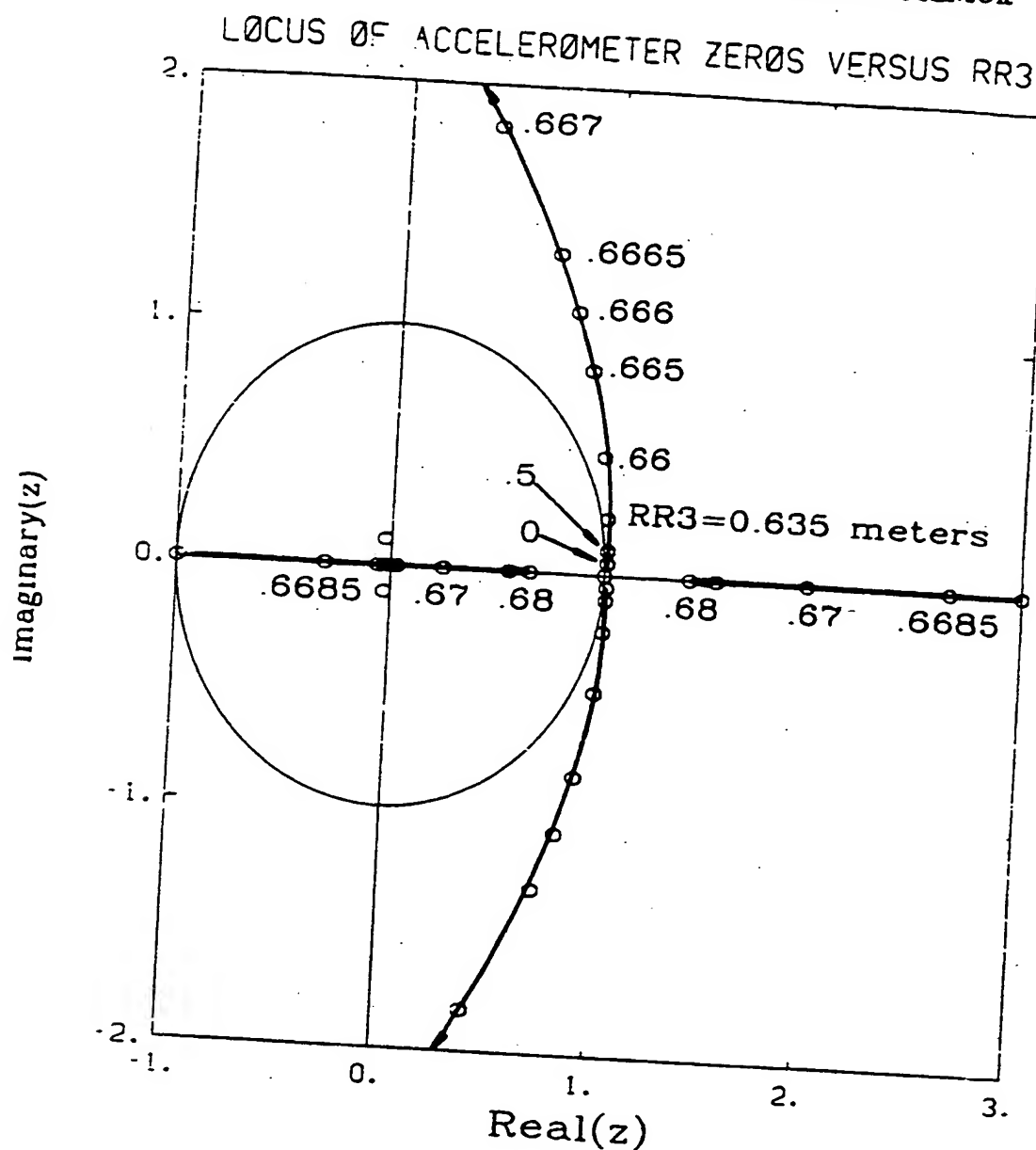


Figure 3.2: Locus of the Zeros of the Transfer Function to the Accelerometer Output as a Function of the Accelerometer Height above the Wheel Axis

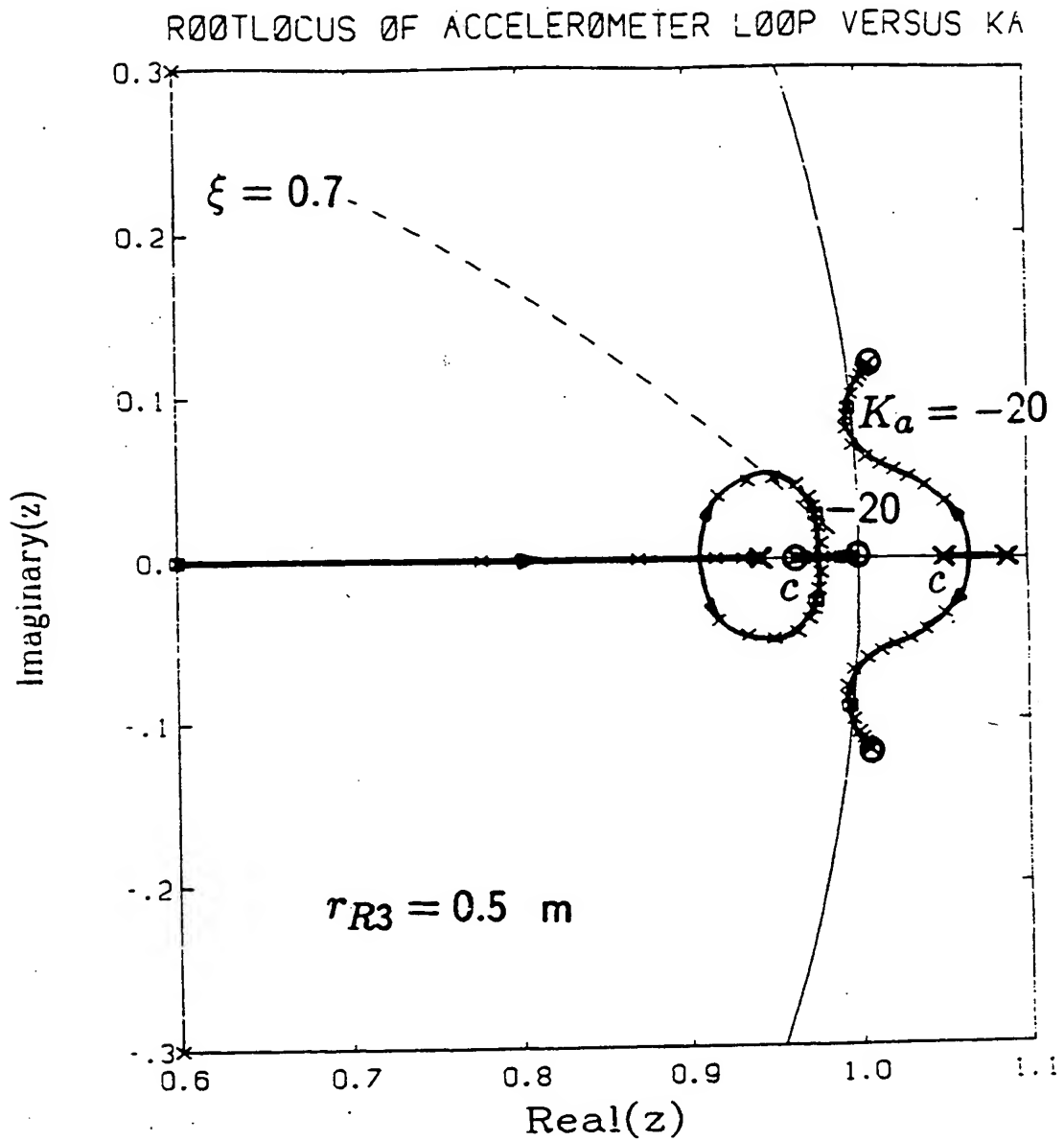
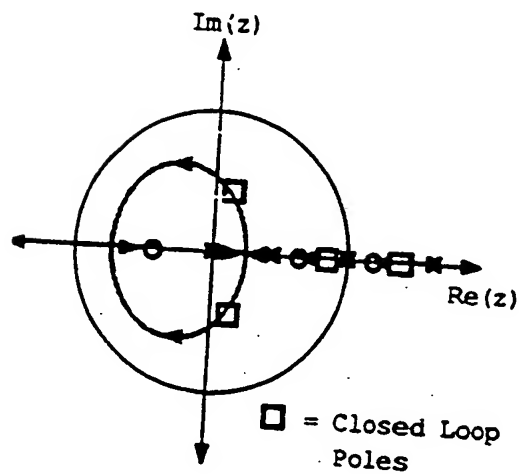
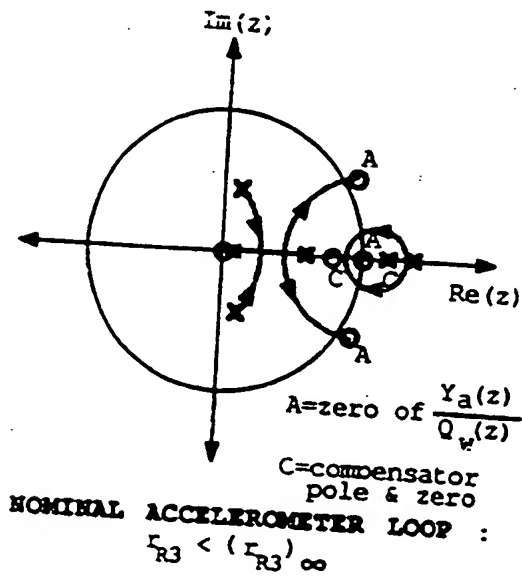


Figure 3.3: Longitudinal Accelerometer Feedback Loop RootLocus when the Accelerometer are placed too Low on the Frame

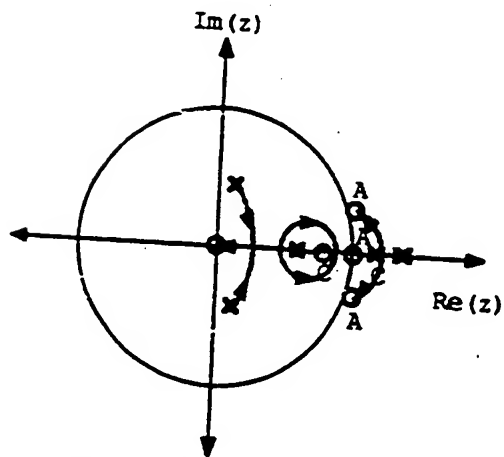
34 CHAPTER 3. LONGITUDINAL SYSTEM WITH ACCELEROMETER SENSOR



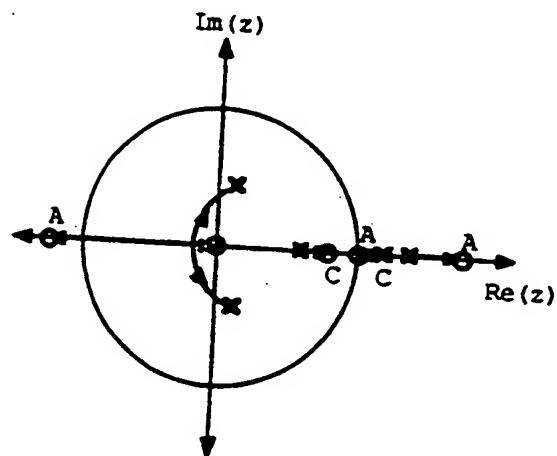
TACHOMETER LOOP COMPENSATION



NOMINAL ACCELEROMETER LOOP :
 $r_{R3} < (r_{R3})_{\infty}$



ACCELEROMETER LOOP for
 $r_{R3} \ll (r_{R3})_{\infty}$



ACCELEROMETER LOOP for
 $r_{R3} > (r_{R3})_{\infty}$

Figure 3.4: Rootloci for the Longitudinal System Designed Compensators Designed by Successive Loop Closures

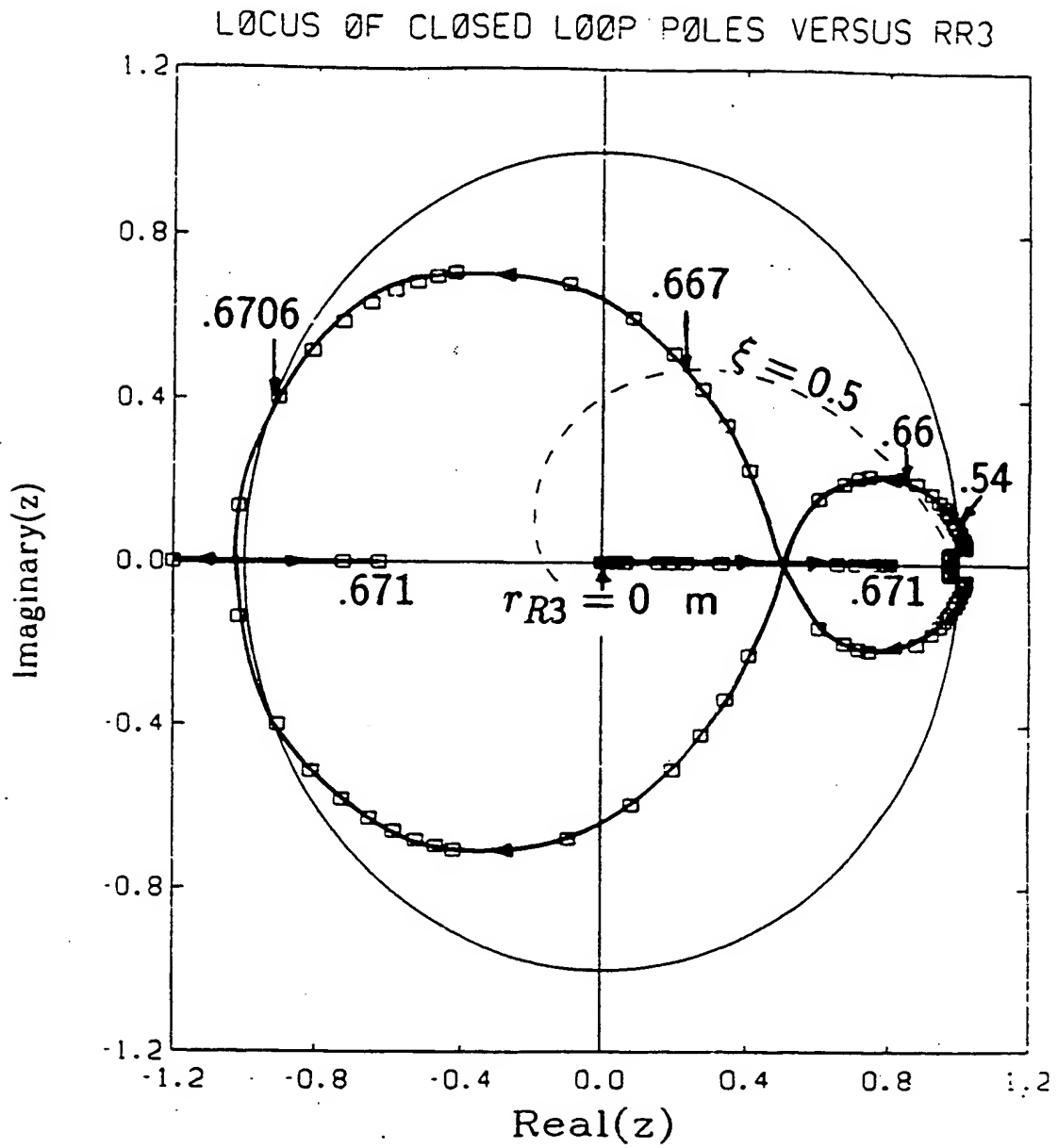


Figure 3.5: Rootlocus for the Closed Loop Longitudinal System as a Function of the Accelerometer Height above the Wheel Axle

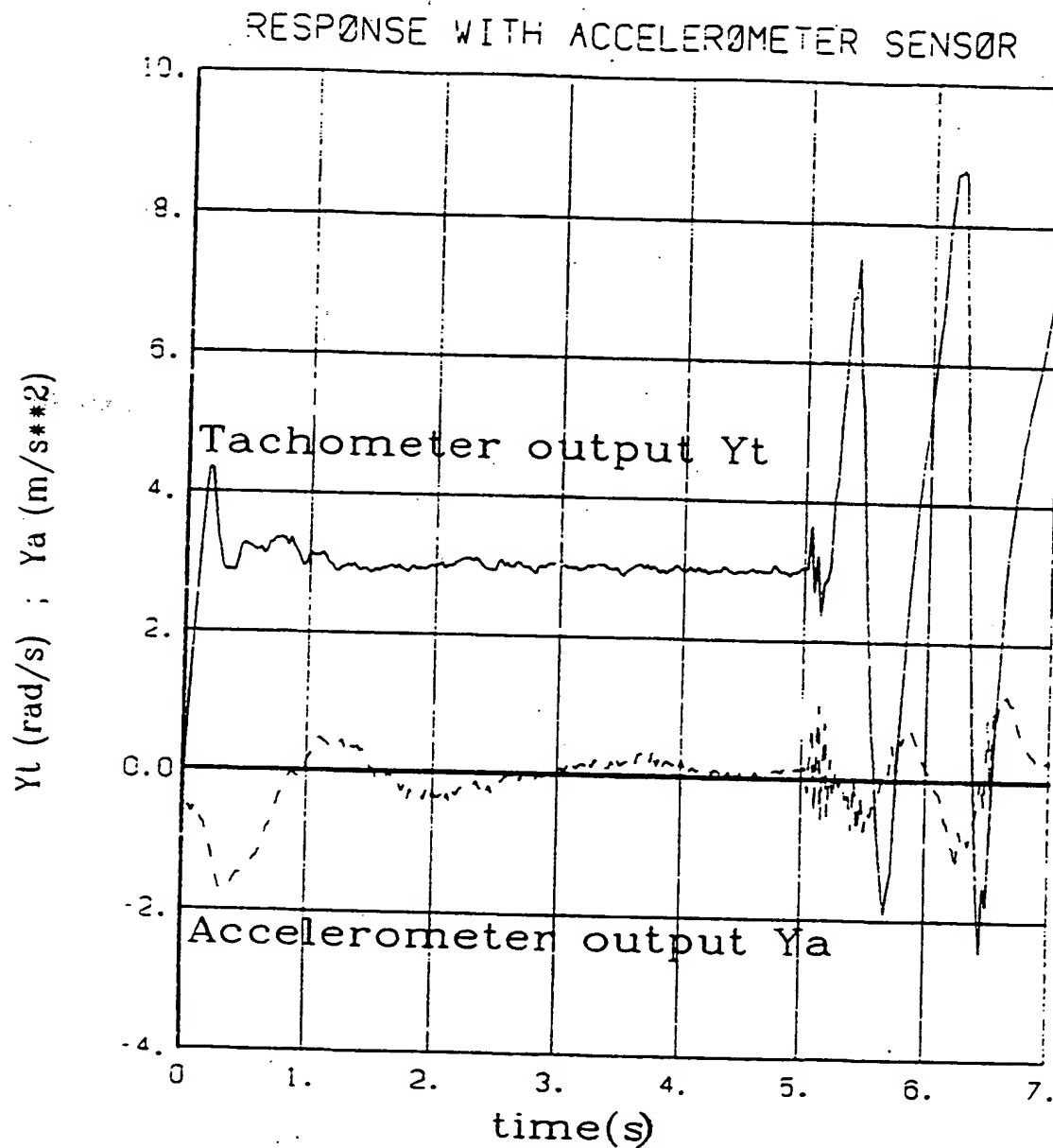


Figure 3.6: Measured Time History of Longitudinal System Signals during an Experimental Stabilization Test

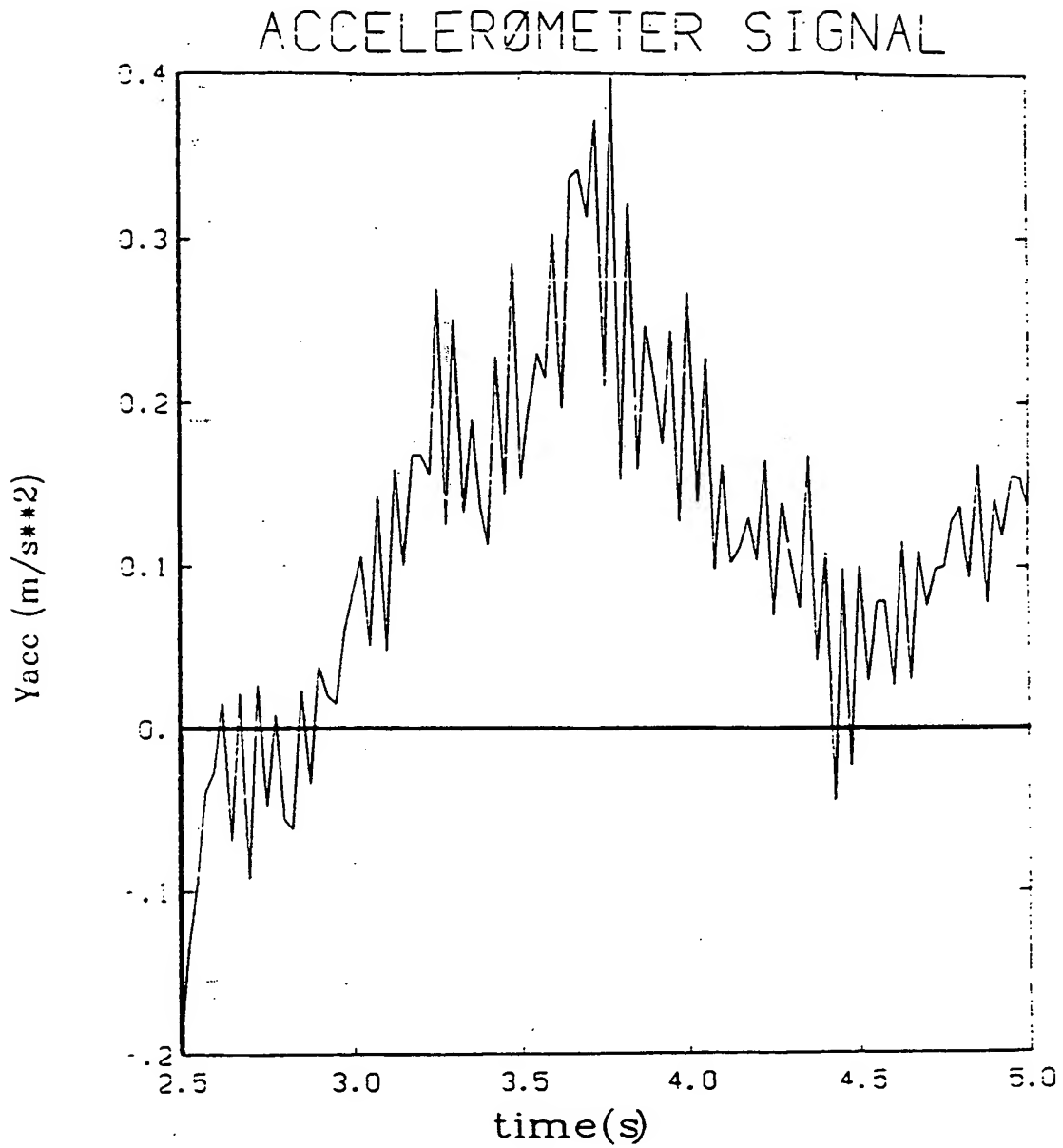


Figure 3.7: Typical Longitudinal Acceleration Measurement while the Unicycle is Moving at a Wheel Speed of 3 rad/sec.

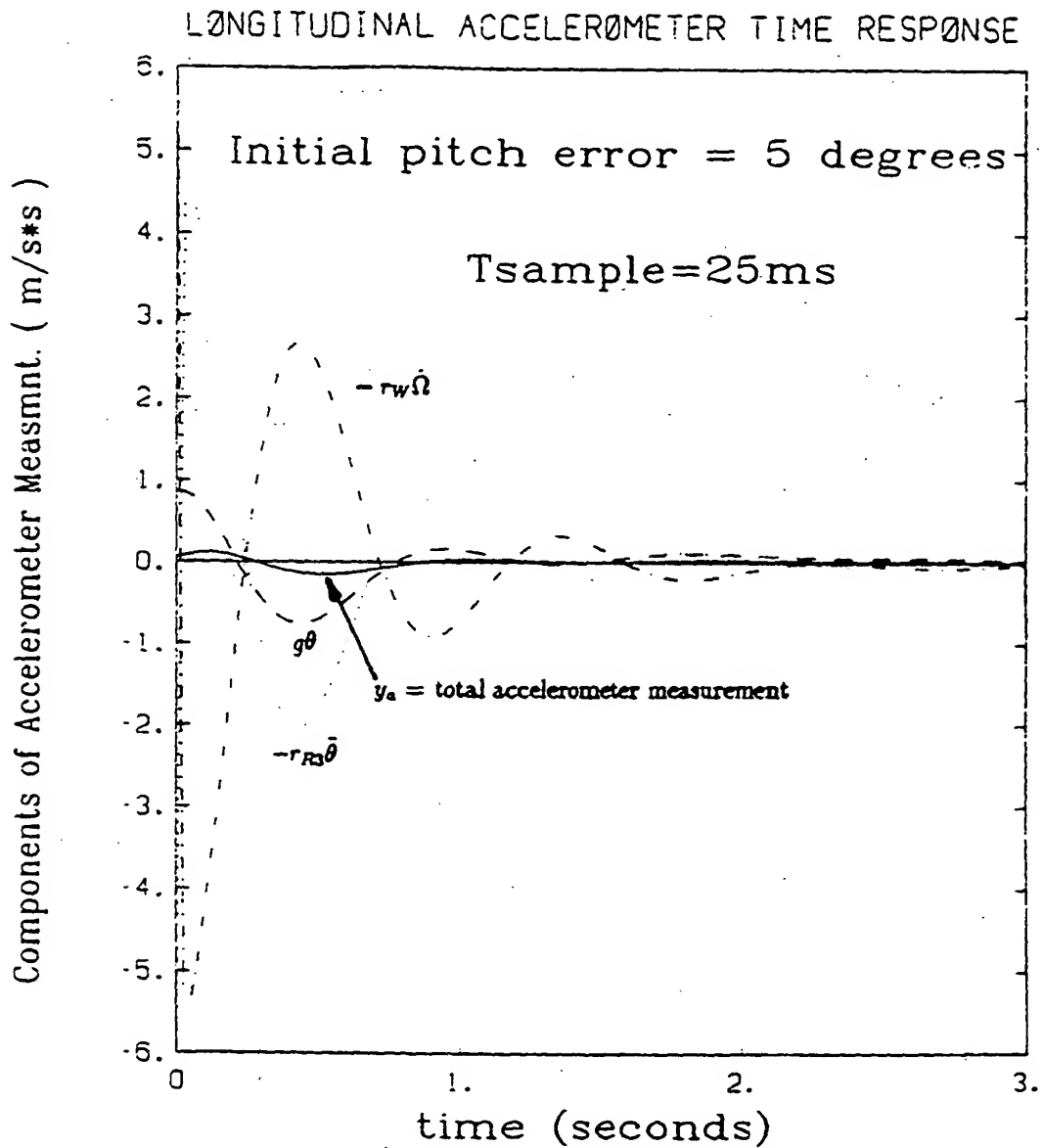


Figure 3.8: The Time Responses of the Longitudinal Accelerometer Measurement and its Components during a Simulation of a Balance Recovery Sequence

Chapter 4

Longitudinal System with Vertical Sensor

4.1 Introduction

We have shown in the previous chapter that an accelerometer measures not only the pitch attitude, but also accelerations proportional to the frame pitch acceleration and wheel angular acceleration. These additional terms create zeros in the transfer function to the accelerometer output, which makes the control system difficult to design and very sensitive to plant parameter changes. In this chapter we will show that a sensor which measures the pitch attitude only, will not have these undesirable zeros.

4.2 Control system design with pitch sensor

The compensator designed by successive loop closure is shown in section 0.5. The tachometer feedback loop was closed first with a first order integral error compensator. This provides a high low-frequency loop gain to decrease the nonlinear effects of the drive system. The root locus of this inner loop is shown in Figure 0.9.

The transfer function to the pitch sensor output has a zero at $z = 1$ and another at $z = -1.78$, as shown in the listing of section 0.5.1. The outer loop compensation is

much easier to design due to the absence of the pair of complex zeros just outside the unit circle, associated with the accelerometer transfer function.

In the accelerometer case, the root locus (Figure 0.5) from the unstable region of the z -plane had to pass through the 'barrier' of three zeros to enter the unit circle. In the present case only one zero at $z = 1$ is present with a pitch sensor. With a simple first order compensator consisting of a pole at $z = 1.03$ and a zero at $z = 0.95$ the longitudinal system can be stabilized. The root locus of Figure 0.11 shows that the loop gain was adjusted until the dominant closed loop poles were well damped.

The second problem which existed with the accelerometer sensor transfer function, was that the pair of complex zeros just outside the unit circle strongly attracted the high frequency branch of the root locus. It made it difficult to obtain well damped low frequency closed loop poles before the high frequency poles became too lightly damped (Figure 0.5). It was also possible that the branches from the unstable openloop poles went directly to these complex zeros outside the unit circle instead of into the stable region of the z -plane (Figure 3.3). In the case of the pitch sensor, the transfer function zeros (apart from the one at $z = 1$) are at $z = -1.78$ and $z = -\infty$. They therefore have much less influence on the behaviour of the low frequency root loci. The high frequency closed loop poles remain well damped (Figure 0.10) and become unstable only at high loop gains of $|K_p| > 150$.

Figure 0.12 shows a simulation of the time response of the closed loop system to a 1 rad/sec step command. It is well damped and settles to the commanded speed in approximately 5 seconds.

4.3 Experimental tests of the control system

A vertical gyro would be able to measure the frame pitch angle with respect to earth's gravity vector irrespective of the inclination of the terrain over which the unicycle robot

3.4.2 LQG design method

An optimal continuous time regulator was designed first, as described in section N.4. We have included integral error feedback of the wheel speed so that we will be able to accurately control the unicycle speed by means of an external command. The cost function that was minimized to obtain the optimal state feedback gains, contained a single factor for the relative weight between the integral error on the wheel speed and the amount of control energy used. This weighting factor was varied to obtain a ratio which provided good damping on the regulator eigenvalues (Figure N.6) and a step response which reached the commanded speed in approximately 5 seconds (Figure N.7).

Since we did not have an apriori knowledge of the process and measurement noise characteristics, we assumed values for the accelerometer and tachometer measurement noise spectral densities, based on a visual inspection of the relative amount of noise present in these two signals during experiments. The process noise spectral density was then varied until the eigenvalues of the estimator were in the same s-plane region as the regulator eigenvalues. The optimal continuous time estimator gains that were obtained are shown in section N.6 and the theoretical step response of the closed loop system with noise inputs, is shown in Figure N.11.

Using the same sampling period as for the successive loop closure compensator, a discrete equivalent of the continuous time LQG compensator was designed in section O.2. The algorithm by Van Loan [Van Loan] was used to calculate the weighting matrices in the discrete time performance index, which will produce the same performance as the original continuous time system.

The discrete time estimator design was performed by first converting the process noise spectral density to an equivalent process noise covariance matrix for the discrete case, by the duality of the regulator performance index conversion (Appendix D of [Bryson 1]). It is shown in the same reference that a measurement noise spectral

3.4 Longitudinal system LQG design

3.4.1 Motivation for using an LQG compensator

Compensators consisting of an optimal regulator and estimator have several attractive properties which we hoped would address some of the problems encountered with stabilizing the longitudinal system. First of all, the design process is highly automated and it usually results in a closed loop system with a good transient response. For the successive loop closure compensator design described in the previous section, an iterative process was required to obtain a closed loop system in which all the modes were reasonably well damped ($\xi < 0.5$). Even with this simple longitudinal plant model, the choice of which loops to close first, the positions of compensator poles, zeros and loop gains is a bit of an art. Compensators designed by minimizing linear quadratic cost functions will make coordinated use of the measurements and can design state feedback gains for closed loop systems that meet reasonable performance requirements. The designer can specify the closed loop performance in terms of a cost function which weights the relative importance of keeping state errors small and using reasonable amounts of control energy.

The state estimator design can be optimized if the statistical nature of the process and measurement noise is known. Even if these characteristics are known only by approximation, the compensators designed by linear quadratic gaussian (LQG) techniques provide good noise filtering as well as phase recovery. This is an important improvement over the successive loop closure design where we would like to filter the noisy accelerometer signal, but have difficulty in compensating for the phase loss associated with it.

Another advantage is that it is easy to solve the problem of long calculation delays in the microprocessor by designing a prediction estimator. It calculates the control command at the end of the current sampling period, based on the measurements at the beginning of the sample period, allowing a full sample period for the microprocessor to perform the calculations.

26 CHAPTER 3. LONGITUDINAL SYSTEM WITH ACCELEROMETER SENSOR

the unicycle is initially pitched forward at an angle of 5 degrees. The maximum magnitude of the accelerometer signal is just 0.15 m/s^2 . Plots of the components of the accelerometer signal, as expressed in equation 3.9 are also shown. It shows that while some of the components may be reasonably large, they add up in such a way that the measured output of the accelerometer sensor is always small. This causes the pitch attitude information that is essential for the control system to maintain balance to be lost in the noise present in the practical situation.

It seems logical to attempt to low pass filter the accelerometer signal before it is read into the microprocessor. Suppose we add a first order filter on the accelerometer output. This places an additional pole on the positive real z-axis in upper righthand diagram of Figure 3.4. The root locus of the closed loop system now has a branch which moves to $-\infty$ on the real axis. Without repeating the whole design process here, it can be stated that the sensitivity problems discussed in the previous section are aggravated by addition of low pass filtering. Physically it means that the phase lag of a low pass filter causes the attitude information required by the control system, to arrive later in time. In an unstable system it is obviously advantageous to have attitude information available to the controller as soon as possible.

We conclude that, even though accelerometers can in theory be used as attitude sensors, practical applications are unlikely to succeed. The accelerometers measure both the pitch attitude and the frame acceleration at the position where they are mounted. The transfer function to the accelerometer output contains zeros whose locations are not only highly sensitive to parameter variations, but also make it difficult to design low order compensators which will stabilize the unstable eigenvalues of the plant.

Furthermore, the component of the accelerometer signal which contains the attitude information is small (maximum $\cong 0.15 \text{ m/s}^2 = 1.5\%$ of the earth's gravity acceleration). It is therefore required that the accelerometers have high sensitivity, but the sensors then become susceptible to vibrations of the robot frame as it moves along uneven terrain.

3.3. COMPENSATOR DESIGN BY SUCCESSIVE LOOP CLOSURE

25

real axis. The unstable pole will therefore always be destabilized as it is attracted to the zero on the positive real axis for increasing loop gain.

A schematic diagram which summarizes the findings of the longitudinal successive loop closure compensator studies is shown in Figure 3.4. Figure 3.5 shows a plot of how the closed loop pole positions change as the accelerometer height deviates from the nominal value of 0.653 m. It shows that the requirement for stability is

$$0.54 < r_{R3} < 0.6707 \text{ m}$$

If the system is expected to be well damped (closed loop poles within the $\xi = 0.5$ curve in the z-plane) the range of acceptable r_{R3} values is actually still more restricted.

3.3.3 Experimental Results

The successive loop closure compensator of section 0.4 was coded in the FORTH computer language and implemented in the on board microprocessor of the unicycle. The computer code is given in section P.1. After executing an algorithm for 5 seconds to bring the unicycle up to a nominal speed of $\Omega_0 = 3.0$ rad/sec while hand holding the robot vertical, the accelerometer feedback loop was closed. Figure 3.6 shows the two measurements during a typical experimental run. The system went unstable when the accelerometer feedback loop was closed and the unicycle released at $t = 5$ seconds. Attempts to adjust the compensator parameters and accelerometer height experimentally to obtain stability were unsuccessful.

Figure 3.7 shows a plot of the accelerometer signal measured during the period between 2.5 and 5.0 seconds of the previous experiment. Noise in the signal can be as high as 0.25 m/s^2 peak to peak from one sample to the next. This noise is caused by high frequency vibrations of the frame due to unevenness in the wheel drive system and the ground surface.

Figure 3.8 shows the theoretical time response of the accelerometer measurement if

24 CHAPTER 3. LONGITUDINAL SYSTEM WITH ACCELEROMETER SENSOR

$r_{R3} = (r_{R3})_{\infty}$. For example for r_{R3} changing from only 3.25 cm lower than $(r_{R3})_{\infty}$ (i.e. - 5%) to 3.25 cm higher than $(r_{R3})_{\infty}$ (i.e. + 5%), the zero locations have changed all the way from $z = 1 \pm j0.24$ through $z = \pm \infty$ to $z = 1 \pm 0.24$.

Since these zeros are points to which two of the root locus branches progress, the closed loop system pole locations are also very sensitive to the choice of r_{R3} . Even if r_{R3} is known exactly, equation 3.9 shows that the accelerometer signal is a function of $r_{R3}\bar{\theta}$, so that differences between the real plant and the theoretical model which cause the actual pitch acceleration ($\bar{\theta}$) to differ more than $\pm 5\%$ from the theoretical pitch acceleration, will cause the same dramatic shift in the accelerometer zero locations.

Figure 3.3 illustrates what happens to the root loci if the accelerometer is mounted too low on the frame. In this case where $r_{R3} = 0.5$ m the root loci from the unstable region of the z -plane converge toward the two complex zeros outside the unit circle instead of toward the zero at $z = 1$ and the compensation zero as in the nominal design shown in Figure 0.5. The accelerometer height, r_{R3} , should therefore not be too low because it creates a 'barrier' of zeros which makes it difficult for the root loci from the unstable region of the z -plane to slip through into the unit circle.

If the accelerometer is placed at the nominal design position, $r_{R3} = 0.653$ m the system can be stabilized. Inspection of the root locus of Figure 0.5 shows that although we may stabilize the system, we will not necessarily obtain satisfactory system performance. The damping on the low frequency branches of the root loci becomes better than $\xi = 0.7$ at fairly high loop gains ($K_a > 20$), at which point the damping on the high frequency branches of the rootloci is rapidly decreasing to unacceptably low values.

Placing the accelerometer near $(r_{R3})_{\infty} = 0.6675$ m would not be sensible because of the great sensitivity of the accelerometer zero and closed loop pole positions described earlier. Equation 3.13 shows that for $r_{R3} > (r_{R3})_{\infty}$ the accelerometer zeros are on the

Section 0.4 describes the design of the lowest order compensator that stabilizes the plant. It consists of an inner loop with proportional feedback of the tachometer measurement and an outer loop with a first order compensator on the accelerometer feedback signal. Closing a tight tachometer feedback loop first has the advantage of decreasing the effect of mechanical nonlinearities in the wheel drive system. The major nonlinearity is Coulomb friction which could be removed by means of an offset torque which depends on the sign of the wheel speed. Unfortunately the relatively inexpensive belt and sprocket drive system used in the robot's wheel drive system also causes time varying friction losses which depend on the angular positions of the gears. The most effective way of minimizing the effects of these varying torque losses is by closing a tight (high gain) tachometer feedback loop first.

An integral error feedback compensator on the tachometer feedback signal will increase the low frequency gain in the inner loop and the block diagram of Figure 0.6 shows how this can be incorporated in the design. For the purpose of finding the minimum order compensator, however, proportional feedback only will be used.

The nominal compensator design was obtained through an iterative process and inspection of the root loci and step responses as the loops were closed and the compensator parameters adjusted. The root locus of Figure 0.5 shows that it is theoretically possible to find a compensator which stabilizes the unstable modes of the unicycle by using an accelerometer sensor. The simulation results in Figure 3.1 show that the maximum pitch angle from which the longitudinal control system can recover without exceeding the maximum available motor torque ($(Q_w)_{max} = 15.12 \text{ N} \cdot \text{m}$) is about 5 degrees.

3.3.2 Robustness of the longitudinal controller

We have shown in section 3.2 that the zeros of the transfer function to the accelerometer output change as a function of r_{AS} , the height above the wheel axis where it is mounted. The plot of the zero locations in the z-plane (Figure 3.2) shows large changes of the zero positions for small variations in the accelerometer height, especially in the vicinity of

These are the two nonholonomic constraint equations for the unicycle motion. Choose the generalized coordinates to describe the position of the unicycle in inertial space to be:

$$\begin{aligned}
 q_1 &= x ; \quad \dot{q}_1 = \dot{x} \\
 q_2 &= y ; \quad \dot{q}_2 = \dot{y} \\
 q_3 &= \bar{w} ; \quad \dot{q}_3 = \dot{\bar{w}} \\
 &= \bar{\Omega} \\
 q_4 &= \phi ; \quad \dot{q}_4 = \dot{\phi} \\
 q_5 &= \psi ; \quad \dot{q}_5 = \dot{\psi} \\
 q_6 &= \theta ; \quad \dot{q}_6 = \dot{\theta} \\
 q_7 &= \nu ; \quad \dot{q}_7 = \dot{\nu} \\
 &= \dot{\eta}
 \end{aligned}$$

Because the unicycle is usually close to vertical the coordinates

$$\phi, \theta \text{ and their derivatives are small} \quad (\text{B.5})$$

$$x, y, \bar{w}, \psi, \nu \text{ are not necessarily small} \quad (\text{B.6})$$

Calculate the kinetic and potential energy of the unicycle:

B.1 Wheel

1. Translational kinetic energy of the wheel:

The position vector from the origin of the inertial reference frame to the center of mass of the wheel is:

$$\begin{aligned}
 \vec{r}_0 &= x\hat{a}_1 + y\hat{a}_2 + r_W\hat{w}_3 \\
 &= (x + r_W s\phi s\psi)\hat{a}_1 + (y - r_W s\phi c\psi)\hat{a}_2 + r_W c\phi\hat{a}_3 \quad (\text{B.7})
 \end{aligned}$$

$$\begin{aligned}
 \dot{\vec{r}}_0 &= (\dot{x} + r_W \dot{\phi} c\phi s\psi + r_W s\phi \dot{\psi} c\psi)\hat{a}_1 \\
 &+ (\dot{y} - r_W \dot{\phi} s\phi c\psi + r_W s\phi \dot{\psi} s\psi)\hat{a}_2 \\
 &- r_W \dot{\phi} s\phi\hat{a}_3 \quad (\text{B.8})
 \end{aligned}$$

Appendix B

EOMs by using Lagrange's Method

Refer to Figures in Appendix A.

Let (x,y) be the coordinates of the ground contact point P of the wheel, in the inertial reference frame $\hat{a}_1, \hat{a}_2, \hat{a}_3$.

Let $\dot{\psi}$ be the rotational speed of the wheel about its axle.

The velocity of the ground contact point P is then:

$$\mathbf{v} = r_W \dot{\psi} \hat{\mathbf{a}}_3 \quad (\text{B.1})$$

The no slip condition of the rolling of the wheel implies

$$\begin{aligned} \dot{x} &= v \cos \psi = r_W \dot{\psi} \cos \psi \\ \dot{y} &= v \sin \psi = r_W \dot{\psi} \sin \psi \end{aligned} \quad (\text{B.2})$$

or rewritten in the differential form:

$$1 \cdot dx - r_W \cos \psi \, d\psi = 0 \quad (\text{B.3})$$

$$1 \cdot dy - r_W \sin \psi \, d\psi = 0 \quad (\text{B.4})$$

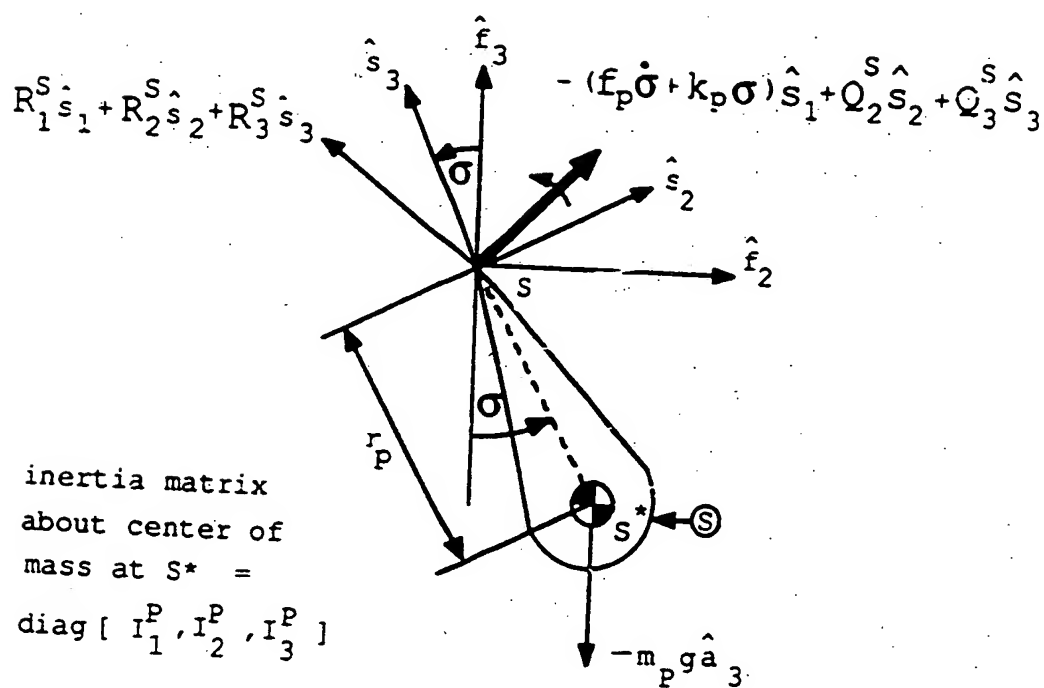
LATERAL PENDULUM:

Figure A.8: Lateral Sensor Pendulum Frame Free Body Diagram

LONGITUDINAL PENDULUM :

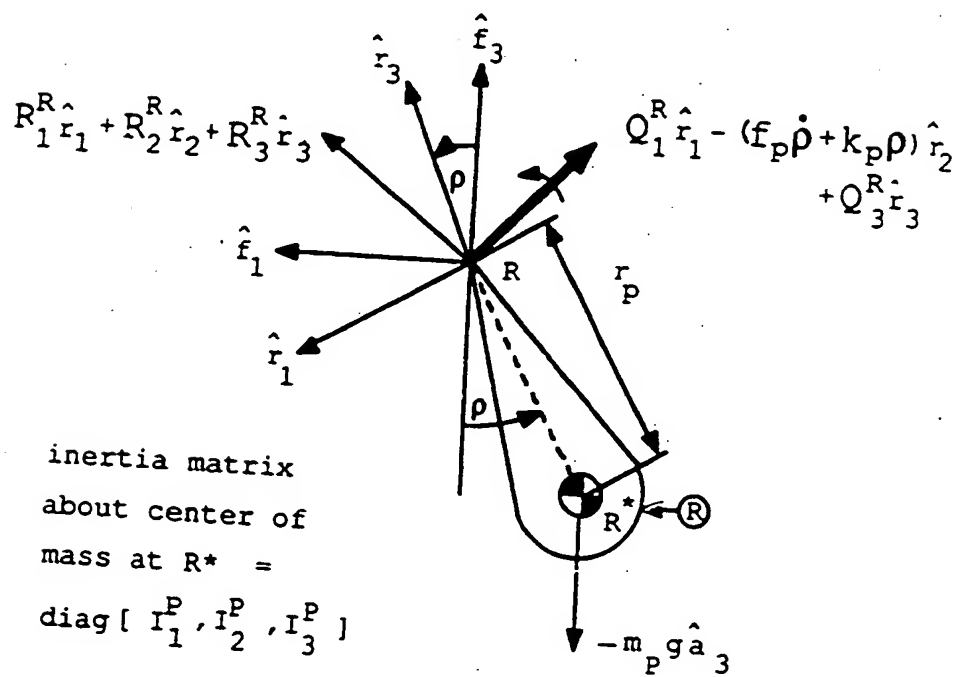


Figure A.7: Longitudinal Sensor Pendulum Frame Free Body Diagram

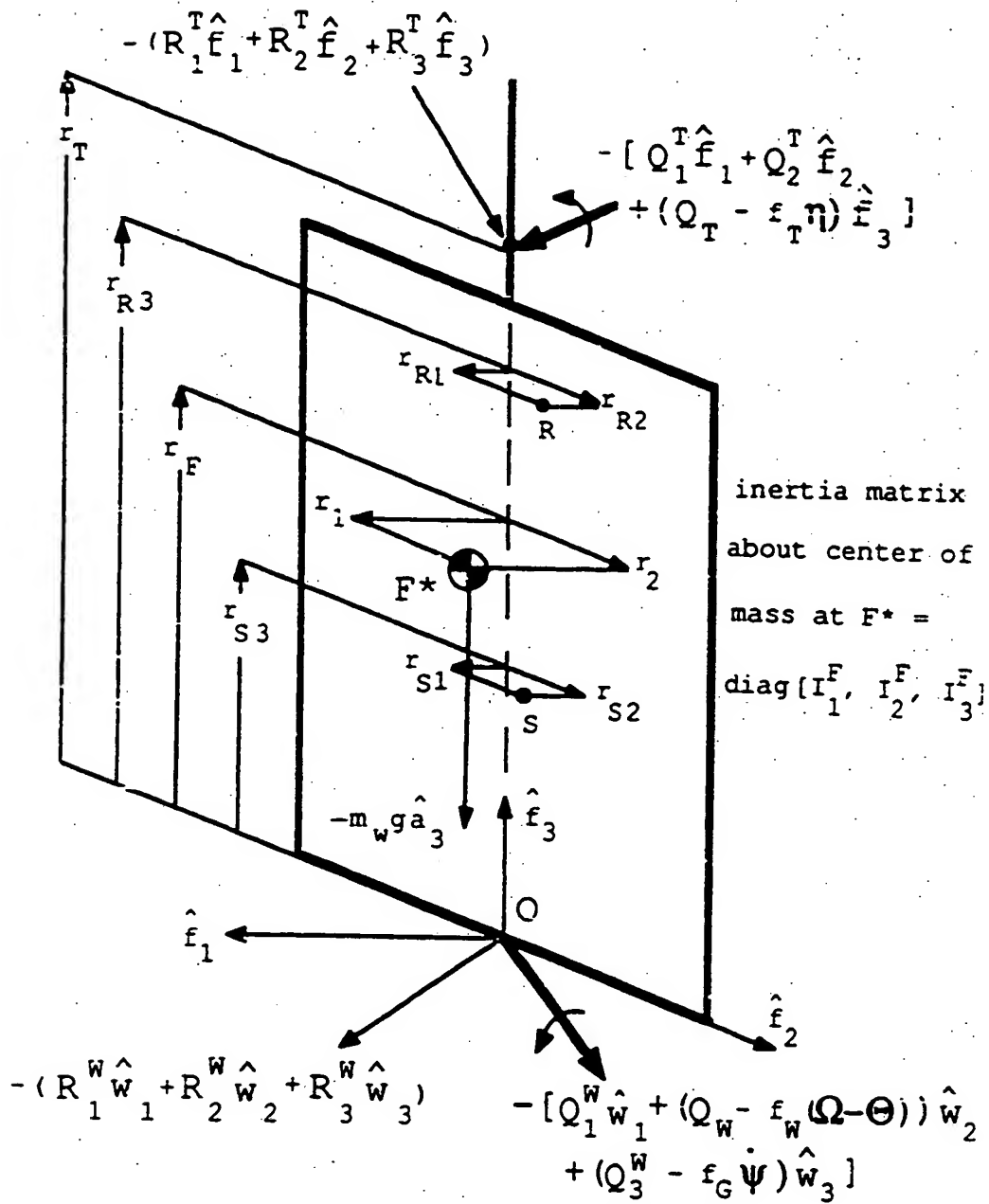
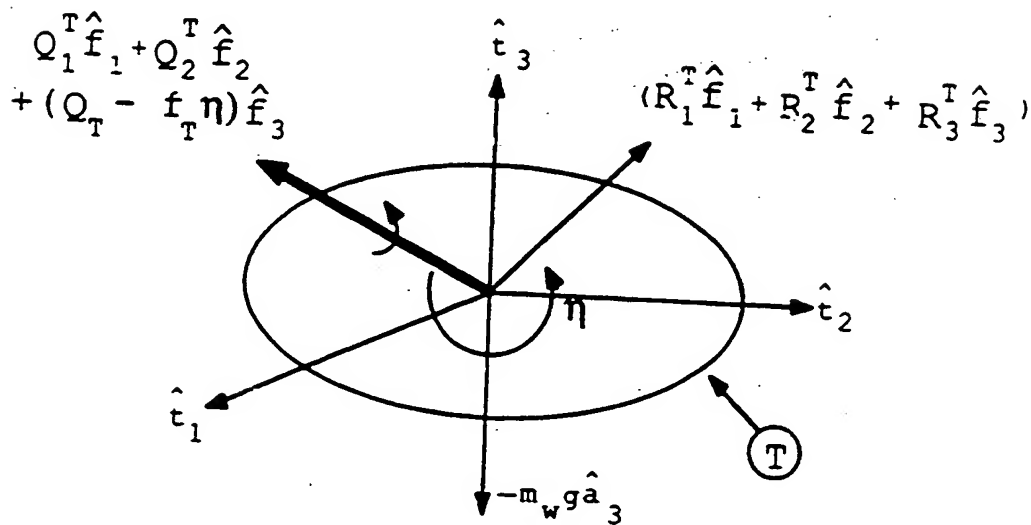


Figure A.6: Unicycle Frame Free Body Diagram

TURNTABLE:



inertia matrix about
center of mass =

$$\text{diag}[I_1^W, I_2^W, I_3^W]$$

turntable angular velocity
relative to frame F :

$$\bar{\eta} = \eta_0 + \eta$$

Figure A.5: Turntable Free Body Diagram

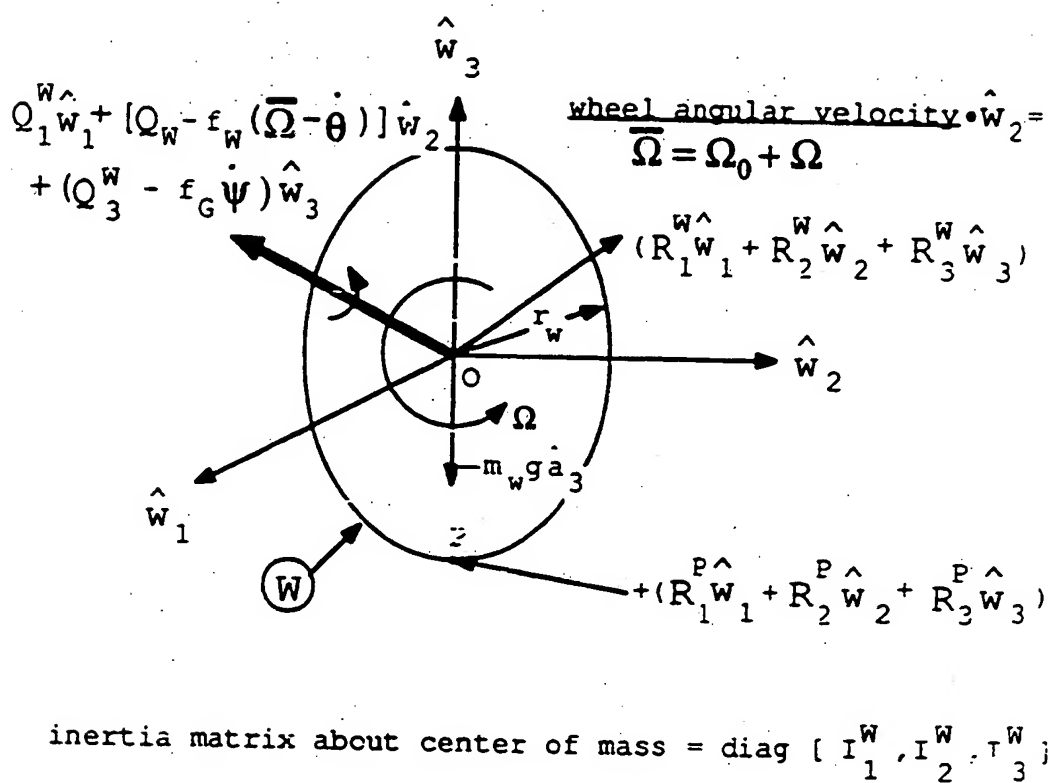
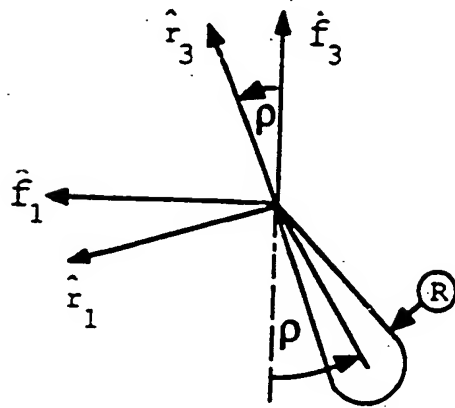
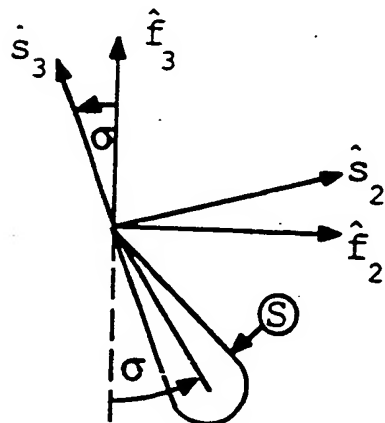
WHEEL:

Figure A.4: Wheel Free Body Diagram



	\hat{f}_1	\hat{f}_2	\hat{f}_3
\hat{r}_1	$\cos \rho$	0	$-\sin \rho$
\hat{r}_2	0	1	0
\hat{r}_3	$\sin \rho$	0	$\cos \rho$

LONGITUDINAL PENDULUM



	\hat{f}_1	\hat{f}_2	\hat{f}_3
\hat{s}_1	1	0	0
\hat{s}_2	0	$\cos \sigma$	$\sin \sigma$
\hat{s}_3	0	$-\sin \sigma$	$\cos \sigma$

LATERAL PENDULUM

Figure A.3: Coordinate Frame Translation Definitions 2

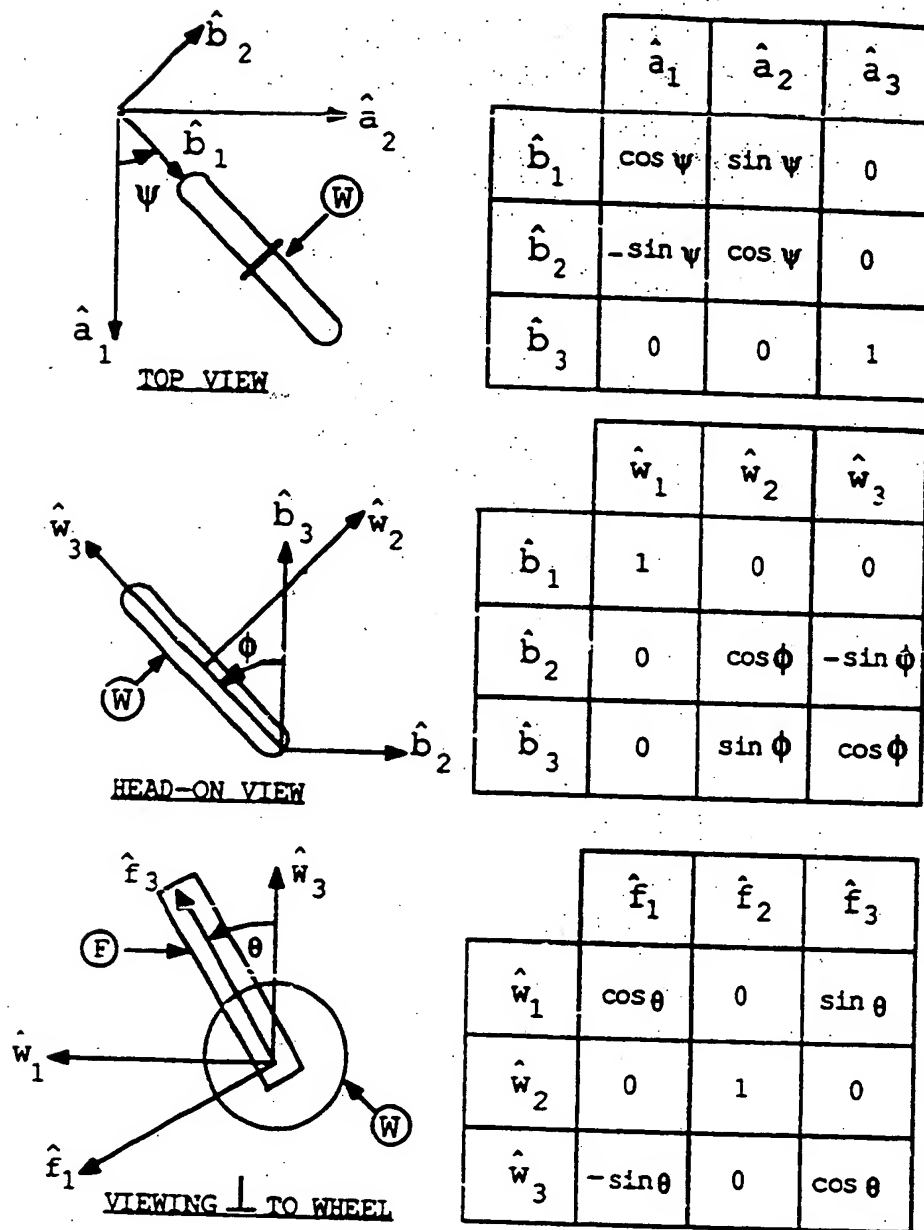


Figure A.2: Coordinate Frame Translation Definitions 1

A.12. SUMMARY OF THE SYSTEM DYNAMIC EQUATIONS

89

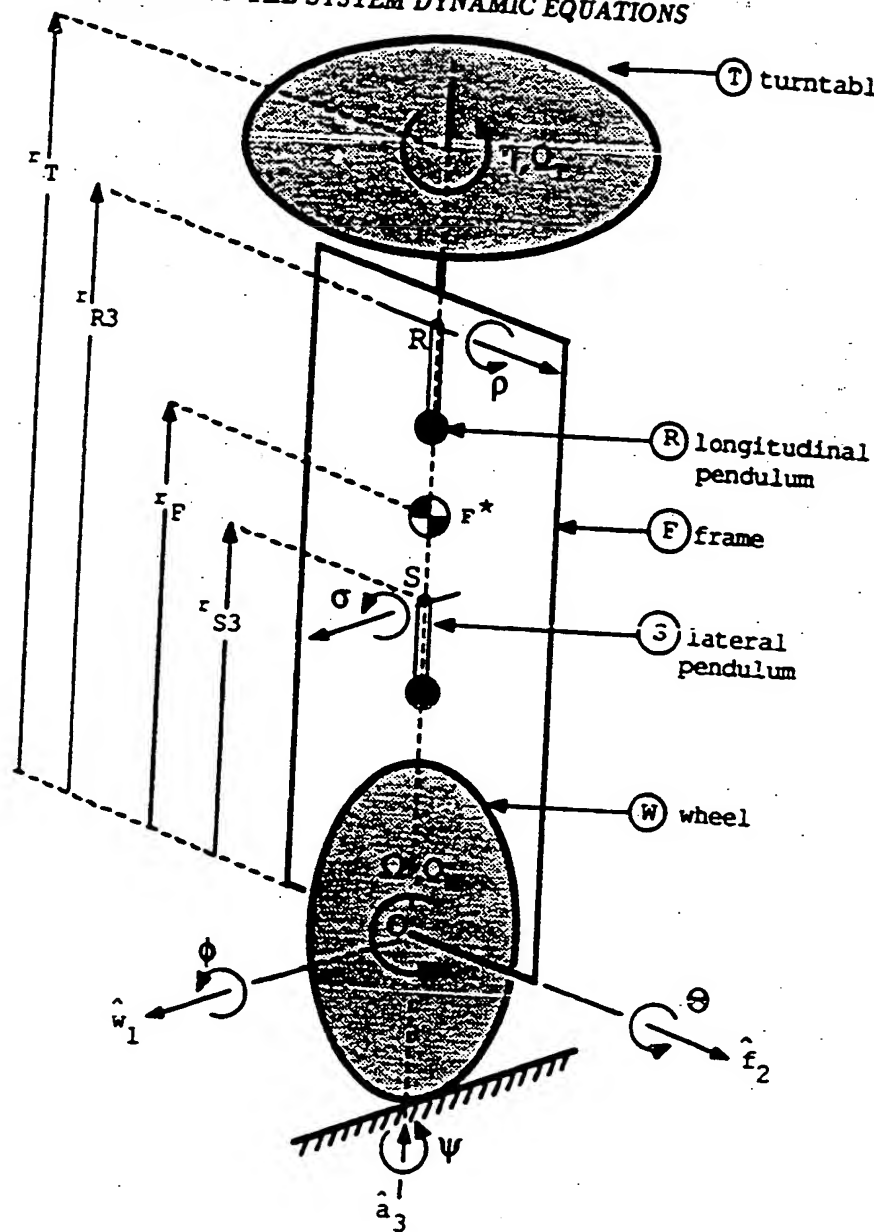


Figure A.1: Unicycle Schematic Diagram

APPENDIX A. EOMS BY NEWTON-EULER MECHANICS

Lateral State Vector : $[\phi, \psi, \eta, \dot{\phi}, \dot{\psi}, \dot{\eta}]^T$

Longitudinal State Vector: $[\dot{\theta}, \Omega, \dot{\rho}, \theta, \rho]^T$

Lateral Control Variable: Q_T

Longitudinal Control Variable: Q_W

The 7 degrees of freedom are: $\phi, \psi, \theta, \Omega, \eta, \sigma, \rho$

A.12. SUMMARY OF THE SYSTEM DYNAMIC EQUATIONS

87

$$I_3^T \ddot{\psi} + I_3^T \dot{\eta} = -f_T \eta - f_T \eta_0 + Q_T \quad (A.92)$$

Lateral Sensor Pendulum Dynamics:

$$\begin{aligned} & + [I_1^S + m_p r_p (r_p - r_{S3} - r_w)] \ddot{\phi} + [I_1^S + m_p r_p^2] \ddot{\sigma} + m_p r_p r_{S1} \ddot{\psi} \\ & = -m_p r_p r_w \Omega_0 \dot{\phi} - f_p \dot{\sigma} - m_p r_p g \phi - (k_p + m_p r_p g) \sigma \end{aligned} \quad (A.93)$$

A.12.2 Longitudinal system

Frame Pitch Dynamics:

$$\begin{aligned} & - m_F r_1 r_2 \ddot{\phi} - m_F r_F r_2 \ddot{\psi} + [I_2^F + I_2^T + m_F r_F^2 + m_T r_T^2 + m_F r_1^2] \ddot{\theta} \\ & + (m_F r_F + m_T r_T) r_w \dot{\Omega} \\ & = I_3^T \eta_0 \dot{\phi} + f_w \Omega - f_w \dot{\theta} + (m_F r_F + m_T r_T) g \theta \\ & + m_F r_1 g + f_w \Omega_0 - Q_w \end{aligned} \quad (A.94)$$

Wheel Rotational Dynamics:

$$\begin{aligned} & - m_F r_w r_2 \ddot{\psi} + (m_T r_T + m_F r_F) r_w \ddot{\theta} \\ & + [I_2^W + (m_w + m_F + m_T) r_w^2] \ddot{\Omega} \\ & = -f_w \dot{\Omega} + f_w \dot{\theta} - f_w \Omega_0 + Q_w \end{aligned} \quad (A.95)$$

Longitudinal Sensor Pendulum Dynamics:

$$\begin{aligned} & + m_p r_p r_{R2} \ddot{\psi} + [I_2^R + m_p r_p (r_p - r_{R3})] \ddot{\rho} - m_p r_p r_w \dot{\Omega} + [I_2^R + m_p r_p^2] \ddot{\rho} \\ & = -f_p \dot{\rho} - m_p r_p g \theta - [k_p + m_p r_p g] \rho \end{aligned} \quad (A.96)$$

A.12 Summary of the system dynamic equations

The 30 equations of motion for the 5 rigid bodies contain internal reaction forces and moments, which can be eliminated to obtain the dynamic equations of motion for the unicycle.

The algebra for eliminating the internal reaction forces and moments will not be shown here.

The equations of motion for the unicycle lateral and longitudinal dynamics are:

A.12.1 Lateral system

Wheel and Frame Yaw Dynamics:

$$\begin{aligned}
 & - [m_F(r_W + r_F)r_1]\ddot{\phi} + [I_3^W + I_3^F + m_F(r_1^2 + r_2^2)]\ddot{\psi} \\
 & - m_F r_F r_2 \ddot{\theta} - m_F r_W r_2 \ddot{\Omega} \\
 & = -I_2^W \ddot{\Omega}_0 \dot{\phi} - [f_G + m_F r_W r_1 \Omega_0] \dot{\psi} + f_T \eta \\
 & - m_F r_1 g \phi - m_F r_2 g \theta + f_T \eta_0 - Q_T
 \end{aligned} \tag{A.90}$$

Gyroscopic Coupling Dynamics:

$$\begin{aligned}
 & - [I_1^W + I_1^F + I_1^T + (m_W + m_F + m_T)r_W^2 + m_T r_T(2r_W + r_T)] \\
 & + m_F r_F(2r_W + r_F) + m_F r_2^2] \ddot{\phi} + m_F r_1(r_W + r_F) \ddot{\psi} + m_F r_1 r_2 \ddot{\theta} \\
 & = -[I_2^W + (m_W + m_F + m_T)r_W^2 + (m_F r_F + m_T r_T)r_W] \Omega_0 \dot{\psi} \\
 & - [(m_W + m_F + m_T)r_W + m_F r_F + m_T r_T] g \phi + I_3^T \eta_0 \dot{\theta} + m_F r_2 g
 \end{aligned} \tag{A.91}$$

Turntable Rotational Dynamics :

A.11 Rotational EOMs of lateral sensor pendulum

A.11.1 Applied moments about S^*

Refer to Figure A.8.

1. Reaction, spring and damping moments:

$$\vec{M} = -(f_p \dot{\sigma} + k_p \sigma) \hat{s}_1 + Q_2^S \hat{s}_2 + Q_3^S \hat{s}_3 \quad (\text{A.85})$$

2. Moment due to reaction forces at hinge point
- S
- :

$$\begin{aligned} \vec{M} &= \vec{r}^{S^*S} \times \vec{R}^S \\ &= r_p \hat{s}_3 \times (R_1^S \hat{s}_1 + R_2^S \hat{s}_2 + R_3^S \hat{s}_3) \\ &= -r_p R_2^S \hat{s}_1 + r_p R_1^S \hat{s}_2 \end{aligned} \quad (\text{A.86})$$

A.11.2 Rotational equations of motion of S

$$-f_p \dot{\sigma} - k_p \sigma - r_p R_2^S = I_1^S (\ddot{\phi} + \ddot{\sigma}) \quad (\text{A.87})$$

$$Q_2^S + r_p R_1^S = I_2^S \ddot{\theta} \quad (\text{A.88})$$

$$Q_3^S = I_3^S \ddot{\psi} \quad (\text{A.89})$$

A.10.3 Forces acting on S

1. Gravity force:

$$\begin{aligned}
-m_p g \hat{a}_3 &= -m_p g [\phi \hat{f}_2 - \theta \hat{f}_1 + \hat{f}_3] \\
&= m_p g \theta \hat{s}_1 - m_p g \phi (\hat{s}_1 - \sigma \hat{s}_3) - m_p g (\sigma \hat{s}_2 - \hat{s}_3) \\
&= m_p g \theta \hat{s}_1 - m_p g (\phi + \sigma) \hat{s}_2 - m_p g \hat{s}_3
\end{aligned} \tag{A.80}$$

2. Reaction forces at S:

$$R_1^S \hat{s}_1 + R_2^S \hat{s}_2 + R_3^S \hat{s}_3 \tag{A.81}$$

A.10.4 Translational equations of motion of S

$$R_1^S + m_p g \theta = m_p [r_W \dot{\Omega} + (r_{S3} - r_p) \ddot{\theta} - r_{S2} \ddot{\psi}] \tag{A.82}$$

$$\begin{aligned}
R_2^S - m_p g (\phi + \sigma) &= m_p [r_W \Omega_0 \dot{\psi} + (r_p - r_W - r_{S3}) \ddot{\phi} \\
&\quad + r_p \ddot{\sigma} + r_{S1} \ddot{\psi}]
\end{aligned} \tag{A.83}$$

$$R_3^S - m_p g = m_p [r_{S2} \ddot{\phi} - r_{S1} \ddot{\theta}] \tag{A.84}$$

A.10 Translational EOMs of lateral sensor pendulum

A.10.1 Absolute angular velocity of the \hat{s} -frame

Refer to Figure A.8 and Figure A.3

$${}^A\bar{\omega}^S \cong (\dot{\phi} + \dot{\sigma})\hat{s}_1 + \dot{\theta}\hat{s}_2 + \dot{\psi}\hat{s}_3 \quad (A.74)$$

A.10.2 Absolute translational acceleration of S^*

$${}^A\bar{a}^{S^*} = \bar{a}^S + {}^A\bar{\omega}^S \times \bar{r}^{SS^*} + {}^A\bar{\omega}^S \times ({}^A\bar{\omega}^S \times \bar{r}^{SS^*}) \quad (A.75)$$

\bar{a}^S can be obtained from equation A.31 by appropriate substitution:

$$\begin{aligned} \bar{a}^S = & (r_W\dot{\Omega} + r_{S3}\dot{\theta} - r_{S2}\dot{\psi})\hat{s}_1 \\ & + [r_{S1}\dot{\psi} - (r_W + r_{S3})\dot{\phi} + r_W\Omega_0\dot{\psi}]\hat{s}_2 \\ & + (r_{S2}\dot{\phi} - r_{S1}\dot{\theta})\hat{s}_3 \end{aligned} \quad (A.76)$$

$$\begin{aligned} {}^A\bar{\omega}^S \times \bar{r}^{SS^*} = & [(\dot{\phi} + \dot{\sigma})\hat{s}_1 + \dot{\theta}\hat{s}_2 + \dot{\psi}\hat{s}_3] \times (-r_p\hat{s}_3) \\ = & -r_p\dot{\theta}\hat{s}_1 + r_p(\dot{\phi} + \dot{\sigma})\hat{s}_2 \end{aligned} \quad (A.77)$$

$$\bar{\omega}^S \times (\bar{\omega}^S \times \bar{r}^{SS^*}) = 0 \quad (A.78)$$

$$\begin{aligned} {}^A\bar{a}^{S^*} = & [r_W\dot{\Omega} + (r_{S3} - r_p)\dot{\theta} - r_{S2}\dot{\psi}]\hat{s}_1 \\ & + [r_W\Omega_0\dot{\psi} + (r_p - r_W - r_{S3})\dot{\phi} + r_p\dot{\sigma} + r_{S1}\dot{\psi}]\hat{s}_2 \\ & + [r_{S2}\dot{\phi} - r_{S1}\dot{\theta}]\hat{s}_3 \end{aligned} \quad (A.79)$$

A.9 Rotational EOMs of Ingit. sensor pendulum

A.9.1 Applied moments about R

Refer to Figure A.7

1. Reaction, spring and damping moments :

$$Q_1^R \hat{r}_1 - (f_p \dot{\rho} + k_p \rho) \hat{r}_2 + Q_3^R \hat{r}_3 \quad (\text{A.69})$$

2. Moment due to reaction forces at hinge point R:

$$\begin{aligned} \vec{M} &= \vec{r}^{R^R} \times \vec{R}^R \\ &= r_p \hat{r}_3 \times (R_1^R \hat{r}_1 + R_2^R \hat{r}_2 + R_3^R \hat{r}_3) \\ &= -r_p R_2^R \hat{r}_1 + r_p R_1^R \hat{r}_2 \end{aligned} \quad (\text{A.70})$$

A.9.2 Rotational equations of motion of R

$$Q_1^R - r_p R_2^R = I_1^R \ddot{\phi} \quad (\text{A.71})$$

$$-f_p \dot{\rho} - k_p \rho + r_p R_1^R = I_2^R (\ddot{\theta} + \ddot{\rho}) \quad (\text{A.72})$$

$$Q_3^R = I_3^R \ddot{\psi} \quad (\text{A.73})$$

$${}^A\bar{w}^R \times ({}^A\bar{w}^R \times \bar{r}^{RR}) = 0 \quad (\text{A.62})$$

$$\begin{aligned} {}^A\bar{a}^{RR} = & [r_W\bar{\Omega} + (r_{R3} - r_p)\bar{\theta} - r_{R2}\bar{\psi} - r_p\bar{\rho}]\bar{r}_1 \\ & + [r_{R1}\bar{\psi} + r_W\Omega_0\bar{\psi} + (r_p - r_W - r_{R3})\bar{\phi}]\bar{r}_2 \\ & + (r_{R2}\bar{\phi} - r_{R1}\bar{\theta})\bar{r}_3 \end{aligned} \quad (\text{A.63})$$

A.8.3 Forces acting on R

1. Gravity force;

$$\begin{aligned} -m_p g \bar{a}_3 &= -m_p g (\phi \bar{w}_2 + \bar{w}_3) \\ &= -m_p g [\phi \bar{f}_2 - \theta \bar{f}_1 + \bar{f}_3] \\ &= -m_p g [\phi \bar{r}_2 - \theta \bar{r}_1 - \rho \bar{r}_1 + \bar{r}_3] \\ &= m_p g (\theta + \rho) \bar{r}_1 - m_p g \phi \bar{r}_2 - m_p g \bar{r}_3 \end{aligned} \quad (\text{A.64})$$

2. Reaction forces at R:

$$R_1^R \bar{r}_1 + R_2^R \bar{r}_2 + R_3^R \bar{r}_3 \quad (\text{A.65})$$

A.8.4 Translational equations of motion of R

$$R_1^R + m_p g (\theta + \rho) = m_p [r_W \bar{\Omega} + (r_{R3} - r_p) \bar{\theta} - r_p \bar{\rho} - r_{R2} \bar{\psi}] \quad (\text{A.66})$$

$$R_2^R - m_p g \phi = m_p [r_W \Omega_0 \bar{\psi} + (r_p - r_W - r_{R3}) \bar{\phi} + r_{R1} \bar{\psi}] \quad (\text{A.67})$$

$$R_3^R - m_p g = m_p [r_{R2} \bar{\phi} - r_{R1} \bar{\theta}] \quad (\text{A.68})$$

A.8 Translational EOMs of longit. sensor pendulum

The dynamic equations of motion of two small passive sensor pendulums are included in the unicycle model. The purpose is to investigate the possibility of determining the unicycle attitude information from measurements of the angles that the lateral and longitudinal sensor pendulums make with respect to the unicycle frame.

A.8.1 Absolute angular velocity of the \hat{r} -frame

Refer to Figure A.7 and Figure A.3.

It is assumed that the sensor pendulums have negligible mass and inertia compared to the rest of the unicycle. In deriving the equations of motion, only forces exerted by the unicycle frame on the pendulums are taken into account. Forces and moments exerted by the sensor pendulums on the rest of the unicycle are small and are therefore neglected in the analysis.

$${}^A\bar{\omega}^R \cong \dot{\phi}\hat{r}_1 + (\dot{\theta} + \dot{\rho})\hat{r}_2 + \dot{\psi}\hat{r}_3 \quad (A.58)$$

A.8.2 Absolute translational acceleration of R^*

$${}^A\bar{a}^{R^*} = \bar{a}^R + {}^A\bar{\omega}^R \times \bar{r}^{RR^*} + {}^A\bar{\omega}^R \times ({}^A\bar{\omega}^R \times \bar{r}^{RR^*}) \quad (A.59)$$

\bar{a}^R can be obtained from equation A.31 by appropriate substitution.

$$\begin{aligned} \bar{a}^R = & (r_W\dot{\Omega} + r_{R3}\ddot{\theta} - r_{R2}\ddot{\psi})\hat{r}_1 \\ & + [r_{R1}\ddot{\psi} - (r_W + r_{R3})\ddot{\phi} + r_W\Omega_0\dot{\phi}]\hat{r}_2 \\ & + (r_{R2}\ddot{\phi} - r_{R1}\ddot{\theta})\hat{r}_3 \end{aligned} \quad (A.60)$$

$$\begin{aligned} {}^A\bar{\omega}^R \times \bar{r}^{RR^*} &= [\dot{\phi}\hat{r}_1 + (\dot{\theta} + \dot{\rho})\hat{r}_2 + \dot{\psi}\hat{r}_3] \times (-r_p\hat{r}_3) \\ &= -r_p(\dot{\theta} + \dot{\rho})\hat{r}_1 + r_p\dot{\phi}\hat{r}_2 \end{aligned} \quad (A.61)$$

A.7.3 Rotational equations of motion of T

$$Q_1^T = I_1^T \dot{\phi} + I_3^T \eta_0 \dot{\theta} \quad (\text{A.55})$$

$$Q_2^T = I_2^T \dot{\theta} - I_3^T \eta_0 \dot{\phi} \quad (\text{A.56})$$

$$Q_T - f_T \eta_0 - f_T \eta = I_3^T (\dot{\psi} + \dot{\eta}) \quad (\text{A.57})$$

A.7 Rotational equations of motion of turntable

A.7.1 Angular momentum of turntable T

Refer to Figure A.5

Absolute angular velocity of the \hat{f} -frame from equation A.25:

$${}^A\bar{\omega}^F = \dot{\phi}\hat{f}_1 + \dot{\theta}\hat{f}_2 + \dot{\psi}\hat{f}_3 \quad (\text{A.49})$$

Angular momentum of T:

$$\bar{H} = H_1\hat{f}_1 + H_2\hat{f}_2 + H_3\hat{f}_3 \quad (\text{A.50})$$

where:

$$\begin{aligned} H_1 &= I_1^T \dot{\phi} \\ H_2 &= I_2^T \dot{\theta} \\ H_3 &= I_3^T (\dot{\psi} + \dot{\eta}) = I_3^T (\dot{\psi} + \eta_0 + \eta) \end{aligned}$$

Note : η is measured in relation to frame F

$$\dot{\bar{M}} = \dot{\bar{H}} = (\dot{\bar{H}})_r + {}^A\bar{\omega}^F \times \bar{H} \quad (\text{A.51})$$

$$(\dot{\bar{H}})_r = I_1^T \dot{\phi}\hat{f}_1 + I_2^T \dot{\theta}\hat{f}_2 + I_3^T (\dot{\psi} + \dot{\eta})\hat{f}_3 \quad (\text{A.52})$$

$${}^A\bar{\omega}^F \times \bar{H} = \begin{vmatrix} \hat{f}_1 & \hat{f}_2 & \hat{f}_3 \\ \dot{\phi} & \dot{\theta} & \dot{\psi} \\ I_1^T \dot{\phi} & I_2^T \dot{\theta} & I_3^T (\dot{\psi} + \eta_0 + \eta) \end{vmatrix} = I_3^T \eta_0 \dot{\theta}\hat{f}_1 - I_3^T \eta_0 \dot{\phi}\hat{f}_2 \quad (\text{A.53})$$

A.7.2 Applied moments to T

$$Q_1^T \hat{f}_1 + Q_2^T \hat{f}_2 + (Q_T - f_T \bar{\eta})\hat{f}_3 \quad (\text{A.54})$$

A.6 Translational equations of motion of turntable

A.6.1 Forces acting on T

Refer to Figure A.5

1. Reaction forces from frame, F:

$$R_1^T \hat{f}_1 + R_2^T \hat{f}_2 + R_3^T \hat{f}_3 \quad (\text{A.43})$$

2. gravity :

$$+ m_T g \hat{a}_3 = -m_T g \theta \hat{f}_1 - m_T g \phi \hat{f}_2 - m_T g \hat{f}_3 \quad (\text{A.44})$$

A.6.2 Absolute acceleration of T

The acceleration of T can be obtained from equation A.31 by letting $r_F \leftarrow r_T$,
 $r_1 = r_2 = 0$

$$\ddot{a}^T = (r_W \dot{\Omega} + r_T \ddot{\theta}) \hat{f}_1 + [r_W \Omega_0 \dot{\psi} - (r_W + r_T) \ddot{\phi}] \hat{f}_2 \quad (\text{A.45})$$

A.6.3 Translational equations of motion of T

$$R_1^T + m_T g \theta = m_T (r_W \dot{\Omega} + r_T \ddot{\theta}) \quad (\text{A.46})$$

$$R_2^T - m_T g \phi = m_T [r_W \Omega_0 \dot{\psi} - (r_W + r_T) \ddot{\phi}] \quad (\text{A.47})$$

$$R_3^T - m_T g = 0 \quad (\text{A.48})$$

(A.41)

$$\begin{aligned}
 & -Q_1^W \theta - Q_3^W + f_T \eta_0 + f_T \eta - Q_T \\
 & + r_1 R_2^W - r_2 R_1^W + r_2 R_3^W \theta + r_1 R_2^T - r_2 R_1^T = I_3^F \ddot{\psi}
 \end{aligned}$$

(A.42)

A.5. ROTATIONAL EQUATIONS OF MOTION OF FRAME F

75

$$\begin{aligned}
 &= [r_2 R_3^T + (r_T - r_F) R_2^T] \dot{f}_1 \\
 &+ [(r_F - r_T) R_1^T - r_1 R_3^T] \dot{f}_2 \\
 &+ [r_1 R_2^T - r_2 R_1^T] \dot{f}_3
 \end{aligned} \tag{A.38}$$

A.5.2 Rotational equations of motion for F

from equation A.25 :

$${}^A \bar{w}^F = \dot{\phi} \hat{f}_1 + \dot{\theta} \hat{f}_2 + \dot{\psi} \hat{f}_3 \tag{A.39}$$

Using Euler's equations of motion:

$$M_1 = I_1 \dot{w}_1 + (I_3 - I_2) w_2 w_3$$

$$M_2 = I_2 \dot{w}_2 + (I_1 - I_3) w_1 w_3$$

$$M_3 = I_3 \dot{w}_3 + (I_2 - I_1) w_1 w_2$$

where:

M_i = applied moments

$w_1 = \dot{\phi}$ and $\dot{w}_1 = \ddot{\phi}$,

$w_2 = \dot{\theta}$ and $\dot{w}_2 = \ddot{\theta}$,

$w_3 = \dot{\psi}$ and $\dot{w}_3 = \ddot{\psi}$

Note that all products $w_i w_j \cong 0$ in Euler's Equation.

A.5.3 Rotational equations of motion of frame F

$$\begin{aligned}
 &Q_3^W \theta - Q_1^W - Q_1^T \\
 &+ r_2 R_1^W \theta + r_2 R_3^W - r_F R_2^W + r_2 R_3^T + (r_T - r_F) R_2^T = I_1^F \ddot{\phi}
 \end{aligned} \tag{A.40}$$

$$\begin{aligned}
 &f_W \Omega_0 + f_W \Omega - f_W \dot{\theta} - Q_W - Q_2^T + r_F R_1^W \\
 &- r_F R_3^W \theta - r_1 R_1^W \theta - r_1 R_3^W + (r_F - r_T) R_1^T - r_1 R_3^T = I_2^F \ddot{\theta}
 \end{aligned}$$

A.5 Rotational equations of motion of frame F

A.5.1 Applied moments about F

Refer to Figure A.6

1. From wheel:

$$\begin{aligned}
 & -Q_1^W \dot{w}_1 - (Q_W - f_W \bar{\Omega}) \dot{w}_2 - Q_3^W \dot{w}_3 \\
 & = -Q_1^W (\dot{f}_1 + \theta \dot{f}_3) - [Q_W - f_W (\bar{\Omega} - \dot{\theta})] \dot{f}_2 - Q_3^W (-\theta \dot{f}_1 + \dot{f}_3) \\
 & = (Q_3^W \theta - Q_1^W) \dot{f}_1 + f_W \Omega_0 + f_W \Omega - f_W \dot{\theta} - Q_W \dot{f}_2 - (Q_1^W \theta + Q_3^W) \dot{f}_3
 \end{aligned} \tag{A.35}$$

2. From turntable:

$$-Q_1^T \dot{f}_1 - Q_2^T \dot{f}_2 - (Q_T - f_T \eta) \dot{f}_3 = -Q_1^T \dot{f}_1 - Q_2^T \dot{f}_2 + (f_T \eta_0 + f_T \eta - Q_T) \dot{f}_3 \tag{A.36}$$

3. Due to reaction forces at O:

$$\begin{aligned}
 \bar{M} &= \bar{r}^{F^O} \times \bar{R}^W \\
 &= \begin{vmatrix} \dot{f}_1 & \dot{f}_2 & \dot{f}_3 \\ -r_1 & -r_2 & -r_F \\ R_3^W \theta - R_1^W & -R_2^W & -(R_1^W \theta + R_3^W) \end{vmatrix} \\
 &= [r_2 R_1^W \theta + r_2 R_3^W - r_F R_2^W] \dot{f}_1 \\
 &\quad + [r_F R_1^W - r_F R_3^W \theta - r_1 R_1^W \theta - r_1 R_3^W] \dot{f}_2 \\
 &\quad + [r_1 R_2^W - r_2 R_1^W + r_2 R_3^W \theta] \dot{f}_3
 \end{aligned} \tag{A.37}$$

4. Due to reaction forces at T:

$$\begin{aligned}
 \bar{M} &= \bar{r}^{F^T} \times \bar{R}^T \\
 &= \begin{vmatrix} \dot{f}_1 & \dot{f}_2 & \dot{f}_3 \\ -r_1 & -r_2 & (r_T - r_F) \\ -R_1^T & -R_2^T & -R_3^T \end{vmatrix}
 \end{aligned}$$

A.4. TRANSLATIONAL EQUATIONS OF MOTION OF FRAME

73

$$\vec{r}^{OF} = r_1 \hat{f}_1 + r_2 \hat{f}_2 + r_F \hat{f}_3 \quad (\text{A.27})$$

$$\begin{aligned} {}^A \vec{\omega}^F \times \vec{r}^{OF} &= \begin{vmatrix} \dot{f}_1 & \dot{f}_2 & \dot{f}_3 \\ \bar{\phi} & \bar{\theta} & \bar{\psi} \\ r_1 & r_2 & r_F \end{vmatrix} \\ &= (r_F \bar{\theta} - r_2 \bar{\psi}) \hat{f}_1 + (r_1 \bar{\psi} - r_F \bar{\phi}) \hat{f}_2 + (r_2 \bar{\phi} - r_1 \bar{\theta}) \hat{f}_3 \end{aligned} \quad (\text{A.28})$$

$${}^A \vec{\omega}^F \times ({}^A \vec{\omega}^F \times \vec{r}^{OF}) = 0 \text{ because it involves products of small angular rates} \quad (\text{A.29})$$

$$\begin{aligned} \vec{a}_0 &= r_W \dot{\Omega} \hat{w}_1 + r_W (\Omega_0 \dot{\psi} - \dot{\phi}) \hat{w}_2 \\ &= r_W \dot{\Omega} (\hat{f}_1 + \theta \hat{f}_3) + r_W (\Omega_0 \dot{\psi} - \dot{\phi}) \hat{f}_2 \end{aligned} \quad (\text{A.30})$$

$$\vec{a}^F = (r_W \dot{\Omega} + r_F \bar{\theta} - r_2 \bar{\psi}) \hat{f}_1 + [r_1 \bar{\psi} - (r_W + r_F) \bar{\phi} + r_W \Omega_0 \dot{\psi}] \hat{f}_2 + (r_2 \bar{\phi} - r_1 \bar{\theta}) \hat{f}_3 \quad (\text{A.31})$$

A.4.3 Translational equations of motion of frame F

$$R_3^W \theta - R_1^W - R_1^T + m_F g \theta = m_F (r_W \dot{\Omega} + r_F \bar{\theta} - r_2 \bar{\psi}) \quad (\text{A.32})$$

$$-R_2^W - R_2^T - m_F g \phi = m_F [r_1 \bar{\psi} - (r_W + r_F) \bar{\phi} + r_W \Omega_0 \dot{\psi}] \quad (\text{A.33})$$

$$-R_1^W \theta - R_3^W - R_3^T - m_F g = m_F (r_2 \bar{\phi} - r_1 \bar{\theta}) \quad (\text{A.34})$$

A.4 Translational equations of motion of frame

A.4.1 Forces acting on F

Refer to Figure A.6

1. Reaction forces from wheel, W:

$$\begin{aligned}
 & -R_1^W \hat{w}_1 - R_2^W \hat{w}_2 - R_3^W \hat{w}_3 \\
 & = -R_1^W (\dot{f}_1 + \theta \dot{f}_3) - R_2^W \dot{f}_2 - R_3^W (-\theta \dot{f}_1 + \dot{f}_3) \\
 & = (R_3^W \theta - R_1^W) \dot{f}_1 - R_2^W \dot{f}_2 - (R_1^W \theta + R_3^W) \dot{f}_3
 \end{aligned} \tag{A.22}$$

2. Reaction forces from turntable, T:

$$-R_1^T \dot{f}_1 - R_2^T \dot{f}_2 - R_3^T \dot{f}_3 \tag{A.23}$$

3 Gravity:

$$\begin{aligned}
 -m_F g \hat{a}_3 &= -m_F g (\phi \hat{w}_2 + \hat{w}_3) \\
 &= -m_F g (\phi \dot{f}_2 - \theta \dot{f}_1 + \dot{f}_3) \\
 &= m_F g \theta \dot{f}_1 - m_F g \phi \dot{f}_2 - m_F g \dot{f}_3
 \end{aligned} \tag{A.24}$$

A.4.2 Absolute translational acceleration of F

Referring to Figure A.2, the absolute angular velocity of the F frame is:

$${}^A \vec{\omega}^F \cong \dot{\phi} \hat{f}_1 + \dot{\theta} \hat{f}_2 + \dot{\psi} \hat{f}_3 \tag{A.25}$$

The acceleration of the center of mass of the unicycle frame, F, is:

$$\vec{a}^F = \vec{a}_0 + {}^A \vec{\omega}^F \times \vec{r}^{OF} + {}^A \vec{\omega}^F \times ({}^A \vec{\omega}^F \times \vec{r}^{OF}) \tag{A.26}$$

where \vec{a}_0 is known from equation A.5

A.3. ROTATIONAL EQUATIONS OF MOTION OF WHEEL:

71

A.3.4 Rotational equations of motion of the wheel

$$Q_1^W + r_W R_2^P = I_1^W \ddot{\phi} - I_2^W \Omega_0 \dot{\phi} \quad (\text{A.19})$$

$$Q_W - f_W(\Omega_0 + \Omega - \dot{\theta}) - r_W R_1^P = I_2^W \dot{\Omega} \quad (\text{A.20})$$

$$Q_3^W - f_G \dot{\phi} = I_3^W \ddot{\psi} + I_2^W \Omega_0 \dot{\phi} \quad (\text{A.21})$$

A.3.3 Angular momentum of the wheel

the angular momentum of the wheel is:

$$\begin{aligned}\vec{H} &= H_1 \hat{w}_1 + H_2 \hat{w}_2 + H_3 \hat{w}_3 \\ &= I_1^W \dot{\phi} \hat{w}_1 + I_2^W (\Omega_0 + \Omega) \hat{w}_2 + I_3^W \dot{\psi} \hat{w}_3\end{aligned}\quad (\text{A.15})$$

Since the components of the angular velocity are taken along the principal axes of the wheel, the angular momentum is given by:

$$\begin{aligned}H_i &= I_i^W w_i \\ w_i &= \text{component of wheel speed} \\ \dot{\Omega} &= (\Omega_0 + \Omega) = \text{wheel rotational speed}\end{aligned}$$

Using Euler's Law for rotational motion of rigid bodies, equate the total applied moment about the center of mass of the wheel to the change of angular momentum:

$$\vec{M} = \dot{\vec{H}} = \frac{d\vec{H}}{dt} + {}^A \vec{\omega}^W \times \vec{H} \quad (\text{A.16})$$

$$\vec{H}_r = I_1^W \dot{\phi} \hat{w}_1 + I_2^W \dot{\Omega} \hat{w}_2 + I_3^W \dot{\psi} \hat{w}_3 \quad (\text{A.17})$$

$${}^A \vec{\omega}^W \times \vec{H} = \begin{vmatrix} \dot{w}_1 & \dot{w}_2 & \dot{w}_3 \\ \dot{\phi} & 0 & \dot{\psi} \\ I_1^W \dot{\phi} & I_2^W (\Omega_0 + \Omega) & I_3^W \dot{\psi} \end{vmatrix} = -I_2^W \Omega_0 \dot{\psi} \hat{w}_1 + I_2^W \Omega_0 \dot{\phi} \hat{w}_3 \quad (\text{A.18})$$

A.3 Rotational equations of motion of wheel:

A.3.1 Applied moments about O

Referring to Figure A.4:

1. The applied moments at the center of mass are:

$$Q_1^W \hat{w}_1 + [Q_W - f_W(\bar{\Omega} - \dot{\theta})] \hat{w}_2 + (Q_3^W - f_G \dot{\psi}) \hat{w}_3 \quad (A.12)$$

where:

Q_W : wheel drive torque

f_W : viscous wheel axle friction

f_G : assumed viscous friction at ground

2. Moments due to reaction forces at ground contact P:

$$\begin{aligned} \vec{M} &= \vec{r}^{OP} \times \vec{R}^P \\ &= -r_W \hat{w}_3 \times (R_1^P \hat{w}_1 + R_2^P \hat{w}_2 + R_3^P \hat{w}_3) \\ &= +r_W R_2^P \hat{w}_1 - r_W R_1^P \hat{w}_2 \end{aligned} \quad (A.13)$$

A.3.2 Absolute angular velocity of the \hat{w} -frame

$$\begin{aligned} {}^A \vec{\omega}^W &= \dot{\phi} \hat{w}_1 + \dot{\psi} \hat{b}_3 \\ &= \dot{\phi} \hat{w}_1 + \dot{\psi} (s\phi \hat{w}_2 + c\phi \hat{w}_3) \\ &\cong \dot{\phi} \hat{w}_1 + \dot{\psi} \hat{w}_3 \end{aligned} \quad (A.14)$$

$$\begin{aligned}\vec{w} \times \vec{v} &= \begin{vmatrix} \dot{w}_1 & \dot{w}_2 & \dot{w}_3 \\ \dot{\phi} & 0 & \dot{\phi} \\ r_W(\Omega_0 + \Omega) & -r_W\dot{\phi} & 0 \end{vmatrix} \\ &= r_W\Omega_0\dot{\phi}\dot{w}_2\end{aligned}$$

$$\vec{a}_0 = r_W\dot{\Omega}\dot{w}_1 + r_W(\Omega_0\dot{\phi} - \dot{\phi})\dot{w}_2 \quad (\text{A.5})$$

A.2.2 Forces acting on W

Refer to Figure A.4 for the wheel freebody diagram:

1. Reaction forces at O :

$$R_1^W \dot{w}_1 + R_2^W \dot{w}_2 + R_3^W \dot{w}_3 \quad (\text{A.6})$$

2. Reaction forces at P :

$$R_1^P \dot{w}_1 + R_2^P \dot{w}_2 + R_3^P \dot{w}_3 \quad (\text{A.7})$$

3. Gravity :

$$-m_W g \hat{a}_3 \cong -m_W g \phi \dot{w}_2 - m_W g \dot{w}_3 \quad (\text{A.8})$$

A.2.3 Translational equations of motion of wheel

By application of Newton's laws of motion, the three components of the forces acting on the wheel are equated to the wheel mass multiplied by the appropriate acceleration component:

$$R_1^P + R_1^W + 0 = m_w r_W \dot{\Omega} \quad (\text{A.9})$$

$$R_2^P + R_2^W - m_w g \phi = m_w r_W (\Omega_0 \dot{\phi} - \dot{\phi}) \quad (\text{A.10})$$

$$R_3^P + R_3^W - m_w g = 0 \quad (\text{A.11})$$

A.2 Translational equations of motion of wheel

A.2.1 Linear acceleration of point O

Referring to Figure A.2 the absolute angular velocity of the wheel is

$$\begin{aligned}\vec{\omega} &= \dot{\psi}\vec{b}_3 + \dot{\phi}\vec{w}_1 + \vec{\Omega}\vec{w}_2 \\ &= \dot{\psi}(s\phi\vec{w}_2 + c\phi\vec{w}_3) + \dot{\phi}\vec{w}_1 + \vec{\Omega}\vec{w}_2\end{aligned}$$

Linearization assumptions made throughout the analysis are:

1. Angles and perturbation angular rates are small compared to 1 radian and Ω_0 respectfully.
2. $\sin \phi \cong \phi$ and $\cos \phi \cong 1$.
3. Products of small angles and angular rates are negligible.
4. $\vec{\Omega} = \Omega_0 + \vec{\Omega}$

where:

Ω_0 = constant component of wheel angular velocity; it can be large.

Ω = small perturbation of wheel angular velocity.

with these assumptions, $\vec{\omega}$ can be approximated by:

$$\vec{\omega} \cong \dot{\phi}\vec{w}_1 + (\Omega_0 + \Omega)\vec{w}_2 + \dot{\psi}\vec{w}_3 \quad (\text{A.1})$$

Assuming no slip at the ground contact point, P, the velocity of the center of mass of the wheel, O, is :

$$\begin{aligned}\vec{v} &= \vec{\omega} \times r_W \vec{w}_3 \\ &= r_W (\Omega_0 + \Omega) \vec{w}_1 - r_W \dot{\phi} \vec{w}_2\end{aligned} \quad (\text{A.2})$$

acceleration of O is :

$$\vec{a}_O = (\vec{v})_r + \vec{w} \times \vec{v} \quad (\text{A.3})$$

where \vec{w} = absolute angular velocity of \vec{w} - frame

$$= \dot{\psi}\vec{b}_3 + \dot{\phi}\vec{w}_1 \cong \dot{\phi}\vec{w}_1 + \dot{\psi}\vec{w}_3 \quad (\text{A.4})$$

Appendix A

EOMs by Newton-Euler Mechanics

A.1 Definition of variables

In this appendix we will derive the dynamic equations of motion (abbreviated EOMs) [for the unicycle robot] by using Newton-Euler mechanics. A schematic diagram of the unicycle model is shown in Figure A.1 and the coordinate frames for the various parts are given in Figures A.2 and A.8. The symbols used in the thesis are given in the table at the beginning of this document.

6.3. CONCLUSION

65

performing the mechanical and electrical designs and constructing the robot. However, during this research a few interesting and satisfying control systems aspects could be tested experimentally with the vehicle. As the partial list of recommendations indicate, future researchers are in a good position to concentrate their efforts on investigating and testing several more interesting control aspects.

This research casts one of the human's fascinating control capabilities into the terms of the control system engineer's language. The process illustrates both the inadequacies and the power of modern control theory.

The shortcomings are evident when we recognize the multitude of sensory inputs that a person uses as well as the effortless application of nonlinear and multiple control actions. Adaptive control and model reference control is part of a person's everyday living. All of these topics are intensive research areas in modern control theory.

The strength of modern control is illustrated by this research which shows that we have the mathematical, theoretical and computational power in hand to start emulating some of the human's more advanced control abilities in a machine. It also illustrates the importance of obtaining sufficient physical insight into the process and identifying the principal configurational, sensory and control aspects, before we can effectively apply control system theory in practice.

This research is an illustration of how control system techniques can be applied to assist normal persons in tasks which require unusual skills or to help disabled persons perform normal tasks. Apart from these, the research has a wider application in providing artificial stability for inherently unstable physical systems.

64 CHAPTER 6. SUMMARY OF CONTRIBUTIONS AND RECOMMENDATIONS

obtain the pitch angle. The measurement of the original accelerometer signal can then be filtered with a long time constant to correct for drift errors.

This so called complimentary filtering technique is essentially the same as that used in a vertical gyro. A rate gyro which measures the pitch rate, combined with the current accelerometer, will probably be a cheaper solution to the sensor problem than using a vertical gyro.

- Stabilize near zero speed

The lateral motions are uncontrollable at zero speed by twisting the wheel through small angles. Preliminary simulations have shown that the unicycle can be stabilized near zero speed if it is commanded to perform small forward-backward oscillations about a fixed point. This conjecture should be investigated because it can produce interesting results on controlling a dynamic system which oscillates between a controllable and an uncontrollable state. An alternative way of controlling the unicycle at low speeds, would be by turning the wheel into the roll direction and then using the longitudinal control system to erect the unicycle.

- Nonlinear lateral control system

The twisting motions performed by a unicycle rider's body at very low speeds are large amplitude (± 30 degrees), which leads us to expect that a nonlinear on-off type controller on the turntable torque might provide stabilization.

6.3 Conclusion

The investigation into computer stabilization of a unicycle robot has yielded valuable insights into the dynamics, control and sensing aspects involved in the process.

A major part of our time resources had to be devoted to selecting the equipment,

- Lateral control system design

Chapter 5 points out that if an accelerometer is used as the lateral attitude sensor, similar problems exist in designing a robust control system as in the longitudinal case. An LQG controller using a measurement of the turntable angular velocity and the frame roll angle, was proposed. We showed that this controller would provide acceptable performance for wheel speeds in the range of approximately $\pm 5\%$ of the nominal design speed and that compensator gain scheduling should be used if the unicycle is to be operated over a wide speed range. The design was not tested experimentally, but we expect it to perform satisfactorily if good roll attitude information is available and an effective gain scheduling scheme is implemented.

6.2 Recommendations for future research

- Test lateral control system

A roll angle sensor using a trailer wheel which extends sideways from the frame should be constructed. It can be used to test a lateral stabilization algorithm using linear control at a constant wheel speed and on a horizontal floor. A gain scheduling algorithm can be developed to control the robot over a range of wheel speeds for which the lateral plant dynamics change significantly.

- Inertial vertical sensor or additional sensors

A vertical gyro should be mounted on the unicycle robot, so that frame roll and pitch angles relative to vertical can be measured. This would permit the vehicle to travel on surfaces which are inclined and rough.

It is possible that another non ground contact sensor in addition to the single accelerometer, might relieve the sensitivity of the closed loop system design. If we have a measurement of the pitch rate or pitch acceleration, we can perform a single or double integration on these measurements respectively, to

62 CHAPTER 6. SUMMARY OF CONTRIBUTIONS AND RECOMMENDATIONS

Candidate longitudinal control systems were designed using an accelerometer as the balance sensor. Since these sensors do not measure the attitude alone, (see section above), the pitch attitude information required by the control system, depends heavily on the accuracy of the plant dynamic model. We have shown that the transfer function to the accelerometer output has zeros which make it difficult to design a robust control system. These zeros can be relocated to more convenient positions in the s -plane by changing the location of the accelerometer on the robot frame, but the resulting zero positions are extremely sensitive to small changes in the sensor location. The maximum acceleration of the unicycle frame is on the order of only 3% of gravity acceleration during typical maneuvers. The accelerometers were designed with adequate resolution to measure signals in this range, but during experimental tests it was found that frame vibration noise due to the roughness of the terrain over which the robot traveled was of the same order of magnitude as the desired signal.

For these reasons above, none of the candidate control systems described in Chapter 3 could stabilize the unicycle robot by means of a single accelerometer as the main balance sensor. An important contribution of this research, however, is the investigation of the theoretical and experimental reasons why accelerometers have limited capabilities as attitude sensors.

Chapter 4 shows that if a vertical sensor is available, a robust longitudinal control system can be designed. The control system is based on a direct measurement of the kinematic variable which indicates the attitude, instead of relying on an indirect measurement and the accuracy of the plant model. By performing experiments on a horizontal surface and measuring the robot frame angle with respect to the ground, we experimentally demonstrated the performance of a robust control system with good stiffness to stabilize a unicycle longitudinally.

wheel torque has three components:

1. The forward acceleration of the center of the wheel.
2. The backward acceleration of the point on the frame where the accelerometer is mounted.
3. $g\theta$, where g = gravitational force per unit mass, and θ is the deviation of the frame from vertical.

The first two signals are large and of opposite sign. The third signal, the one of interest to us, never becomes very large for a successful stabilization scheme (the maximum value of θ observed using the trailer sensor was about .5 degrees). Thus we were looking for a very small signal in the presence of the difference of two other large signals. A little additive random noise in the accelerometer signal obscures the difference between the two large signals and makes estimation of the small signal $g\theta$ almost impossible.

Theoretically, there is a point on the frame where the first two signals exactly cancel each other. However a change in vertical location of only a millimeter or two causes the difference in these two signals to be larger than $g\theta$ with $\theta = 0.5$ degrees, i.e. the total signal is very sensitive to the location to the location of the transfer function zeros (from wheel torque to accelerometer signal) to vertical location of the accelerometer.

Optical or inertial sensors which could be mounted on the unicycle to provide vertical information of the required accuracy were too expensive for the financial resources available for this research. Instead we built a simple mechanical device which measured the robot frame's angle with respect to the ground. This allowed experimental testing of balance control algorithms on smooth horizontal floor surfaces.

- Longitudinal control system design and tests

60 CHAPTER 6. SUMMARY OF CONTRIBUTIONS AND RECOMMENDATIONS

unicycle. The result is a robot with interesting unstable open loop dynamics, which can serve as a test bed for modern control system techniques.

- Emulation of a human riding a unicycle

The actuation methods and sensor information used by a human riding a unicycle were evaluated in Chapter 2. Observations of a human's control actions and calculations of a person's mass and inertia properties were combined to propose a mechanical robot configuration which could emulate the important features. We constructed such a one wheeled robot with an on-board power supply, actuators, sensors and microprocessors to perform the active stabilization task.

- Dynamic model for a unicycle robot

The linearized dynamic equations of motion that describe the lateral and longitudinal model of a one wheeled robot were derived. It was shown that the lateral and longitudinal dynamics decouple under certain reasonable conditions and that the lateral dynamics vary with the unicycle speed due to the gyroscopic effect of the rotating wheel. Physical explanations for the dynamic system modes and the zeros of transfer functions from the actuators to the various sensors, were presented.

- Evaluation of balance sensors

We tried first to use accelerometers on the unicycle robot to determine the deviation of the frame from vertical. This choice was motivated by the desire to emulate the balance sensing capability of the human ear, and on considerations of cost. Furthermore, theoretical analysis showed that we should be able to determine the vertical directly by placing the accelerometer at a particular vertical location.

However, in practice, we were unable to stabilize the longitudinal motions of the unicycle using an accelerometer. We believe the reason for this is as follows. The longitudinal accelerometer signal in response to an impulse in

Chapter 6

Summary of Contributions and Recommendations

In this chapter we summarize the main contributions of this research and propose recommendations for future research into active stabilization of unstable vehicles.

6.1 Contributions

- Research topic

The automatic stabilization of a unicycle was made possible by means of a unique combination of state of the art computer hardware and modern control systems analysis and design tools. Since this research commenced, several sources mentioned that the idea of a computer stabilized unicycle has appeared elsewhere. Only one reference of a practical application could be found in the literature [Iguchi], but the control method there does not bear any relationship to the way a human controls a unicycle. Using new, compact, and powerful microprocessors, the research in this thesis resulted in a one wheeled robot with all its computational and electrical power on board, to emulate the longitudinal stabilization used by a human riding a

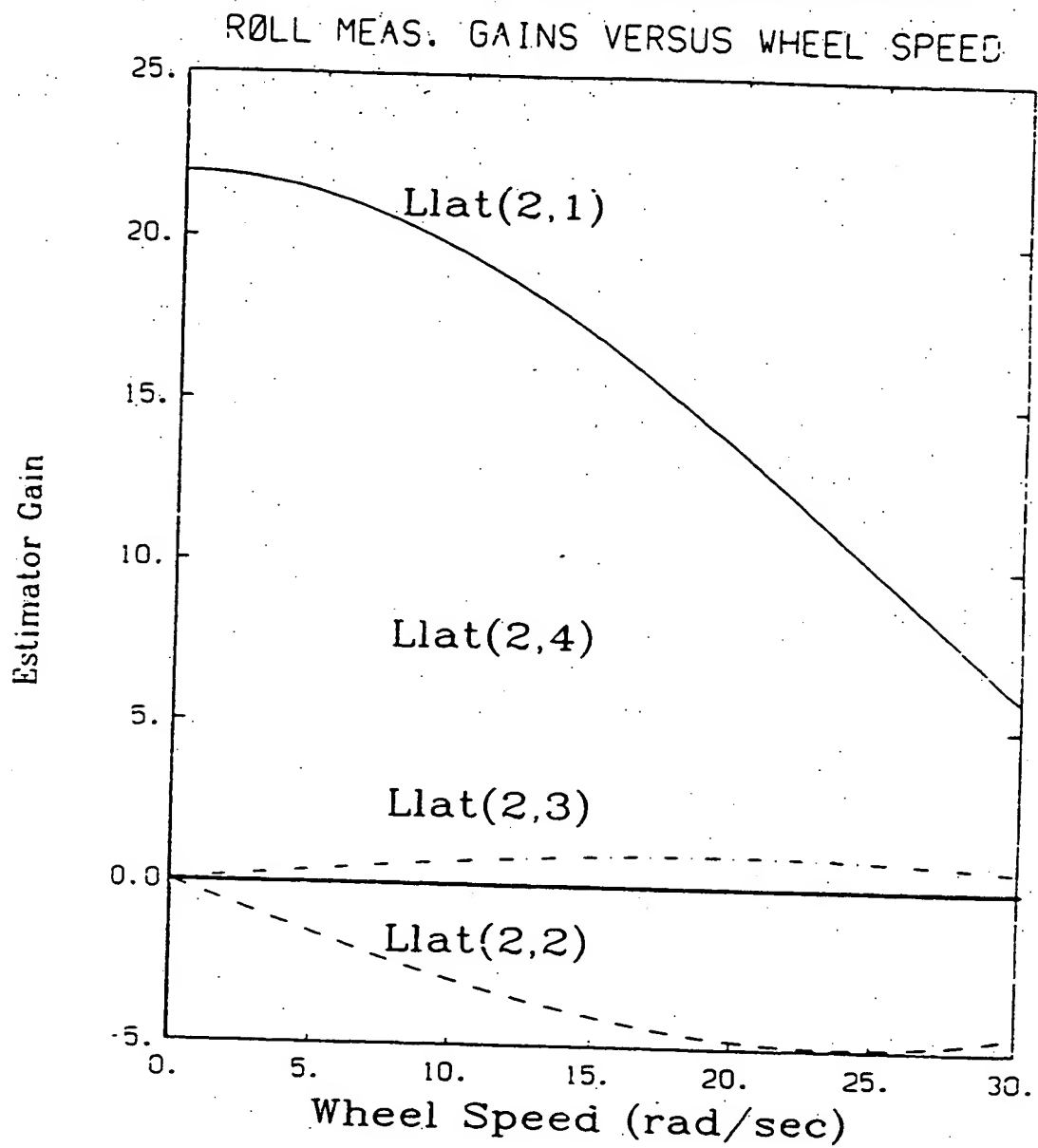


Figure 5.5: Lateral System Optimal Estimator Gains on the Roll Angle Measurement, as a Function of the Wheel Speed

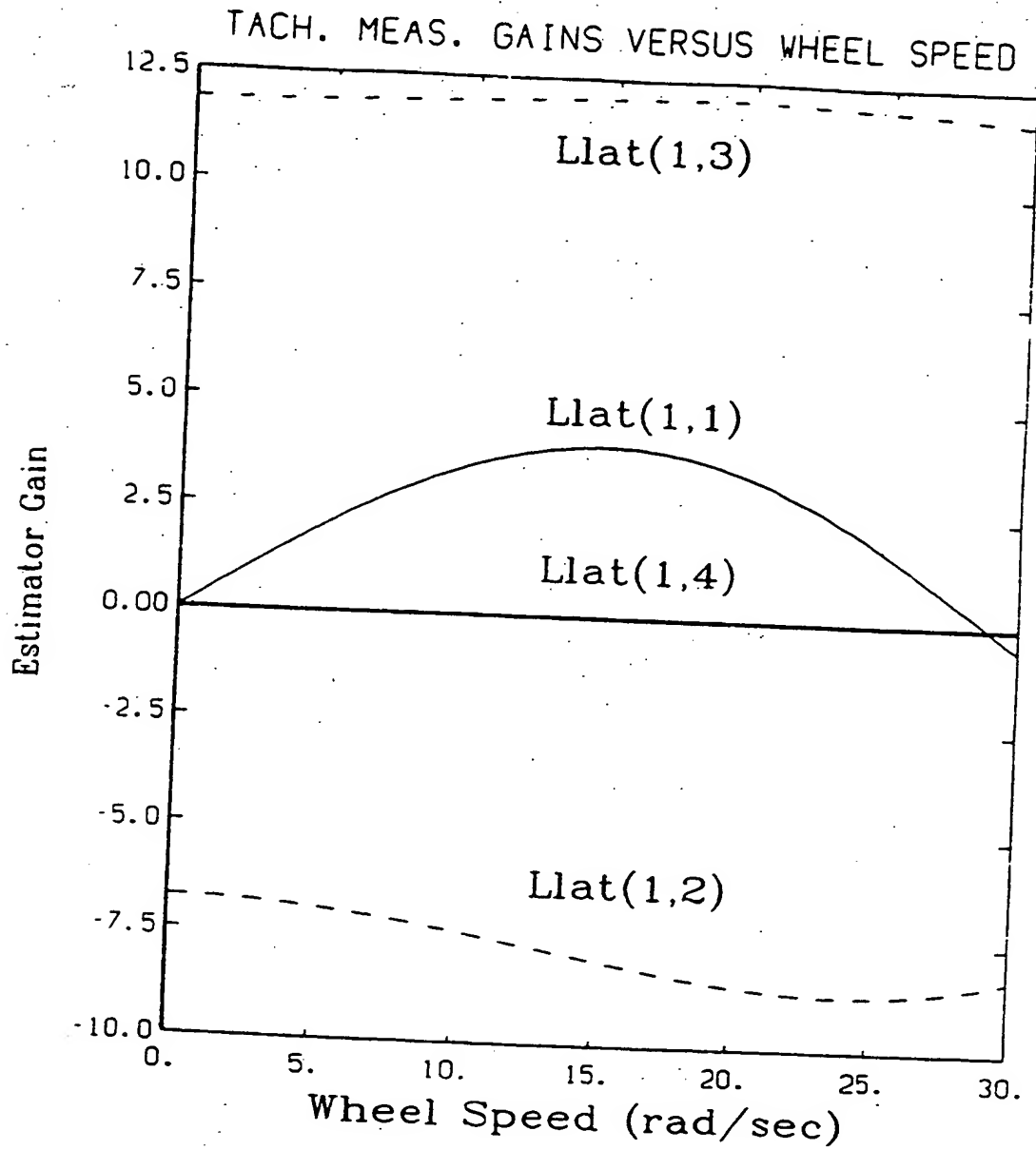


Figure 5.4: Lateral System Optimal Estimator Gains on the Turntable Tachometer Measurement, as a Function of the Wheel Speed

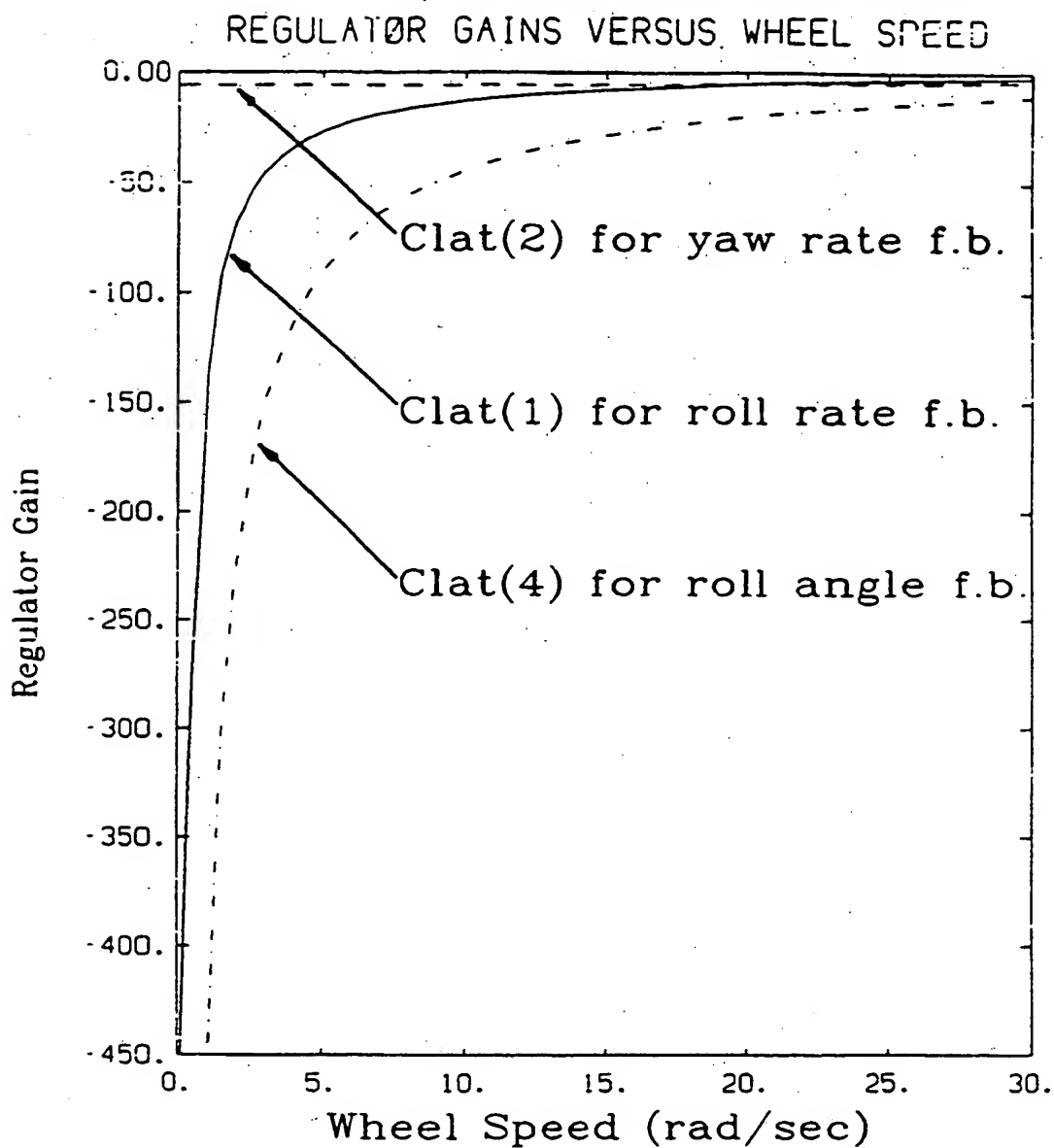


Figure 5.3: Lateral System Optimal Regulator Gains as a Function of the Wheel Speed

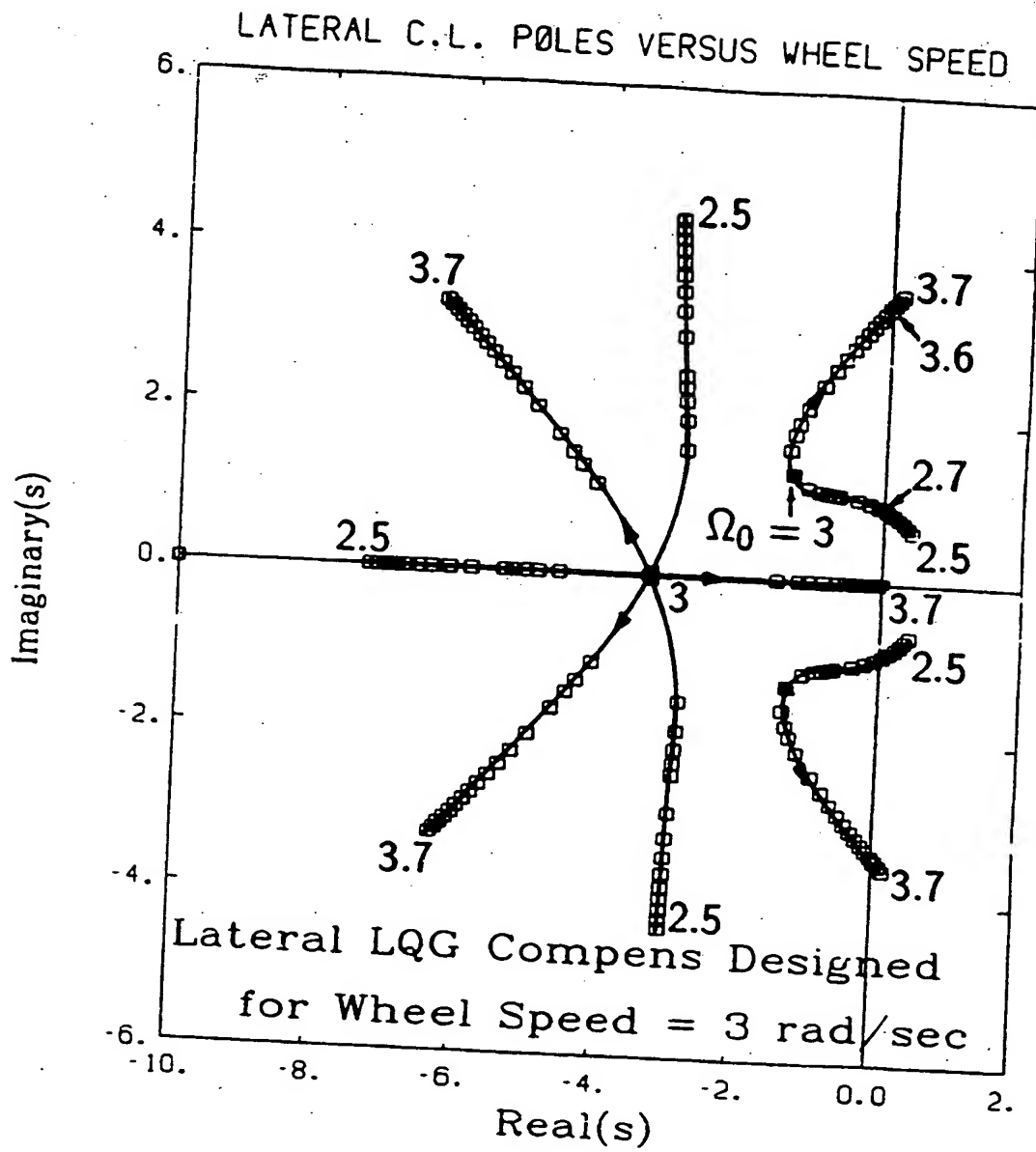
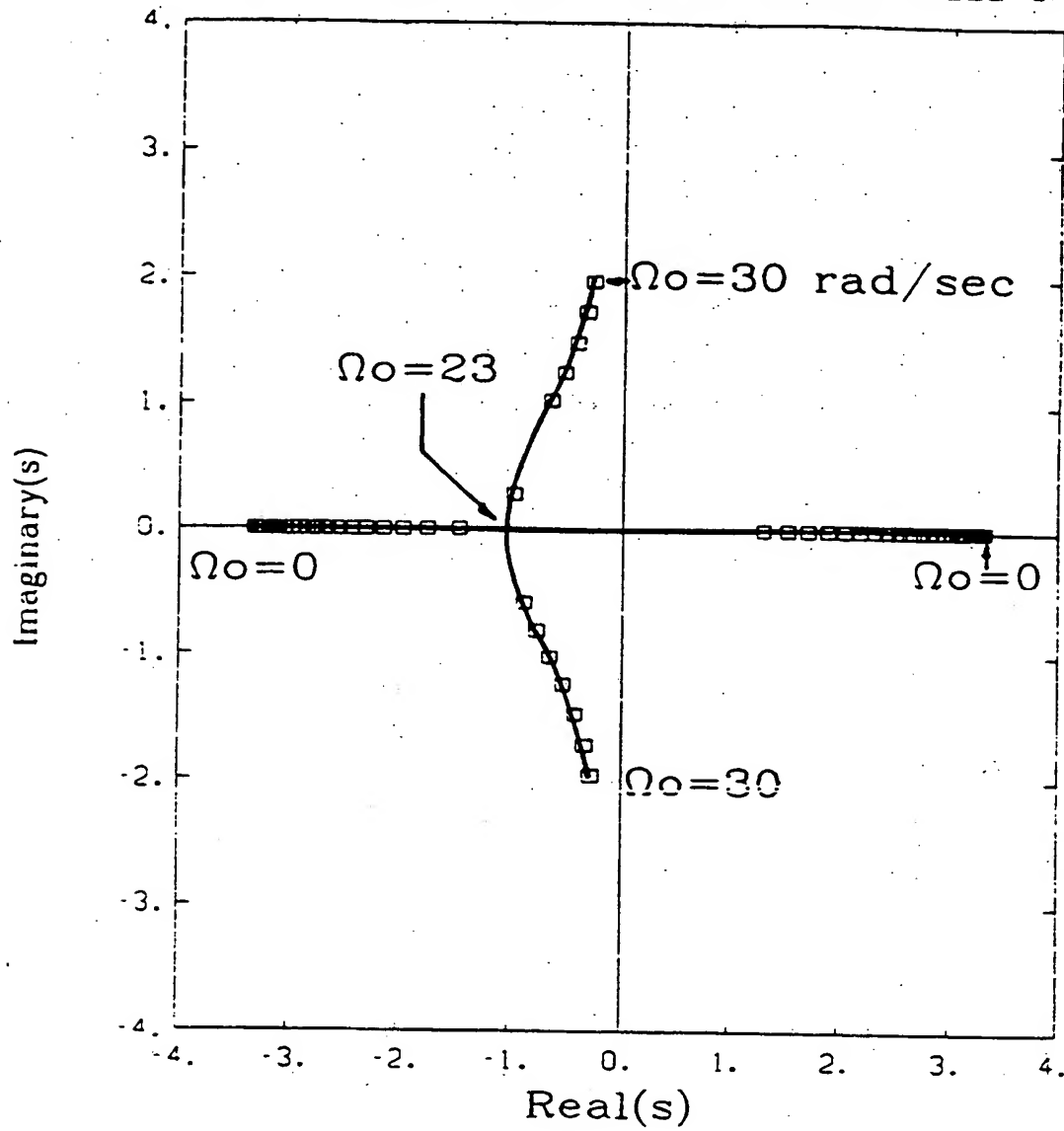


Figure 5.2: Lateral System Closed Loop Poles as a Function of the Wheel Speed for an LQG compensator designed for 3 rad/sec

LOCUS OF LATERAL PLANT POLES VERSUS WHEEL SPEED

Figure 5.1: Dependence of the Lateral Plant Eigenvalues on the Wheel Speed, Ω_o

speeds. At zero wheel speed, the roll gains become infinitely large, since it is obviously impossible to stabilize the unicycle robot by twisting the frame about the vertical axis. However, a scheme where the wheel is turned towards the direction that the robot is falling and then using the longitudinal control system to erect the unicycle, can work at low wheel speeds.

Plots of the estimator gains on the tachometer and roll angle measurements are shown in Figures 5.4 and 5.5 respectively. It is evident that gain scheduling on the estimator gains will also be required as the wheel speed changes. It is interesting to note that none of the estimator gains become excessively large at any speed as the regulator gains did. Also notice that at zero wheel speed, measurement of the turntable tachometer speed η is used to improve the estimate of the yaw rate and turntable speed only ($Llat(1,1) = Llat(1,4) = 0$) while the measurement of the roll angle sensor is used to improve the roll angle and roll rate estimate ($Llat(2,2) = Llat(2,3) = 0$).

From the investigations in this chapter it is concluded that the lateral system can be stabilized at nonzero wheel speeds by twisting the turntable. Appropriate sensors would be a tachometer to measure the turntable speed and a roll angle sensor. If the unicycle is to operate over a wide range of forward speeds, some form of scheduling of the compensator gains with wheel speed will be required.

the amount of control torque used. The ratio of these two weighting factors was varied to obtain a closed loop response which would let the yaw rate reach the commanded value in approximately 5 seconds (Figure Q.2).

A full order state estimator was designed by assuming the same noise spectral densities as for the longitudinal system design. Section Q.4 shows the optimal regulator and estimator gains as well as the regulator and estimator poles.

The design above was for a nominal wheel speed of $\Omega_0 = 3$ rad/sec. All the closed loop poles are well damped ($\xi \geq 0.7$) and the real parts of the estimator eigenvalues are comparable to those of the regulator eigenvalues. If we use the compensator gains for the nominal wheel speed of 3 rad/sec, but vary the wheel speed, the closed loop eigenvalues of the system change as shown in Figure 5.2. Since the lateral plant eigenvalues change as a function of wheel speed, the closed loop system will remain stable for

$$2.7 < \Omega_0 < 3.6 \text{ rad/sec}$$

The range for acceptable closed loop response is probably even smaller (in the order of $\Omega_0 \pm 5\%$) so that gain scheduling will be required for the lateral control system. If we use the same cost function, but the different lateral plant models for the range of possible wheel speeds, the optimal regulator feedback gains as a function of the wheel speed, can be calculated. The regulator gain on the integral error of the yaw rate (e) and the feedback gain on the turntable speed (η) remain constant for all wheel speed values. Figure 5.3 shows how the other regulator gains should be varied to minimize the cost function at different wheel speeds. The yaw rate feedback gain remains relatively constant, but the feedback gains on the roll angle and rate changes significantly, especially at lower wheel speeds.

It is evident that if some form of a compensator gain scheduling technique is used, the regulator gains will have to be changed rapidly with wheel speed at low wheel

5.3. LATERAL SYSTEM LQG DESIGN

51

coincide with the plant poles at 3.29 rad/sec, at which point the inverted pendulum modes would become unobservable through the accelerometer measurement.

$$(rs_3)_{unobs} = 0.699 \text{ m}$$

The point of unobservability is just 4 mm removed from the 'ideal' accelerometer height, which shows that the closed loop design will be very sensitive to plant parameter changes if an accelerometer is used as a balance sensor. Furthermore, the point of unobservability will also change as a function of the wheel speed because the inverted pendulum time constants change as shown in Figure 5.1.

It is concluded that it would not be advisable to use an accelerometer as the lateral balance sensor. A roll angle sensor has only one zero at $s = 0$ in its transfer function from the control torque. The unobservability matrix shows that the two inverted pendulum modes are observable from a roll angle sensor (see the third row of the OBS matrix in the print-out of section Q.3.1). A lateral compensator using a roll angle sensor will be used to design a balance control system.

5.3 Lateral system LQG design

A linear quadratic gaussian (LQG) compensator is designed by minimizing the expected value of a quadratic cost function which weighs the relative importance of keeping state errors small and using reasonable amounts of control torque. We will use the same performance index in designing optimal compensators for the range of wheel speeds at which the unicycle robot is likely to travel.

An optimal continuous time regulator was designed as described in section Q.4. We included integral error feedback of yaw rate so that the unicycle robot may be steered by an external command. The cost function that was minimized to obtain the optimal feedback gains weighed the integral of yaw rate error against

Two of the accelerometer transfer function zeros are at

$$s = \pm \sqrt{\frac{g\bar{J}_{22} - r_W J_{24}}{(J_{22} - I_{21})r_W + J_{22}r_{S3}}} \quad (5.13)$$

The third accelerometer zero at $s = 0$ does not appear in equation 5.12 because it is cancelled by the pole at $s = 0$ due to the zero turntable friction assumption. Equation 5.13 shows that the locations of the accelerometer zeros are independent of the wheel speed Ω_0 .

By substitution of the parameters from appendix M into equation 5.13 we see that the pair of zeros are at infinity for the accelerometer mounted at the critical height of

$$\begin{aligned} (r_{S3})_{\infty} &= \frac{(I_{21} - \bar{J}_{22})r_W}{J_{22}} \\ &= 0.695 \text{ m} \end{aligned} \quad (5.14)$$

For $r_{S3} < (r_{S3})_{\infty}$ the accelerometer transfer function has a pair of complex zeros on the imaginary axis. An impulse torque on the turntable motor will cause the frame acceleration to increase initially and then recede back to zero. For $r_{S3} > (r_{S3})_{\infty}$ the accelerometer zeros are on the positive and negative real axis. The frame acceleration at this height will therefore have a nonminimum phase behaviour to an impulsive turntable torque. The physical meaning of the zeros at $\pm j\infty$ when $r_{S3} = (r_{S3})_{\infty}$ is therefore that the frame will have no initial acceleration at this height, for an impulsive control torque. The point on the frame acts as a virtual pivot point during motions, with points above and below $(r_{S3})_{\infty}$ on the frame accelerating in opposite directions.

Theoretically the best place to locate the accelerometer would be at $(r_{S3})_{\infty}$. From the print-out in section Q.3.1 we notice that, for a nominal wheel speed of $\Omega_0 = 3$ rad/sec, the lateral plant eigenvalues are at approximately 3.29 rad/sec. We can use equation 5.13 to solve for the height $(r_{S3})_{\text{unob}}$ when the accelerometer zeros

5.2. LATERAL SYSTEM CHARACTERISTICS

49

Taking the Laplace transform of the equations above and eliminating $\dot{\eta}$, we obtain the transfer functions to the roll angle and yaw rate:

$$\frac{\Phi(s)}{Q_T(s)} = \frac{-J_{22}B}{(I_{21}s^2 - J_{24})(As + f_G) - J_{22}J_{11}I_{33}s} \quad (5.4)$$

$$\frac{s\Psi(s)}{Q_T(s)} = \frac{-B(I_{21}s^2 - J_{24})}{(I_{21}s^2 - J_{24})(As + f_G) - J_{22}J_{11}I_{33}s} \quad (5.5)$$

where

$$\begin{aligned} A &= I_{33}I_{12} - I_{13}I_{32} \\ B &= I_{33} + I_{13} \end{aligned} \quad (5.6)$$

From equation Q.18 the accelerometer measurement is

$$y_a(t) = -(r_W + r_{S3})\ddot{\phi} + r_W\Omega_0\dot{\phi} + g\phi \quad (5.7)$$

Taking the Laplace transform, 5.7 becomes:

$$y_a(s) = [g - (r_W + r_{S3})s^2]\Phi(s) + r_W\Omega_0s\Psi(s) \quad (5.8)$$

Substitute equations 5.4 and 5.5 into 5.8 to obtain the transfer function:

$$\frac{y_a(s)}{Q_T(s)} = \frac{J_{22}B[(r_W + r_{S3})s^2 - g] - r_W\Omega_0B(I_{21}s^2 - J_{24})}{(I_{21}s^2 - J_{24})(As + f_G) - J_{22}J_{11}I_{33}s} \quad (5.9)$$

if we define

$$\bar{J}_{22} = I_1^W + m_W r_W^2 + m_F r_W(r_W + r_F) + m_T r_W(r_W + r_T) \quad (5.10)$$

we notice from equation Q.13 that

$$J_{22} = \bar{J}_{22}\Omega_0 \quad (5.11)$$

and the accelerometer transfer function can be rewritten as

$$\frac{y_a(s)}{Q_T(s)} = \frac{B\Omega_0\{\bar{J}_{22}[(r_W + r_{S3})s^2 - g] - r_W(I_{21}s^2 - J_{24})\}}{(I_{21}s^2 - J_{24})(As + f_G) - J_{22}J_{11}I_{33}s} \quad (5.12)$$

unicycle yaw modes in the measurement of the turntable speed relative to the frame.

The transfer function to the accelerometer measurement has three zeros: one at $s = 0$ and two at ± 1.0284 rad/sec on the imaginary axis of the s -plane. The position of the two zeros which are not at the origin, is a function of the height r_{S3} of the accelerometer above the wheel axle, but not a function of the wheel speed, as we will show later.

If an accelerometer is used as a balance sensor the control system designer is confronted with the same problems encountered in the longitudinal control system design. First of all, the three zeros on the imaginary axis cause a 'barrier' of zeros which makes it difficult to design a compensator which will bring the root loci from the unstable poles in the right half of the s -plane to the left half plane.

We will now proceed to calculate the accelerometer zero positions analytically and show that their locations are very sensitive to changes in r_{S3} and plant parameter changes:

The lateral plant dynamics from equation Q.6 are:

$$I_{12}\ddot{\psi} + I_{13}\dot{\eta} = J_{11}\dot{\phi} - f_G\dot{\psi} - Q_T \quad (5.1)$$

$$I_{21}\ddot{\phi} = J_{22}\dot{\psi} + J_{24}\phi \quad (5.2)$$

$$I_{32}\ddot{\psi} + I_{33}\dot{\eta} = Q_T \quad (5.3)$$

where the coefficients of the state variables are defined in equations Q.7 through Q.14.

The viscous friction constant f_T has been ignored in the equations above since it has no effect on the zero locations.

5.2. LATERAL SYSTEM CHARACTERISTICS

47

frame yaw angle and turntable angular position are not shown, since we do not presently intend to control these variables.

At nonzero wheel speeds, the gyroscopic effect of the wheel changes the eigenvalues of the inverted pendulum modes. Figure 5.1 shows that, as the wheel speed increases, the time constants of these modes become longer. The particular wheel drive motor used in the robot can reach a maximum rotor speed of 7000 revolutions per minute. With the 24:1 reduction gear system, this entails a maximum wheel speed of approximately 30 rad/sec. Figure 5.1 shows that at this speed the inverted pendulum modes have changed from real eigenvalues to a pair of stable complex eigenvalues in the s -plane. It is evident that the lateral control system will have to adjust its compensator gains as the wheel speed changes.

The system characteristics listed in section Q.3.1 are for a nominal wheel speed of $\Omega_0 = 3$ rad/sec. The controllability vector CTR shows that all modes are controllable from the turntable torque.

The output distribution matrix is shown for three possible sensors:

- a tachometer measuring the turntable speed relative to the frame
- an accelerometer mounted on the frame with its sensitive axis in the lateral direction
- a roll angle sensor, which could consist of a vertical gyro or a device for measuring the frame angle relative to a horizontal surface, as described for the longitudinal system in the previous chapter.

The transfer function from the turntable torque to the tachometer output shows that three of the four eigenvalues are nearly cancelled by zeros and that consequently only the residue of the mode at $s = 0.238$ rad/sec is not small. This makes physical sense since we cannot expect to see much of the inverted pendulum and

Chapter 5

Lateral Control System

5.1 Introduction

In this chapter the lateral system transfer functions for different sensors at different wheel speeds, will be evaluated. A continuous time LQG compensator is designed and the dependence of the compensator gains on the wheel speed is discussed.

5.2 Lateral System Characteristics

The dynamic equations of motion of the decoupled lateral system are given in Appendix Q, equation Q.6. The yaw angle ψ , the roll angle ϕ , the turntable speed η relative to the frame and the turntable torque Q_T , are the variables associated with the lateral system dynamics.

After substitution of the mechanical parameters from appendix M into the dynamic equations, we can evaluate the plant eigenvalues. As shown in the listing of section Q.3.1, the openloop system consists of two eigenvalues at approximately plus and minus 3.29 rad/sec in the s -plane. The unstable eigenvalue is associated with the lateral inverted pendulum mode of the unicycle robot. Two other modes near $s = 0$ are shown in the print-out. One is associated with the yaw rate of the unicycle and the other with the turntable angular speed relative to the frame. The modes at $s = 0$ associated with the

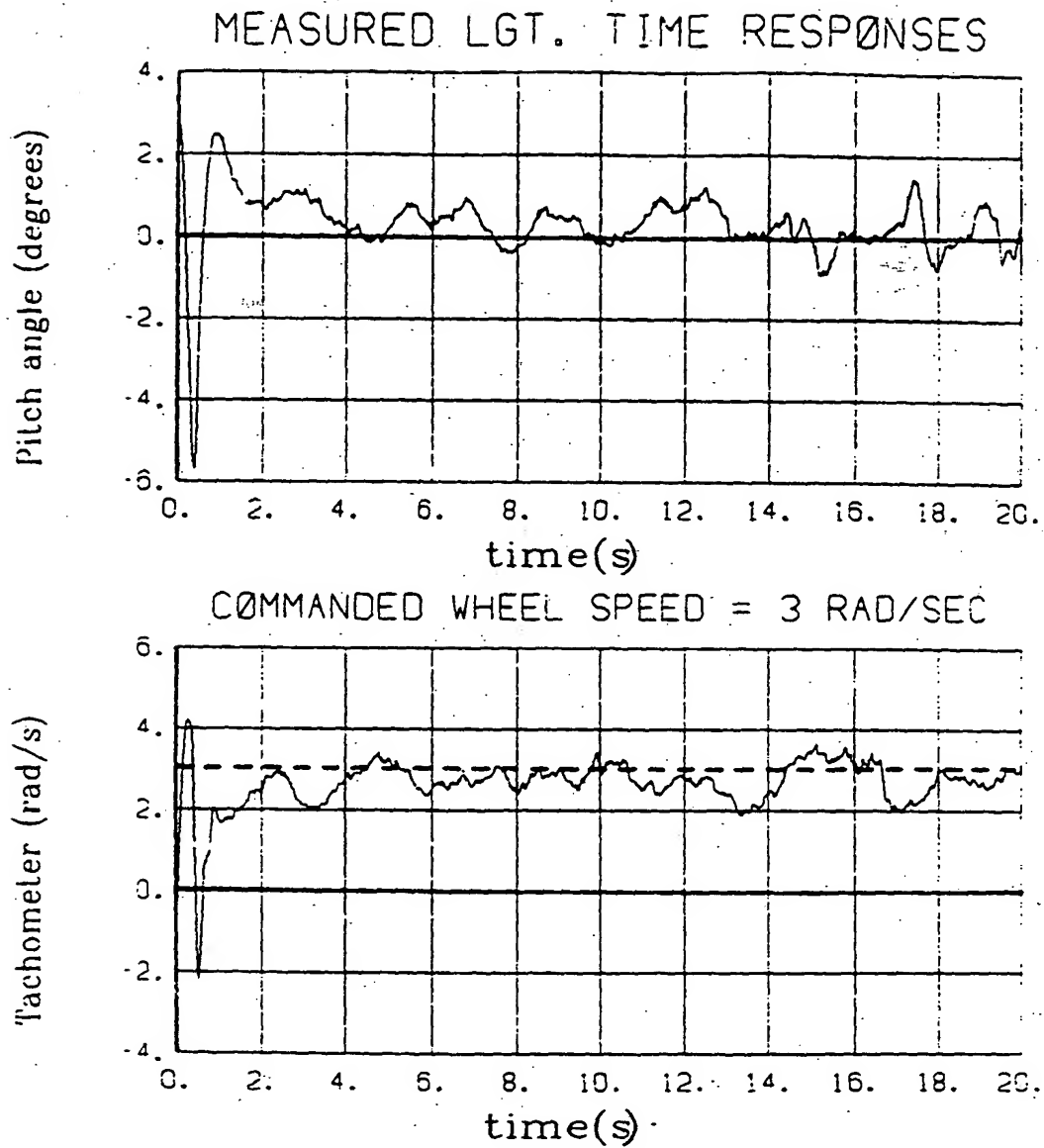


Figure 4.3: Pitch Angle and Wheel Speed Measurements at 3 rad/sec Commanded Wheel Speed

MEASURED LGT. TIME RESPONSES

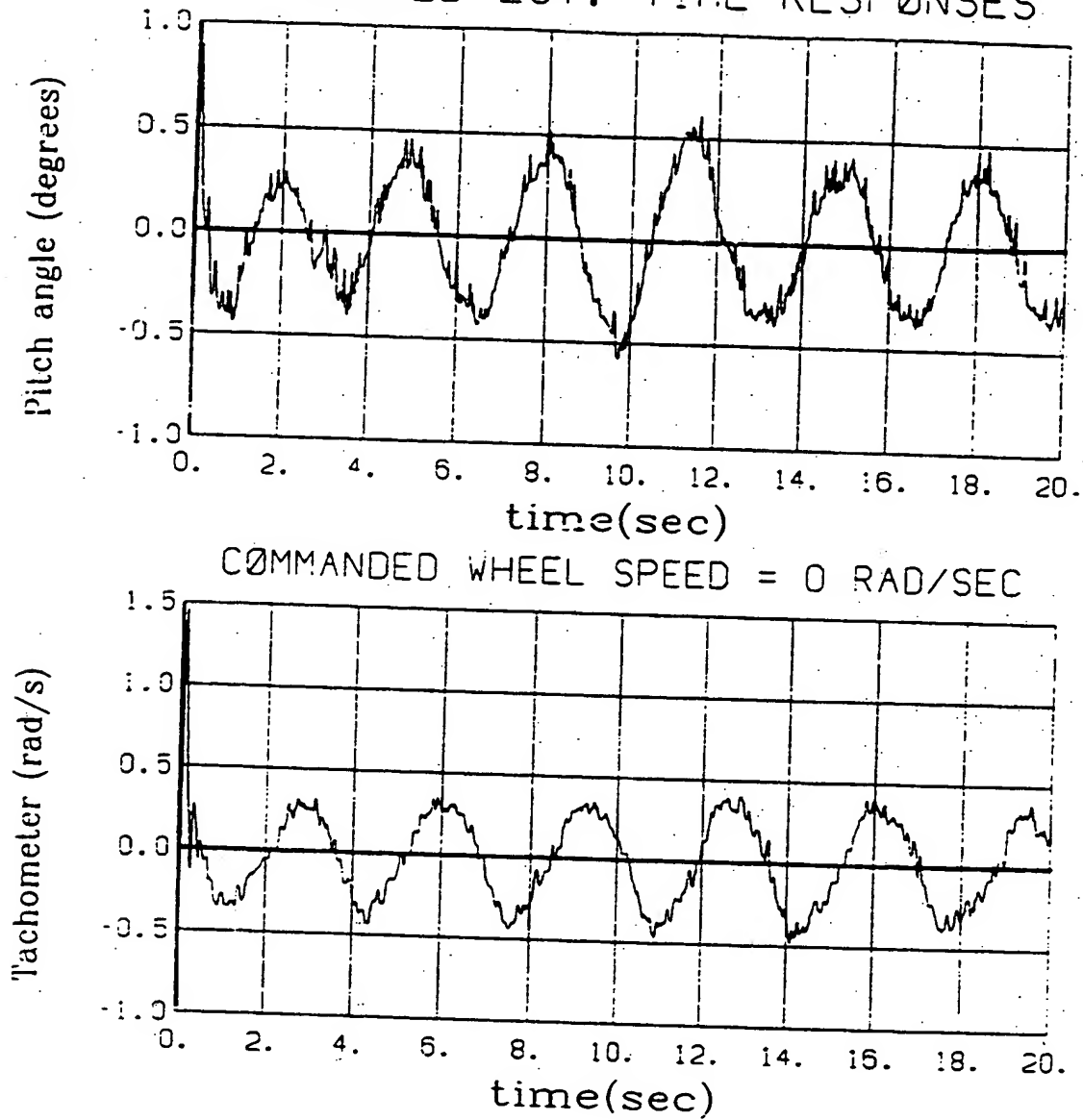


Figure 4.2: Pitch Angle and Wheel Speed Measurements at Zero Commanded Wheel Speed

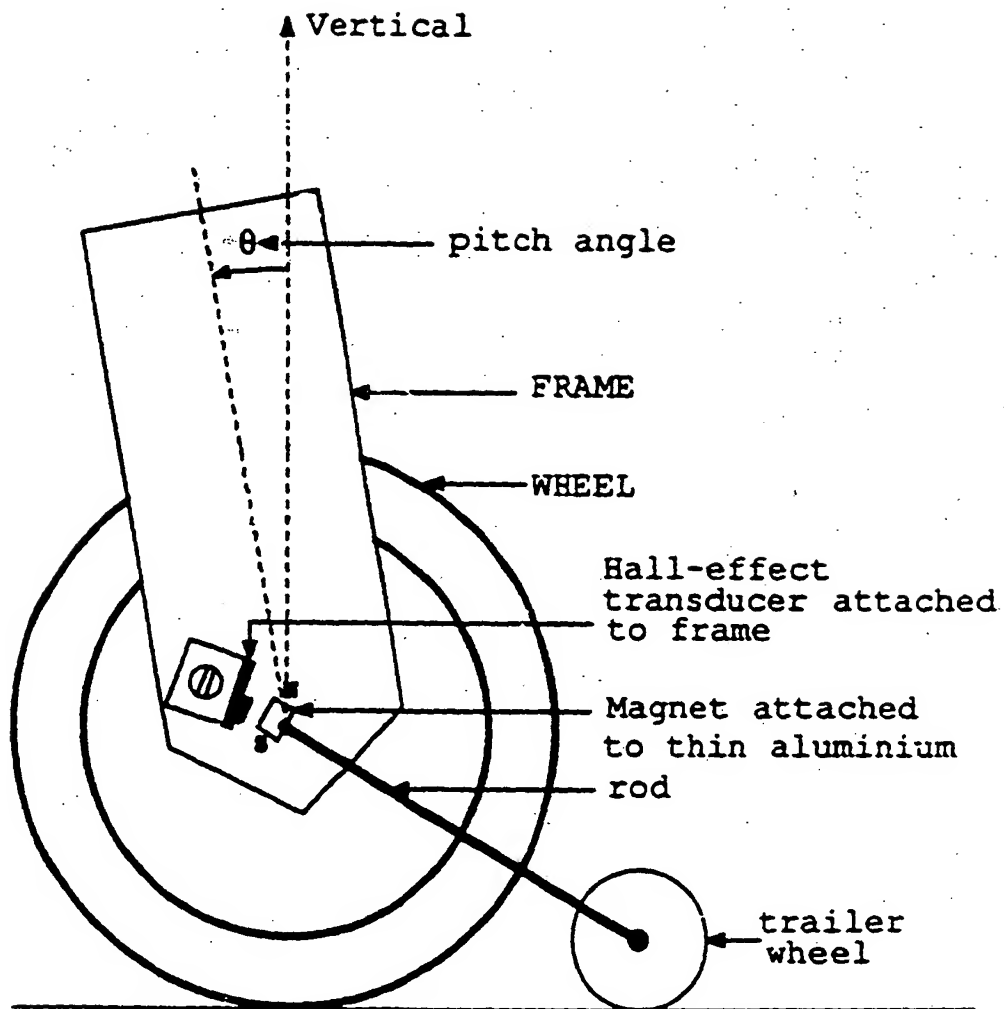


Figure 4.1: Mechanical Design of Frame Pitch Angle Sensor

the 25 ms sample period. The dominant pole pair therefore has an undamped natural frequency of $\omega_n = 1.2$ rad/sec and a damping ratio of $\xi = 0.54$, for which the closed loop bandwidth is approximately $1.5\omega_n = 1.8$ rad/sec = 0.29 Hz. We notice that the frequency of the oscillations in Figure 4.2 are approximately 0.3 Hz which corresponds to the closed loop system's bandwidth.

The controlled system has good disturbance rejection. An impulse applied to the system by means of a fist blow at the turntable height, merely causes the robot to move forward a few centimeters, after which it re-establishes balancing on the spot. The stiffness of the system is illustrated by the fact that a person grabbing hold of the top of the robot and shaking it longitudinally, cannot destabilize the control system as long as the maximum control torque on the motor and the linear range of the pitch sensor (± 5 degrees) are not exceeded.

The performance of the closed loop system when the unicycle robot moves along at a constant commanded wheel speed of 3 rad/sec (0.585 m/s), is illustrated by the measurements shown in Figure 4.3. In this test the robot still stabilized well, although the maximum pitch angle reached approximately 1 degree from vertical occasionally. This greater error can be attributed to the fact that the linoleum tiled floor surface in the hallway where the tests were performed, had a noticeable degree of unevenness.

4.4 Conclusion

These experimental results illustrate that the model for the unicycle longitudinal dynamics is accurate and that, given accurate pitch information, a digital control system can perform the balancing function with good stiffness and robustness characteristics.

4.3. EXPERIMENTAL TESTS OF THE CONTROL SYSTEM

41

travels. A vertical gyro [Kayton] consists of a two degree-of-freedom gyro whose spin axis is nominally vertical, with two nominally horizontal specific force sensors mounted on the inner gimbal. Signals from these specific force sensors are filtered with a fairly long time constant (in the order of minutes) and used to torque the gyro gimbals to correct for gyro drift effects. This technique of complimentary filtering combines a gyro sensor with good short time response with the time average of the specific force sensor to obtain a good measure of the vertical.

Inertial sensors of this type with good accuracy (say 5% of the maximum expected unicycle pitch angle of \pm degrees) are quite expensive. If, however, we perform the experiments on a reasonably horizontal floor, we can construct a simple device as shown in Figure 4.1 to prove in principle that a compensator using a vertical reference input, can stabilize the unicycle robot. It measures the frame angle relative to the floor surface by means of a Hall-effect transducer and a small magnet. This sensor is linear for small pitch angles between \pm 5 degrees. Details on the electronic interface and calibration of these transducers are shown in Figures H.15 and H.16 in Appendix H.

The control algorithm was coded in FORTH for the on board microprocessor (section P.3). It uses a sampling period of 25 ms ($f_{sample} = 40$ Hz) as before.

The closed loop system performed excellently during experimental tests. Figure 4.2 shows a plot of the actual pitch angle and wheel speed measurements during a stabilization test at zero commanded wheel speed. Although only twenty seconds of data are shown, the robot can balance until the batteries are run down. The maximum pitch angle is about 0.5 degree and the robot slowly oscillates at a period of approximately 3 seconds while the wheel traverses a distance of \pm 5 cm to keep the wheel axle below the unicycle's center of mass.

The closed loop system has a dominant pole pair at $z = 0.983 \pm j0.0249$ (see PITCHLOPP in section 0.5.1) which corresponds to s -plane poles at $s = 1.2e \pm j2.15$ for

unicycle into the desired direction. He uses his knowledge (gained by experience) of the nonlinear friction characteristics of the wheel on the ground to apply the correct torque profile to end up in the desired direction. Simultaneously, the rider would lean into the turn to counteract the effect of the ground reaction force and the inertia of his body, which would tend to let the rider fall towards the direction that he had been travelling. To emulate just one such a control action on a robot obviously would be prohibitively complex. The goal is therefore to identify and emulate only the most important control actions of a human rider.

The first and probably the most important simplification is that we assume that we can model the human riding on a unicycle with a linear process. Thereby we choose to represent the rider and unicycle by a finite number of connected rigid bodies and assume that the relative angular position and rate motions are small. We also assume that the control torques and other kinematic variables are continuous functions of time. The restriction to a linear system analysis can be changed later to include studies of nonlinear control methods, but it is reasoned that for the initial studies, we should deal with a linear system model. This not only gives insight into the basic issues involved in controlling a unicycle, but also gives access to the most powerful mathematical and control systems techniques available at present. The assumption of a linear system is also not so unrealistic, because experienced unicycle riders do not execute large amplitude motions when traveling in a straight line or while turning slowly.

We believe that the most basic configuration that will represent the major parts and motions of a human on a unicycle consists of three rigid bodies. As shown in the schematic diagram of Figure A.1 it consists of a wheel, a frame to present the unicycle frame and lower part of the rider's body and a rotary turntable which presents the rider's twisting torso and arms. The most important way in which a human rider maintains longitudinal stability is by means of the torques exerted on the pedals of the wheel. The forward and backward leaning action of the rider is of lesser importance and was not implemented in the robot in order to simplify the mechanical design.

Chapter 2

Dynamic Model for the Unicycle Robot

2.1 Dynamics of a human riding a unicycle

The process of a human riding a unicycle is quite complex. Not only does a person use a multitude of sensory inputs to monitor the process, but the control actions themselves are nonlinear. As is the case with most skills learned by a human, many of the control feedback loops are closed at a subconscious level. When we attempt to emulate the process of a human riding a unicycle by a computer stabilized one wheeled robot, we first have to simplify the human's actions into mathematical and mechanical models which can be simulated and implemented in a laboratory.

A person on a unicycle maintains longitudinal stability by pedaling faster or slower, by leaning his torso forward or backward and by moving his arms forward and backward. Lateral stability is obtained by leaning his torso sideways, pulling an arm in or stretching it out and by steering the wheel into the direction that he is falling by twisting motions at the hip joints. Many of these control actions are rather jerky. For example, when a person wants to change direction on a unicycle, he would use his torso and outstretched arms as a reaction inertia to suddenly twist the lower part of his body and the

2.2 Mechanical design of the unicycle robot

The unicycle robot that was designed, consists of three parts: a wheel, a frame on which the drive motors, sensors and electronics are mounted, and a battery pack on top of the frame which can rotate about the vertical axis.

The robot was specifically designed with mass and dimensional properties similar to those of a human riding on a unicycle. This allowed interesting performance comparisons, since the open-loop time constants in the two cases are similar. Although these dimensions and weight make the robot less transportable, it gives the designer more freedom to select equipment without being too concerned about physical size. Enough batteries could also be mounted on the robot to supply electrical power for extended periods of up to two hours of continuous testing without recharging.

Consider a young person of about 50 kg (110 lb) mass. The mass can be roughly divided equally between the body above and below the hips. The upper part of the body that performs the twisting motions will be approximated by a 25 kg cylinder of 0.2 m radius. The moment of inertia about the vertical axis is therefore approximately

$$I_{torso} = \frac{1}{2}MR^2 = 0.5 \text{ kg} \cdot \text{m}^2$$

This compares well with the turntable (battery pack) inertia of $I_3^T = 0.5028 \text{ kg} \cdot \text{m}^2$.

The rider's legs, which are usually slightly bent when resting on the pedals, are approximated by two 12.5 kg cylinders of $r = 8.5 \text{ cm}$ in radius (r) and spaced a distance (d) of 0.1 m apart. The moment of inertia about the vertical centerline between them is given by

$$I_{legs} = 2\left[\frac{1}{2}mr^2 + md^2\right] = 0.34 \text{ kg} \cdot \text{m}^2$$

This inertia is close to the robot's frame plus electronics inertia of $I_3^F = 0.3635 \text{ kg} \cdot \text{m}^2$.

2.1. DYNAMICS OF A HUMAN RIDING A UNICYCLE

7

Observation of a human riding a unicycle shows that lateral stability is obtained largely by continuously twisting the wheel in order to steer towards the direction that he is falling. The ground reaction at the contact point between the wheel and the ground applies a moment to the unicycle which rolls it back to vertical. A turntable mounted on top of the robot with its axis of rotation along the centerline of the unicycle is used to simulate the rider's torso and arms.

We show in Appendix F that the unicycle can be stabilized by sideways leaning actions only, but that the yaw angular momentum is uncontrollable from the lean actuator. We decided to exclude the sideways leaning action from the mechanical robot in order to simplify the construction.

A person uses several sensory systems to monitor the stabilization process while riding a unicycle. The four major sensors used to determine orientation with respect to vertical are the vestibular system, visual system, proprioceptive sensors and tactile sensors [Borah] and [Ormsby]. The vestibular system is the primary orientation system of the human and consists of the semicircular canals (which measure angular velocity of the head) and the otolith organs (which respond to linear accelerations and to changes in orientation with respect to the gravity vector). Proprioceptive cues are obtained from limb position signals and muscle length and tension afferents, from which the brain can infer which dynamic forces are acting on the body, based on the person's experience in coordination. A person can also determine his orientation with respect to vertical from tactile pressure cues on the various parts of his body which are in contact with his environment. Finally eye sight is used, which in combination with a person's experience in deducing the direction of vertical from clues in his environment, gives an indication of his lateral and longitudinal orientation. All these sensory inputs are combined in the human brain to determine the spatial orientation of his body. It is obviously impossible to use sensors on the robot with all the sophistication mentioned above.

robot is shown in Figure 2.1 and more detailed drawings are contained in Appendix L. The microprocessor rack is mounted in the middle of the frame between the two motors and the two servo amplifiers on either side of it on the outside of the frame.

2.3 Dynamics of the unicycle robot

The unicycle robot may be modeled as three interconnected rigid bodies as shown in the schematic diagram of Figure A.1. The various coordinate transformations required to describe the relative angular motions of the three rigid bodies are defined in Figures A.2 and A.3.

In Appendix A the dynamic equations of motion are derived by using Newton-Euler mechanics. Each part of the unicycle is considered as a free rigid body with gravity forces, control torques and reaction forces and torques from adjoining bodies acting on it. It also includes the dynamics of two sensor pendulums R and S mounted to the frame which can freely swing in the longitudinal and lateral directions respectively. The derivations make provision for mounting the sensor pendulums anywhere on the unicycle frame.

The equations are generalized to include the situation where the center of mass of the frame is displaced away from the vertical centerline of the robot. Inclusion of the products of inertia into the dynamic equations of motion would significantly complicate the mathematics. Therefore the robot was designed with its mass distribution as symmetrical as possible about the longitudinal and lateral planes which intersect in the vertical centerline. This would cause the products of inertia to be negligibly small or zero (section 7-2, [Greenwood]). It is assumed that the wheel rolls on the ground without slipping, which places a nonholonomic constraint on the dynamic equations. The dynamic equations are derived for a nonzero nominal turntable speed, which produces coupling between the longitudinal and lateral plant dynamics.

2.2. MECHANICAL DESIGN OF THE UNICYCLE ROBOT

9

The center of mass for the unicycle robot above the wheel axle is given by

$$r^* = \frac{m_{FTF} + m_{TTT}}{m_F + m_T} = 0.63 \text{ m}$$

which would be located at approximately hip height for a rider sitting on a unicycle.

The mechanical parameters of the robot and the measurement methods are given in Appendix M. The calculations above do not include all the inertia properties of the unicycle plus rider, and only serve as an indication that during the robot construction an attempt was made to let the mechanical system approximate the real life situation.

The reader may wonder why the heavy battery pack is placed at the top of the unicycle robot. Placing the center of mass high not only emulates the real case of a human on a unicycle, but is also advantageous from a control systems point of view. If we consider the unicycle as a simple inverted pendulum, the higher the center of mass is, the larger is the fall-down time constant of the open-loop system. This permits a slower sampling frequency in the control microprocessor, so that it has more time to complete the calculations of the balance algorithm. Furthermore, during balance recovery actions, the wheel drive torque has to accelerate the wheel until its axle is below the center of mass of the unicycle. As we show in section L.2 the effective inertia that the torque has to accelerate depends on the height of the center of mass of the superstructure (frame and turntable). When the center of mass of the superstructure is just above the wheel axle height, the control torque has to accelerate almost all of the superstructure's as well as the wheel's inertia during stabilization actions. If, on the other hand, the superstructure's center of mass is high above the wheel axle, only the wheel's inertia needs to be accelerated (see equations L.4 and L.5).

The frame of the robot was made out of aluminum. All of the more complicated parts were made on a numerically coded milling machine to provide a light but rigid structure to which the motors, gear systems, servo amplifiers, computer rack, sensor electronics and the rotary battery pack could be mounted. A drawing of the unicycle

equal to zero for the whole unicycle.

- set the vertical component of the moment about the vertical centerline equal to zero for the whole unicycle and include the applied ground friction torque.
- set the moment about the axle of the wheel equal to zero for the frame plus turntable and include the applied torque Q_W and wheel drive friction torque.
- set the moment about the axle of the turntable equal to zero for the turntable and include the applied torque Q_T and the turntable drive friction torque.

The resulting equations in sections C.2 and C.3 serve as an additional confirmation that the dynamic model for the system is derived correctly.

2.4 Selection of actuators and the drive system

One of the aims of this research project was to build a robot that can stabilize itself without any connections to its environment other than the wheel touching the ground. Therefore both its actuators and power source should be on-board. Direct current motors and batteries offer a convenient solution to this requirement.

The choice between direct drive or geared drive systems was dictated by cost. While the former offers advantages of a simpler mechanical design and none of the nonlinearities associated with geared drive systems, these motors were too expensive for the budget of the project. The direct current servo motors (Infranor) that were selected have low inertia armatures which allows high angular acceleration of the rotor and can run at low speeds with full output torque and no cogging. A 316 watt motor was selected for the wheel drive system because the robot is expected to stabilize itself while continuously running at a forward speed as high as 3 meters per second (10 km/h). A smaller 151 watt motor was selected for the turntable drive system. The maximum speeds for these motors are 7000 and 10 000 revolutions per minute for the large and small motor respectively.

2.3. DYNAMICS OF THE UNICYCLE ROBOT

11

The dynamic equations for the three parts of the unicycle with the two sensor pendulums are obtained after eliminating all the internal reaction forces and moments. It results in an eleventh order system with two forcing functions, the wheel torque and the turntable torque. The equations are summarized in section A.12 and presented in state space form in Appendix D.

As a means of checking the equations of motion, the derivation was repeated by using Lagrange's equations in Appendix B. This method is based on the physical principle that the time rate of change of the scalar generalized momentum p_i is equal to the generalized force Q_i due to the applied forces plus an inertial generalized force due to motion in the other generalized coordinates (section 6-6, [Greenwood]). Often the Q_i 's are derivable from a potential function, which is the potential energy of the unicycle in the gravity field of earth, in the present case. This method avoids the need to eliminate all the reaction forces as in Appendix A. The no-slip condition on the wheel is a nonholonomic constraint equation and is included into Lagrange's equation as shown in section B.3.1.

In the Lagrange's method derivation, we did not include the sensor pendulums and asymmetry of the frame since we only wanted to check the dynamic equations of motion. The summary of the dynamic equations of section B.4 indeed confirms that the previous equations are correct.

A third very useful method for checking the dynamic equations of motion is described in Appendix C. It is based on D'Alembert's principle which states that the laws of static equilibrium apply to a dynamical system if the inertial forces, as well as the actual external forces, are considered as applied forces acting on the system (section 1-5, [Greenwood]). After determining the D'Alembert forces, D'Alembert torques and gravitational forces on the three parts of the unicycle, the following procedure ([Bryson 3]) provides the dynamic equations of motion:

- set the two horizontal components of the moment about the ground contact point

A precision cable and polyurethane chain drive system and aluminum gears were used to reduce the motor speeds and increase the motor torques. This system requires no lubrication and the gear ratios can easily be adjusted by using different belt and gear sizes. An effort was made to select optimum gear ratios for the drive systems. For the wheel drive system it is desirable to select a gear ratio which matches the motor rotor inertia to the effective inertia of the longitudinal system dynamics, so that maximum wheel acceleration can be obtained. This will enable the quickest recovery from longitudinal balance disturbances. Appendix K shows how the wheel acceleration as a function of the gear ratio can be derived from the dynamic equations of motion. For the robot parameters listed in Appendix M, a 24:1 gear reduction is near the optimum value for the wheel drive system.

Lateral system stability is maintained by continuously steering into the direction that the unicycle is falling. The optimal gear ratio for the turntable drive system would therefore be the ratio that gives maximum yaw acceleration. Appendix G uses the lateral system dynamic equations of motion and plant parameters to calculate that the optimal gear ratio would be approximately 72:1. The practical limitations of the three stage gear reduction system that was constructed limited the gear ratio to 60:1, but this results in a maximum yaw acceleration that is 98% of the optimum.

Pulse width modulated amplifiers ([Galil Motion]) were used to drive the servo motors. The particular models that were used modulate the 48 V d.c. supply from the batteries to supply a regulated current to the motors. They can continuously supply 10 A to each motor. The servo amplifier receives a reference voltage from the digital-to-analog interface card in the on-board microprocessor, which commands a torque in the motor. The digital computer interface electronics is described in more detail in Appendix L.

2.5 Selection and construction of sensors

The control system needs information on the angular rates of the wheel and the turntable relative to the frame. The turntable speed can be very low and tachometers give poor results at low angular rates. It was therefore decided to use position encoders on the motor rotor shafts to obtain angular velocity information. This method, which is described in detail in Appendix I, uses a high frequency clock to count the number of clock pulses during each pulse from the position encoder as it rotates. The pulse count can then be inverted in the microprocessor to obtain angular velocity information. This method can provide high resolution angular rate information by the appropriate selection of the counter clock frequency and counter register length.

Several balance sensors were considered. As we will show in a later chapter, the ideal sensors would measure the pitch and roll angles of the unicycle with respect to vertical. Instruments which can indicate vertical in the presence of external accelerations other than gravity on the instrument are quite complex [Wrigley]. Vertical gyros, free gyros and optical vertical reference systems can provide this information, but all of these were too expensive for the budget of the project.

Passive sensor pendulums were considered as a means of obtaining vertical reference. All the modes of the unicycle dynamic system are theoretically available from the measurement of the passive sensor pendulum angles relative to the unicycle frame. Unfortunately the commercial instruments of this type do not have the required resolution and some of their parameters (eg. damping factor) are temperature dependent. Furthermore, it is shown in Appendix E that the inverted pendulum modes can be unobservable if the passive sensor pendulums are mounted at the wrong heights.

Rate gyros can be used to measure roll and pitch rates. The inverted pendulum modes are observable from these measurements, but unfortunately these instruments are also fairly expensive.

Analyses in section N.3 and Q.3 show that the inverted pendulum modes are observable from measurements of accelerometers mounted on the unicycle frame. We decided to use this type of sensor because it would allow the robot to ride on inclined terrain and accelerometers of adequate sensitivity could be constructed at an affordable cost. Simulations have shown (see later chapters) that the maximum lateral and longitudinal accelerations are in the order of 0.1 m/s^2 . Appendix H describes how servo accelerometers with an accuracy of about 0.0033 m/s^2 were constructed by careful mechanical, optical and electronic design.

If we are prepared to do tests on horizontal surfaces only, the unicycle can pull a light carriage with position sensors to measure the roll and pitch angles directly. We constructed such a sensor by means of a small magnet and a Hall effect transistor to measure the unicycle frame's pitch angle relative to a horizontal floor surface. This provided an inexpensive way to demonstrate experimentally that the unicycle robot could be stabilized if the vertical orientation information was available to the control system.

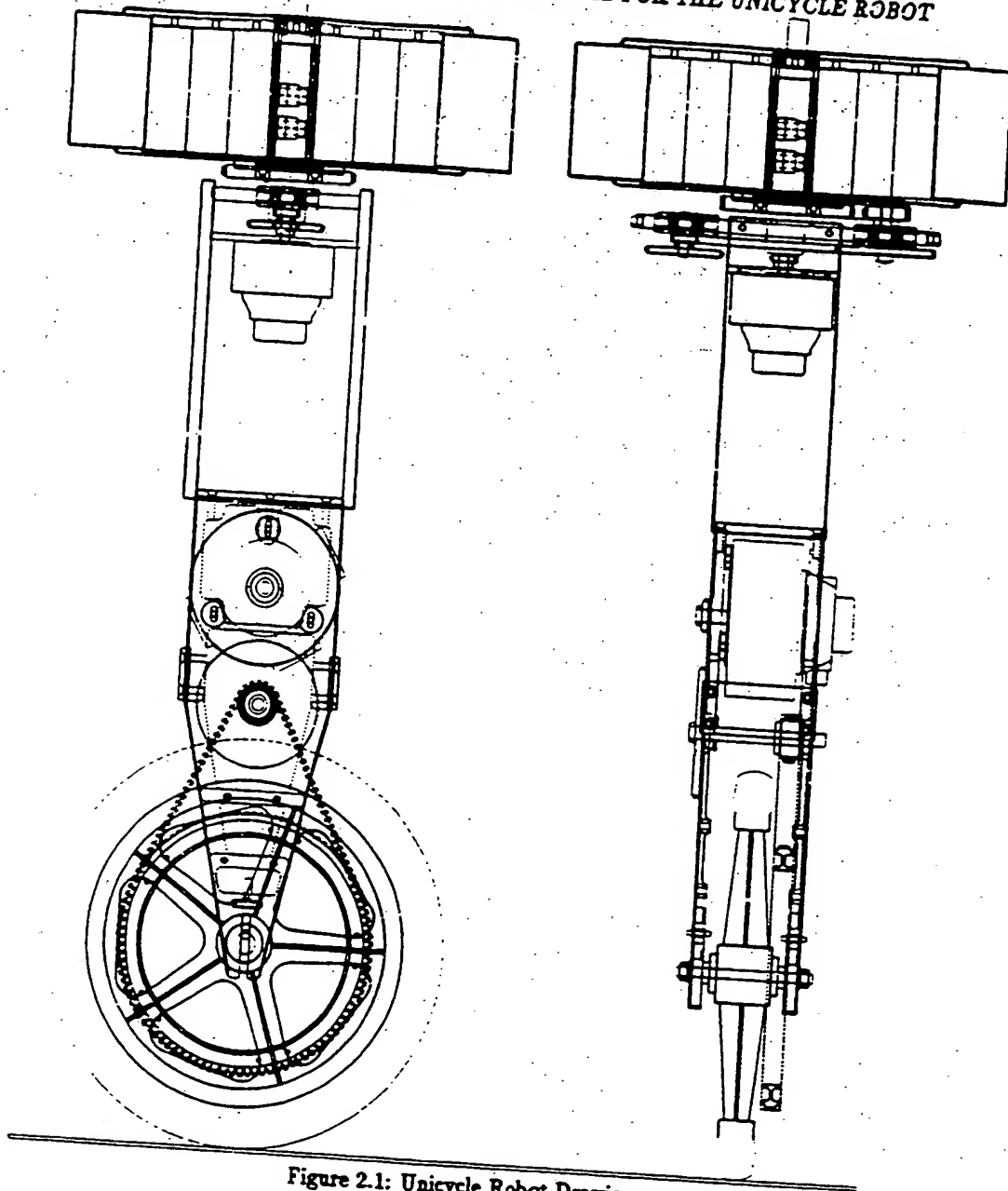


Figure 2.1: Unicycle Robot Drawing

Chapter 3

Longitudinal System with Accelerometer Sensor

3.1 Introduction

A significant simplification of the control system design can be obtained if the lateral and longitudinal system dynamics can be decoupled. Inspection of the system dynamic equations presented at the end of Appendix A, shows that it is indeed possible to decouple the lateral and longitudinal dynamics if the nominal turntable angular rotation speed η_0 is zero and the unicycle frame has left-right symmetry about a vertical plane, i.e. $r_1 = r_2 = 0$. The first requirement implies that the turntable rotation speeds should always be so slow that the gyroscopic effect of this rotating inertia does not significantly couple lateral motions into the longitudinal dynamics. Previous research efforts [Iguchi] have in fact used a fast rotating gyro on the unicycle to slow down the time constants associated with the falling down of the unicycle. Since the purpose of this thesis is to emulate the control method of a human riding a unicycle, where this form of gyroscopic stabilization is absent, the requirement that η_0 must be zero is compatible with the goal of this research.

The second requirement that the center of mass of the unicycle must be on the line

18 CHAPTER 3. LONGITUDINAL SYSTEM WITH ACCELEROMETER SENSOR

of geometric symmetry has been met by the mechanical design and construction of the robot as discussed in the previous chapter.

The dynamic equations of motion for the decoupled longitudinal system are given in Appendix N, equations N.3 and N.4. The pitch angle θ , the wheel perturbation speed Ω and the wheel drive torque Q_w are the variables associated with the longitudinal system dynamics.

3.2 Longitudinal system characteristics

After substituting the measured mechanical parameters into the dynamic equations, we can determine the longitudinal system characteristics. As shown in section N.3 the eigenvalues of the openloop system consist of two poles at approximately plus and minus 7 rad/s in the s-plane. The unstable pole is associated with the inverted pendulum mode of the unicycle, when it falls forward or backward. The third eigenvalue near the origin of the s-plane corresponds to the rigid body horizontal velocity mode for the unicycle as a whole. The fourth mode associated with the wheel's angular position is not shown because we do not intend to control the unicycle's position. Inspection of the modal controllability matrix shows that all modes are controllable from the wheel torque.

A tachometer is mounted on the wheel drive motor shaft. We assume that drive belt elasticity and backlash are negligible so that the tachometer measures the relative speed between the wheel and the unicycle frame. The transfer function from the motor torque to the tachometer measurement has two zeros at approximately plus and minus 2.8 rad/s. The physical meaning of the zero locations can be interpreted after a few calculations:

Simplify equations N.3 and N.4 to

$$I_{11}\ddot{\theta} + I_{12}\ddot{\Omega} = J\dot{\theta} - Q_w \quad (3.1)$$

$$I_{12}\ddot{\theta} + I_{22}\ddot{\Omega} = Q_w \quad (3.2)$$

3.2. LONGITUDINAL SYSTEM CHARACTERISTICS

19

The viscous friction constant f_v has been ignored since it has no effect on the zero locations.

Since the tachometer reading is

$$y_t = \Omega - \dot{\theta} \quad (3.3)$$

we can rewrite equations 3.1 and 3.2 to

$$(I_{11} + I_{12})\ddot{\theta} + I_{12}\dot{y}_t = J\dot{\theta} - Q_W \quad (3.4)$$

$$(I_{12} + I_{22})\ddot{\theta} + I_{22}\dot{y}_t = Q_W \quad (3.5)$$

Take the Laplace transform of the above two equations, eliminate $\Theta(s)$ and solve

$$\frac{Y_t(s)}{Q_W(s)} = \frac{(I_{11} + 2I_{12} + I_{22})s^2 - J}{s[(I_{11}I_{22} - I_{12}^2)s^2 - JI_{22}]} \quad (3.6)$$

The zero locations are at

$$\begin{aligned} s &= \pm \sqrt{\frac{J}{I_{11} + 2I_{12} + I_{22}}} \\ &= \pm \sqrt{\frac{(m_F r_F + m_T r_T)g}{I_2^W + m_W r_W^2 + I_2^F + m_F(r_W + r_F)^2 + I_2^T + m_T(r_W + r_T)^2}} \end{aligned} \quad (3.7)$$

If we close a tachometer feedback loop with proportional feedback and command a tachometer speed y_c

$$Q_W = K(y_c - y_t) \quad (3.8)$$

the root loci of two of the closed loop poles approach the zero locations and the other closed loop pole moves to infinity as K becomes large. This implies that with the tightest feedback loop closed on the tachometer measurement, the time constant associated with the instability of the longitudinal system can at best be lengthened to that at the zero locations. With a tight feedback loop a command of $y_c = 0$ implies no relative movement between the wheel and the frame. In this locked wheel situation the unicycle falls over more slowly (longer time constant) than the free wheel condition (shorter time constant associated with the open loop pole positions). Notice that equation 3.7 gives

20 CHAPTER 3. LONGITUDINAL SYSTEM WITH ACCELEROMETER SENSOR

exactly the eigenvalues associated with a unicycle pitching over with a locked wheel.

An accelerometer mounted on the unicycle frame measures the specific force at the point where it is located. Its output is a signal given by equation N.16:

$$y_a(t) = g\theta - r_w\ddot{\Omega} - r_{R3}\ddot{\theta} \quad (3.9)$$

where r_w is the wheel radius and r_{R3} is the height above the wheel axle where the accelerometer is located. The transfer function from the wheel torque to the accelerometer output has an equal number of poles and zeros (3) due to the direct feedthrough term from the wheel torque to the accelerometer measurement (see equation N.16). One of the zeros is at the origin of the s -plane and the locations of the other two zeros vary as a function of the accelerometer height r_{R3} . The locations of these zeros have a significant effect on the closed loop system behaviour and we now proceed to determine these zero locations.

The transfer functions $\frac{\theta(s)}{Q_w(s)}$ and $\frac{\Omega(s)}{Q_w(s)}$ can be calculated from the longitudinal system equations 3.1 and 3.2:

$$\frac{\Omega(s)}{Q_w(s)} = \frac{(I_{11} + I_{12})s^2 - J}{s[(I_{11}I_{22} - I_{12}^2)s^2 - JI_{22}]} \quad (3.10)$$

$$\frac{\theta(s)}{Q_w(s)} = \frac{-(I_{22} + I_{12})s}{s[(I_{11}I_{22} - I_{12}^2)s^2 - JI_{22}]} \quad (3.11)$$

Laplace transform 3.9 and substitute 3.10 and 3.11 into it:

$$\frac{Y_a(s)}{Q_w(s)} = \frac{s\{[(I_{12} + I_{22})r_{R3} - (I_{11} + I_{12})r_w]s^2 + r_wJ - g(I_{12} + I_{22})\}}{s[(I_{11}I_{22} - I_{12}^2)s^2 - JI_{22}]} \quad (3.12)$$

For the case with nonzero friction, the pole will not be exactly at $s = 0$ and thus will not be canceled by the zero at the origin.

The zeros of the accelerometer transfer function are given by

$$s = 0$$

$$\text{and } s = \pm j \sqrt{\frac{g(I_{12} + I_{22}) - r_wJ}{(I_{11} + I_{12})r_w - (I_{12} + I_{22})r_{R3}}} \quad (3.13)$$

3.2. LONGITUDINAL SYSTEM CHARACTERISTICS

21

By substitution of the parameters from Appendix M into the equation above we see that the pair of zeros are at infinity for the accelerometer mounted at the critical height of

$$\begin{aligned}(r_{R3})_{\infty} &= \frac{(I_{11} + I_{12})r_W}{(I_{12} + I_{22})} \\ &= 0.6675 \text{ m}\end{aligned}\tag{3.14}$$

If an accelerometer were placed at $r_{R3} = (r_{R3})_{\infty}$, it would have zero initial response to an impulse on the wheel torque. With the accelerometer at this height the direct feedthrough term from the control torque Q_W to the accelerometer output y_a becomes zero. It is confirmed by equation N.16 where the coefficient of Q_W , namely $r_{R3}G_1 + r_W G_2$, vanishes when $r_{R3} = (r_{R3})_{\infty}$.

For $r_{R3} < (r_{R3})_{\infty}$ the accelerometer transfer function has a pair of complex zeros and for $r_{R3} > (r_{R3})_{\infty}$ the zeros are on the positive and negative real axis. The location of the zeros is thus very sensitive to small deviations in r_{R3} if r_{R3} is in the vicinity of $(r_{R3})_{\infty}$.

Another undesirable situation occurs when r_{R3} is such that the accelerometer zeros cancel the inverted pendulum poles of the plant. These modes then become unobservable from the accelerometer measurement, which defeats the purpose for which the accelerometer was used in the first place. We can solve for this critical height from equation 3.12:

$$\begin{aligned}(r_{R3})_{\text{unobs}} &= \frac{JI_{12}r_W + (I_{11}I_{22} - I_{12}^2)g}{JI_{22}} \\ &= 0.721 \text{ m}\end{aligned}\tag{3.15}$$

The physical explanation for the existence of this point of unobservability is that, if the unicycle was allowed to fall over in the plane of the wheel, this point would move straight down, i.e. it would have no horizontal acceleration. If we think of the spring-mass analogy of the accelerometer, it is clear that such an instrument mounted at this height, with its sensitive axis pointing along the direction of the unicycle travel, will

22 CHAPTER 3. LONGITUDINAL SYSTEM WITH ACCELEROMETER SENSOR

have a zero output. An accelerometer mounted at this point on the unicycle is analogous to the case where an accelerometer is mounted on the bob of a simple pendulum.

A method to identify the longitudinal system dynamic model experimentally is described in section N.3.2. One of the problems of identifying an unstable plant is that its variables do not stay within small perturbation ranges for very long (in the order of one second in this case). The small angles assumption is basic to deriving a valid linearized model for the unicycle dynamics (Appendices A, B and C). A partial identification of the system transfer functions was obtained by hanging the unicycle upside down by its wheel. The dynamic model then changes from an inverted to an ordinary pendulum to which we can apply sinusoidal test signals and measure frequency responses. In section N.3.2 the conclusion is drawn that the actual plant model is acceptably close to the theoretical model because their frequency responses agree to within 2 dB in gain and 10 degrees in phase over the frequency spectrum of signals present in the dynamic system during typical maneuvers.

3.3 Compensator design by successive loop closure

3.3.1 Nominal design

Control systems designed by successive loop closure techniques can produce compensators of low order. This is advantageous when the compensator is implemented in a microprocessor, which takes a finite time to calculate the control command. The shorter this time is, the faster sampling rate can be used, which usually improves the quality of the dynamic response. Several other considerations for the sampling rate selection are discussed in section O.1.

The longitudinal dynamics are modified to include the delay time between the instant that the measurements are made and the time that the control command is issued (see section N.3.2).

The translational kinetic energy of the wheel is:

$$\begin{aligned} T_W^{tr} &= \frac{1}{2} m_W \dot{\vec{r}}_0 \cdot \dot{\vec{r}}_0 \\ &= \frac{1}{2} m_W [\dot{x}^2 + \dot{y}^2 + r_W^2 \dot{\phi}^2 + r_W^2 \dot{\psi}^2 s^2 \phi \\ &\quad + 2r_W \dot{x}(\phi c \phi s \psi + \psi s \phi c \psi) - 2r_W \dot{y}(\psi s \phi s \psi - \phi c \phi c \psi)] \end{aligned}$$

2. Rotational kinetic energy of the wheel:

absolute angular velocity of the wheel is:

$$\begin{aligned} \vec{\omega}^W &= \dot{\psi} \vec{a}_3 + \dot{\phi} \vec{b}_1 + \dot{\omega} \vec{w}_2 \\ &= \dot{\phi} \vec{w}_1 + (\dot{\omega} + \dot{\psi} s \phi) \vec{w}_2 + \dot{\psi} c \phi \vec{w}_3 \end{aligned} \quad (B.9)$$

The rotational kinetic energy of the wheel is:

$$T_W^{rot} = \frac{1}{2} I_1^W \dot{\phi}^2 + \frac{1}{2} I_2^W (\dot{\omega} + \dot{\psi} s \phi)^2 + \frac{1}{2} I_3^W \dot{\psi}^2 c^2 \phi \quad (B.10)$$

3. Potential energy of the wheel:

$$\begin{aligned} V_W &= m_W g z_0 \\ &= m_W g r_W c \phi \end{aligned} \quad (B.11)$$

B.2 Frame

1. Translational kinetic energy of the frame:

The position vector from the origin of the inertial reference frame to the center of mass of the frame is:

$$\begin{aligned} \vec{r}_F &= \vec{r}_0 + r_F \vec{f}_3 \\ &= [x + (r_W + r_{Fc \theta}) s \phi s \psi + r_{Fs \theta} c \psi] \vec{a}_1 \\ &\quad + [y - (r_W + r_{Fc \theta}) s \phi c \psi + r_{Fs \theta} s \psi] \vec{a}_2 \\ &\quad + [(r_W + r_{Fc \theta}) c \phi] \vec{a}_3 \end{aligned} \quad (B.12)$$

$$\dot{\vec{r}}_F = \dot{x} \vec{a}_1 + \dot{y} \vec{a}_2 + \dot{z} \vec{a}_3 \quad (B.13)$$

APPENDIX B. EOMS BY USING LAGRANGE'S METHOD

where:

$$\begin{aligned} \dot{x}_F &= \dot{x} + r_W(\dot{\phi}c\phi s\psi + \dot{\psi}s\phi c\psi) \\ &+ r_F[\dot{\theta}(c\theta c\psi - s\theta s\phi s\psi) + \dot{\psi}(c\theta s\phi c\psi - s\theta s\psi) + \dot{\phi}c\theta c\phi s\psi] \end{aligned} \quad (B.14)$$

$$\begin{aligned} \dot{y}_F &= \dot{y} + r_W(\dot{\psi}s\phi s\psi - \dot{\phi}c\phi c\psi) \\ &+ r_F[\dot{\theta}(s\theta s\phi c\psi + c\theta s\psi) + \dot{\psi}(s\theta c\psi + c\theta s\phi s\psi) - \dot{\phi}c\theta c\phi c\psi] \end{aligned} \quad (B.15)$$

$$\dot{z}_F = -r_W\dot{\phi}s\phi - r_F(\dot{\theta}s\theta c\phi + \dot{\phi}c\theta s\phi) \quad (B.16)$$

The translational kinetic energy of the frame is

$$T_F^tr = \frac{1}{2}m_F(\dot{x}_F^2 + \dot{y}_F^2 + \dot{z}_F^2) \quad (B.17)$$

2. Rotational kinetic energy of the frame:

The absolute angular velocity of the frame is:

$$\begin{aligned} {}^A\vec{\omega}^F &= \dot{\psi}\hat{a}_3 + \dot{\phi}\hat{b}_1 + \dot{\theta}\hat{f}_2 \\ &= (\dot{\phi}c\theta - \dot{\psi}c\phi s\theta)\hat{f}_1 + (\dot{\theta} + \dot{\psi}s\phi)\hat{f}_2 + (\dot{\phi}s\theta + \dot{\psi}c\phi c\theta)\hat{f}_3 \end{aligned} \quad (B.18)$$

The rotational kinetic energy of the frame is:

$$\begin{aligned} T_F^{rot} &= \frac{1}{2}I_1^F(\dot{\phi}c\theta - \dot{\psi}c\phi s\theta)^2 + \frac{1}{2}I_2^F(\dot{\theta} + \dot{\psi}s\phi)^2 \\ &+ \frac{1}{2}I_3^F(\dot{\phi}s\theta + \dot{\psi}c\phi c\theta)^2 \end{aligned} \quad (B.19)$$

3. Potential energy of the frame:

$$\begin{aligned} V_F &= m_W g z_F \\ &= m_F g (r_W + r_F c\theta) c\phi \end{aligned} \quad (B.20)$$

B.3 Turntable

1. Translational kinetic energy of the turntable:

The translational kinetic energy of the turntable can be found by simply substituting r_H for r_F in equations B.13 through B.17:

$$\begin{aligned} \dot{x}_T &= \dot{x} + r_W(\dot{\phi}c\phi s\psi + \dot{\psi}s\phi c\psi) \\ &+ r_T[\dot{\theta}(c\theta c\psi - s\theta s\phi s\psi) + \dot{\psi}(c\theta s\phi c\psi - s\theta s\psi) + \dot{\phi}c\theta c\phi c\psi] \end{aligned} \quad (B.21)$$

$$\begin{aligned} \dot{y}_T &= \dot{y} + r_W(\dot{\psi}s\phi s\psi - \dot{\phi}c\phi c\psi) \\ &+ r_T[\dot{\theta}(s\theta s\phi c\psi + c\theta s\psi) + \dot{\psi}(s\theta c\psi + c\theta s\phi s\psi) - \dot{\phi}c\theta c\phi c\psi] \end{aligned} \quad (B.22)$$

$$\dot{z}_T = -r_W\dot{\phi}s\phi - r_T(\dot{\theta}s\theta c\phi + \dot{\phi}c\theta s\phi) \quad (B.23)$$

The translational kinetic energy of the turntable is

$$T_T^T = \frac{1}{2}m_T(\dot{x}_T^2 + \dot{y}_T^2 + \dot{z}_T^2) \quad (B.24)$$

2. Rotational kinetic energy of the turntable:

the absolute angular velocity of the turntable is:

$$\begin{aligned} \mathbf{A}^T_T &= \mathbf{A}^F_T + \dot{\nu}\hat{f}_3 \\ &= (\dot{\psi}c\theta - \dot{\phi}c\phi s\theta)\hat{f}_1 + (\dot{\theta} + \dot{\psi}s\phi)\hat{f}_2 + (\dot{\phi}s\theta + \dot{\psi}c\phi c\theta + \dot{\nu})\hat{f}_3 \end{aligned} \quad (B.25)$$

The rotational kinetic energy of the turntable is:

$$\begin{aligned} T_T^R &= \frac{1}{2}I_1^T(\dot{\psi}c\theta - \dot{\phi}c\phi s\theta)^2 + \frac{1}{2}I_2^T(\dot{\theta} + \dot{\psi}s\phi)^2 \\ &+ \frac{1}{2}I_3^T(\dot{\phi}s\theta + \dot{\psi}c\phi c\theta + \dot{\nu})^2 \end{aligned} \quad (B.26)$$

3. Potential energy of the turntable:

The potential kinetic energy of the turntable can be found by substituting r_T for r_F in equation B.20:

$$V_F = m_T g(r_W + r_T c\theta) c\phi \quad (B.27)$$

B.3.1 The Lagrangian and Lagrange's equation

The Lagrangian is

$$L = T_{tot} - V_{tot} \quad (B.28)$$

and Lagrange's equation for a system with n generalized coordinates, q_i , and m nonholonomic constraint equations, ϕ_j , is:

$$\frac{d}{dt} \left(\frac{\partial L}{\partial \dot{q}_i} \right) - \frac{\partial L}{\partial q_i} = \sum_{j=1}^m \lambda_j a_{ji} + Q_i \quad (B.29)$$

(for $i = 1, 2, \dots, n$)

where Q_i are the generalized forces which are not derivable from a potential function (the applied torques from the motors and friction in this case)

$$a_{ji} \equiv \frac{\partial \phi_j}{\partial \dot{q}_i} \quad (B.30)$$

where ϕ_j are the constraint equations of the system.

See [Greenwood] chapter 6, [Pars] chapters 6 through 8, [Rosenberg] chapter 15 and [Whittaker] chapter 2 for details.

Note:

It would be tempting to substitute \dot{x} and \dot{y} from the constraint equations B.2 into the kinetic energy terms, in order to eliminate two of the generalized coordinates (x and y) and simplify the system of equations.

As pointed out in [Rosenberg], chapter 14, this will lead to the wrong answer since the constraint equations are nonholonomic (not integrable). Embedding of constraint equations are only possible with holonomic constraint equations. Trying to embed nonholonomic constraint equations to eliminate the use of Lagrange multipliers violates the dynamical principles on which the derivation of Lagrange's equations are based (the principle of work done during virtual displacements).

Simplify the expressions for the total translational kinetic energy by defining:

$$A_x \equiv \dot{z} + r_W(\dot{\phi}c\phi s\psi + \dot{\psi}s\phi c\psi) \quad (\text{B.31})$$

$$B_x \equiv \dot{\theta}(c\theta c\psi - s\theta s\phi s\psi) + \dot{\psi}(c\theta s\phi c\psi - s\theta s\psi) + \dot{\phi}c\theta c\phi s\psi \quad (\text{B.32})$$

$$A_y \equiv \dot{y} + r_W(\dot{\psi}s\phi s\psi + \dot{\phi}c\phi c\psi) \quad (\text{B.33})$$

$$B_y \equiv \dot{\theta}(s\theta s\phi c\psi - c\theta s\psi) + \dot{\psi}(s\theta c\psi + c\theta s\phi s\psi) - \dot{\phi}c\theta c\phi c\psi \quad (\text{B.34})$$

$$A_z \equiv r_W\dot{\phi}s\phi \quad (\text{B.35})$$

$$B_z \equiv -(\dot{\theta}s\theta c\phi + \dot{\phi}c\theta s\phi) \quad (\text{B.36})$$

The total translational kinetic energy then becomes:

$$\begin{aligned} T_{\text{tot}}^{\text{tr}} &= T_W^{\text{tr}} + T_F^{\text{tr}} + T_T^{\text{tr}} \\ &= \frac{1}{2}(m_W + m_F + m_T)(A_x^2 + A_y^2 + A_z^2) \\ &\quad + (m_F r_F + m_T r_T)(A_x B_x + A_y B_y + A_z B_z) \\ &\quad + \frac{1}{2}(m_F r_F^2 + m_T r_T^2)(B_x^2 + B_y^2 + B_z^2) \end{aligned} \quad (\text{B.37})$$

The total rotational kinetic energy is:

$$\begin{aligned} T_{\text{tot}}^{\text{rot}} &= \frac{1}{2}I_1^W \dot{\phi}^2 + \frac{1}{2}I_2^W (\dot{\psi} + \dot{\psi}s\phi)^2 + \frac{1}{2}I_3^W \dot{\psi}^2 c^2\phi \\ &\quad + \frac{1}{2}(I_1^F + I_1^T)(\dot{\phi}c\theta - \dot{\psi}c\phi s\theta)^2 + \frac{1}{2}(I_2^F + I_2^T)(\dot{\theta} + \dot{\psi}s\phi)^2 \\ &\quad + \frac{1}{2}(I_3^F + I_3^T)(\dot{\phi}s\theta + \dot{\psi}c\phi c\theta)^2 \\ &\quad + \frac{1}{2}I_3^T[2\dot{\psi}(\dot{\phi}s\theta + \dot{\psi}c\phi c\theta) + \dot{\nu}^2] \end{aligned} \quad (\text{B.38})$$

The negative of the total potential energy is

$$-V_{\text{tot}} = -(m_W + m_F + m_T)r_W g c\phi - (m_F r_F + m_T r_T)g c\theta c\phi \quad (\text{B.39})$$

APPENDIX B: EOMS BY USING LAGRANGE'S METHOD

define:

$$m_{tot} = m_W + m_F + m_T \quad (B.40)$$

$$m_1 = m_F r_F + m_T r_T \quad (B.41)$$

$$m_2 = m_F r_F^2 + m_T r_T^2 \quad (B.42)$$

The Lagrangian then becomes:

$$\begin{aligned} L &= T_{tot}^{tr} + T_{tot}^{rot} - V_{tot} \\ &= \frac{1}{2} m_{tot} (A_x^2 + A_y^2 + A_z^2) + m_1 (A_x B_x + A_y B_y + A_z B_z) \\ &\quad + \frac{1}{2} m_2 (B_x^2 + B_y^2 + B_z^2) \\ &\quad + \frac{1}{2} I_1^W (\dot{\phi}^2 + \frac{1}{2} I_2^W (\dot{\psi} + \dot{\psi}_s \phi)^2 + \frac{1}{2} I_3^W \dot{\psi}^2 \epsilon^2 \phi) \\ &\quad + \frac{1}{2} (I_1^F + I_1^T) (\dot{\phi} c \theta - \dot{\psi} c \phi s \theta)^2 + \frac{1}{2} (I_2^F + I_2^T) (\dot{\theta} + \dot{\psi}_s \phi)^2 \\ &\quad + \frac{1}{2} (I_3^F + I_3^T) (\dot{\phi} s \theta + \dot{\psi} c \phi c \theta)^2 + \frac{1}{2} I_3^T [2i (\dot{\phi} s \theta + \dot{\psi} c \phi c \theta) + i^2] \\ &\quad - m_{tot} r_W g c \phi - m_1 g c \theta c \phi \end{aligned} \quad (B.43)$$

Substitute the Lagrangian into Lagrange's equation for each of the generalized coordinates.

Under stabilized conditions, the angles θ and ϕ and their derivatives are small. The small angle approximations in $\phi \cong \phi$, $\cos \phi \cong 1$, $\theta \phi \cong 0$ etc. are used to simplify the equations.

1. $q_1 = x$:

$$\begin{aligned} \frac{\partial L}{\partial \dot{x}} &= m_{tot} (A_x) + m_1 B_x \\ &\cong m_{tot} [\dot{x} + r_W (\dot{\phi} s \psi + \dot{\psi} \phi c \psi)] + m_1 [\dot{\theta} c \psi + \dot{\psi} (\phi c \psi - \theta s \psi) + \dot{\phi} s \psi] \end{aligned} \quad (B.44)$$

$$\frac{d}{dt} \left(\frac{\partial L}{\partial \dot{x}} \right) \cong m_{tot}(\ddot{x} + r_W \ddot{\phi} s \psi) + m_1(\ddot{\theta} c \psi + \dot{\phi} s \dot{\psi}) \quad (B.45)$$

where the assumption $\dot{\psi}, \ddot{\psi} \ll 1$ has been used to simplify the equation.

$$\frac{\partial L}{\partial x} = 0 \quad (B.46)$$

from equations B.3 and B.4

$$a_{11} = 1 \quad (B.47)$$

$$a_{12} = 0 \quad (B.48)$$

substitute into Lagrange's equation:

$$m_{tot}(\ddot{x} + r_W \ddot{\phi} s \psi) + m_1(\ddot{\theta} c \psi + \dot{\phi} s \dot{\psi}) = \lambda_1 \quad (B.49)$$

2. $q_2 = y$:

$$\begin{aligned} \frac{\partial L}{\partial \dot{y}} &= m_{tot}(A_y) + m_1 B_y \\ &\cong m_{tot}[\dot{y} + r_W(\dot{\psi} \phi s \psi + \dot{\phi} c \psi)] + m_1[\dot{\theta} s \psi + \dot{\psi}(\theta c \psi - \phi s \psi) - \dot{\phi} c \psi] \end{aligned} \quad (B.50)$$

$$\frac{d}{dt} \left(\frac{\partial L}{\partial \dot{y}} \right) \cong m_{tot}(\ddot{y} - r_W \ddot{\phi} c \psi) + m_1(\ddot{\theta} s \psi - \dot{\phi} c \dot{\psi}) \quad (B.51)$$

$$\frac{\partial L}{\partial y} = 0 \quad (B.52)$$

$$a_{12} = 0 \quad (B.53)$$

$$a_{22} = 1 \quad (B.54)$$

substitute into Lagrange's equation:

$$m_{tot}(\ddot{y} - r_W \ddot{\phi} c \psi) + m_1(\ddot{\theta} s \psi - \dot{\phi} c \dot{\psi}) = \lambda_2 \quad (B.55)$$

APPENDIX B. EOMS BY USING LAGRANGE'S METHOD

3. $q_3 = \bar{w}$:

$$\frac{\partial L}{\partial \bar{w}} = I_2^W (\ddot{w} + \dot{w}s\phi) \quad (B.56)$$

$$\begin{aligned} \frac{d}{dt} \left(\frac{\partial L}{\partial \dot{\bar{w}}} \right) &\cong I_2^W (\ddot{w} + \dot{w}s\phi + \dot{\phi}c\phi) \\ &\cong I_2^W \ddot{w} \end{aligned} \quad (B.57)$$

$$\frac{\partial L}{\partial \bar{w}} = 0 \quad (B.58)$$

$$a_{13} = -r_W c\phi \quad (B.59)$$

$$a_{23} = -r_W s\phi \quad (B.60)$$

$$Q_w = Q_W \quad (B.61)$$

substitute into Lagrange's equation:

$$I_2^W \ddot{w} = -r_W c\phi \lambda_1 - r_W s\phi \lambda_2 + Q_W \quad (B.62)$$

4. $q_4 = \phi$:

$$\begin{aligned} \frac{\partial L}{\partial \phi} &= m_{tot}(A_x r_W s\phi - A_y r_W c\phi) \\ &\cong (m_{tot} r_W + m_1)(A_x s\phi - A_y c\phi) + (m_1 r_W + m_2)(B_x s\phi - B_y c\phi) \\ &\quad + I_1^W \dot{\phi} + (I_1^F + I_1^T)(\dot{\phi} - \dot{\psi}\theta) + (I_3^F + I_3^T)\dot{\phi}\theta + I_3^T \dot{\psi}\theta \end{aligned} \quad (B.63)$$

$$\begin{aligned} \frac{d}{dt} \left(\frac{\partial L}{\partial \dot{\phi}} \right) &= (m_{tot} r_W + m_1)[\ddot{x}s\phi - \ddot{y}c\phi + r_W \dot{\phi} + \dot{\psi}(\dot{x}c\phi + \dot{y}s\phi)] \\ &\quad + I_1^{tot} + m_1 r_W + m_2 \dot{\phi} + I_3^T \dot{\psi}\theta \end{aligned} \quad (B.64)$$

$$\frac{\partial L}{\partial \phi} \cong (m_{tot} r_W + m_1)\dot{\psi}(\dot{x}c\phi + \dot{y}s\phi) + I_2^W \ddot{w}\dot{\phi} + (m_{tot} r_W + m_1)g\phi \quad (B.65)$$

$$a_{14} = 0 \quad (\text{B.66})$$

$$a_{24} = 0 \quad (\text{B.67})$$

$$Q_4 = 0 \quad (\text{B.68})$$

substitute into Lagrange's equation:

$$\begin{aligned} & (m_{tot}r_W + m_1)(\bar{x}s\dot{\psi} - \bar{y}c\dot{\psi}) + I_1^{tot} + m_{tot}r_W^2 + 2m_1r_W + m_2)\ddot{\phi} + I_3^T\dot{\phi} \\ & = I_2^W\ddot{\psi} + (m_{tot}r_W + m_1)g\phi \end{aligned} \quad (\text{B.69})$$

5. $q_5 = \psi$:

$$\frac{\partial L}{\partial \psi} \cong (m_{tot}r_W + m_1)\phi(\bar{x}c\dot{\psi} + \bar{y}s\dot{\psi}) + I_2^W\ddot{\psi} + I_3^{tot}\dot{\psi} + I_3^T\dot{\nu} \quad (\text{B.70})$$

$$\begin{aligned} \frac{d}{dt} \left(\frac{\partial L}{\partial \dot{\psi}} \right) &= (m_{tot}r_W + m_1)\{\phi(\bar{x}c\dot{\psi} + \bar{y}s\dot{\psi}) + \phi[\bar{x}c\dot{\psi} - \bar{y}s\dot{\psi}]\} \\ &+ I_2^W(\ddot{\psi} + \ddot{\phi}) + I_3^{tot}\ddot{\psi} + I_3^T\ddot{\nu} \end{aligned} \quad (\text{B.71})$$

$$\frac{\partial L}{\partial \psi} \cong (m_{tot}r_W + m_1)[\phi(\bar{x}c\dot{\psi} + \bar{y}s\dot{\psi}) + \phi(\bar{x}c\dot{\psi} + \bar{y}s\dot{\psi})] \quad (\text{B.72})$$

$$a_{15} = 0 \quad (\text{B.73})$$

$$a_{25} = 0 \quad (\text{B.74})$$

$$Q_5 = 0 \quad (\text{B.75})$$

Notice that $Q_5 \neq -Q_T$ because the torque Q_T does not act around the axis about which the coordinate under consideration (ψ) rotates.

Substitute into Lagrange's equation:

$$I_3^{tot}\ddot{\psi} + I_3^T\ddot{\nu} + I_2^W\ddot{\psi} - (m_{tot}r_W + m_1)\phi(\bar{x}c\dot{\psi} + \bar{y}s\dot{\psi}) = 0 \quad (\text{B.76})$$

APPENDIX B. EOMS BY USING LAGRANGE'S METHOD

6. $q_6 = \theta$:

$$\frac{\partial L}{\partial \theta} \cong m_1(\dot{z}c\psi + \dot{y}s\psi + r_w\dot{\psi}) + (I_2^F + I_2^T + m_2)(\dot{\theta} + \dot{\psi}) \quad (B.77)$$

$$\frac{d}{dt} \left(\frac{\partial L}{\partial \dot{\theta}} \right) \cong m_1[\ddot{z}c\psi + \ddot{y}s\psi] + (I_2^F + I_2^T + m_2)\ddot{\theta} \quad (B.78)$$

$$\frac{\partial L}{\partial \theta} \cong I_3^T \dot{\psi} + m_1 g \theta \quad (B.79)$$

$$a_{16} = 0 \quad (B.80)$$

$$a_{26} = 0 \quad (B.81)$$

$$Q_6 = -Q_w \quad (B.82)$$

Substitute into Lagrange's equation:

$$(I_2^F + I_2^T + m_2)\ddot{\theta} + m_1(\ddot{z}c\psi + \ddot{y}s\psi) = I_3^T \ddot{\psi} + m_1 g \theta - Q_w \quad (B.83)$$

7. $q_7 = \nu$:

$$\frac{\partial L}{\partial \nu} = I_3^T [\dot{\phi}c\theta + \dot{\psi}c\phi c\theta + \dot{\nu}] \quad (B.84)$$

$$\frac{d}{dt} \left(\frac{\partial L}{\partial \dot{\nu}} \right) = I_3^T (\ddot{\phi} + \ddot{\nu}) \quad (B.85)$$

$$\frac{\partial L}{\partial \nu} = 0 \quad (B.86)$$

$$a_{17} = 0 \quad (B.87)$$

$$a_{27} = 0 \quad (B.88)$$

$$Q_7 = Q_T \quad (B.89)$$

Substitute into Lagrange's equation:

$$I_3^T(\ddot{\psi} + \ddot{\nu}) = Q_T \quad (\text{B.90})$$

Eliminate x and y coordinates from the dynamic equations:
from B.2:

$$\ddot{x} = r_W \ddot{\omega} c\psi \quad (\text{B.91})$$

$$\ddot{y} = r_W \ddot{\omega} s\psi \quad (\text{B.92})$$

$$\ddot{\bar{x}} = r_W(\ddot{\omega} c\psi - \dot{\omega} \dot{\psi} s\psi) \quad (\text{B.93})$$

$$\ddot{\bar{y}} = r_W(\ddot{\omega} s\psi + \dot{\omega} \dot{\psi} c\psi) \quad (\text{B.94})$$

Eliminate $\ddot{\bar{x}}$ from B.49:

$$m_{tot} r_W (\ddot{\omega} c\psi - \dot{\omega} \dot{\psi} s\psi + \dot{\phi} s\psi) + m_1 (\ddot{\theta} c\psi + \dot{\phi} s\psi) = \lambda_1 \quad (\text{B.95})$$

Eliminate $\ddot{\bar{y}}$ from B.55:

$$m_{tot} r_W (\ddot{\omega} s\psi + \dot{\omega} \dot{\psi} c\psi - \dot{\phi} c\psi) + m_1 (\ddot{\theta} s\psi - \dot{\phi} c\psi) = \lambda_2 \quad (\text{B.96})$$

Eliminate λ_1 and λ_2 from B.62:

$$(I_2^W + m_{tot} r_W^2) \ddot{\omega} + (m_F r_{FF} + m_T r_{TT}) r_W \ddot{\theta} = Q_W \quad (\text{B.97})$$

Eliminate \ddot{x} , \ddot{y} , $\ddot{\bar{x}}$ and $\ddot{\bar{y}}$ from B.69:

$$\begin{aligned} & (I_1^{tot} + m_{tot} r_W^2 + 2m_1 r_W + m_2) \ddot{\phi} + I_3^T \ddot{\nu} \dot{\theta} \\ & = (I_2^W + m_{tot} r_W^2 + m_1 r_W) \ddot{\omega} \dot{\psi} + (m_{tot} r_W + m_1) g \phi \end{aligned} \quad (\text{B.98})$$

Eliminate $\ddot{\bar{x}}$ and $\ddot{\bar{y}}$ from B.76:

$$I_3^{tot} \ddot{\psi} + I_3^T \ddot{\nu} + I_2^W \ddot{\omega} \dot{\phi} = 0$$

but from B.90:

$$\begin{aligned} I_3^T(\ddot{\psi} + \dot{\nu}) &= Q_T \\ (I_3^W + I_3^F)\ddot{\psi} + I_2^W\dot{\omega}\dot{\phi} &= -Q_T \end{aligned} \quad (\text{B.99})$$

Eliminate \ddot{x} and \ddot{y} from B.83:

$$(I_2^F + I_2^T + m_2)\ddot{\theta} + m_1 r_W \ddot{\omega} = I_3^T \dot{\nu} \dot{\phi} + m_1 g \theta - Q_W \quad (\text{B.100})$$

B.4 Summary of unicycle dynamic equations

Note that:

$$\dot{\omega} \equiv \Omega_0 + \Omega \quad (\text{B.101})$$

$$\dot{\nu} \equiv \eta_0 + \eta \quad (\text{B.102})$$

B.4.1 Lateral system dynamic equations

Wheel and Frame Yaw Dynamics:

$$(I_3^W + I_3^F)\ddot{\psi} + I_2^W \Omega_0 \dot{\phi} = -Q_T \quad (\text{B.103})$$

Gyroscopic Coupling Dynamics:

$$\begin{aligned} & [I_1^W + I_1^F + I_1^T + (m_W + m_F + m_T)r_W^2 + 2r_W(m_{FTF} + m_{TTT}) \\ & + (m_F r_F^2 + m_T r_T^2)]\ddot{\phi} + I_3^T \eta_0 \dot{\theta} \\ & = [I_2^W + (m_W + m_F + m_T)r_W^2 + (m_{FTF} + m_{TTT})r_W]\Omega_0 \dot{\psi} \\ & + [(m_W + m_F + m_T)r_W + (m_{FTF} + m_{TTT})]g\phi \end{aligned} \quad (\text{B.104})$$

Turntable Rotational Dynamics:

$$I_3^T(\ddot{\psi} + \dot{\eta}) = Q_T \quad (\text{B.105})$$

B.4.2 Longitudinal system dynamic equations

Frame Pitch Dynamics:

$$\begin{aligned}
 & \{I_2^F + I_2^T + m_F r_F^2 + m_T r_T^2\} \ddot{\theta} + (m_F r_F + m_T r_T) r_W \dot{\Omega} \\
 & = I_3^T \eta_0 \dot{\phi} + (m_F r_F + m_T r_T) g \theta - Q_W
 \end{aligned}
 \tag{B.106}$$

Wheel Rotational Dynamics:

$$[I_2^W + (m_W + m_F + m_T) r_W^2] \ddot{\Omega} + (m_F r_F + m_T r_T) r_W \ddot{\theta} = Q_W
 \tag{B.107}$$

These are the same dynamic equations as those obtained in Appendix A where Newtonian mechanics were used to derive the equation of motion.

The cross coupling terms are absent in the results of the Lagrangian derivation because they were not taken into account.

Appendix C

EOMs by using D'Alembert's Principle

C.1 Procedure

The following procedure avoids finding internal forces and torques in deriving the equations of motion. It is based on D'Alembert's principle which states that the laws of static equilibrium apply to a dynamical system if the inertial forces, as well as the actual external forces, are considered as applied forces acting on the system.

- Determine the following torques and forces:

- (1) D'Alembert torques acting on wheel, frame and turntable.
- (2) D'Alembert forces acting on wheel, frame and turntable.
- (3) Gravitational forces acting on wheel, frame and turntable.

- Determine five equations of motion:

- (1) - (2) Set the two quasi-horizontal components of moment about P (wheel contact point with ground) equal to zero for whole unicycle.
- (3) Set the vertical components of moment about P (wheel contact point with ground) equal to zero for whole unicycle, and include the external friction torque $-f_G\psi$.
- (4) Set moment about axle of wheel equal to zero for frame plus turntable and include applied and friction torques $-Q_W - f_W(\dot{\Omega} - \dot{\theta})$.
- (5) Set moment about axle of turntable to zero for turntable, and include applied and friction torques $Q_T - f_T\dot{\eta}$.

D'Alembert Torque:

- Wheel:

$$-(I_1^W \ddot{\phi} - I_2^W \Omega_0 \dot{\psi}) \dot{w}_1 - I_2^W \dot{\Omega} \dot{w}_2 - (I_3^W \ddot{\psi} + I_2^W \Omega_0 \dot{\phi}) \dot{w}_3 \quad (C.1)$$

- Frame:

$$-I_1^F \ddot{\phi} \dot{f}_1 - I_2^F \ddot{\theta} \dot{f}_2 - I_3^F \ddot{\psi} \dot{f}_3 \quad (C.2)$$

- Turntable:

$$-(I_1^T \ddot{\phi} + I_3^T \eta_0 \dot{\phi}) \dot{f}_1 - (I_2^T \ddot{\theta} - I_3^T \eta_0 \dot{\phi}) \dot{f}_2 - I_3^T (\ddot{\psi} + \dot{\eta}) \dot{f}_3 \quad (C.3)$$

D'Alembert Forces:

- Wheel:

$$-m_W r_W [\dot{\Omega} \dot{w}_1 + (\Omega_0 \dot{\psi} - \dot{\phi}) \dot{w}_2] \quad (C.4)$$

- Frame:

$$-m_F (r_W \dot{\Omega} + r_F \ddot{\theta}) \dot{f}_1 - m_F [-(r_W + r_F) \ddot{\phi} + r_W \Omega_0 \dot{\phi}] \dot{f}_2 \quad (C.5)$$

- Turntable:

$$-m_T (r_W \dot{\Omega} + r_T \ddot{\theta}) \dot{f}_1 - m_T [r_W \Omega_0 \dot{\psi} - (r_W + r_T) \ddot{\phi}] \dot{f}_2 \quad (C.6)$$

Gravitational Forces:

- Wheel:

$$-m_W g(-\phi \ddot{w}_2 - \ddot{w}_3) \quad (C.7)$$

- Frame:

$$m_F g(\theta \ddot{f}_1 - \phi \ddot{f}_2 - \ddot{f}_3) \quad (C.8)$$

- Turntable:

$$m_T g(\theta \ddot{f}_1 - \phi \ddot{f}_2 - \ddot{f}_3) \quad (C.9)$$

 \ddot{w}_1 Component of Moment about P for Whole Cycle

$$\begin{aligned} 0 = & -(I_1^W \ddot{\phi} - I_2^W \Omega_0 \dot{\phi}) + m_W r_W [g\phi + r_W (\Omega_0 \dot{\phi} - \ddot{\phi})] \\ & - I_1^F \ddot{\phi} + m_F (r_W + r_F) [g\phi - (r_W + r_F) \ddot{\phi} + r_W \Omega_0 \dot{\phi}] \\ & - (I_1^T \ddot{\phi} + I_3^T \eta_0 \dot{\phi}) + m_T (r_W + r_T) [g\phi - (r_W + r_T) \ddot{\phi} + r_W \Omega_0 \dot{\phi}] \end{aligned} \quad (C.10)$$

 \ddot{w}_2 Component of Moment about P for Whole Cycle

$$\begin{aligned} 0 = & -I_2^W \ddot{\Omega} - m_W r_W^2 \ddot{\Omega} \\ & - I_2^F \ddot{\theta} + m_F (r_W + r_F) [-r_W \ddot{\Omega} - r_F \ddot{\theta}] + m_F r_F g \theta \\ & - (I_2^T \ddot{\theta} - I_3^T \eta_0 \dot{\phi}) + m_T (r_W + r_T) [-r_W \ddot{\Omega} - r_T \ddot{\theta}] + m_T r_T g \theta \end{aligned} \quad (C.11)$$

 \ddot{w}_3 Component of Moment about P for Whole Cycle

$$0 = -(I_3^W \ddot{\psi} + I_2^W \Omega_0 \dot{\phi}) - I_3^F \ddot{\psi} - I_3^T (\ddot{\psi} + \ddot{\eta}) - f_G \dot{\psi} \quad (C.12)$$

 \ddot{f}_2 Component of Moment about O for Frame and Turntable

$$\begin{aligned} 0 = & -I_2^F \ddot{\theta} + m_F r_F [g\theta - r_W \ddot{\Omega} - r_F \ddot{\theta}] \\ & - (I_2^T \ddot{\theta} - I_3^T \eta_0 \dot{\phi}) + m_T r_T [g\theta - r_W \ddot{\Omega} - r_T \ddot{\theta}] + f_W (\ddot{\Omega} - \ddot{\theta}) - Q_W \end{aligned} \quad (C.13)$$

 \ddot{f}_3 Component of Moment about Q for Turntable

$$0 = -I_3^T (\ddot{\psi} + \ddot{\eta}) + Q_T - f_T \ddot{\eta} \quad (C.14)$$

Subtract equation C.14 from C.12:

$$0 = -(I_3^W \ddot{\psi} + I_2^W \Omega_0 \dot{\phi}) - I_3^F \ddot{\psi} + f_T \ddot{\eta} - Q_T - f_G \dot{\psi} \quad (C.15)$$

Subtract equation C.13 from C.11:

$$\begin{aligned} 0 &= -[I_2^W + (m_W + m_F + m_T)r_W^2]\ddot{\Omega} - (m_F r_F - m_T r_T)r_W \ddot{\theta} \\ &\quad - f_W(\ddot{\Omega} - \ddot{\theta}) + Q_W \end{aligned} \quad (C.16)$$

C.2 Lateral equations of motion

from C.15:

$$(I_3^W + I_3^F)\ddot{\psi} = -I_2^W \Omega_0 \dot{\phi} - f_G \dot{\psi} + f_T \ddot{\eta} - Q_T \quad (C.17)$$

from C.10:

$$\begin{aligned} &[I_1^W + I_1^F + I_1^T + m_W r_W^2 + m_F(r_W + r_F)^2 + m_T(r_W + r_T)^2]\ddot{\phi} \\ &= [I_2^W + m_W r_W^2 + m_F r_W(r_W + r_F) + m_T r_W(r_W + r_T)]\Omega_0 \dot{\psi} \\ &\quad + [m_W r_W + m_F(r_W + r_F) + m_T(r_W + r_T)]g\phi - I_3^T \eta_0 \ddot{\theta} \end{aligned} \quad (C.18)$$

from C.14:

$$I_3^T(\ddot{\psi} + \ddot{\eta}) = -f_T \ddot{\eta} + Q_T \quad (C.19)$$

C.3 Longitudinal equations of motion

from C.13:

$$\begin{aligned} &[I_2^F + I_2^T + m_F r_F^2 + m_T r_T^2]\ddot{\theta} + (m_F r_F + m_T r_T)r_W \ddot{\Omega} \\ &= I_3^T \eta_0 \dot{\phi} + (m_F r_F + m_T r_T)g\theta + f_W(\ddot{\Omega} - \ddot{\theta}) - Q_W \end{aligned} \quad (C.20)$$

from C.16:

$$\begin{aligned} &(m_F r_F + m_T r_T)r_W \ddot{\theta} + [I_2^W + (m_W + m_F + m_T)r_W^2]\ddot{\Omega} \\ &= -f_W(\ddot{\Omega} - \ddot{\theta}) + Q_W \end{aligned} \quad (C.21)$$

APPENDIX C. EOMS BY USING D'ALEMBERT'S PRINCIPLE

These last 5 equations, derived by using generalized D'Alembert forces and summing moments about fixed points, are the same as the dynamic equations of motion derived in Appendix A and B. In Appendix A Newton's equations were used to derive the equations of motion and in Appendix B an energy approach and Lagrange's equation was used.

Appendix D

State Space Form of the EOMs

The system dynamic equations from Appendix A can be written in matrix form as:

$$\bar{I}\dot{\bar{x}} = \bar{F}\bar{x} + \bar{G}u + \bar{K}w \quad (\text{D.1})$$

The matrix equation can be converted to the standard state space form:

$$\begin{aligned} \dot{\bar{x}} &= \bar{I}^{-1}\bar{F}\bar{x} + \bar{I}^{-1}\bar{G}u + \bar{I}^{-1}\bar{K}w \\ &= Fx + Gu + Kw \end{aligned} \quad (\text{D.2})$$

The dynamic equations in matrix form are shown on the next page:

APPENDIX D STATE SPACE FORM OF THE EOMS

$$= \begin{bmatrix} \bar{I}_{1,1} & \bar{I}_{1,2} & 0 & 0 & 0 & 0 & \bar{I}_{1,7} & \bar{I}_{1,8} & 0 & 0 & 0 \\ \bar{I}_{2,1} & \bar{I}_{2,2} & 0 & 0 & 0 & 0 & \bar{I}_{2,7} & 0 & 0 & 0 & 0 \\ 0 & \bar{I}_3^T & \bar{I}_3^T & 0 & 0 & 0 & 0 & 0 & 0 & 0 & 0 \\ \bar{I}_{4,1} & \bar{I}_{4,2} & 0 & \bar{I}_{4,4} & 0 & 0 & 0 & 0 & 0 & 0 & 0 \\ 0 & 0 & 0 & 0 & 1 & 0 & 0 & 0 & 0 & 0 & 0 \\ 0 & 0 & 0 & 0 & 0 & 1 & 0 & 0 & 0 & 0 & 0 \\ \bar{I}_{7,1} & \bar{I}_{7,2} & 0 & 0 & 0 & 0 & \bar{I}_{7,7} & \bar{I}_{7,8} & 0 & 0 & 0 \\ 0 & \bar{I}_{8,2} & 0 & 0 & 0 & 0 & \bar{I}_{8,7} & \bar{I}_{8,8} & 0 & 0 & 0 \\ 0 & \bar{I}_{9,2} & 0 & 0 & 0 & 0 & \bar{I}_{9,7} & \bar{I}_{9,8} & \bar{I}_{9,9} & 0 & 0 \\ 0 & 0 & 0 & 0 & 0 & 0 & 0 & 0 & 0 & 1 & 0 \\ 0 & 0 & 0 & 0 & 0 & 0 & 0 & 0 & 0 & 0 & 1 \end{bmatrix} \begin{bmatrix} \phi \\ \dot{\phi} \\ \eta \\ \sigma \\ \dot{\phi} \\ \sigma \\ \bar{\theta} \\ \Omega \\ \bar{\rho} \\ \dot{\sigma} \\ \dot{\rho} \end{bmatrix}$$

$$= \begin{bmatrix} \bar{F}_{1,1} & \bar{F}_{1,2} & f_T & 0 & \bar{F}_{1,5} & 0 & 0 & 0 & 0 & \bar{F}_{1,10} & 0 \\ 0 & \bar{F}_{2,2} & 0 & 0 & \bar{F}_{2,5} & 0 & \bar{F}_{2,7} & 0 & 0 & 0 & 0 \\ 0 & 0 & -f_T & 0 & 0 & 0 & 0 & 0 & 0 & 0 & 0 \\ 0 & \bar{F}_{4,2} & 0 & -f_p & \bar{F}_{4,5} & \bar{F}_{4,6} & 0 & 0 & 0 & 0 & 0 \\ 1 & 0 & 0 & 0 & 0 & 0 & 0 & 0 & 0 & 0 & 0 \\ 0 & 0 & 0 & 1 & 0 & 0 & 0 & 0 & 0 & 0 & 0 \\ \bar{F}_{7,1} & 0 & 0 & 0 & 0 & 0 & -f_W & f_W & 0 & \bar{F}_{7,10} & 0 \\ 0 & 0 & 0 & 0 & 0 & 0 & f_W & -f_W & 0 & 0 & 0 \\ 0 & 0 & 0 & 0 & 0 & 0 & 0 & 0 & -f_p & \bar{F}_{9,10} & \bar{F}_{9,11} \\ 0 & 0 & 0 & 0 & 0 & 0 & 1 & 0 & 0 & 0 & 0 \\ 0 & 0 & 0 & 1 & 0 & 0 & 0 & 0 & 1 & 0 & 0 \end{bmatrix} \begin{bmatrix} \phi \\ \dot{\phi} \\ \eta \\ \sigma \\ \dot{\phi} \\ \sigma \\ \bar{\theta} \\ \Omega \\ \bar{\rho} \\ \theta \\ \rho \end{bmatrix}$$

$$+ \begin{bmatrix} -1 & 0 \\ 0 & 0 \\ 1 & 0 \\ 0 & 0 \\ 0 & 0 \\ 0 & 0 \\ 0 & -1 \\ 0 & 1 \\ 0 & 0 \\ 0 & 0 \\ 0 & 0 \end{bmatrix} \begin{bmatrix} Q_T \\ Q_W \end{bmatrix} + \begin{bmatrix} 0 & f_T & 0 \\ \bar{K}_{2,1} & 0 & 0 \\ 0 & -f_T & 0 \\ 0 & 0 & 0 \\ 0 & 0 & 0 \\ 0 & 0 & 0 \\ \bar{K}_{7,1} & 0 & f_W \\ 0 & 0 & -f_W \\ 0 & 0 & 0 \\ 0 & 0 & 0 \\ 0 & 0 & 0 \end{bmatrix} \begin{bmatrix} g \\ \eta_0 \\ \Omega_0 \end{bmatrix}$$

where the coefficients of the matrices are :

$$\bar{I}_{1,1} = -[m_F(r_W + r_F)r_1]$$

$$\bar{I}_{1,2} = [I_3^W + I_3^F + m_F(r_1^2 + r_2^2)]$$

$$\bar{I}_{1,7} = -m_F r_F r_2$$

$$\bar{I}_{1,8} = -m_F r_W r_2$$

$$\bar{F}_{1,1} = -I_2^W \Omega_0$$

$$\bar{F}_{1,2} = -[f_G + m_F r_W r_1 \Omega_0]$$

$$\bar{F}_{1,5} = -m_F r_1 g$$

$$\bar{F}_{1,10} = -m_F r_2 g$$

$$\begin{aligned} \bar{I}_{2,1} = & -[I_1^W + I_1^F + I_1^T + (m_W + m_F + m_T)r_W^2 + m_T r_T(2r_W + r_T) \\ & + m_F r_F(2r_W + r_F) + m_F r_2^2] \end{aligned}$$

$$\bar{I}_{2,2} = m_F r_1(r_W + r_F)$$

$$\bar{I}_{2,7} = m_F r_1 r_2$$

APPENDIX D. STATE SPACE FORM OF THE EOMS

$$\bar{F}_{2,2} = -[I_2^W + (m_W + m_F + m_T)r_W^2 + (m_F r_F + m_T r_T)r_W]\Omega_0$$

$$\bar{F}_{2,5} = -[(m_W + m_F + m_T)r_W + m_F r_F + m_T r_T]g$$

$$\bar{F}_{2,7} = I_3^T \eta_0$$

$$\bar{K}_{2,1} = m_F r_2$$

$$\bar{I}_{4,1} = [I_1^S + m_p r_p(r_p - r_{S3} - r_W)]$$

$$\bar{I}_{4,2} = m_p r_p r_{S1}$$

$$\bar{I}_{4,4} = [I_1^S + m_p r_p^2]$$

$$\bar{F}_{4,2} = -m_p r_p r_W \Omega_0$$

$$\bar{F}_{4,5} = -m_p r_p g$$

$$\bar{F}_{4,6} = -(k_p + m_p r_p g)$$

$$\bar{I}_{7,1} = -m_F r_1 r_2$$

$$\bar{I}_{7,2} = -m_F r_F r_2$$

$$\bar{I}_{7,7} = \{I_2^F + I_2^T + m_F r_F^2 + m_T r_T^2 + m_F r_1^2\}$$

$$\bar{I}_{7,8} = (m_F r_F + m_T r_T) r_W$$

$$\bar{F}_{7,1} = I_3^T \eta_0$$

$$\bar{F}_{7,10} = (m_F r_F + m_T r_T) g$$

$$\bar{K}_{7,1} = m_F r_1$$

$$\bar{I}_{8,2} = -m_F r_W r_2$$

$$\bar{I}_{8,7} = (m_T r_T + m_F r_F) r_W$$

$$\bar{I}_{8,8} = [I_2^W + (m_W + m_F + m_T) r_W^2]$$

$$\bar{I}_{9,2} = m_p r_p r_{R2}$$

$$\bar{I}_{9,7} = [I_2^R + m_p r_p (r_p - r_{R2})]$$

$$\bar{I}_{9,8} = -m_p r_p r_W$$

$$\bar{I}_{9,9} = [I_2^R + m_p r_p^2]$$

$$\bar{F}_{9,10} = -m_p r_p g$$

$$\bar{F}_{9,11} = -[k_p + m_p r_p g]$$

Appendix E

Attitude by Means of a Sensor Pendulum

The purpose of this investigation is to determine whether the modes of an inverted pendulum in a gravity field are observable from a measurement of the deflection angle of a small sensor pendulum mounted on the inverted pendulum. The modal observability as a function on the sensor pendulum location is calculated. A physical explanation for the unobservability of the inverted pendulum modes in the sensor pendulum measurement when the sensors are mounted at a certain height on the unicycle frame, is presented.

E.1 Dynamic equations of motion

1. Inverted pendulum dynamics:

Refer to Figure E.1:

Description of parameters:

m_I = mass of inverted pendulum.

J_I^I = moment of inertia of inverted pendulum about an axis passing through the center of mass, I^* , of the inverted pendulum, and parallel to the \hat{i}_2 unit

vector.

m_p = mass of sensor pendulum.

J_2^P = moment of inertia of sensor pendulum about an axis passing through the center of mass, P^* , of the sensor pendulum, and parallel to the \hat{i}_2 unit vector.

r_I = distance from the inverted pendulum support point to it's center of mass, I^* .

r_H = distance from the inverted pendulum support point to the sensor pendulum's hinge point.

r_p = distance from the sensor pendulum's hinge point to it's center of mass, P^* .

Acceleration of c.m. I^* of inverted pendulum : $r_I \ddot{\theta} \hat{i}_1$

moment balance about O:

$$r_I \hat{i}_3 \times \{m_I g \hat{i}_1 - m_I g \hat{i}_3 - m_I r_I \ddot{\theta} \hat{i}_1\} = J_2^I \ddot{\theta} \hat{i}_2$$

where the last term in the brackets above is the D'Alembert force.

Equation of Motion of Inverted Pendulum:

$$(J_2^I + m_I r_I^2) \ddot{\theta} = m_I r_I g \theta \quad (E.1)$$

Laplace transform:

$$\Theta(s) = \frac{s\theta(o) + \dot{\theta}(o)}{s^2 - w_I^2} \quad (E.2)$$

$$\text{where } w_I^2 = \frac{m_I r_I g}{J_2^I + m_I r_I^2}$$

so that the time response is an unstable exponentially growing function:

$$\theta(t) = \theta(o) \cosh w_I t + \frac{\dot{\theta}(o)}{w_I} \sinh w_I t \quad (E.3)$$

APPENDIX E. ATTITUDE BY MEANS OF A SENSOR PENDULUM

2. Sensor pendulum dynamics:

Refer to Figure E.2:

angular velocity of \hat{p} frame:

$${}^A\bar{\omega}^P = (\bar{\theta} + \bar{\gamma})\hat{p}_2 \quad (E.4)$$

acceleration of hinge point H:

$$\begin{aligned} \bar{a}^H &= r_H \bar{\theta} \hat{i}_1 \\ &\cong r_H \bar{\theta} \hat{p}_1 \end{aligned} \quad (E.5)$$

acceleration of P^* of the sensor pendulum:

$$\begin{aligned} \bar{a}^{P^*} &= \bar{a}^H + {}^A\bar{\omega}^P \times \bar{r}^{HP^*} + {}^A\bar{\omega}^P \times ({}^A\bar{\omega}^P \times \bar{r}^{HP^*}) \\ &= r_H \bar{\theta} \hat{p}_1 + (\bar{\theta} + \bar{\gamma})\hat{p}_2 \times (-r_p \hat{p}_3) + 0 \\ &= [(r_H - r_p)\bar{\theta} - r_p \bar{\gamma}] \hat{p}_1 \end{aligned} \quad (E.6)$$

moment balance about hinge point H:

$$(-r_p \hat{p}_3) \times \{m_p g (\bar{\theta} + \bar{\gamma}) \hat{p}_1 - m_p g \hat{p}_3 - m_p [(r_H - r_p)\bar{\theta} - r_p \bar{\gamma}] \hat{p}_1\} = J_2^P (\bar{\theta} + \bar{\gamma}) \hat{p}_2$$

Equation of Motion of Sensor Pendulum:

$$[J_2^P + m_p r_p (r_p - r_H)] \bar{\theta} + [J_2^P + m_p r_p^2] \bar{\gamma} = -m_p r_p g (\bar{\theta} + \bar{\gamma}) \quad (E.7)$$

define:

$$C = J_2^P + m_p r_p (r_p - r_H)$$

$$D = J_2^P + m_p r_p^2$$

$$E = -m_p r_p g$$

rewrite E.7 as :

$$C \bar{\theta} + D \bar{\gamma} = E (\bar{\theta} + \bar{\gamma}) \quad (E.8)$$

Transfer function from inverted pendulum angle to angle measured by sensor pendulum:

Laplace transform for equation E.7

$$\frac{\Lambda(s)}{\Theta(s)} = - \left(\frac{Cs^2 - E}{Ds^2 - E} \right) \quad (\text{E.9})$$

Notes:

1.

$$\lim_{s \rightarrow 0} \frac{\Lambda}{\Theta} = -1$$

$$\Rightarrow \gamma|_{t=\infty} = -\theta|_{t=\infty}$$

so the measured angle is the negative of the attitude angle in steady state, as it should be.

2. For this case with no damping on the pendulum, there are two poles at :

$$\begin{aligned} s &= \pm \sqrt{\frac{E}{D}} \\ &= \pm j \sqrt{\frac{m_p r_p g}{J_p + m_p r_p^2}} \end{aligned}$$

where: $J_p \equiv J_2^p$

3. The zeros for the transfer function are at :

$$\begin{aligned} s &= \pm \sqrt{\frac{E}{C}} \\ &= \pm \sqrt{\frac{-m_p r_p g}{J_p + m_p r_p (r_p - r_H)}} \end{aligned}$$

APPENDIX E. ATTITUDE BY MEANS OF A SENSOR PENDULUM

- (a) If $J_p + m_p r_p (r_p - r_H) > 0$; i.e. when $r_H < r_p + \frac{J_p}{m_p r_p}$:

\Rightarrow 2 complex zeros at

$$s = \pm j \sqrt{\frac{m_p r_p g}{J_p + m_p r_p (r_p - r_H)}}$$

See Figure E.3.

- (b) If $J_p + m_p r_p (r_p - r_H) < 0$; i.e. when $r_H > r_p + \frac{J_p}{m_p r_p}$:

\Rightarrow 2 real zeros at

$$s = \pm \sqrt{\frac{m_p r_p g}{|J_p + m_p r_p (r_p - r_H)|}}$$

See Figure E.4.

A non minimum phase behaviour of the sensor pendulum will occur due to the right half plane zero.

4. It is evident from Figure E.4 that the sensor pendulum could be mounted at a critical height, $(r_H)_{crit}$, where the zeros will cancel the inverted pendulum poles. This is the situation where unobservability of the inverted pendulum modes occur. Several methods for calculating the condition for unobservability will now be presented.

E.2 Observability matrix

$$\begin{aligned} \ddot{\theta} &= \frac{m_I r_I g}{J_I^I + m_I r_I^2} \theta \\ \ddot{\gamma} &= -\frac{m_p r_p g}{J_2^P + m_p r_p^2} (\theta + \gamma) \\ &\quad - \frac{[J_2^P + m_p r_p (r_p - r_H)] m_p r_p g}{(J_2^P + m_p r_p^2)(J_I^I + m_I r_I^2)} \theta \end{aligned}$$

define:

$$\begin{aligned} P &= \frac{m_I r_I g}{J_2^I + m_I r_I^2} \\ H &= -\frac{g}{J_2^P + m_P r_P^2} \left\{ m_P r_P + \frac{m_I r_I [J_2^P + m_P r_P (r_P - r_H)]}{J_2^I + m_I r_I^2} \right\} \\ Q &= -\frac{m_P r_P g}{J_2^P + m_P r_P^2} \end{aligned} \quad (\text{E.10})$$

The state space representation of the system is:

$$\begin{bmatrix} \ddot{\theta} \\ \ddot{\gamma} \\ \dot{\theta} \\ \dot{\gamma} \end{bmatrix} = \begin{bmatrix} 0 & 0 & P & 0 \\ 0 & 0 & H & Q \\ 1 & 0 & 0 & 0 \\ 0 & 1 & 0 & 0 \end{bmatrix} \begin{bmatrix} \theta \\ \gamma \\ \dot{\theta} \\ \dot{\gamma} \end{bmatrix} \quad (\text{E.11})$$

or:

$$\dot{x} = Fx$$

if γ only is measured \Rightarrow output matrix:

$$M = [0 \ 0 \ 0 \ 1]$$

Observability matrix is

$$\begin{aligned} O &= \begin{bmatrix} M \\ MF \\ MF^2 \\ MF^3 \end{bmatrix} \\ &= \begin{bmatrix} 0 & 0 & 0 & 1 \\ 0 & 1 & 0 & 0 \\ 0 & 0 & H & Q \\ H & Q & 0 & 0 \end{bmatrix} \end{aligned} \quad (\text{E.12})$$

$$\det O = - \begin{vmatrix} 0 & 1 & 0 \\ 0 & 0 & H \\ H & Q & 0 \end{vmatrix} - Q \begin{vmatrix} 0 & 0 & 0 \\ 0 & 1 & 0 \\ H & Q & 0 \end{vmatrix} = -H^2 \quad (E.13)$$

system will become unobservable when:

$$\det O = 0 = -H^2$$

i.e. when:

$$H = 0 = -\frac{g}{J_2^P + m_p r_p^2} \left\{ m_p r_p + \frac{m_I r_I (J_2^P + m_p r_p (r_p - r_H))}{J_2^I + m_I r_I^2} \right\} \quad (E.14)$$

The critical height for the location of the sensor pendulum when unobservability of the inverted pendulum modes occurs, is:

$$\begin{aligned} (r_H)_{crit} &= r_p + \frac{1}{m_p r_p} \left[J_2^P + \frac{m_p r_p}{m_I r_I} (J_2^I + m_I r_I^2) \right] \\ &= \frac{J_2^I + m_I r_I^2}{m_I r_I} + \frac{J_2^P + m_p r_p^2}{m_p r_p} \end{aligned} \quad (E.15)$$

E.3 Physical explanation for modal unobservability

rewrite the dynamic equations for the sensor pendulum Equation E.7 as:

$$[J_2^P + m_p r_p^2] \ddot{\gamma} + m_p r_p g \gamma = -\{[J_2^P + m_p r_p (r_p - r_H)] \ddot{\theta} + m_p r_p g \theta\} \quad (E.16)$$

define:

Term1 : $[J_2^P + m_p r_p(r_p - r_H)]\ddot{\theta}$

Term 2: $m_p r_p g \theta$

The terms on the right hand side can be considered to be the forcing functions on the motion of the sensor pendulum. If the right hand side becomes zero, the behavior of $\theta(t)$ does not influence the motion of $\gamma(t)$, and this is when the unstable modes associated with $\theta(t)$ cannot be sensed by the measurement of $\gamma(t)$.

Term 1 is dependent on the location of the sensor pendulum hinge point, and is the moment on the sensor pendulum due to the acceleration of the inverted pendulum I.

Term 2 is the moment on the sensor pendulum due to the effect of gravity vector change as θ changes.

From the dynamic equations of motion of the inverted pendulum I, we have:

$$\ddot{\gamma} = \frac{m_I r_I g}{(J_2^I + m_I r_I^2)} \theta \quad (E.17)$$

Substitute in equation above and set right hand side = 0:

$$[J_2^P + m_p r_p(r_p - r_H)] \frac{m_I r_I g}{(J_2^I + m_I r_I^2)} \theta + m_p r_p g \theta = 0$$

solve for the critical r_H where unobservability occurs:

$$(r_H)_{crit} = \frac{J_2^I + m_I r_I^2}{m_I r_I} + \frac{J_2^P + m_p r_p^2}{m_p r_p} \quad (E.18)$$

which is the same result as obtained in equation E.2.

E.4 Unobservability by pole-zero cancellation

The modal unobservability condition can be predicted by calculating the r_H where the zeros of $\frac{\Gamma(s)}{\theta(s)}$ cancel the poles of the inverted pendulum: from equation E.9 the

zeros of $\frac{\Lambda(s)}{\delta(s)}$ are where:

$$s^2 = \frac{E}{C} = -\frac{m_p r_p g}{J_2^P + m_p r_p (r_p - r_H)} \quad (E.19)$$

the poles of the inverted pendulum are at :

$$s^2 = \frac{m_I r_I g}{J_2^I + m_I r_I^2} \quad (E.20)$$

pole-zero cancellation occurs when above two equations are set equal. Solve for $(r_H)_{crit}$:

$$-\frac{m_p r_p g}{J_2^P + m_p r_p (r_p - r_H)} = \frac{m_I r_I g}{J_2^I + m_I r_I^2}$$

$$(r_H)_{crit} = \frac{J_2^I + m_I r_I^2}{m_I r_I} + \frac{J_2^P + m_p r_p^2}{m_p r_p} \quad (E.21)$$

E.5 Unobservability by inspection of the F matrix

The point of unobservability can be found by inspection of the dynamics matrix in the state space representation of the inverted and sensor pendulum: From the F matrix in equation E.11

$$\begin{aligned} \ddot{\gamma} = & -\frac{g}{J_2^P + m_p r_p^2} \left\{ m_p r_p + \frac{m_I r_I [J_2^P + m_p r_p (r_p - r_H)]}{J_2^I + m_I r_I^2} \right\} \theta \\ & - \frac{m_p r_p g}{J_2^P + m_p r_p^2} \gamma \end{aligned} \quad (E.22)$$

Note that if the coefficient of θ above becomes zero, the dynamics of $\ddot{\gamma}$ is not affected by the motions of θ , which indicates unobservability of the unstable modes associated with θ by sensing γ only.

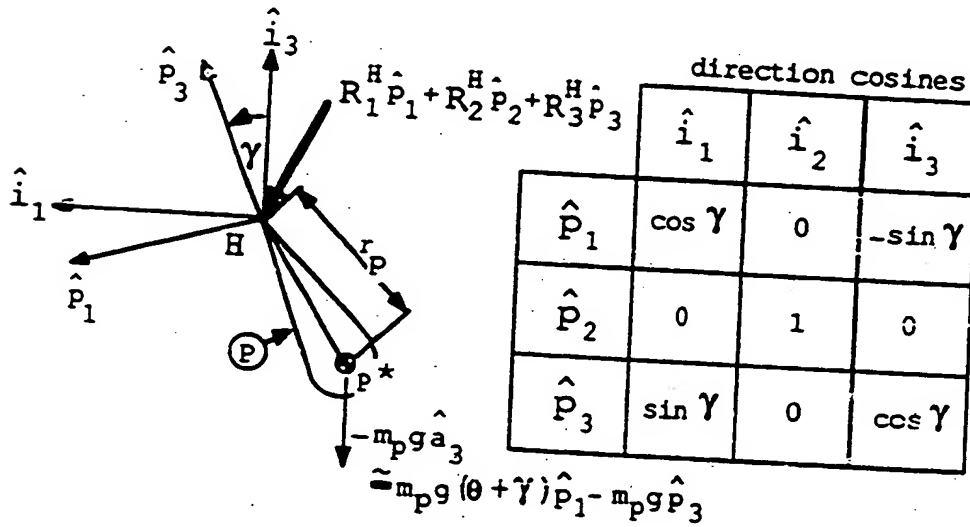
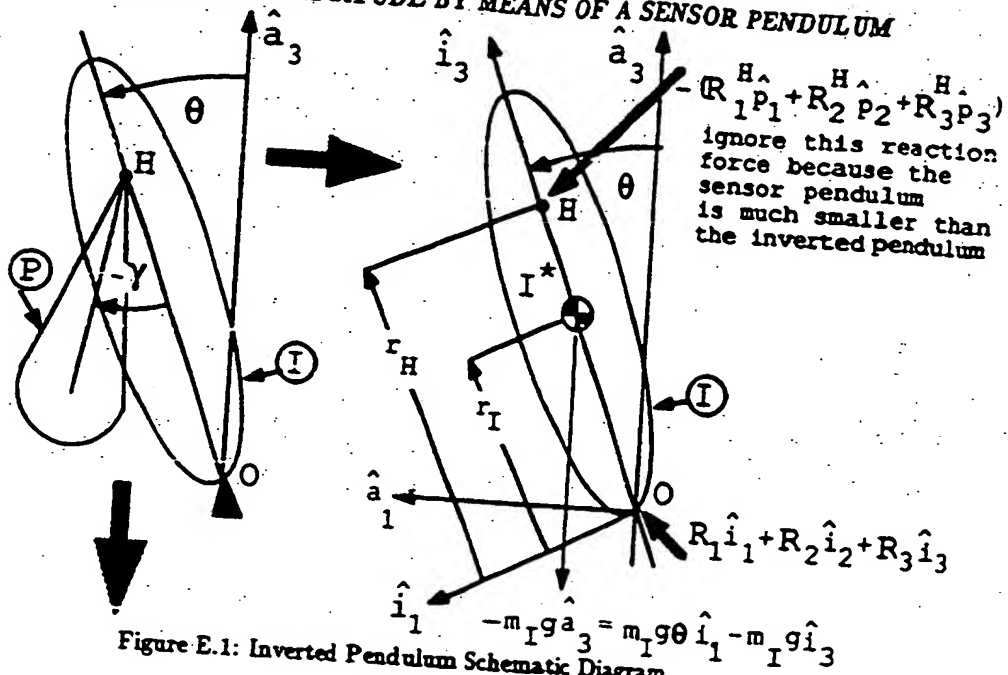
Solve for the value of r_H where the coefficient of θ becomes = 0.

$$(r_H)_{crit} = \frac{J_2^I + m_I r_I^2}{m_I r_I} + \frac{J_2^P + m_P r_P^2}{m_P r_P} \quad (E.23)$$

Conclusion:

Several approaches to solve for the critical location of the sensor pendulum in this simple two body system, were presented. When the critical location for a sensor pendulum in more complex dynamic systems is sought, it will be evident that some approaches may provide the critical sensor position easier than others.

APPENDIX E. ATTITUDE BY MEANS OF A SENSOR PENDULUM



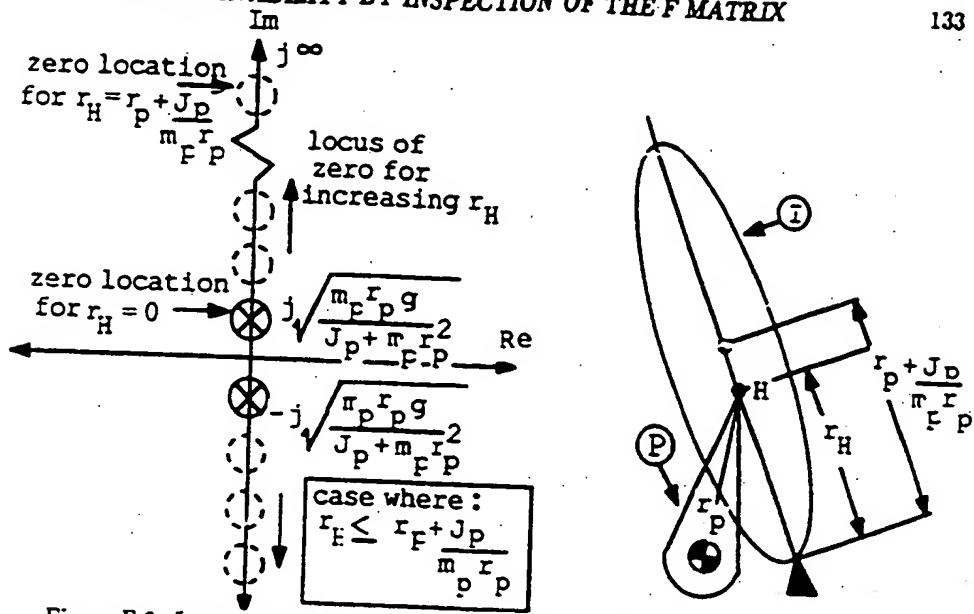


Figure E.3: Locus of Imaginary Axis Zeros as a Function of Sensor Pendulum Height

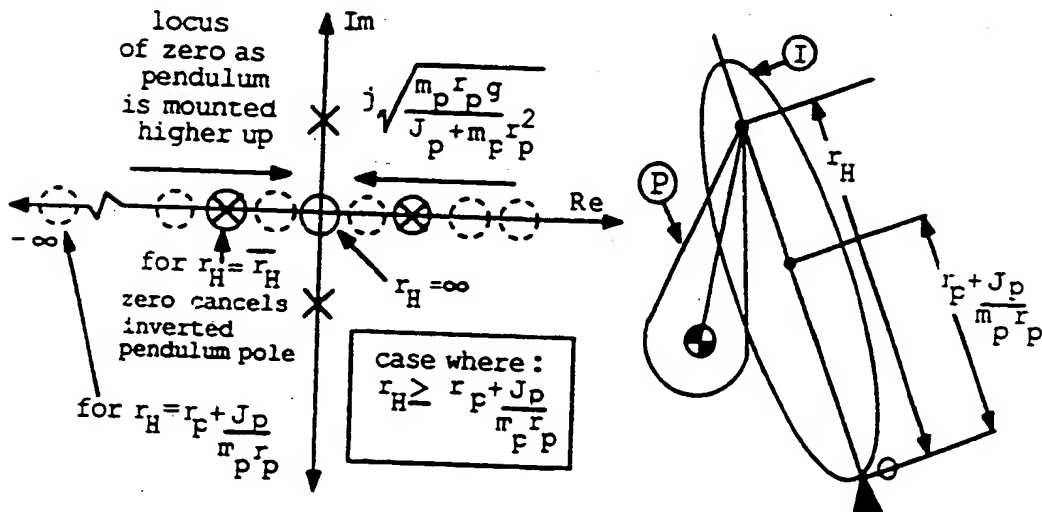


Figure E.4: Locus of Real Axis Zeros as a Function of Sensor Pendulum Height

Appendix F

Unicycle Robot Steered by Sideways Leaning

The unicycle robot can be stabilized and steered by means of a sideways leaning of the rider's body. Figure F.1 shows a schematic diagram of a wheel and a body of which the upper part can lean out of the plane of the wheel. The lower part (L) simulates the rider's legs and the upper part (B) the sideways leaning part of a person's torso. The dynamic equations of motion for this configuration are derived and the lateral system characteristics are evaluated in this appendix.

F.1 Dynamic Equations

The following procedure avoids finding internal forces and torques in deriving the equations of motion.

- Determine the following torques and forces:
 - (1) D'Alembert torques acting on wheel, legs and body.
 - (2) D'Alembert forces acting on wheel, legs and body.

(3) Gravitational forces acting on wheel, legs and body.

- Determine five equations of motion:

(1) - (2) Set the two horizontal components of the moment about P (wheel contact point with ground) equal to zero for the whole unicycle.

(3) Set the vertical component of the moment about P equal to zero for the whole unicycle, and include the external friction torque $-f_G\dot{\psi}$.

(4) Set the moment about the axle of the wheel equal to zero for the legs and body and include the applied torque Q_W .

(5) Set the moment about the sideways lean axle of the body equal to zero and include the applied lean torque Q_B .

D'Alembert Torque:

- Wheel:

$$-(I_1^W \ddot{\phi} - I_2^W \Omega_0 \dot{\psi}) \dot{w}_1 - I_2^W \dot{\Omega} \dot{w}_2 - (I_3^W \ddot{\psi} + I_2^W \Omega_0 \dot{\phi}) \dot{w}_3 \quad (F.1)$$

- Legs:

$$-I_1^L \ddot{\phi} \dot{f}_1 - I_2^L \ddot{\theta} \dot{f}_2 - I_3^L \ddot{\psi} \dot{f}_3 \quad (F.2)$$

- Body:

$$-I_1^B (\ddot{\phi} + \ddot{\beta}) \dot{g}_1 - I_2^B \ddot{\theta} \dot{g}_2 - I_3^B \ddot{\psi} \dot{g}_3 \quad (F.3)$$

D'Alembert Forces:

- Wheel:

$$-m_W r_W [\dot{\Omega} \dot{w}_1 + (\Omega_0 \dot{\psi} - \dot{\phi}) \dot{w}_2] \quad (F.4)$$

- Legs:

$$-m_L (r_W \dot{\Omega} + r_L \ddot{\theta}) \dot{f}_1 - m_L [-(r_W + r_L) \ddot{\phi} + r_W \Omega_0 \dot{\psi}] \dot{f}_2 \quad (F.5)$$

- Body:

$$-m_B [r_W \dot{\Omega} + (r_H + r_B) \ddot{\theta}] \dot{g}_1 - m_B [-(r_W + r_H + r_B) \ddot{\phi} - r_B \ddot{\beta} + r_W \Omega_0 \dot{\psi}] \dot{g}_2 \quad (F.6)$$

Gravitational Forces:

- Wheel:

$$m_W g(-\phi \hat{w}_1 - \hat{w}_3) \quad (F.7)$$

- Legs:

$$m_L g(\theta \hat{f}_1 - \phi \hat{f}_2 - \hat{f}_3) \quad (F.8)$$

- Body:

$$m_B g(\theta \hat{g}_1 - (\phi + \beta) \hat{g}_2 - \hat{g}_3) \quad (F.9)$$

 \hat{w}_1 Component of Moment about P for Whole Unicycle

$$\begin{aligned} 0 = & -(I_1^W \ddot{\phi} - I_2^W \Omega_0 \dot{\phi}) + m_W r_W [g\phi + r_W (\Omega_0 \dot{\phi} - \ddot{\phi})] \\ & - I_1^L + m_L (r_W + r_L) [g\phi - (r_W + r_L) \ddot{\phi} + r_W \Omega_0 \dot{\phi}] - I_2^B (\ddot{\phi} + \ddot{\beta}) \\ & + m_B (r_W + r_H + r_B) [g\phi - (r_W + r_H + r_B) \ddot{\phi} - r_B \ddot{\beta} + r_W \Omega_0 \dot{\phi}] + m_B r_B g\phi \end{aligned} \quad (F.10)$$

 \hat{w}_2 Component of Moment about P for Whole Unicycle

$$\begin{aligned} 0 = & -[I_2^W + m_W r_W^2] \ddot{\Omega} \\ & - I_2^L \ddot{\theta} + m_L (r_W + r_L) [g\theta - (r_L \ddot{\theta} + r_W \ddot{\Omega})] \\ & - I_2^B \ddot{\theta} + m_B (r_W + r_H + r_B) [g\theta - r_W \ddot{\Omega} - (r_H + r_B) \ddot{\theta}] \end{aligned} \quad (F.11)$$

 \hat{w}_3 Component of Moment about P for Whole Unicycle

$$0 = -(I_3^W \ddot{\psi} + I_2^W \Omega_0 \dot{\phi}) - I_3^L \ddot{\psi} - I_3^B \ddot{\psi} - f_G \dot{\phi} \quad (F.12)$$

 \hat{f}_2 Component about O for Legs and Body

$$\begin{aligned} 0 = & -I_2^L \ddot{\theta} + m_L r_L [g\theta - r_L \ddot{\theta} - r_W \ddot{\Omega}] \\ & - I_2^B \ddot{\theta} + m_B (r_H + r_B) [g\theta - r_W \ddot{\Omega} - (r_H + r_B) \ddot{\theta}] - Q_W \end{aligned} \quad (F.13)$$

 \hat{g}_1 Component about H for Body

$$\begin{aligned} 0 = & -I_1^B (\ddot{\phi} + \ddot{\beta}) + m_B r_B [r_W \Omega_0 \dot{\phi} - (r_W + r_H + r_B) \ddot{\phi} - r_B \ddot{\beta} \\ & + g(\phi + \beta)] - Q_B \end{aligned} \quad (F.14)$$

F.2 Lateral equations of motion

from F.12:

$$(I_3^W + I_3^L + I_3^B)\ddot{\phi} = -I_2^W \Omega_0 \dot{\phi} - f_G \dot{\phi} \quad (F.15)$$

from F.10:

$$\begin{aligned} & [I_1^W + m_W r_W^2 + I_1^L + m_L(r_W + r_L)^2 + I_1^B + m_B(r_W + r_H + r_B)^2]\ddot{\phi} \\ & + [I_1^B + m_B r_B(r_W + r_H + r_B)]\ddot{\beta} \\ & = [I_2^W + m_W r_W^2 + m_L r_W(r_W + r_L) + m_B r_W(r_W + r_H + r_B)]\Omega_0 \dot{\phi} \\ & + [m_W r_W + m_L(r_W + r_L) + m_B(r_W + r_H + r_B)]g\phi + m_B r_B g\beta \end{aligned} \quad (F.16)$$

from F.14:

$$\begin{aligned} & [I_1^B + m_B r_B(r_W + r_H + r_B)]\ddot{\phi} + [I_1^B + m_B r_B^2]\ddot{\beta} \\ & = m_B r_W r_B \Omega_0 \dot{\phi} + m_B r_B g(\phi + \beta) - Q_B \end{aligned} \quad (F.17)$$

F.3 Longitudinal equations of motion

from F.11:

$$\begin{aligned} & [I_2^L + m_L r_L(r_W + r_L) + I_2^B + m_B(r_H + r_B)(r_W + r_H + r_B)]\ddot{\theta} \\ & + [I_2^W + m_W r_W^2 + m_L r_W(r_W + r_L) + m_B r_W(r_W + r_H + r_B)]\dot{\Omega} \\ & = [m_L r_L + m_B(r_H + r_B)]g\theta \end{aligned} \quad (F.18)$$

from F.13:

$$\begin{aligned} & [I_2^L + m_L r_L^2 + I_2^B + m_B(r_H + r_B)^2]\ddot{\theta} + [m_L r_L + m_B(r_H + r_B)]r_W \dot{\Omega} \\ & = [m_L r_L + m_B(r_H + r_B)]g\theta - Q_W \end{aligned} \quad (F.19)$$

F.4 Lateral system characteristics

For the purposes of the present study, let the turntable be solidly fixed to the frame. Assume that there is a rotational joint and motor somewhere along the frame at a distance r_H from the wheel axle. The mass and inertia of the original frame is therefore divided in two, with the lower part of the frame simulating the rider's legs (L) and the upper part of the frame together with the turntable simulating the leaning part of the rider's body (B).

In order to divide the frame's mass and inertia, consider the original frame as a rectangular body of width w and height $2r_F$. Its mass is m_F and the inertia about the \hat{f}_1 unit vector passing through its center of mass is

$$I_1^F = \frac{m_F}{12}(w^2 + 4r_F^2) \quad (F.20)$$

so that

$$w = \sqrt{\frac{12I_1^F}{m_F} - 4r_F^2} \quad (F.21)$$

With the hinge point H a distance r_H from the bottom of the frame where it connects to the wheel axle, the mass of the lower part of the frame is

$$m_L = \frac{r_H}{2r_F} m_F \quad (F.22)$$

The center of mass is at

$$r_L = \frac{r_H}{2} \quad (F.23)$$

The inertia of the lower part of the frame is

$$I_1^L = \frac{m_L}{12}(w^2 + 4r_L^2) \quad (F.24)$$

Likewise, the upper part of the frame has mass properties:

$$m_U = \frac{2r_F - r_H}{2r_F} m_F \quad (F.25)$$

$$r_U = \frac{2r_F - r_H}{2} \quad (F.26)$$

$$I_1^U = \frac{m_U}{12}(w^2 + 4r_U^2) \quad (F.27)$$

Now we can combine the mass properties of the upper part of the frame with that of the turntable to find the mass properties of the leaning part of the body (B):

$$m_B = m_U + m_T \quad (F.28)$$

$$r_B = \frac{m_U r_U + m_T(r_T - r_H)}{m_U + m_T} \quad (F.29)$$

$$I_1^B = I_1^U + m_U(r_B - r_U)^2 + I_1^T + m_T(r_T - r_H - r_B)^2 \quad (F.30)$$

By calculating the inertia properties in this manner the eigenvalues associated with the sideways falling of the leaning configuration unicycle as a whole, will be the same as the corresponding eigenvalues of the twisting configuration unicycle.

The lateral system dynamic equations of motion F.15, F.16 and F.17 can be written in state space form if we define the state vector

$$\mathbf{x} = [\phi \ \dot{\phi} \ \ddot{\phi} \ \phi \ \dot{\phi} \ \ddot{\phi}]^T \quad (F.31)$$

$$\begin{bmatrix} I_{11} & 0 & I_{13} & 0 & 0 \\ I_{21} & 0 & I_{23} & 0 & 0 \\ 0 & I_{33} & 0 & 0 & 0 \\ 0 & 0 & 0 & 1 & 0 \\ 0 & 0 & 0 & 0 & 1 \end{bmatrix} \begin{bmatrix} \ddot{\phi} \\ \ddot{\psi} \\ \ddot{\beta} \\ \dot{\phi} \\ \dot{\beta} \end{bmatrix} = \begin{bmatrix} 0 & J_{12} & 0 & J_{14} & J_{15} \\ 0 & J_{22} & 0 & J_{24} & J_{25} \\ J_{31} & -f_G & 0 & 0 & 0 \\ 1 & 0 & 0 & 0 & 0 \\ 0 & 0 & 1 & 0 & 0 \end{bmatrix} \begin{bmatrix} \ddot{\phi} \\ \ddot{\psi} \\ \ddot{\beta} \\ \dot{\phi} \\ \dot{\beta} \end{bmatrix} + \begin{bmatrix} -1 \\ 0 \\ 0 \\ 0 \\ 0 \end{bmatrix} Q_B \quad (F.32)$$

where

$$I_{11} = I_1^B + m_B r_B(r_W + r_H + r_B) \quad (F.33)$$

$$I_{13} = I_1^B + m_B r_B^2 \quad (F.34)$$

$$I_{21} = I_1^W + m_W r_W^2 + I_1^L + m_L(r_W + r_L)^2 + I_1^B + m_B(r_W + r_H + r_B) \quad (F.35)$$

$$I_{23} = I_{11} \quad (F.36)$$

$$I_{32} = I_1^W + I_3^L + I_3^B \quad (F.37)$$

$$J_{12} = m_B r_B r_W \Omega_0 \quad (F.38)$$

$$J_{14} = J_{15} = m_B r_B g \quad (F.39)$$

$$J_{22} = [I_2^W + m_W r_W^2 + m_L r_W (r_W + r_L) + m_B r_W (r_W + r_H + r_B)] \Omega_0 \quad (F.40)$$

$$J_{24} = [m_W r_W + m_L (r_W + r_L) + m_B (r_W + r_H + r_B)] g \quad (F.41)$$

$$J_{25} = J_{14} \quad (F.42)$$

$$J_{31} = -I_2^W \Omega_0 \quad (F.43)$$

$$J_{32} = -f_G \quad (F.44)$$

Multiplication of equation F.32 by the inverse of the first matrix containing the inertia terms, yields the standard state space form of the lateral system dynamic equations;

$$\dot{x} = Fx + Gu \quad (F.45)$$

An analysis of the lateral system characteristics is shown in the listing of section F.4.1. There is one eigenvalue near $s = 0$ which is the yaw rate mode of the robot. The other eigenvalue at $s = 0$ for the yaw angular position mode is not shown. Two pairs of eigenvalues reside on the real axis on either side of the imaginary axis. The eigenvalues at $s = \pm 3.29$ rad/sec are for the sideways unstable pendulum modes of the unicycle as a whole. These modes are at the same frequency as those in the twisting configuration (section Q.3.1), because we have chosen to use the same robot parameters of Appendix M. Two other inverted pendulum modes are at $s = \pm 9.89$ rad/sec due to the leaning part of the body. The location of these eigenvalues change as a function of the hinge height, r_H .

The modal controllability matrix CTR in the print-out shows that the yaw rate mode is uncontrollable from the lean motor torque. Physically it means that if yaw angular momentum is present in the system, it cannot be controlled with the

lean actuator. Fortunately this yaw mode is stable due to the friction losses at the ground contact point of the wheel.

The CTR matrix also indicates limited controllability of the main inverted pendulum modes (at $s = \pm 3.29$ rad/sec) from the lean motor torque. It is possible to stabilize the unicycle by leaning the body, but accurate control of the yaw motions (i.e. steering) cannot be achieved by this control method.

F.4.1 Lateral system analysis

UCTC12/LEANCHAR.CTR

LATERAL SYSTEM CONTROLLED BY LEANING

.....

LATERAL STATES : PHI.DOT; PSI.DOT; BETA.DOT; PHI; BETA

CONTROL INPUT : LEAN MOTOR TORQUE (QB)

UNITS : METERS, RADIANS, SECONDS

.....

LEAN HINGE HEIGHT ABOVE WHEEL AXLE (METERS) :

RH -

0.7000

NOMINAL WHEEL SPEED (RAD/SEC) :

ONEGA0 -

142 APPENDIX F. UNICYCLE ROBOT STEERED BY SIDEWAYS LEANING

3.0

OPENLOOP SYSTEM MATRICES:

.....

FLAT

0.0000	0.7783	0.0000	12.9442	-7.6666
-0.1259	-0.0277	0.0000	0.0000	0.0000
0.0000	-1.3688	0.0000	-22.3357	95.8731
1.0000	0.0000	0.0000	0.0000	0.0000
0.0000	0.0000	1.0000	0.0000	0.0000

GLAT

0.3308
0.0000
-3.7467
0.0000
0.0000

EIGVAL

-0.0279
-3.2935
3.2937
-9.8930
9.8930

EIGVEC

0.0017	1.0000	1.0000	-0.0902	-0.0902
1.0000	0.0386	-0.0379	-0.0012	0.0011
-0.0000	0.2606	0.2607	1.0000	1.0000
-0.0600	-0.3036	0.3036	0.0091	-0.0091

F.4. LATERAL SYSTEM CHARACTERISTICS

143

0.0003 -0.0791 0.0792 -0.1011 0.1011

CTR

-

-0.0000

-0.0034

-0.0034

-1.8725

-1.8725

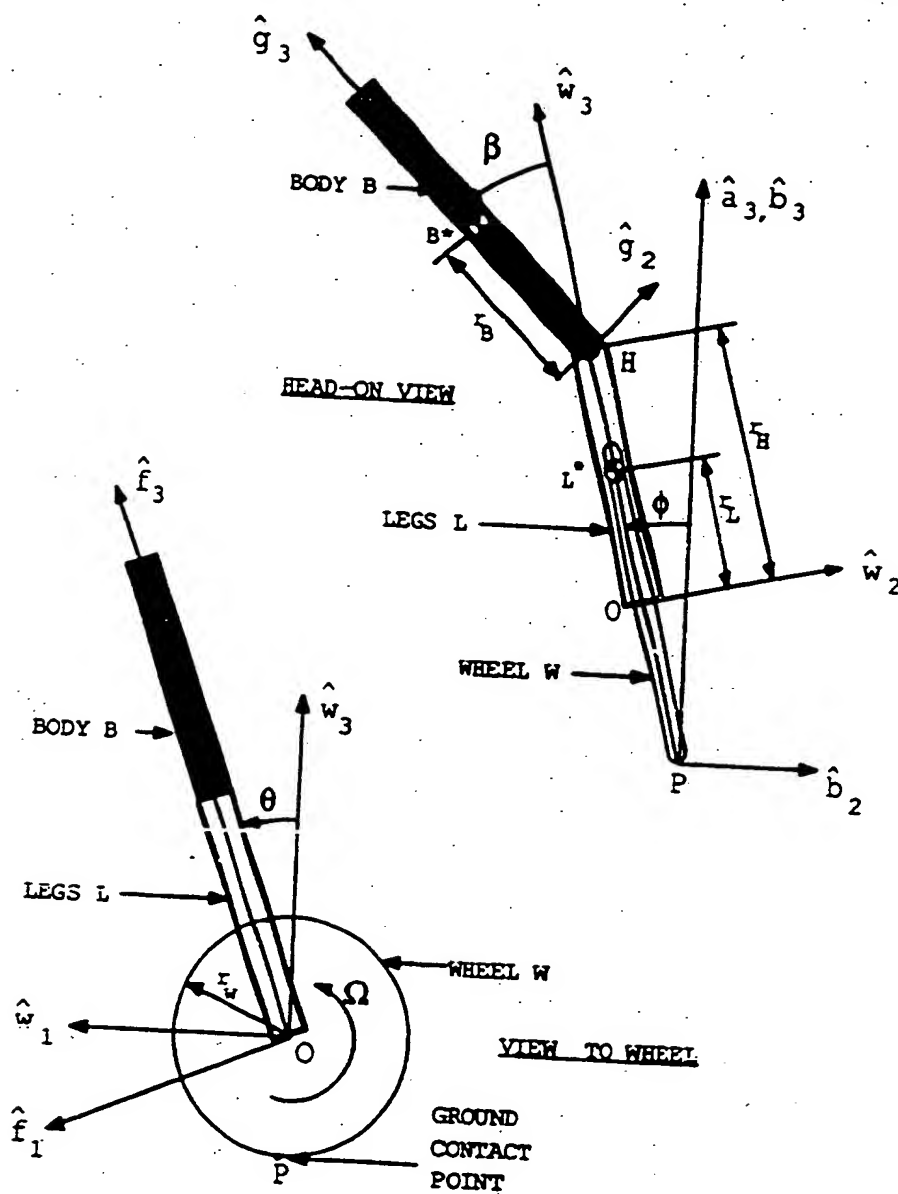


Figure F.1: Steering by Leaning

Appendix G

Gear Ratio for Maximum Yaw Acceleration

G.1 Motivation for the optimal gear ratio

The turntable is used as a null momentum reaction wheel to steer the body of the unicycle. A direct current motor mounted on the unicycle frame drives the turntable through a gear train.

The unicycle control system will compensate for lateral disturbances by steering the vehicle towards the direction that it is falling over. It would therefore be advantageous to calculate the optimal gear ratio of the turntable drive train, that would give maximum yaw acceleration of the frame of the unicycle. The relevant parameters are shown in Figure G.1

G.2 Yaw dynamics with a geared drive system

Obtaining the dynamic equations from Lagrange's method:

Let the generalized coordinates of the lateral system be:

$$q_1 = \psi = \text{yaw angle of the frame}$$

$$q_2 = \bar{\omega} = \text{angle of motor rotor relative to the frame}$$

$$q_3 = \bar{\eta} = \text{angle of turntable relative to the frame}$$

the derivatives of the generalized coordinates are

$$\dot{q}_1 = \dot{\psi}$$

$$\dot{q}_2 = \omega$$

$$\dot{q}_3 = \eta$$

The total kinetic energy of the system is:

$$\begin{aligned} T &= \frac{1}{2}[J_F \dot{\psi}^2 + J_R(\dot{\psi} + \omega)^2 + J_T(\dot{\psi} + \eta)^2] \\ &= \frac{1}{2}[J_F \dot{q}_1^2 + J_R(\dot{q}_1 + \dot{q}_2)^2 + J_T(\dot{q}_1 + \dot{q}_3)^2] \end{aligned} \quad (\text{G.1})$$

The constraint equation of the system is

$$\omega = n\eta \quad \text{or} \quad \dot{q}_2 = \eta \dot{q}_3 \quad (\text{G.2})$$

where n is the gear ratio of the turntable drive system.

The nonholonomic constraint equation is augmented to the Lagrange's equation to give

$$\frac{d}{dt} \left(\frac{\partial T}{\partial \dot{q}_i} \right) - \frac{\partial T}{\partial q_i} = \lambda a_i + Q_i \quad (\text{G.3})$$

where Q_i is a generalized force.

$$a_i \equiv \frac{\partial \phi}{\partial \dot{q}_i} \quad (\text{G.4})$$

where ϕ is the constraint equation of the system

$$\phi = \omega - n\eta = 0 \quad (\text{G.5})$$

rewritten in differential form:

$$1 \cdot d\dot{\omega} - \eta \cdot d\dot{\eta} = 0 \quad (\text{G.6})$$

We can readily identify the a_i coefficients:

$$\begin{aligned} a_1 &= 0 \\ a_2 &= 1 \\ a_3 &= -\eta \end{aligned} \quad (\text{G.7})$$

apply Lagrange's equation for each generalized coordinate:

$q_1 = \psi$:

$$(J_F + J_R + J_T)\ddot{q}_1 + J_R\ddot{q}_2 + J_T\ddot{q}_3 = -T_R \quad (\text{G.8})$$

where T_R is the torque developed between the rotor and it's stator which is fixed to the unicycle frame.

q_2 :

$$J_R(\ddot{q}_1 + \ddot{q}_2) = \lambda + T_R \quad (\text{G.9})$$

q_3 :

$$J_T(\ddot{q}_1 + \ddot{q}_3) = -n\lambda \quad (\text{G.10})$$

Eliminate the Lagrange multipliers by substituting G.9 into G.10:

$$(J_F + nJ_R)\ddot{q}_1 + nJ_R\ddot{q}_2 + J_T\ddot{q}_3 = nT_R \quad (\text{G.11})$$

use the constraint equation to eliminate \ddot{q}_2 from equations G.8 and G.11 to yield the two dynamic equations of motion:

$$(J_F + J_R + J_T)\ddot{q}_1 + (J_T + nJ_R)\ddot{q}_3 = -T_R$$

or in terms of the system coordinates:

$$(J_F + J_R + J_T)\ddot{\psi} + (J_T + nJ_R)\ddot{\eta} = -T_R \quad (\text{G.12})$$

and

$$(J_T + nJ_R)\ddot{q}_1 + (n^2 J_R + J_T)\ddot{q}_3 = nT_R$$

or in terms of the system coordinates:

$$(J_T + nJ_R)\ddot{\psi} + (n^2 J_R + J_T)\ddot{\eta} = nT_R \quad (G.13)$$

we can use equation G.13 to eliminate J_T from equation G.12; which then becomes

$$[J_F + (1 - n)J_R]\ddot{\psi} + n(1 - n)J_R\ddot{\eta} = -(n + 1)T_R \quad (G.14)$$

Equations G.13 and G.14 are now in a form which can be compared with equations of the lateral system derived in Appendices A, B and C where the motor rotor inertias were assumed to be zero.

As we will see later, n is a fairly large number (approximately 70) for the actual unicycle parameters. We can therefore approximate the right hand side of equation G.14 by $-nT_R$.

Eliminate $\ddot{\eta}$ between equations G.13 and G.14:

$$\ddot{\psi} = \frac{-(nJ_R + J_T)nT_R}{J_R(J_T + J_F)n^2 - 2J_T J_R n + J_T(J_F + J_R)} \quad (G.15)$$

To get maximum acceleration as a function of n let $\frac{d\ddot{\psi}}{dn} = 0$

$$n_{opt} = \frac{J_F + J_R}{J_T + J_F + 2J_R} + \sqrt{\left(\frac{J_F + J_R}{J_T + J_F + 2J_R}\right)^2 + \frac{J_T(J_F + J_R)}{J_R(J_T + J_F + 2J_R)}} \quad (G.16)$$

Notice that if $J_T \rightarrow \infty$ i.e. load is held fixed

$$n_{opt} \rightarrow \sqrt{\frac{J_F + J_R}{J_R}} \cong \sqrt{\frac{J_F}{J_R}}$$

Also notice that equation G.16 can be approximated as follows:

$$n_{opt} \cong \underbrace{\frac{J_F}{J_T + J_F}}_{\text{small compared to } 1} + \sqrt{\underbrace{\left(\frac{J_F}{J_T + J_F}\right)^2}_{\text{small compared to } 1} + \frac{J_T J_F}{J_R(J_T + J_F)}}$$

if $J_R < J_T, J_F$ the optimal gear ratio is by good approximation:

$$n_{opt} \cong \sqrt{\frac{J_T J_F}{J_R(J_T + J_F)}} \quad (G.17)$$

G.3 Yaw acceleration as a function of gear ratio

Since the standard gear sizes allow a discrete number of gear ratios only, it is useful to plot equation G.15 as a function of the gear ratio, n . The CTRL-C program latnopt.ctr is used to calculate this function and the resulting plot is shown in Figure G.2.

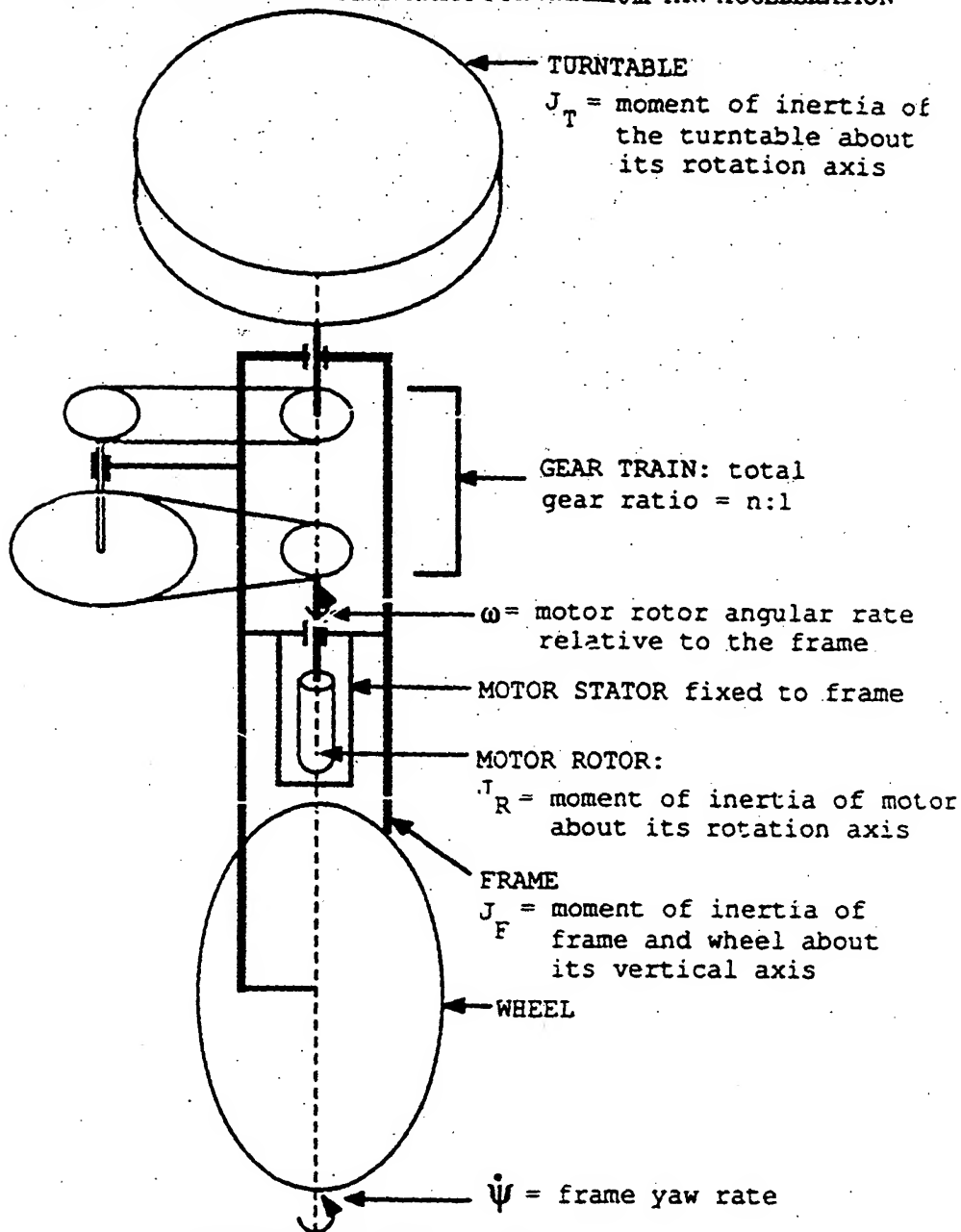


Figure G.1: Turntable Gear Drive Schematic

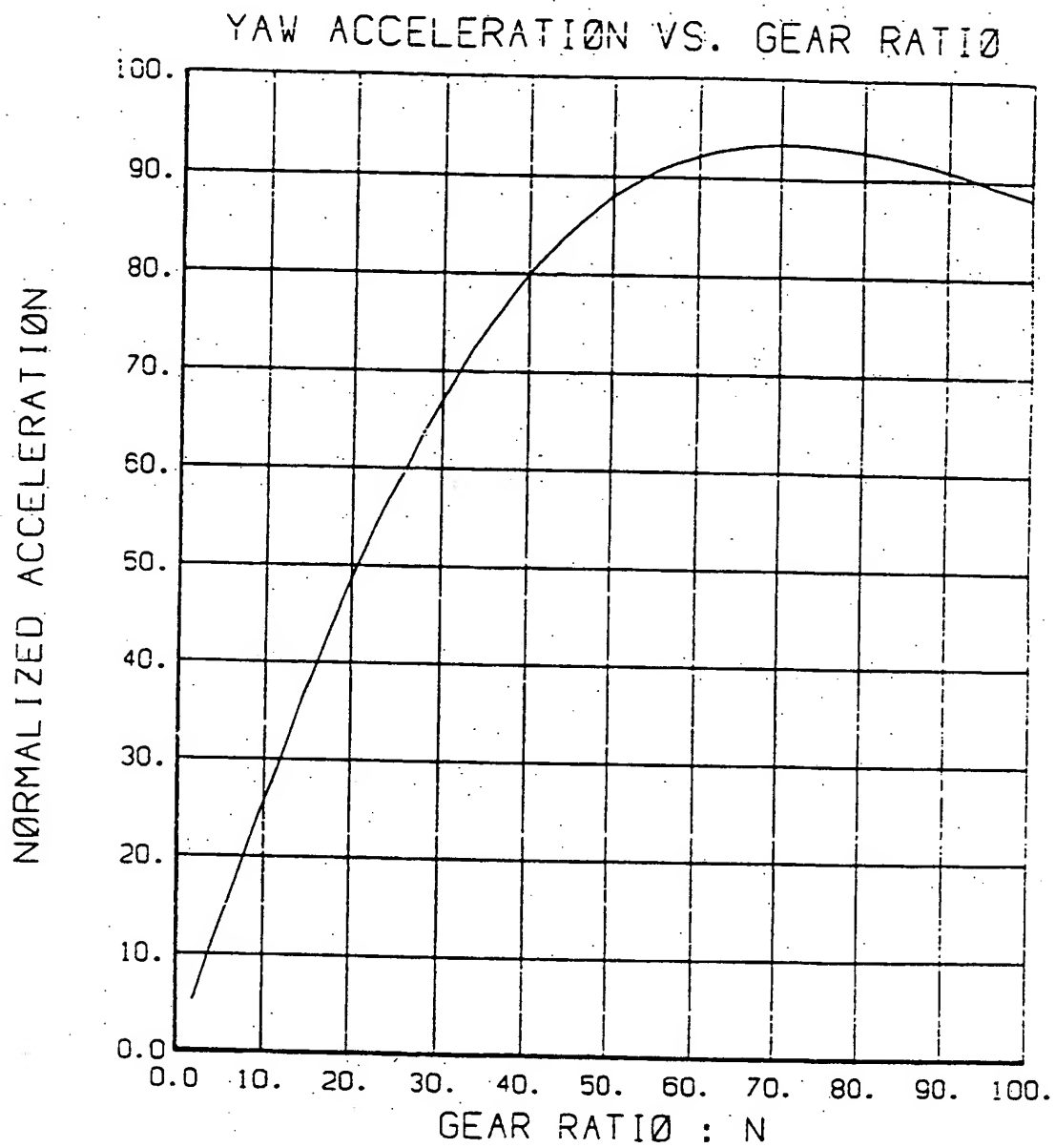


Figure G.2: Normalized Yaw Acceleration as a Function of the Turntable Drive System Gear Ratio

Appendix H

Servo Accelerometer Design

H.1 Introduction

Simulations of the unicycle and control system have shown that the attitude of the vehicle will deviate less than 1 degree from vertical during normal maneuvers. Peak linear acceleration of the frame is expected to be on the order of $0.1m/s^2$. To obtain good attitude and acceleration information, the accelerometer sensor should have an accuracy of approximately one twentieth of the maximum expected value, i.e. $0.005m/s^2$. ($\frac{1}{2000}$ of the earth's gravity acceleration). Commercial servo accelerometers which measure to these accuracies are prohibitively expensive and a custom made accelerometer was designed for the unicycle robot.

H.2 Mechanical design of servo accelerometer

A drawing of the mechanical part of the accelerometer is shown in Figure H.1. It consists of a pendulum suspended by means of a beryllium-copper flexure. Optical pick-off of the position of the pendulum is accomplished by an infra-red light-emitting diode on the pendulum which illuminates a set of photodiodes fixed

to the accelerometer housing.

Electromagnetic actuation of the pendulum is provided by a set of coils on the pendulum and a pair of permanent magnets pressed into the walls of the housing. The physical size and weight of the pendulum was minimized to keep the undamped natural frequency of the pendulum much higher than the bandwidth of the unicycle robot (unicycle bandwidth is less than 1 Hz).

H.3 Feedback control system design

Figure H.2 shows the block diagram of the feedback control system. The purpose of the control system is to generate a current in the actuator coils which will reposition the light beam to the null position on the photo detectors during accelerations. If integral error feedback control is used as shown in the analysis in Figure H.2, the current in the coil is proportional to the acceleration experienced by the accelerometer as long as the frequency content of the acceleration motion is much lower than the closed loop bandwidth of the servo accelerometer.

H.4 Optical pick-off considerations

A Siemens SFH405-2 (Table H.1) infra-red light-emitting diode (LED) was used as a light source. The pendulum arm was specially designed to allow the LED to shine through a narrow slit of 75 μm (0.003 inches) in the bottom of the pendulum. The photo detector is a Siemens SFH204 four-quadrant silicon photodiode (Table H.2). The active units are only 12 μm apart and 100 μm wide and were connected in pairs to sense the beam deviation along one axis only.

An important consideration for the choice of this detector as opposed to two separate phototransistors, is the fact that all the active areas are on the same piece

of silicon substrate, which provides the most similar behaviour of the differential active areas under temperature variations.

The choice of a light beam width of $75\text{ }\mu\text{m}$ for the $100\text{ }\mu\text{m}$ wide active area of the detector results in a maximum to minimum variation of the detector output current for a pendulum motion of only $75\text{ }\mu\text{m}$.

By taking the difference between the output currents from the two active areas, a reasonably linear relationship between pendulum position and detector output signal can be obtained, as shown in figure H.3. The output currents from the photodiodes are in the order of tenths of a μA and the light beamwidth should be chosen wide enough to generate enough photo current without flooding the whole active area. The distance from the light source to the detector was minimized by mechanical design for the same reason.

Temperature drift and other forms of process noise cause errors in the servo accelerometer outputs which cannot be distinguished from actual accelerations. It is shown in the analysis of figure H.4 that the errors due to detector drift can be minimized by maximizing the sensitivity of the photo detector to pendulum position changes. Since one of the few parameters available to the designer to increase this sensitivity is by decreasing the light beamwidth, it is a conflicting requirement to that stated in the previous paragraph. A compromise of making the light beam approximately half as wide as the detector active area was chosen.

In order to compensate for the non-uniformity of the light source and detector sensitivity, the total light received by all the active areas of the detector is regulated to be constant as described in the next section.

H.5 Detector electronics and servo amplifier design

Figure H.5 depicts the electronic circuit diagram for the servo accelerometer. A voltage proportional to the total light received by the photodiode detectors, is compared with a well stabilized 8V reference signal. The difference is used to regulate the current to the LED in order to keep the total received light constant.

A differential amplifier stage converts the difference in the photo currents to a voltage which is proportional to the pendulum displacement. The photodiode package is mounted on a separate printed circuit board which can be repositioned mechanically to receive the light beam in the middle of the detector under zero acceleration conditions. Any remaining offset is corrected for electronically.

The small signals from the photodiodes are susceptible to interference from stray electromagnetics (e.g. 60Hz hum, switching amplifier noise, D.C. motor commutator noise, etc.). All the photodetector electronics are mounted on a miniature circuitboard (Figure H.6) which is positioned on the side of the accelerometer as close to the photodiodes as possible. The whole unit is packaged in a metal box at ground potential, which effectively eliminates any stray environmental electromagnetic influences.

The actuator coil has a $25\ \Omega$ resistance and requires approximately 160 mA to reposition the pendulum to its original position when the accelerometer is turned on its side. A class A servo amplifier is included with feedback to provide the driving current without cross over distortion.

H.6 Openloop frequency response and plant model

The frequency response from the coil current control voltage to the differential photodiode output was measured. The gain and phase responses are plotted in

APPENDIX H. SERVO ACCELEROMETER DESIGN

Figure H.7 and it is seen that the plant response compares well to that of a lightly damped second order system with:

$$\begin{aligned} K_p &= 0.684 && \text{low frequency gain} \\ \omega_n &= 46.6 \text{ Hz} && \text{undamped natural frequency} \\ \xi &= 0.01 && \text{damping factor} \end{aligned}$$

$$\Rightarrow G_p(s) = \frac{K_p \omega_n^2}{s^2 + 2\xi \omega_n s + \omega_n^2}$$

The coil inductance measured 22 mH and together with the 25 Ω coil resistance and 30 Ω series resistor, it forms another plant pole at

$$\omega_p = \frac{R}{L} = \frac{55}{0.022} = 2500 \text{ rad/sec}$$

This pole is at a much higher frequency than the control bandwidth of approximately 200 rad/sec and is therefore ignored in the plant dynamic model.

H.7 Compensation design

The compensator is designed to increase the damping on the lightly damped plant poles and it also adds a pure integrator into the loop to provide zero error to constant acceleration inputs. Two additional zeros are required to draw the closed loop root locus far enough into the left half of the s -plane to provide an acceptably short settling time.

The second order electronic compensator that was selected is shown in Figure H.8.

For unity feed back, the closed loop characteristic polynomial is:

$$1 + G_p(s)G_c(s) = 0, \quad \text{i.e.}$$

$$s^4 + \frac{1}{CR_4}s^3 + \frac{w_n^2}{R_1}\left[\frac{R_2}{K_p} + 1\right]s^2 + \frac{w_n^2}{CR_1R_3R_4}\{[R_3(R_2 + R_4) - R_1R_4]K_p + R_1R_3\}s + \frac{K_p w_n^2}{C^2 R_1 R_4} = 0 \quad (H.1)$$

The desired closed loop poles were chosen to be at the 4th order ITAE positions, therefore the desired closed loop polynomial is:

$$\left[\left(\frac{s}{w_0} + 0.424\right)^2 + (1.263)^2\right]\left[\left(\frac{s}{w_0} + 0.626\right)^2 + (0.4141)^2\right] = 0 \quad (H.2)$$

where w_0 is the desired bandwidth of the compensated closed loop system.

Simplifying equation H.2 gives:

$$s^4 + 2.1w_0s^3 + 3.4w_0^2s^2 + 2.7w_0^3s + w_0^4 = 0 \quad (H.3)$$

Solve for R_i by comparing the coefficients of the powers of s in equation H.1 and equation H.3.

$$R_1 = \frac{K_p w_n^2}{C^2 R_4 w_0^4} \quad (H.4)$$

$$R_2 = \frac{R_1}{K_p} \left[\frac{3.4w_0^2}{w_n^2} - 1 \right] \quad (H.5)$$

$$R_3 = \frac{R_1 R_4 w_n^2 K_p}{w_n^2 [(R_2 + R_4)K_p + R_1] - 2.7w_0^3 C R_1 R_4} \quad (H.6)$$

$$R_4 = \frac{1}{2.1w_0 C} \quad (H.7)$$

A condition that stems from the fact that the resistor values must all be positive, is:

$$(w_0)_{min} > 0.5423w_n \quad (H.8)$$

A CTRL-C program, 'lgtitae.ctr' calculates the required resistor values. The resulting print-out in Section H.8 shows that the compensator results in a pole at $s=0$, one more on the negative real axis and a pair of complex zeros in the left half of the s -plane.

APPENDIX H. SERVO ACCELEROMETER DESIGN

A root locus of the closed loop poles versus the overall loop gain, K , is shown in Figure H.9. The poles are at the ITAE positions for $K=1$. The compensated openloop system frequency response in Figure H.10 shows a 30 degrees phase margin. A low pass filter is added on the output to reduce the output oscillations during impulsive disturbances. The step response in Figure H.11 shows that the closed loop system is reasonably well damped with a settling time of approximately 30 ms.

H.8 ITAE compensator calculation program

PLANT PARAMETERS

KP -

0.6840

FM -

46.6000

ZETA -

0.0100

VM -

292.7964

PLANTPOLES -

1.0d+02 •

-0.0293 + 2.9278i

H.8. ITAE COMPENSATOR CALCULATION PROGRAM

159

-0.0293 - 2.92781

ITAE COMPENSATOR PARAMETERS: ω_0 -DESIRSD C.L. BANDW ; C-CAPACITOR VALUE

ω_0 -

351.3557

C -

1.0000d-07

EXACT RESISTOR VALUES

R1 -

2.8390d+04

R2 -

1.6171d+05

R3 -

2.7493d+03

R4 -

1.3553d+04

NEAREST AVAILABLE RESISTOR VALUES & CAPACITOR SHORT RESISTOR R5

R1 -

28700.0

APPENDIX H. SERVO ACCELEROMETER DESIGN

R2 -

162000.0

R3 -

2870.0

R4 -

14000.0

R5 -

3300000.0

COMPGAIN -

115.7491

COMZEROS -

1.0d+02 *

-0.8088 + 1.9454i

-0.8088 - 1.9454i

COMPOLES -

-714.2857

-3.0303

CLOSED LOOP SYSTEM PARAMETERS

CLZEROS -

1.0d+02 •
 -0.8088 + 1.9454i
 -0.8088 - 1.9454i

CLPOLES =

1.0d+02 •
 -1.5542 + 4.5407i
 -1.5542 - 4.5407i
 -2.0617 + 1.4861i
 -2.0617 - 1.4861i

LOW PASS FILTER ON OUTPUT (WC = CUT-OFF FREQ. IN RAD/SEC) :

WC =

212.8000

H.9 Servo accelerometer calibration

The servo accelerometers were mounted on a dividing head for calibration, using the gravity acceleration and tilt angle relationship to calculate the acceleration input. The dividing head has a 0.1 degree accuracy.

First the servo loop was opened by disconnecting the actuator coil and the accelerometer was positioned vertically (0 m/s^2 acceleration input). The optical detector screws were loosened and the detector was shifted until the differential current in the two halves of the detector was zero. The dividing head was then tilted from -180 degrees to +180 degrees and the differential output voltage of the

APPENDIX H. SERVO ACCELEROMETER DESIGN

optical detector stage was recorded. Figure H.12 shows a reasonably linear range with a steep slope for tilt angles between ± 20 degrees.

Thereafter the servo loop on the lateral accelerometer was closed and the sensor was mounted vertically on the dividing head. The offset on the output voltage was trimmed to the minimum value by means of the potentiometer on the sensor. Figure H.13 shows a plot of the sensor output voltage as a function of the tilt angle. A very linear relationship is obtained for a range of ± 20 degrees. A least squares fit to the data point for the linear region yields:

$$V_{out}^{LAT} = -0.311\phi \quad \text{volt}$$

where ϕ is the roll angle in degrees. Since a $+90$ degree tilt angle corresponds to $1g$ acceleration, the transfer function can be rewritten as:

$$latacc = 0.35048 V_{out}^{LAT} \quad m/s^2$$

where $latacc$ is the lateral acceleration.

The longitudinal accelerometer is calibrated in the same manner and its transfer function is shown in Figure H.14. A least squares fit for the data points gives:

$$V_{out}^{LGT} = -0.3452 \times \theta \quad (\text{volt})$$

where θ is the pitch angle in degrees.

$$lgtacc = -0.31576 V_{out}^{LGT} \quad m/s^2$$

where $lgtacc$ is the longitudinal acceleration.

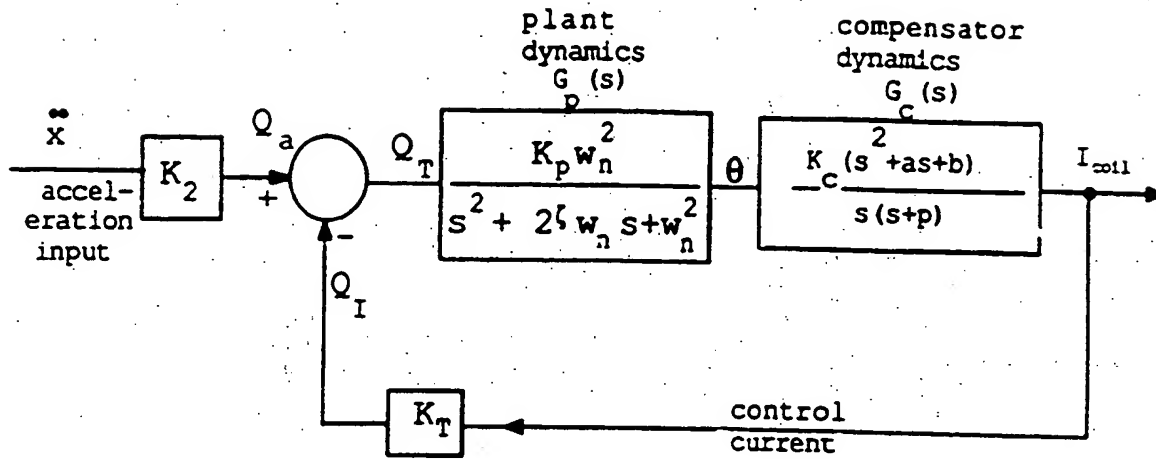
The sensor output voltage drift due to temperature effects measured less than $\pm 10mV$. This is equivalent to $\pm \frac{1}{5000}$ of gravity acceleration or an uncertainty of $\pm \frac{1}{30}$ degree in the measured tilt angle.

H.10 Hall-effect frame angle sensor design

A device to measure the unicycle frame pitch angle was designed by using a trailer wheel that touches the ground, as shown in Figure 4.1. A Hall-effect transducer (91SS12-2 LOHET by MICRO SWITCH, a Honeywell Division) is attached to the unicycle frame, separated from the magnet at the end of the aluminum rod from the trailer wheel by a 2 mm air gap.

The analog electronic interface to the LOHET is shown in Figure H.15. The output of the fourth operational amplifier is connected to the analog-to-digital interface card described in Appendix J.

The sensor was calibrated to determine the output voltage as a function of the pitch angle. The calibration curve is shown in Figure H.16. The sensor is linear over a range of -5 degrees to +5 degrees with a gain of 0.8541 volt/degree.



closed loop transfer function :

$$G_{CL}(s) = \frac{I_{coil}}{\ddot{x}} = \frac{K_2 K_p K_c w_n^2 (s^2 + as + b)}{s(s+p)(s^2 + 2\zeta w_n s + w_n^2) + K_T K_p K_c w_n^2 (s^2 + as + b)}$$

for frequencies much lower than the servo accelerometer closed loop bandwidth:

$$\lim_{s \rightarrow 0} G_{CL}(s) = \frac{I_{coil}}{\ddot{x}} \Big|_{\text{approx steady state}} = \frac{K_2}{K_T} \Rightarrow \text{the coil current is proportional to the acceleration}$$

Figure H.2: Feedback Control System Block Diagram

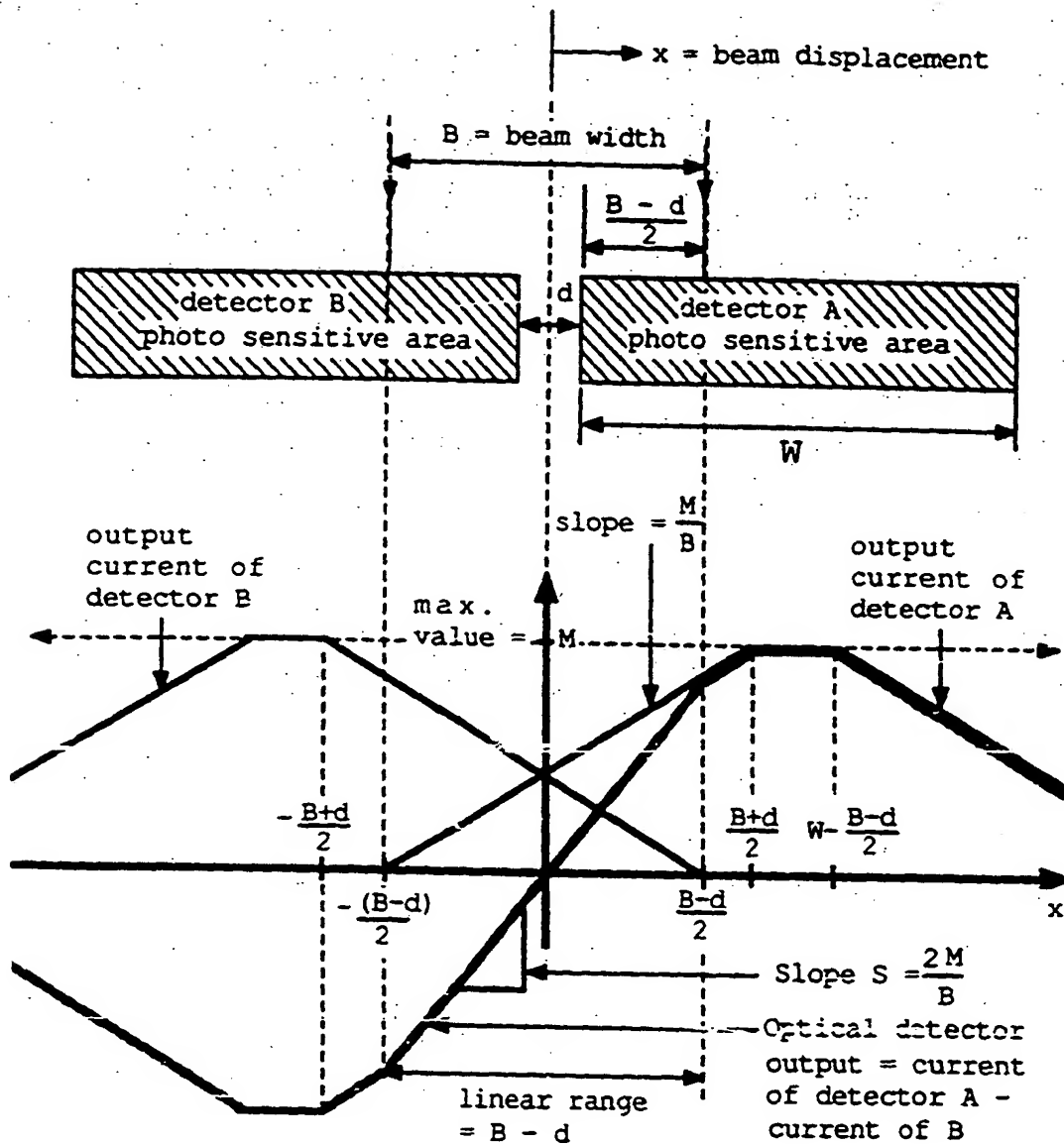
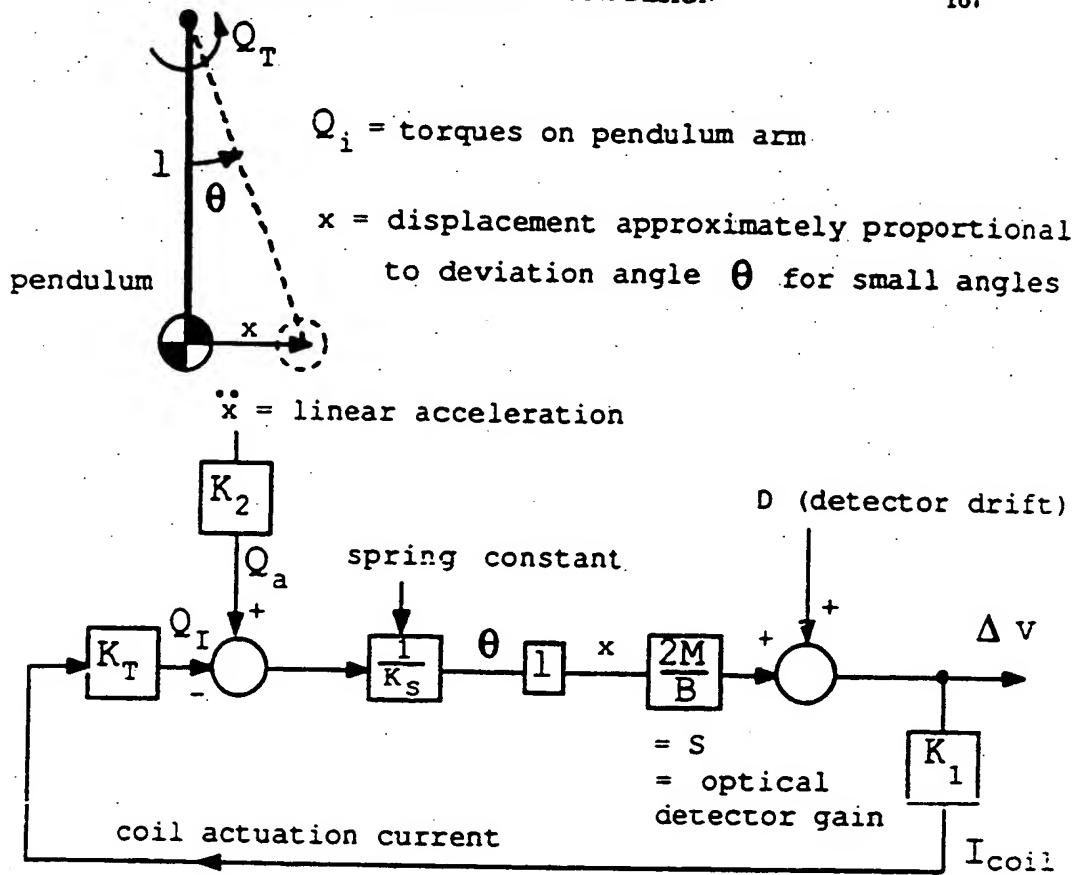


Figure H.3: Relationship between Differential Photodiode Output and Light Beam Position



$$\frac{\Delta v}{\ddot{x}} = \frac{K_2 \frac{1S}{K_s}}{\text{loopgain}} \quad \text{and} \quad \frac{\Delta v}{D} = \frac{1}{\text{loopgain}}$$

$$\therefore \ddot{x} \frac{K_2 1S}{K_s} = \Delta v \times \text{loopgain} = D$$

$$\boxed{\frac{\ddot{x}}{D} = \frac{K_s}{K_2 1S}}$$

\therefore to get the apparent acceleration due to drift D , small, make $S (= \frac{2M}{B})$ as large as possible

make B as small as possible

Figure H.4: Sensitivity to Process Noise Analysis

H.10. HALL-EFFECT FRAME ANGLE SENSOR DESIGN

169

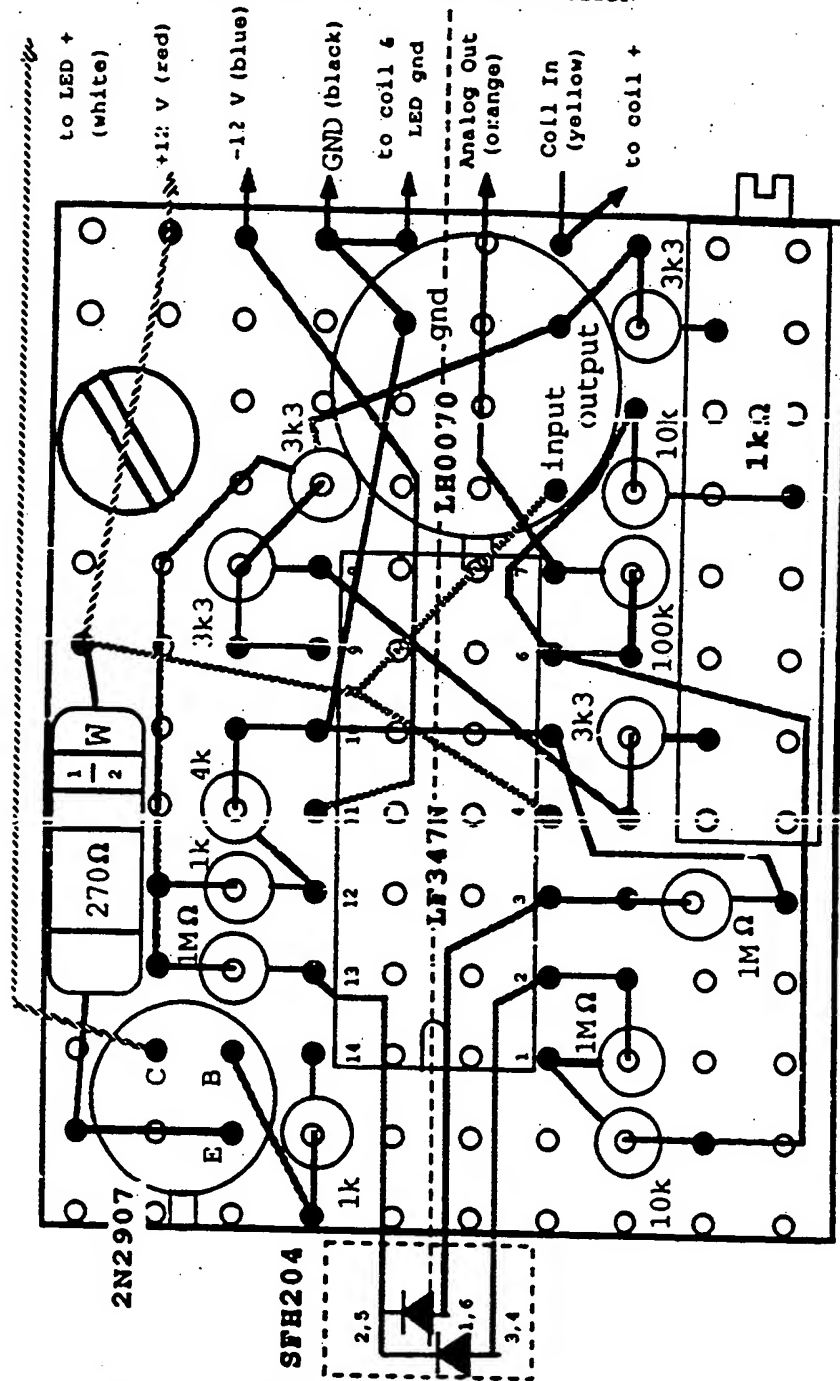


Figure H.6: Opto Electronics Printed Circuit Board Layout

THEORETICAL & MEASURED PLANT FREQUENCY RESPONSE

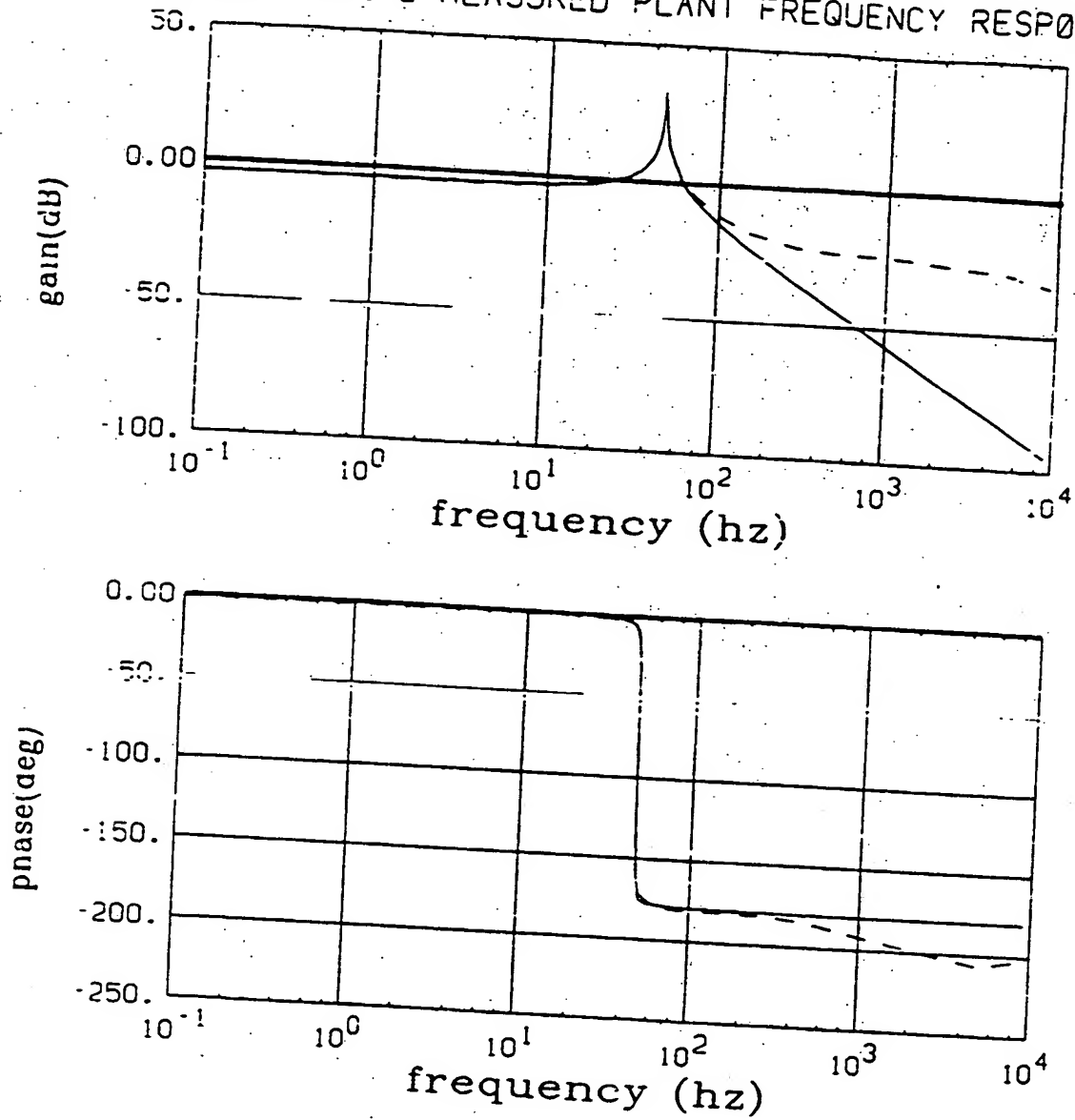
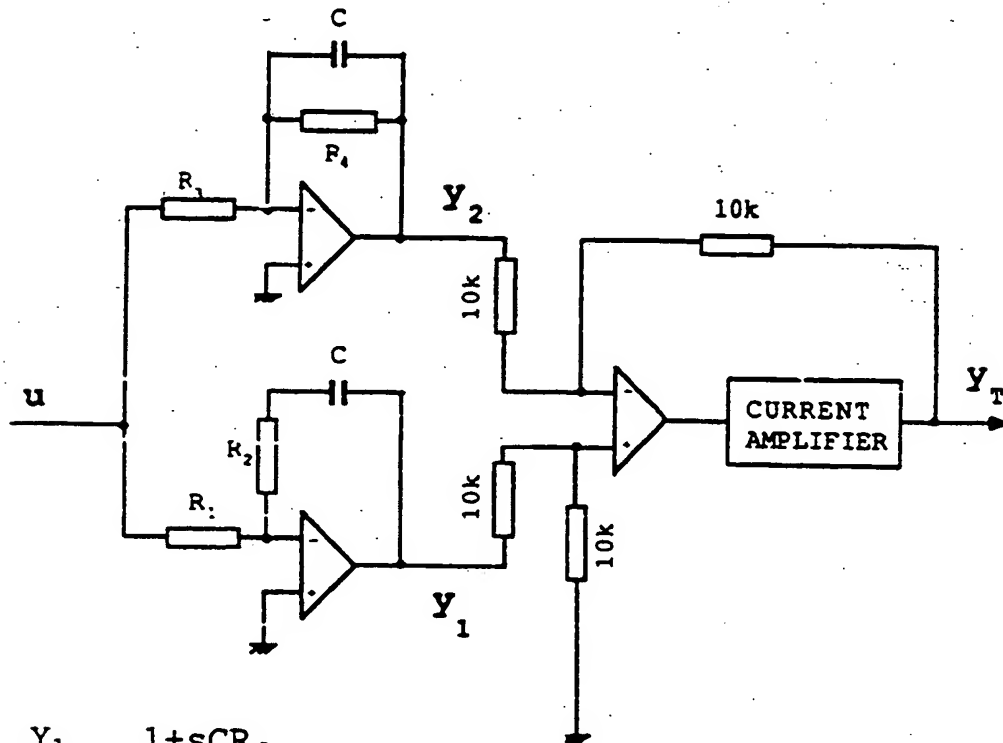


Figure H.7: Plant Measured and Theoretical Frequency Response



$$\frac{Y_1}{U} = - \frac{1+sCR_2}{sCR_1}$$

$$\frac{Y_2}{U} = - \frac{R_4}{R_3} \frac{1}{1+sCR_4}$$

$$Y_T = Y_2 - Y_1$$

$$G_C(s) = \frac{Y_T}{U} = - \frac{C^2 R_2 R_3 R_4 s^2 + C[R_3(R_2 + R_4) - R_1 R_4]s + R_3}{CR_1 R_3 s(1 + sCR_4)}$$

Figure H.8: Second Order Electronic Compensator

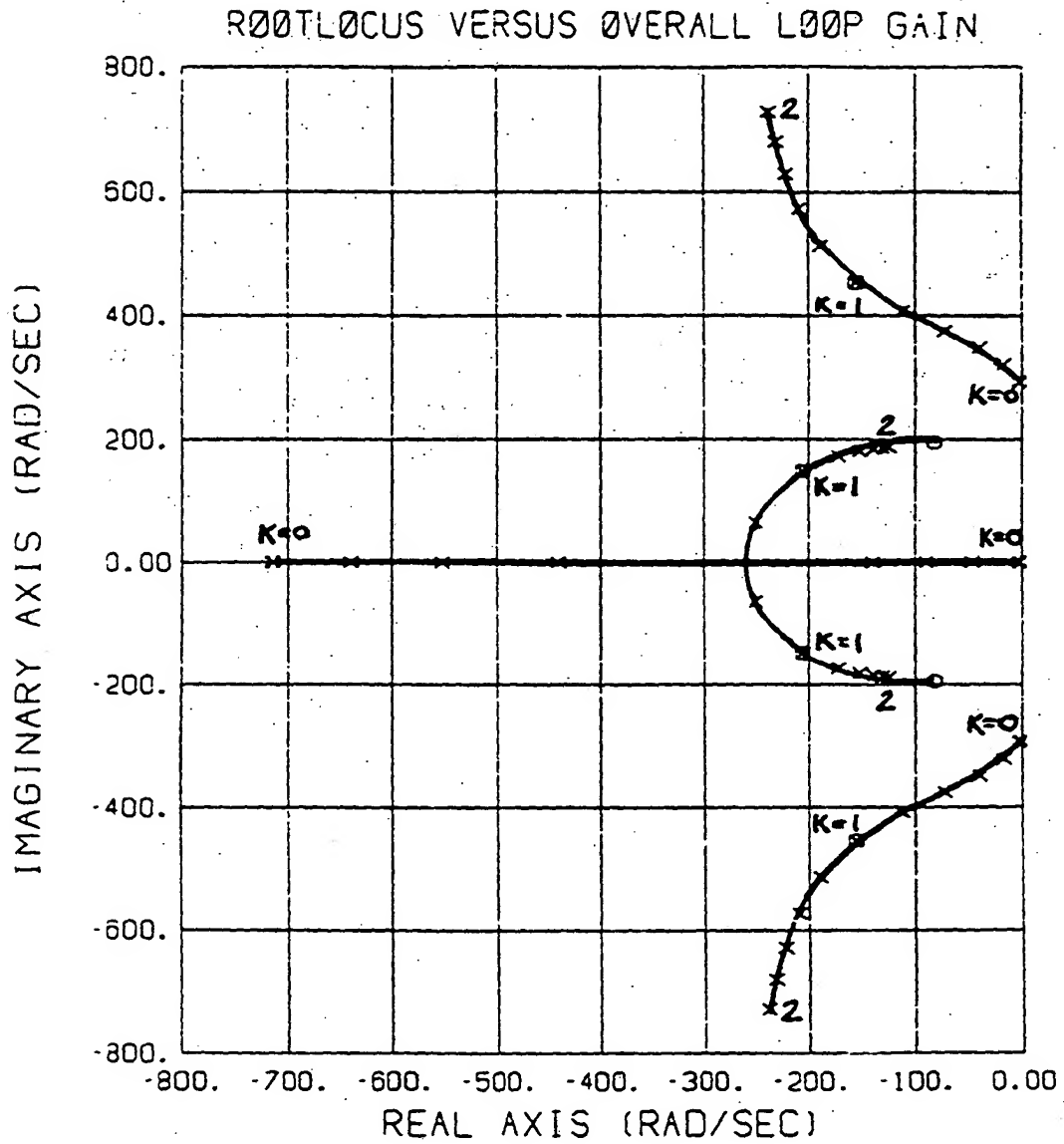


Figure H.9: Closed Loop System Root Locus versus Overall Loop Gain K

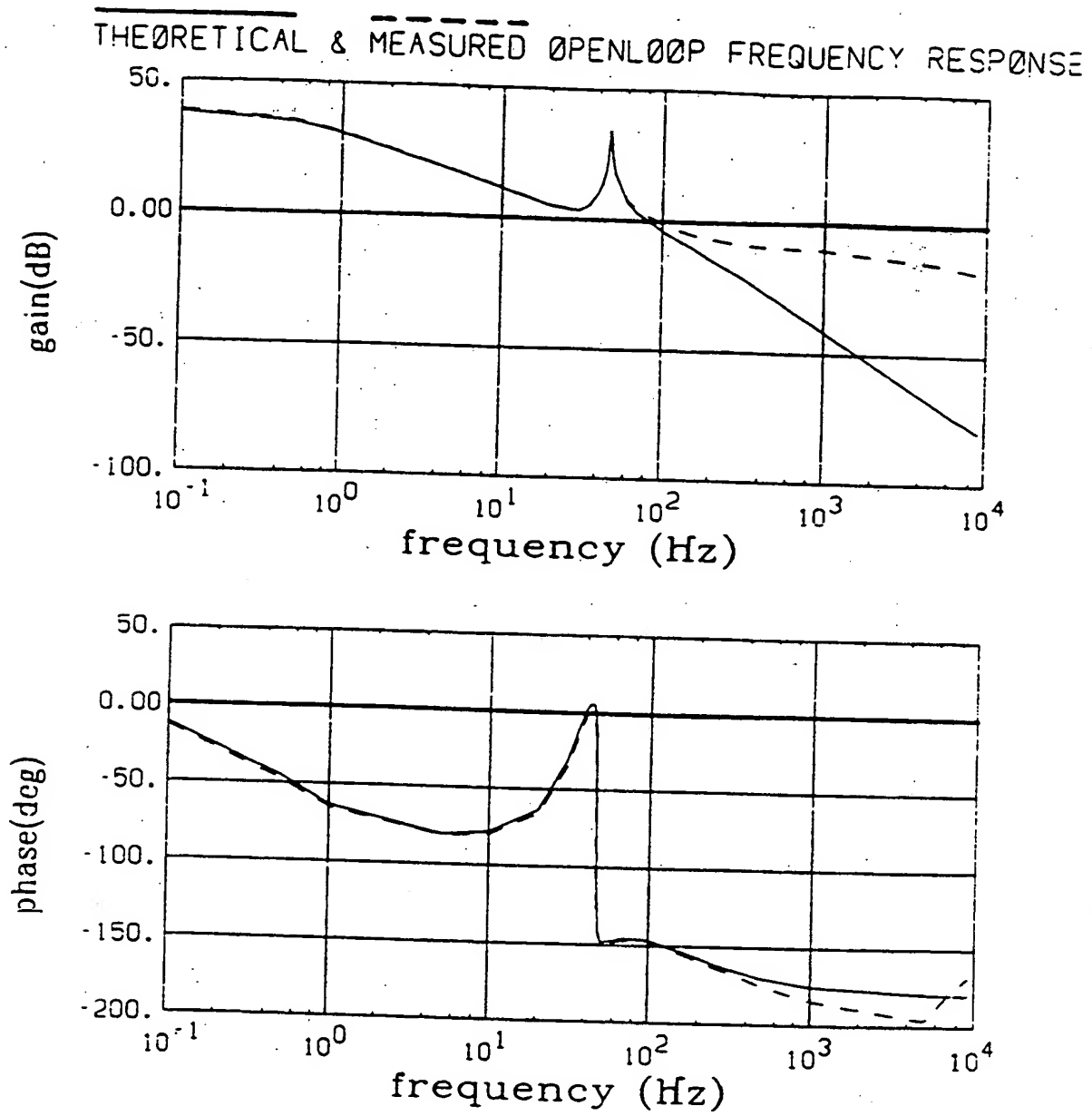


Figure H.10: Servo Accelerometer Openloop Frequency Responses

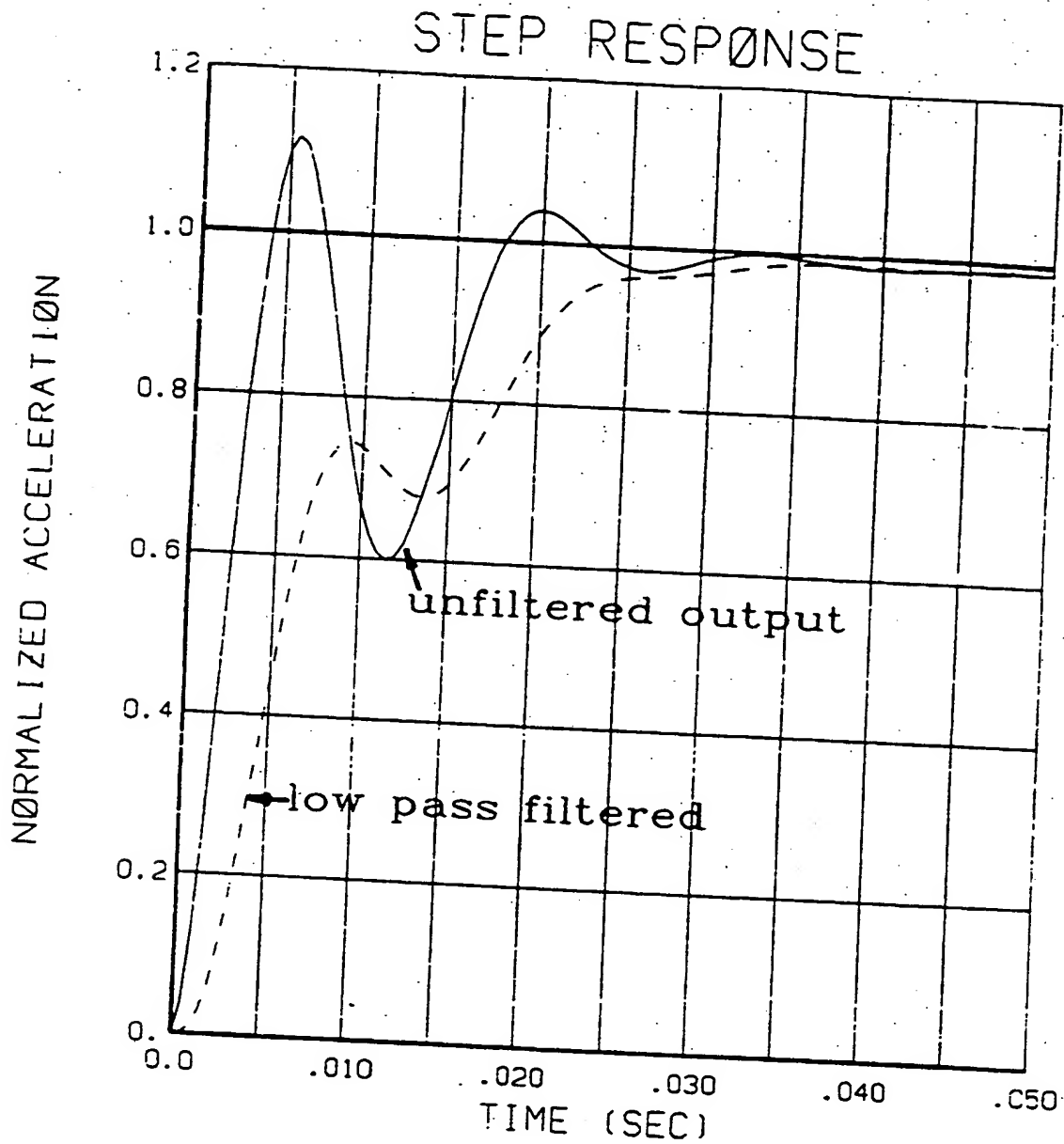


Figure H.11: Theoretical, Step Response of the Closed Loop Servo Accelerometer

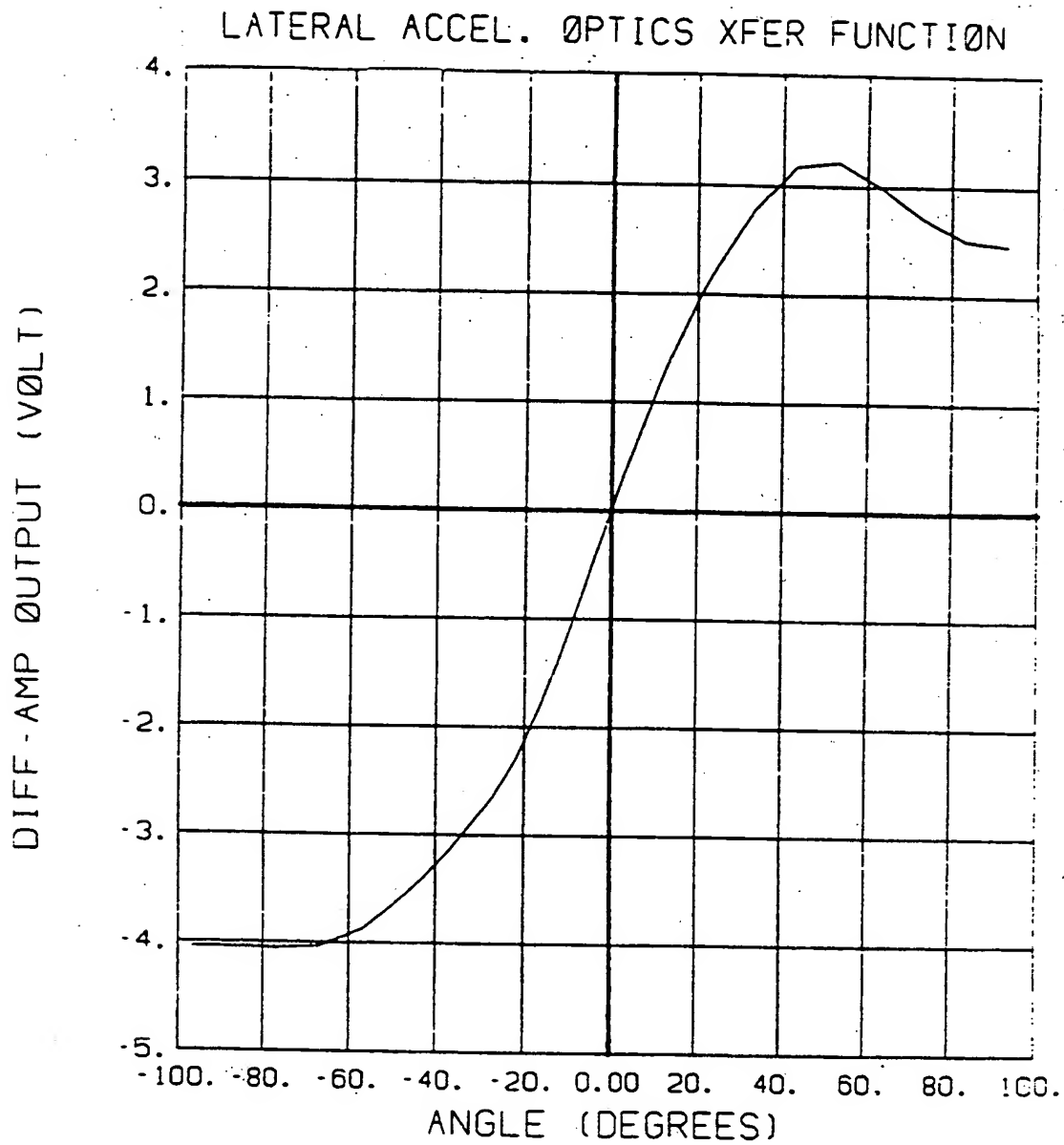


Figure H.12: Differential Output of the Optical Detector as a Function of the Accelerometer Tilt Angle

LATERAL SERVØ-ACCEL. CLOSED LOOP XFER FUNCTION

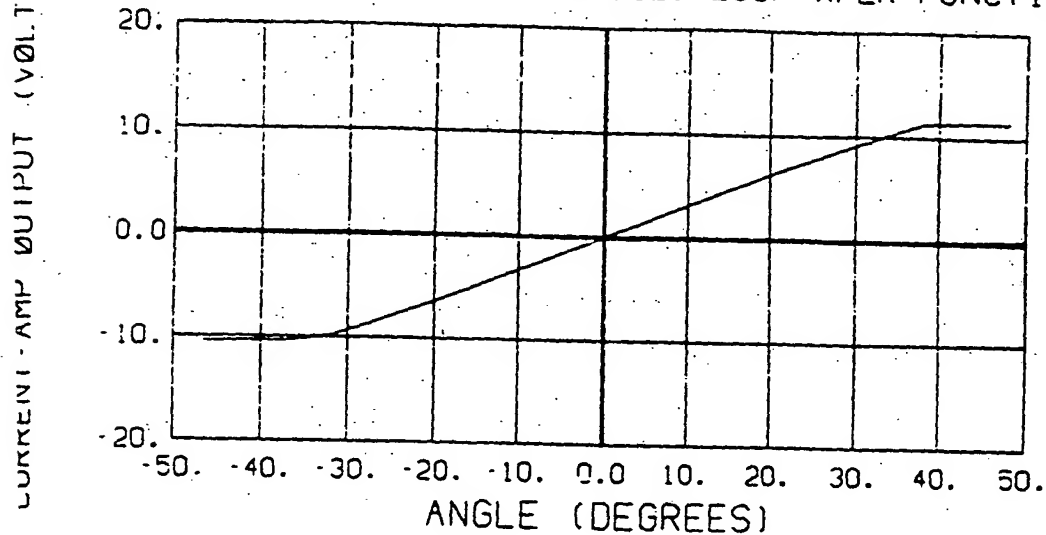


Figure H.13: Measured Transfer Function for the Lateral Accelerometer

LONGIT. SERVØ-ACCEL. CLOSED LOOP XFER FUNCTION

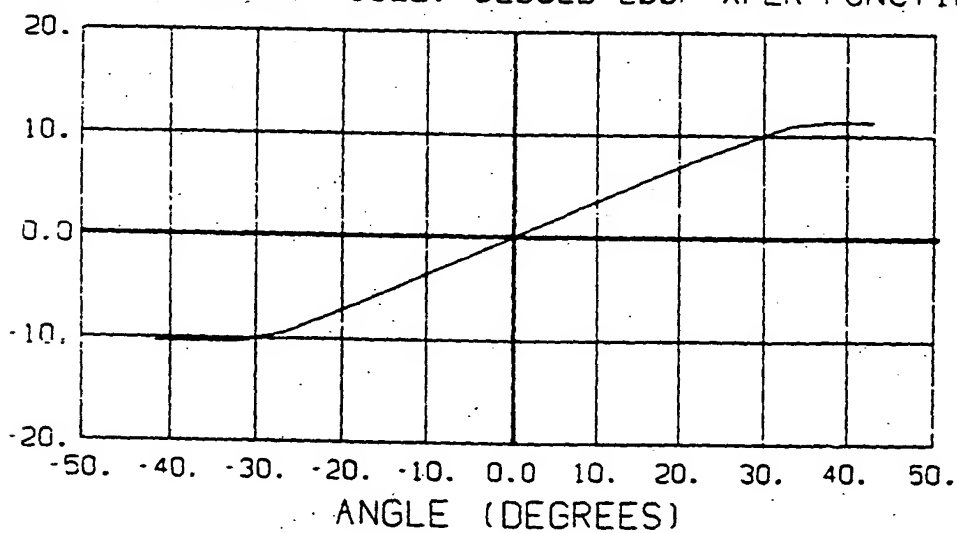


Figure H.14: Measured Transfer Function for the Longitudinal Accelerometer

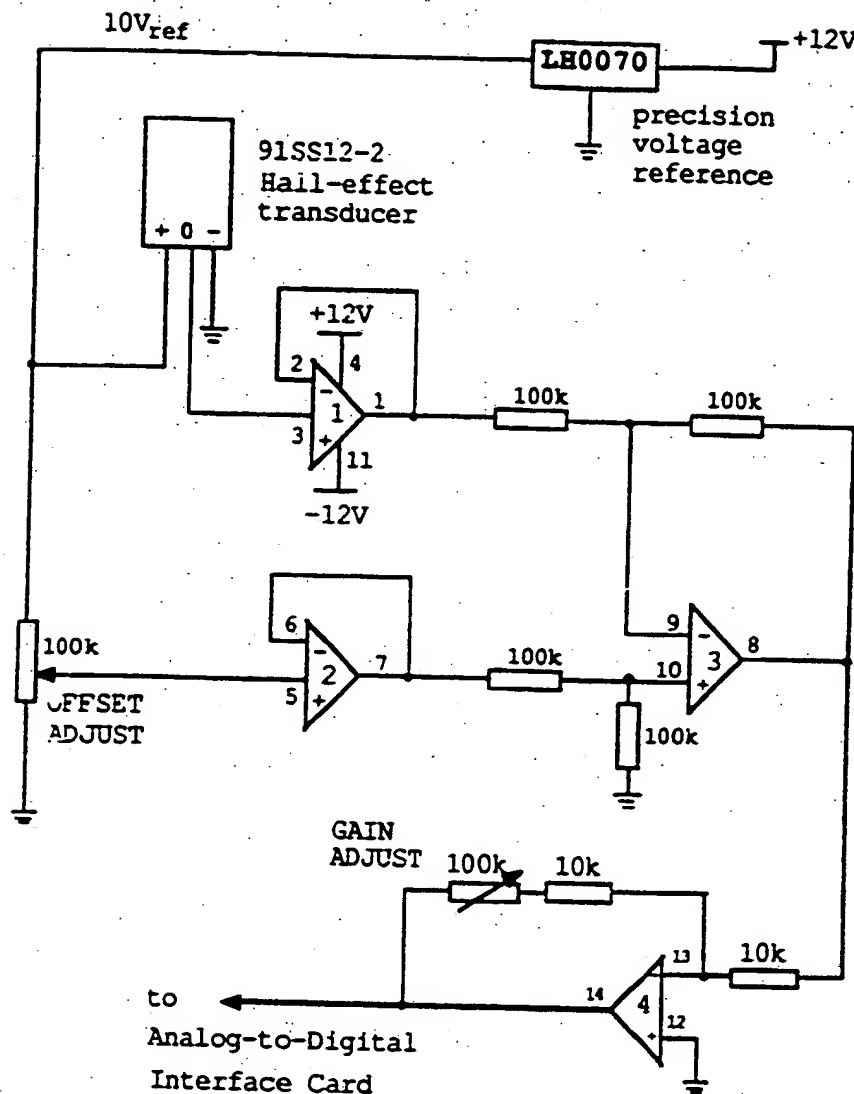


Figure H.15: Hall-effect Transducer Electronic Interface

LONGIT. PITCH SENSOR TRANSFER FUNCTION

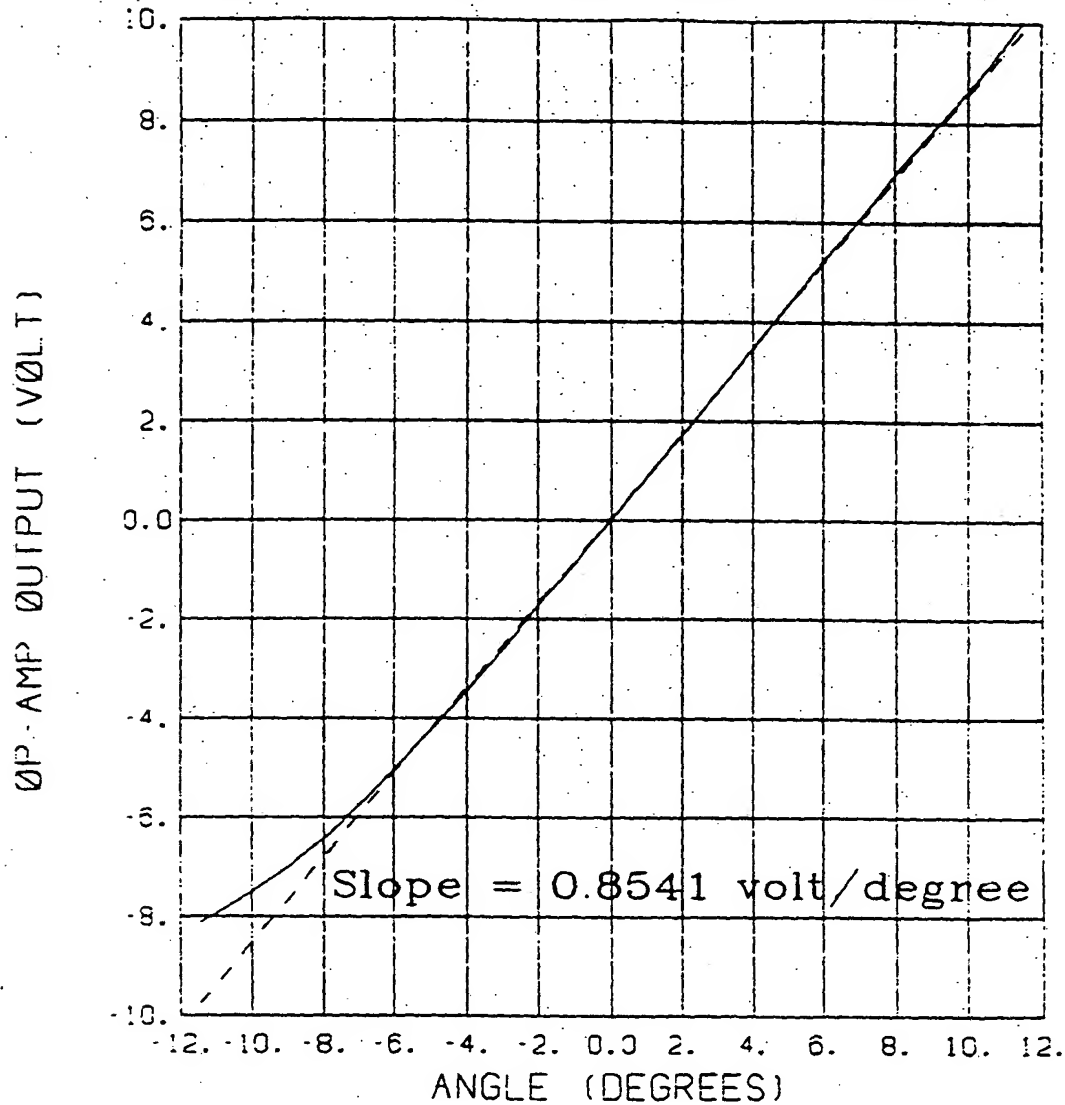
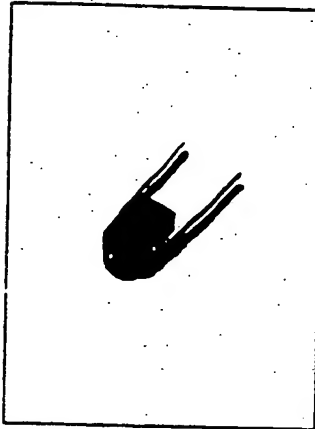


Figure H.16: Measured Transfer Function of the Hall-effect Transducer Pitch Angle Sensor

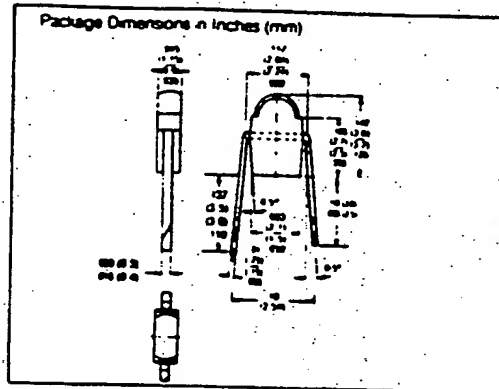
SIEMENS**SFH 405 SERIES****INFRARED EMITTER****FEATURES**

- Miniature Plastic Package
- 1/10" (2.54 mm) Lead Spacing
- Emitter for SFH-305 Phototransistor Detector
- Designed for Maximum Spacing of 10 mm Between Emitter and Detector
- Three Radiant Intensity Groups

DESCRIPTION

The SFH 405 is a GaAs infrared diode which emits radiation at a wavelength in the near infrared. The radiation emitted is excited by current flowing in the forward direction.

The case is transparent plastic with a lens shaped light output. The plastic is slightly smoke colored in order to differentiate between phototransistors of the same type (SFH 305). The terminals are solder pins in 1/10" (2.54 mm) lead spacing. The infrared emitting diodes are grouped according to radiation intensity. SFH 405 is suitable for use as emitter with the phototransistor SFH 305 to effect miniature light barriers with close spacing between sender and receiver up to 10 mm maximum. The cathode is marked with a colored dot.

**Maximum Ratings**

Operating and Storage Temperature	T	-40 to +80	°C
Soldering Temperature			
(Distance from soldering point to package ≥ 2 mm)			
On soldering time $t \leq 3$ s		230	s
From soldering time $t \leq 3$ s		300	s
Junction Temperature		80	°C
Reverse Voltage		5	V
Forward Current		40	mA
Surge Current (0 - 10 μ s, 0 - 10)		1.6	A
Power Dissipation		65	mW
Thermal Resistance		950	°C/W
		850	°C/W

Characteristics ($T_{amb} = 25^{\circ}\text{C}$)

Wavelength $I_f = 40$ mA, $t_f = 20$ ms	λ	950 ± 20	nm
Spectral Bandwidth			
$I_f = 40$ mA, $t_f = 20$ ms	$\Delta\lambda$	55	nm
Half Angle		± 16	°
Active Area		0.25	mm ²
Active Die Area per Die		0.5 \times 0.5	mm ²
Distance Die Surface to Package Surface		1.3 to 1.9	mm
Switching T_r to t_f from 10% to 90% and from 90% to 10% at $I_f = 40$ mA	t	1	ns
Capacitance ($V_a = 0$ V)	C	40	pF
Forward Voltage			
$I_f = 40$ mA		1.25 (± 1.0)	V
Breakdown Voltage ($I_a = 10$ μ A)		30 (± 5)	V
Reverse Current ($V_a = 5$ V)		0.01 (≤ 10)	μ A
Temperature Coefficient of I_f or ϕ_e		-0.55	%/K
Temperature Coefficient of V_f		-15	mV/K
Temperature Coefficient of λ		-0.3	nm/K

Radiant Intensity I_e in Axial Direction Measured at a Solid Angle of $\Omega = 0.68$ sr

Group	SFH 405-2	SFH 405-3	
Radiant Intensity			
$I_f = 40$ mA, $t_f = 20$ ms I_e	≤ 32	≥ 25	mW/sr
Radiant Power P_e at 40 mA			
$t_f = 20$ ms P_e	25	4	mW

Table H.1: Siemens SFH405-2

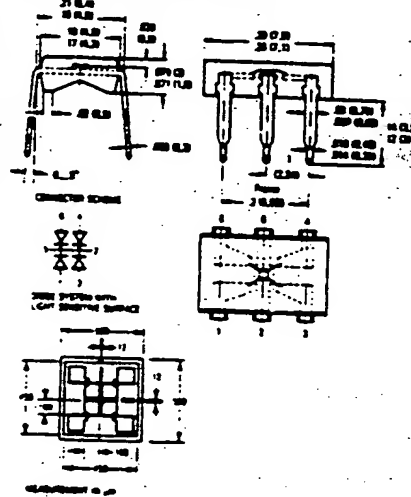
APPENDIX H. SERVO ACCELEROMETER DESIGN

SIEMENS**SFH 204****SILICON FOUR QUADRANT PHOTODIODE****FEATURES**

- Miniature size
- Four quadrant active sections
- Close spacing of contacts, 12 μm
- Can decrease if and by how much a light source has deviated

DESCRIPTION

The SFH 204 silicon planar miniature four quadrant photodiode has application in edge drive, positioning, and path and corner scanning control devices. The active units are spaced at only 12 μm apart from individual contacts. It is therefore possible to get exact positioning with high definition.

Package Dimensions in inches (mm)**Maximum Ratings**

Reverse voltage
Ambient temperature
Storage temperature at a 2mm distance
from the unit bottom at $\leq 3 \text{ s}$
Power dissipation

V_R	12	V
T_A	85	$^{\circ}\text{C}$
T_{stg}	-55...+125	$^{\circ}\text{C}$
P_D	40	mW

Characteristics ($T_{amb} = 25^{\circ}\text{C}$)

Responsivity of the photo element
Spectral sensitivity $\lambda = 880 \text{ nm}$
Dark current ($V_R = 10 \text{ V}$, $f = 1 \text{ kHz}$, $d = 0$)

R	0.11 D-0.00	$\mu\text{A}/\mu\text{W}$
λ	> 0.25	$\mu\text{A}/\mu\text{W}$
I_D	0.01 AC 20	μA

Autobias capabilities

($V_R = 0 \text{ V}$, $f = 1 \text{ kHz}$, $d = 0$)
($V_R = 10 \text{ V}$, $f = 1 \text{ kHz}$, $d = 0$)

C_{in}	2.5	pF
C_{out}	1.5	pF

Rise and fall time of the photodiode

from $\sim 20\%$ to 80% and
from 80% to 10% of the final value

t_r	2	ns
t_f	4	ns

Relative sensitive area

Distance between nearest sensitive areas,
length of the cross-shaped geometry

A	4 \times 0.01	mm^2
A	12 D-10	μm^2

Maximum dimensions of the several components

of the four systems from the main

Δx	< 20	μm
------------	------	---------------

Specifications subject to change without notice.

Siemens Components Inc., Optoelectronics Division, 16000 Hammon Road, Cupertino, California 95014 (408) 253-7910/7911 910-328-0022

Table H.2: Siemens SFH204

Appendix I

Position Encoder and Servo Amplifier Interface

I.1 Introduction

This computer card extracts velocity information from the position encoders mounted on the axes of the turntable and wheel drive motors, and interfaces these signals to the G64 bus of the GESPAC computer. It also takes digital motor current command signals from the computer bus and outputs it as analog signals to the servo amplifiers.

I.2 Position encoder interface

The Datametrix K3DO-200-5SE-4A optical encoder outputs two 0 - 5V square waves in quadrature at 200 pulses per revolution of the motor shaft. On the state transition of one of these signals, a counter is started. It is clocked with a high frequency clock derived from the microprocessor system clock. When the next encoder state transition occurs, the counter's contents is stored in a register, the counter cleared and the process repeated. The number stored in the register can be read by the microprocessor and inverted to obtain motorshaft speed. A schematic

182 APPENDIX I. POSITION ENCODER AND SERVO AMPLIFIER INTERFACE

diagram of the position encoder digital logic is shown in Figure I.1 and Figure I.2. The layout of the components on the interface card is shown in Figure I.3.

I.3 Operation of the logic circuitry

A master clock, SCLK, controls the timing of all the logic transitions of the position encoder interface card, as shown in the timing diagram of Figure I.4. The frequency of SCLK is jumper selectable, and is chosen from considerations discussed in the next section. The two quadrature signals from the position encoder are synchronized with SCLK and the direction of rotation is determined and indicated by the U/\bar{D} . The logic level of this signal is written to the data bus bit zero to indicate the direction of motor rotation to the microprocessor. When the motor stands still or reverses direction hexadecimal FFFF is written to the counter buffer register in the 74LS699 ICs by means of the \overline{CLOAD} strobe.

One clock cycle after the low to high transition of the second phase signal of the position encoder, the upper 15 bits of the counter are loaded into the buffer register (by the RLD strobe) and are available to the upper 15 bits of the data bus. One clock cycle later, the counter is cleared (\overline{CCLR} strobe) and it starts counting the number of clock pulses until the next low to high transition of the second phase of the position encoder occurs.

The lower 5 bits of the address bus is decoded to place the lateral position encoder rate data at peripheral address hexadecimal 800020 and the longitudinal encoder rate data at 800030.

I.4 Selection of the interface clock frequencies

Define:

c = the number of clock pulses counted during one complete cycle of the second phase of the position encoder.

f = the frequency(in Hz) of the master clock of the position encoder logic circuitry.

ω = motor axle angular velocity in rad/sec.

For the encoders which generate 200 pulses per revolution, the motor speed is given by:

$$\omega = \frac{2\pi f}{200c} \quad \text{rad/sec} \quad (L1)$$

From the lateral control system simulations, the maximum turntable speed is expected to be $\eta_{max} = .12$ rad/sec. With the turntable drive gear ratio of 60:1 the maximum lateral drive motor shaft speed will be $60 \times 0.12 = 7.2$ rad/sec. Let the counter on the interface card reach its maximum count of $(2^{15} - 1)$ at 1% of this speed. The lateral encoder interface clock frequency is calculated from equation L1 as:

$$\begin{aligned} f &= \frac{200\omega c}{2\pi} \\ &= \frac{200 \times 0.072 \times (2^{15} - 1)}{2\pi} \\ &= 75.096 \text{ kHz} \end{aligned} \quad (L2)$$

since the clock is derived from a subdivision of the 8MHz microprocessor system clock, a convenient value is

$$LATCLK = \frac{8 \text{ MHz}}{2^8} = 31.25 \text{ kHz} \quad (L3)$$

The typical nominal wheel speed is $\Omega_0 = 3$ rad/sec. The typical maximum perturbation of the nominal wheel speed is $\bar{\Omega} = 0.12$ rad/sec.

184 APPENDIX I. POSITION ENCODER AND SERVO AMPLIFIER INTERFACE

The gear ratio for the wheel drive system is 24:1, so the motor speed at 3 rad/sec wheel speed is:

$$\omega_0 = 3 \times 24 = \frac{2\pi f}{200c} \quad (I4)$$

If the accuracy of the motor speed should be measured to 1% of the maximum perturbation speed, then:

$$\left(\omega_0 + \frac{\tilde{\omega}}{100}\right) = \frac{2\pi f}{200(c-1)} \quad (I5)$$

$$\left(3 + \frac{.12}{100}\right) \times 24 = \frac{2\pi f}{200(c-1)} \quad (I6)$$

eliminate c between equation I4 and I6 to get the optimum clock frequency

$$f = \frac{200\omega_0(100\omega_0 + \tilde{\omega})}{2\pi\tilde{\omega}} \quad (I7)$$

$$= 5.732MHz \quad (I8)$$

Let the master clock frequency for the longitudinal encoder rate interface be the same as the microprocessor clock frequency:

$$LGTCLK = 8MHz \quad (I9)$$

I.5 Servo amplifier interface

The two DC motors are driven with pulse width modulated (PWM) servo amplifiers. These amplifiers have internal current feedback and are adjusted so that a -16V to +10V input signal commands an output current of -10A to +10A to the servo motors.

12 bit Digital-to-Analog Converters(DAC) are used on the computer interface card to convert the digital current command on the microprocessor bus to an analog voltage for the servo amplifiers, as shown in Figure I.5.

Define:

D = digital number supplied to the DAC

B = digital number appearing on the microprocessor bus

V_{out} = output voltage of the DAC

V_{ref} = reference voltage for the DAC output
= 10V

For the DAC and operational amplifiers as configured in Figure 1.5,

$$V_{out} = V_{ref} \left(\frac{D - 2048}{2048} \right) \quad (1.10)$$

where $0 \leq D \leq 4095$

Because of the negative logic of the G64 data bus, a binary value of B written to the DAC will give an output voltage of

$$V_{out} = V_{ref} \left(\frac{2048 - B}{2048} \right) \quad \text{Volt} \quad (1.11)$$

where $0 \leq B \leq 2048$

The lower 5 bits of the address bus is decoded to place the lateral DAC at peripheral address hexadecimal 800000 and the longitudinal DAC at 800010.

186 APPENDIX I. POSITION ENCODER AND SERVO AMPLIFIER INTERFACE

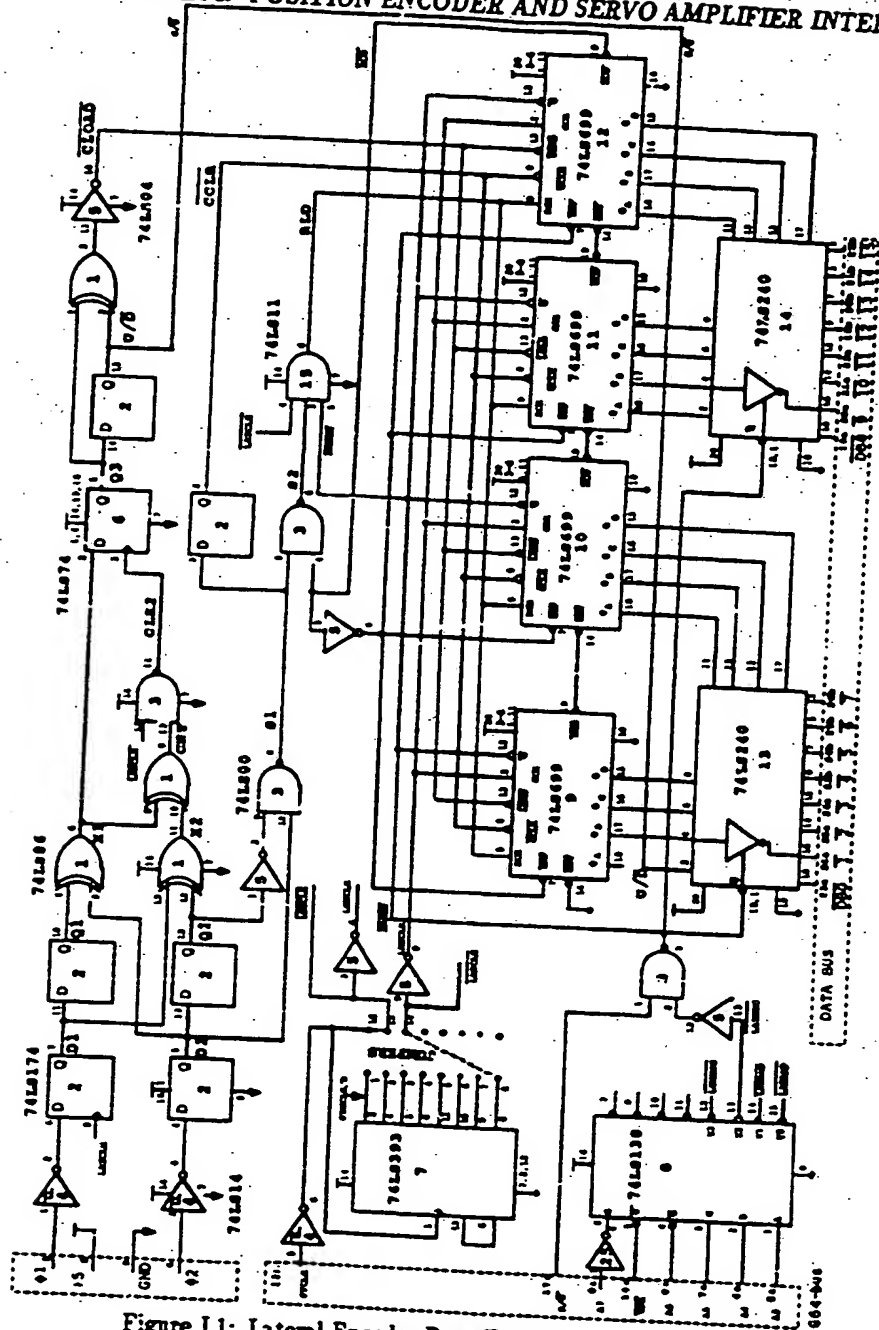


Figure I.1: Lateral Encoder Rate Extraction Logic Diagram

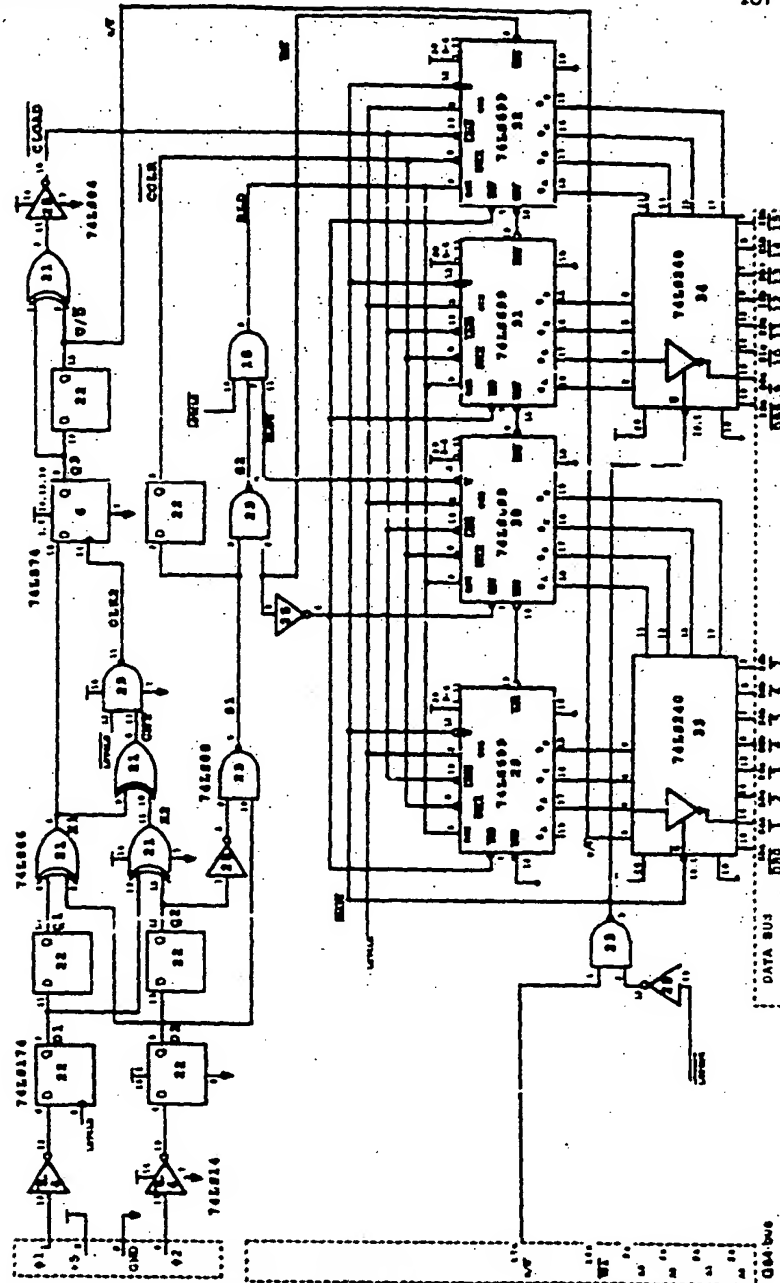


Figure 12: Longitudinal Encoder Rate Extraction Logic Diagram

188 APPENDIX I. POSITION ENCODER AND SERVO AMPLIFIER INTERFACE

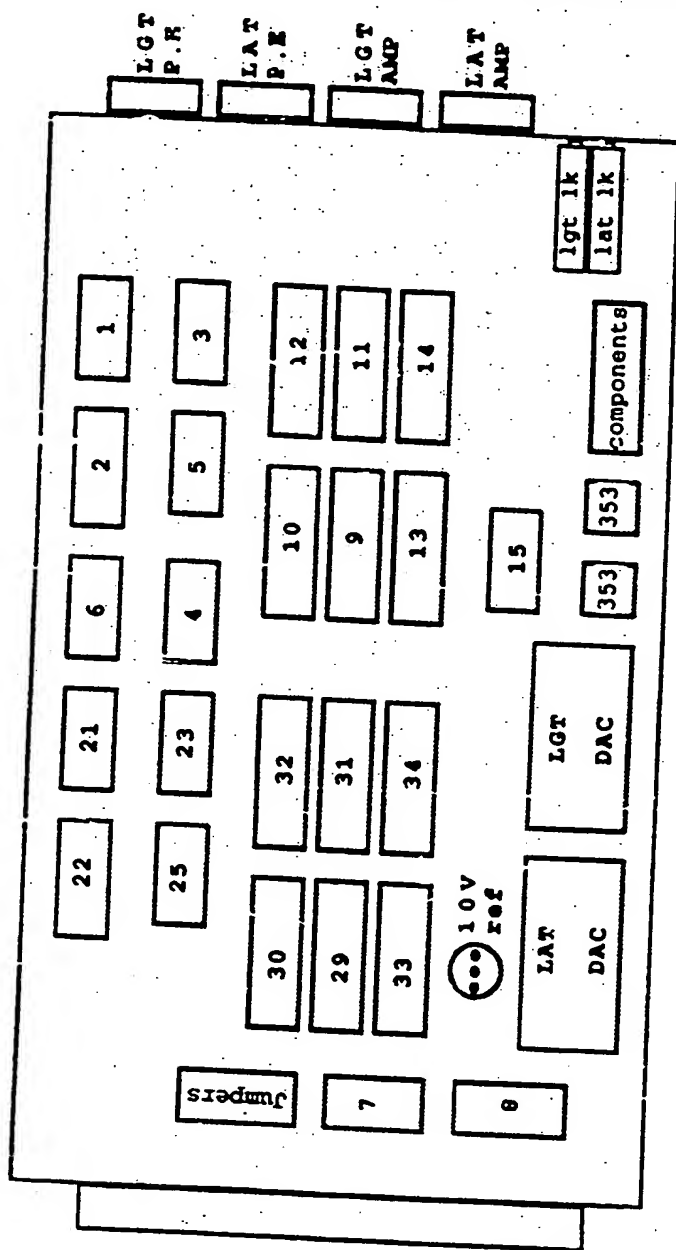


Figure L3: Position Encoder and Servo Amplifier Interface Card Layout

L5. SERVO AMPLIFIER INTERFACE POSITIVE ROTATION

189

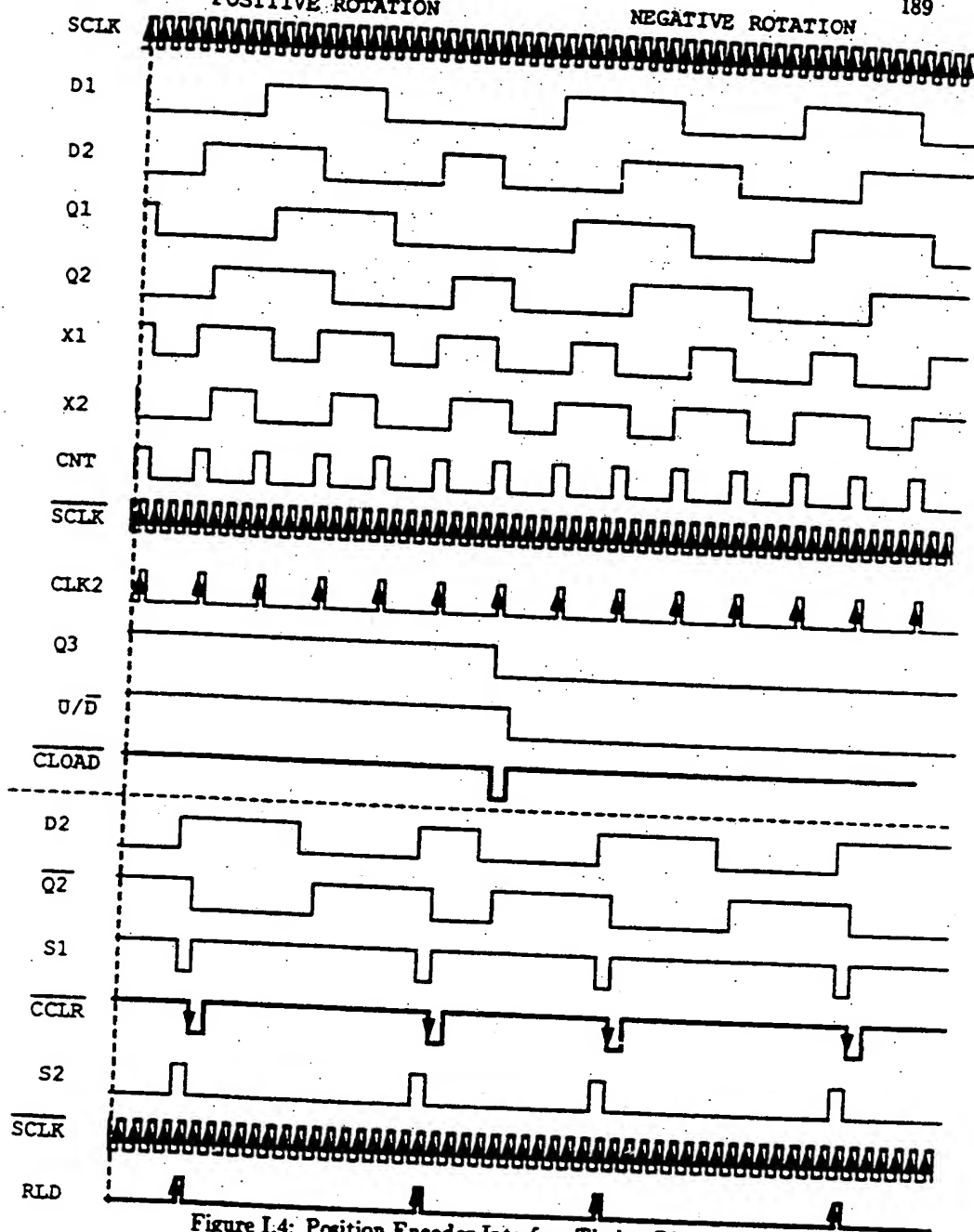


Figure L4: Position Encoder Interface Timing Diagram

190 APPENDIX I. POSITION ENCODER AND SERVO AMPLIFIER INTERFACE

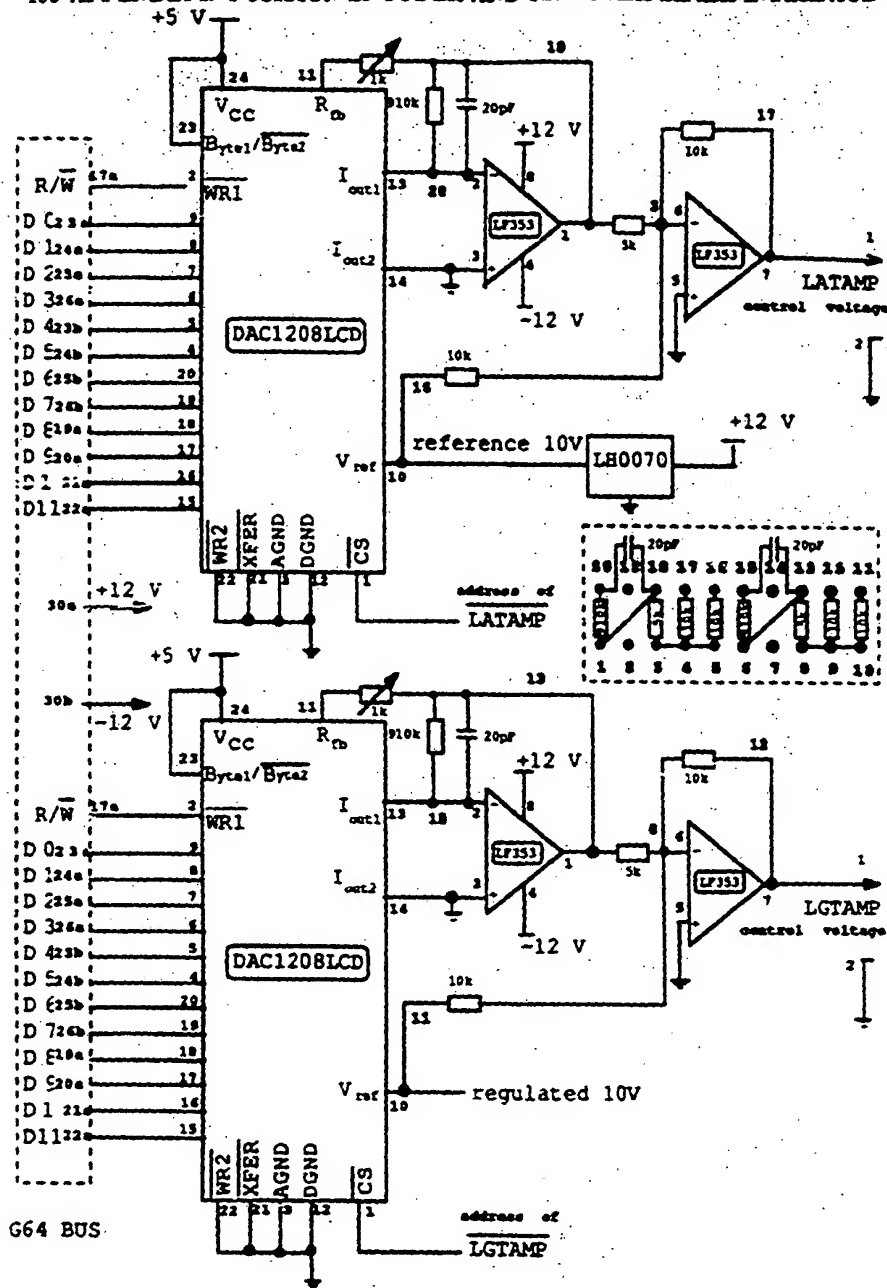


Figure I.5: Digital to Analog Converter Interface to Servo Amplifiers

Appendix J

Analog-to-Digital, Radio and FPP Interface

J.1 Analog-to-Digital interface design

J.1.1 Hardware design

Figure J.1 shows the AD574AJD 12 bit analog-to-digital converter(ADC) from Analog Devices Inc. and its interfacing to the G64 bus. Its peripheral address is \$8000F0 (where the \$ sign implies a hexadecimal number). Up to 8 analog signals with magnitudes between $\pm 10V$ can be multiplexed (by the multiplexer at address \$8000E0) and connected to the sample-and-hold device at peripheral address \$8000D0.

J.1.2 Software for controlling the ADC interface

To read and digitize one analog input channel, the microprocessor executes the following commands:

1. writes the code for the analog channel to be discretized to the multiplexer address \$8000E0. A binary number of 000 on the data bus will correspond to

APPENDIX J. ANALOG-TO-DIGITAL, RADIO AND FPP INTERFACE

the first analog input which is the lateral accelerometer signal. The binary number 001 corresponds to the second analog input which is the longitudinal accelerometer signal.

2. executes a software wait state for $1.8\mu s$ to allow the analog switches in the multiplexers to complete the switching process.
3. writes a '1' on data bus bit 0 to address \$8000D0 to start the sampling process of the LF398A sample and hold device.
4. enters a software wait state for $25\mu s$ which is the required acquisition time for the LF398A to reach within 0.1% of its steady state value.
5. writes a '0' to \$8000D0 to place the sample and hold device into hold mode.
6. writes any number to the ADC address at \$8000F0 to start the analog to digital conversion.
7. enters a software wait state for $35\mu s$ for the ADC to complete the conversion.
8. reads the digitized value of the analog input.
9. repeats steps (1) through (8) to read the other analog input signals.

The FORTH program code to implement this algorithm is shown in section J.1.4.

J.1.3 Binary values of the analog input voltage

The 12 output data lines of the ADC are connected to the 12 least significant bits (LSB) of the microprocessor bus. The 4 most significant bits (MSB) of the databus are masked out in software, because they are meaningless. Because of the negative logic of the G-64 databus the value read from the databus should be subtracted from 4095 to obtain the actual digital output of the ADC.

The ADC null offset is trimmed so that the major carry operation (binary 0111 1111 1111 to 1000 0000 0000) should occur at an analog value of $\frac{1}{2}$ LSB below analog common i.e. - 1.221mV. The full scale calibration is set so that the last

transition (from 1111 1111 1110 to 1111 1111 1111) should occur for an analog value $1\frac{1}{2}$ LSB below the nominal full (9.9963 volts for 10.000 volts full scale). Fitting a straight line through the above two pairs of coordinates gives the analog reading:

$$A_{in} = 10.00366 - 4.884 \times 10^{-3}(4095 - D_{bus})$$

where D_{bus} is the 12 bit value read on the databus.

J.1.4 FORTH Program to drive the ADC converter

(--- Analog to Digital Converter Driver ---)
CR

ONLY FORTH DEFINITIONS

```

HEX 800000 CONSTANT LATDACADDR ( Set LAT DAC's address )
      800010 CONSTANT LGTDACADDR ( Set LGT DAC's address )
      800020 CONSTANT LATENCADDR ( Set LAT Encoder's address )
      800030 CONSTANT LGTENCADDR ( Set LGT Encoder's address )

      8000D0 CONSTANT SHADDR    ( Sample & Hold's address )
      8000E0 CONSTANT MUXADDR   ( Multiplexer's address )
      8000F0 CONSTANT ADCADDR   ( Analog-to-Digital Converter's address )

      0 CONSTANT LATACCMUX      ( MUXCode for Lateral Accelerometer )
      1 CONSTANT LGTACCMUX      ( MUXCode for Longitudinal Accelerometer )

```

CR

DECIMAL

```

.( Loading LATDAC word code) CR
: LATDAC 10000 SWAP - 2048 * 10000 / ( get 12 bit equiv. for output to DAC )
  LATDACADDR V! ; ( write 16 bit word to DAC1 )

```

194 APPENDIX J. ANALOG-TO-DIGITAL, RADIO AND FPP INTERFACE

```

: WAIT4N ( N - ) ( S/W WAIT for n*4 micro-seconds )
0 DO LOOP :

.( Loading MUXSWITCH word code ) CR
: MUXSWITCH ( channels - ) ( switches MUX to specified input channel )
MUXADDR W!
1 WAIT4N : ( waits 4 microsec. for MUX to settle )

.( Loading SAMPLEHOLD word code ) CR
: SAMPLEHOLD ( - ) ( SAMPLE and HOLD command )
1 SRAADDR W! ( sample analog signal )
7 WAIT4N ( waits 28 microsec. for S&H to settle )
0 SRAADDR W! : ( place S&H device in HOLD mode )

.( Loading AD_CONVERTER word code ) CR
: AD_CONVERTER ( - DigitizedValue ) ( Do Analog to Digital Conversion )
1 ADCADDR W! ( Starts A to D Converter )
9 WAIT4N ( Waits 36 microsec. for ADC finish )
ADCADDR W0 : ( Reads the digital result from the ADC )

.( Loading AtoD_CONVERT word code ) CR
: AtoD_CONVERT ( channels - DigitizedValue )
MUXSWITCH ( Complete process for an AtoD Conversion )
SAMPLEHOLD
AD_CONVERTER :

.( Loading RLATACC word code ) CR
: RLATACC ( - LatAcc_Volt ) ( Conv. Analog Volt. from Lateral Accelerometer )
10003660 4884 4095
LATACCNOX AtoD_CONVERT
- - - 1000 / . : ( Output in millivolts )

.( Loading RLGTACC word code ) CR

```



```

: RLGTACC ( - LgtAcc_Volt ) ( Conv. Analog Volt. from Longit. Accelerometer)
10003660 4884 4096
LGTACCWUX AtoD_CONVERT
- * - 1000 / . : ( Output in millivolts )

```

J.2 Radio receiver interface design

J.2.1 Hardware design

The radio receiver emits pulse width modulated (PWM) signals in response to the radio signals received from the radio transmitter. The pulses for each radio channel are repeated every 17.4 ms and has a low voltage of 0V and a high voltage of 4V. The pulse width is 0.82 ms for a maximum negative stick input and 1.72 ms for a maximum positive stick input.

Figure J.2 shows how the 8254 programmable interval timer (PIT) is used to count the number of timer clock pulses during the high level of the PWM signal. The timer interface clock is 4 MHz, half of the microprocessor clock frequency. The count for the maximum positive stick input will therefore be 7280 while the minimum count for full negative stick will be 3280 counts.

The PIT has 3 independently programmable 16 bit counters. The PWM output from channel 1 of the radio receiver is connected to the gate of counter 1 at address \$800082. The PWM output of channel 2 is connected to counter 2 at \$800084.

J.2.2 Software interface

Counters are programmed by writing a control word to address \$800086. Counters 1 and 2 are programmed to operate in Mode 0, by sequentially writing the

APPENDIX J. ANALOG-TO-DIGITAL, RADIO AND FPP INTERFACE

bytes \$70 and \$B0 to the control word upon system initialization. Because of the negative databus logic, the ones complement of these values is actually written out by the microprocessor, namely \$8F and \$4F.

As shown in Figure J.2, the falling edge of the second radio channel pulse is used to generate an interrupt request (IRQ) to the microprocessor.

The interrupt service routine then reads the two count values in the P.I.T. and saves these in the variables for the lateral and longitudinal input commands. The counters are then re-initialized to zero before the interrupt request flip-flop on the P.I.T. interface card is reset to receive the new radio commands about 17 ms later.

A listing of the software code that drives the radio receiver interface is listed in the next section. The interrupt service routine, RADIO-READ, was written in Motorola 68000 assembler code to maximize the speed of the interrupt service routine.

J.2.3 Program to drive the radio receiver interface

```
( --- Radio Receiver Interface Driver --- )
```

```
CR
```

```
ONLY PORT DEFINITIONS
```

```
ALSO ASSEMBLER
```

```
VARIABLE LATPW
```

```
VARIABLE LSTPW
```

```
REX
```

```
800080 CONSTANT RCCOUNTER0 ( Radio Receiver Interface )
```

```
800082 CONSTANT RCCOUNTER1 ( Counter Addresses )
```

J.2. RADIO RECEIVER INTERFACE DESIGN

197

800084 CONSTANT RCCOUNTER2

800086 CONSTANT RCCONTROLWORD (Counter Controlword address)

800090 CONSTANT RCTRIGGER (Trigger address to RESET IRQ flip-flop)

68 CONSTANT LEVEL2_IRQ (Level2 Autovector Address)

DECIMAL

CODE RADIO_READ (Reads Radio Receiver Channels upon IRQ)

MOVE.L DO, -(A7) (saves contents of DO on stack)

MOVE.B #21, RCCONTROLWORD (Latches all counts)

MOVE.V RCCOUNTER1, DO (Reads LSB of Counter1)

MOVE.B DO, LATPW (Save temporary)

MOVE.V RCCOUNTER1, DO (Reads MSB of Counter1)

LSL.W #8, DO

MOVE.B LATPW, DO (Get LSB)

MOVE.V DO, LATPW (Save)

MOVE.V RCCOUNTER2, DO (Reads LSB of Counter2)

MOVE.B DO, LGTPW (Save temporary)

MOVE.V RCCOUNTER2, DO (Reads MSB of Counter2)

LSL.W #8, DO

MOVE.B LGTPW, DO (Get LSB)

MOVE.V DO, LGTPW (Save)

MOVE.B #3F, RCCONTROLWORD (Rewrites Ctrlword to 1)

MOVE.B #0, RCCOUNTER1 (Write LSB of initial counter1)

MOVE.B #0, RCCOUNTER1 (Write MSB of initial counter1)

APPENDIX J. ANALOG-TO-DIGITAL, RADIO AND FPP INTERFACE

MOVE.B \$34F,RCCONTROLWORD (Rewrites Ctrlword to 2)

MOVE.B \$0,RCCOUNTER2 (Write LSB of initial counter2)

MOVE.B \$0,RCCOUNTER2 (Write MSB of initial counter2)

MOVE.B \$1,RCTRIGGER (Reset IRQ flip-flop on Radio Int)

MOVE.L (A7)+,D0 (Restores original value of D0)

RTE (Return from exception routine)

END-CODE

CR

(Loading RADIO_INIT code to Initialize R/Control Interface & Interrupt)

CR

: RADIO_INIT (Initialize Radio Control Interface & Interrupt)

['] RADIO_READ (Initialize Radio Receiver)

LEVEL2_IRQ ! (Level 2 Autovector)

BINARY

10001111 RCCONTROLWORD C! (Set Counters 1,2)

01001111 RCCONTROLWORD C! (for Mode 0)

1 RCTRIGGER C! (Reset IRQ flip-flop on Radio Intf)

DECIMAL ;

: WAGHBIETJIE (Wait a while)

10000 0 DO 1000 1000 * DROP LOOP ;

```
CR
.( Loading R/SHOW code to show R/C Reading on Terminal Screen )
CR

: R/SHOW. ( Show R/C Reading on Terminal Screen )

      BEGIN
      LATTVM W0 5164 - CR 20 SPACES .
      5178 LGTPVM W0 - 10 SPACES .
      WAGBIEITJIE ?TERMINAL
      UNTIL ;
```

J.3 Floating point processor (FPP) interface

The Motorola MC68881 floating point coprocessor interface to the G-64 bus and MC68000 CPU is shown in Figure J.4.

The address decoding locates the base address for the FPP at \$20 000 in memory.

The Mach 2 FORTH Software contains a special floating point instruction set to utilize the floating point processor.

The component layout for interface card described in this appendix is shown in Figure J.5.

J.4 Electrical and electronic wiring diagram

Figure J.6 shows schematically how the electrical and electronic elements on the unicycle robot are interconnected.

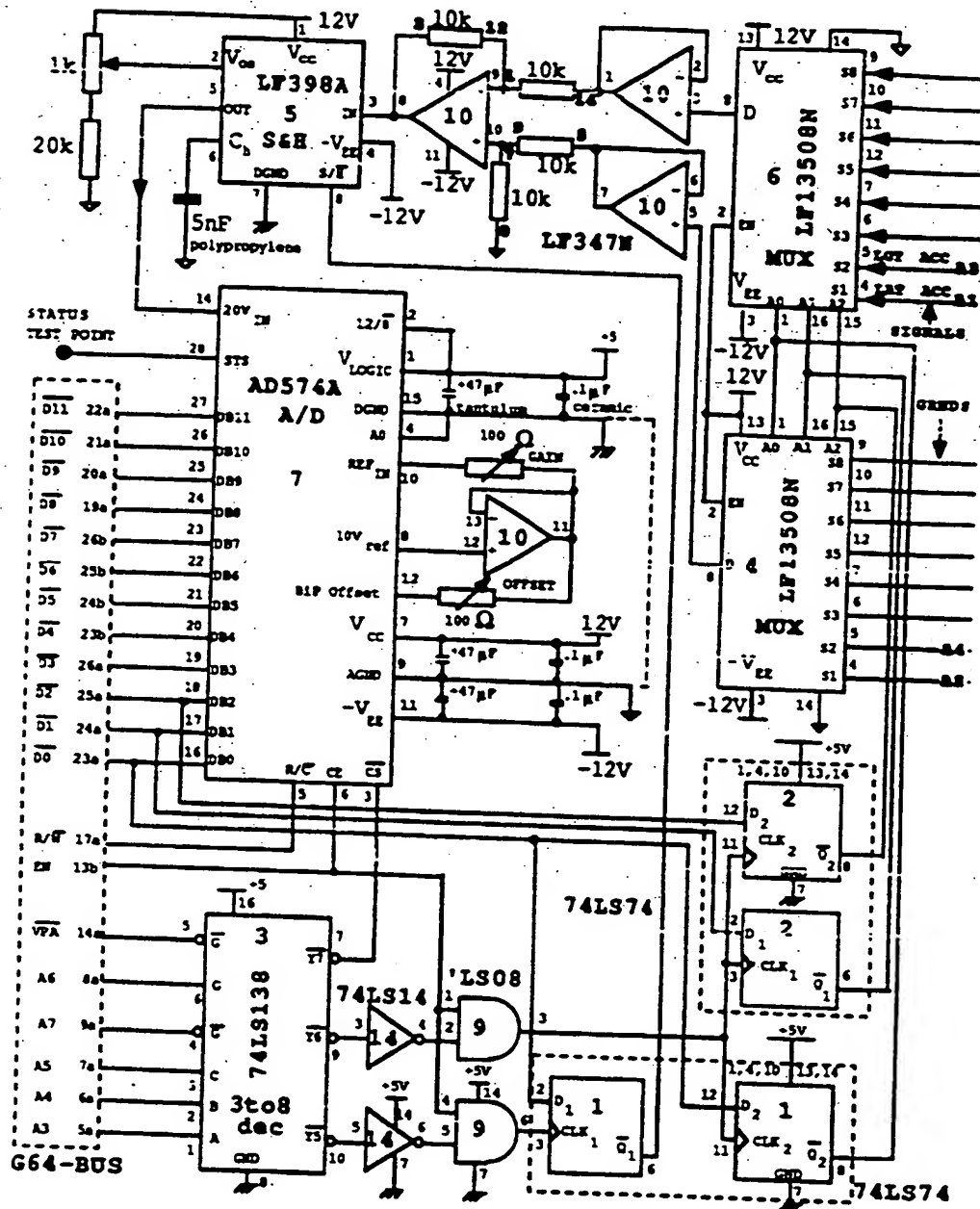
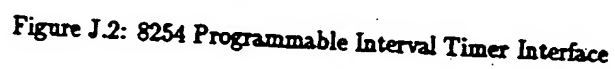


Figure J.1: 12 Bit Analog-to-Digital Converter and 8 Channel Multiplexer Interface

201



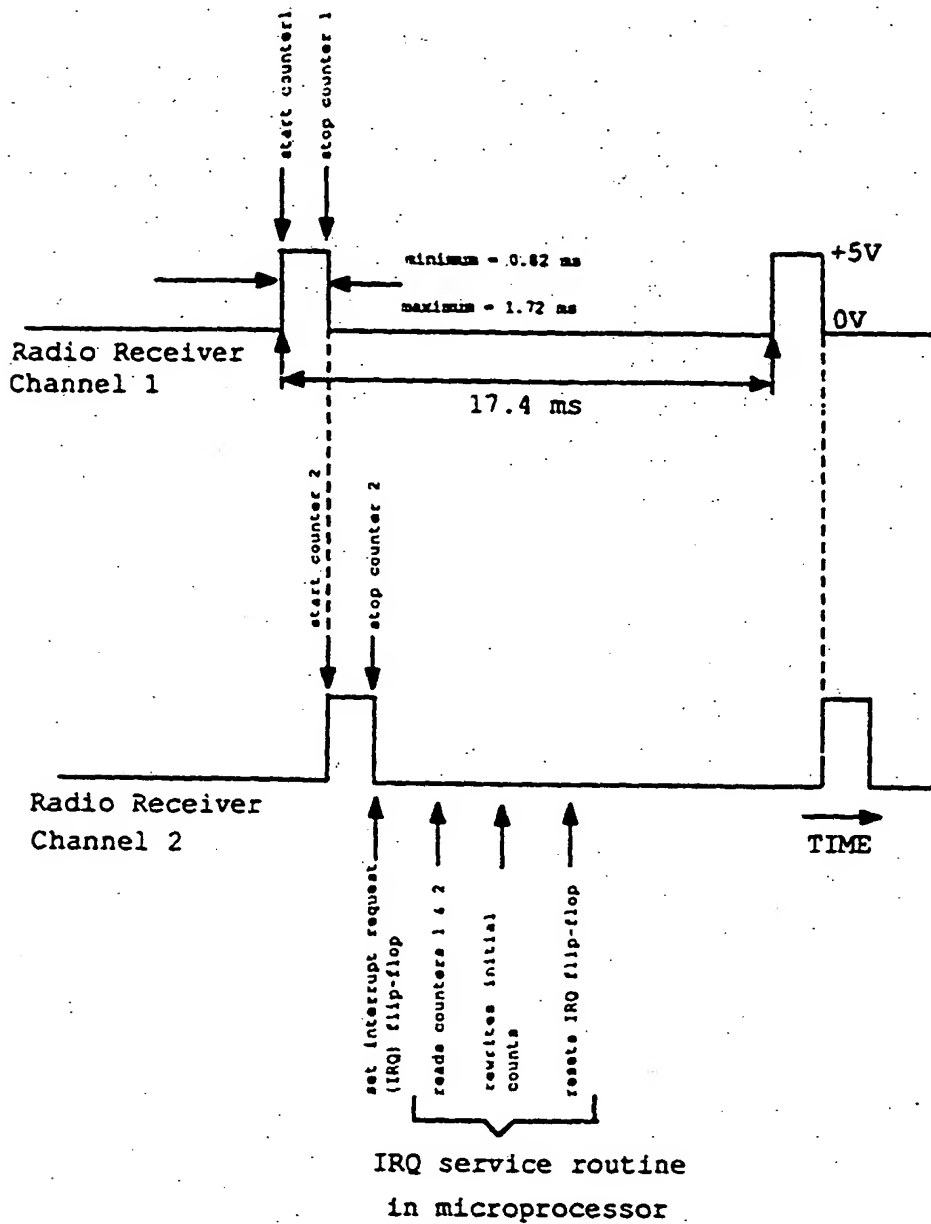


Figure J.3: Radio Receiver Interface Timing Diagram.

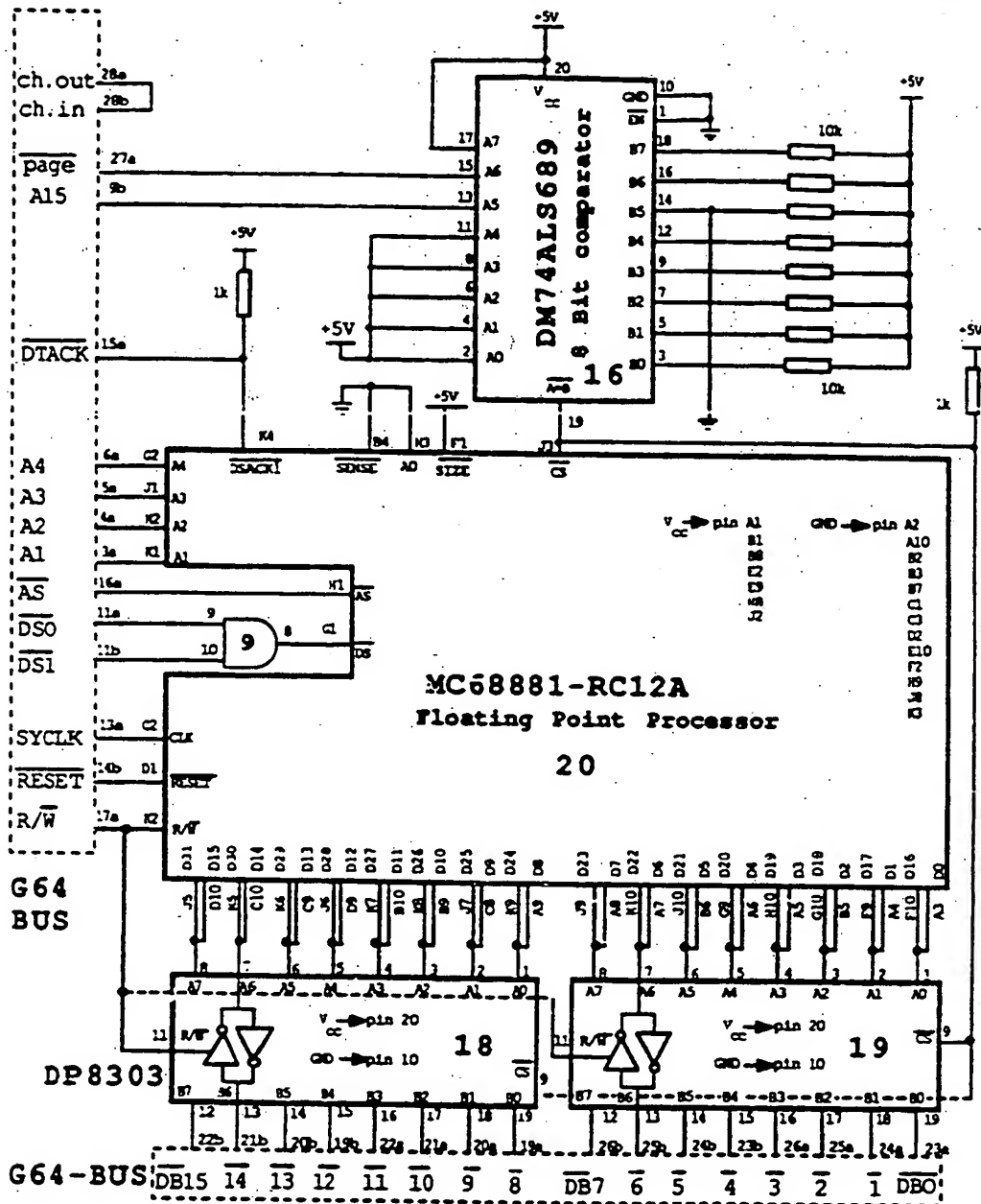


Figure J.4: Floating Point Processor Interface to the G-64 bus and MC68000 CPU

APPENDIX J. ANALOG-TO-DIGITAL, RADIO AND FPP INTERFACE

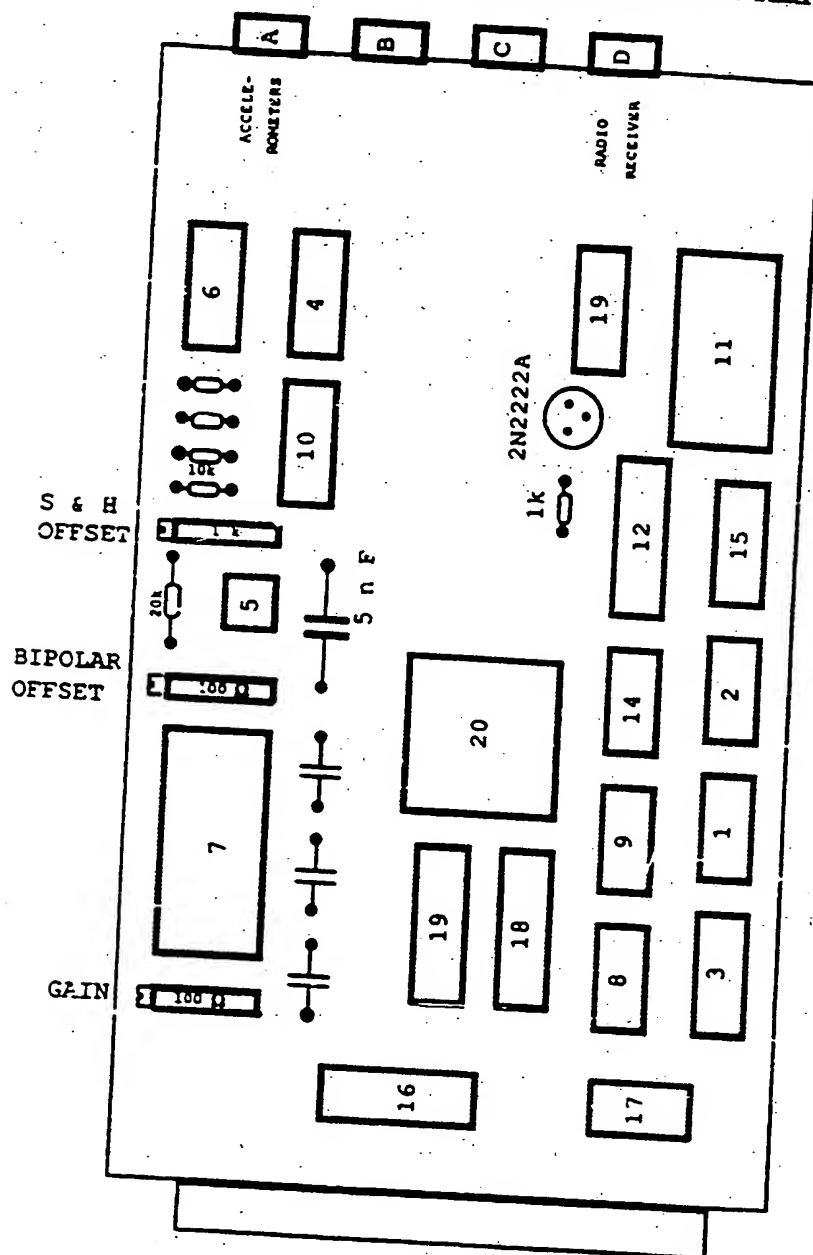


Figure J.5: Interface Board Layout

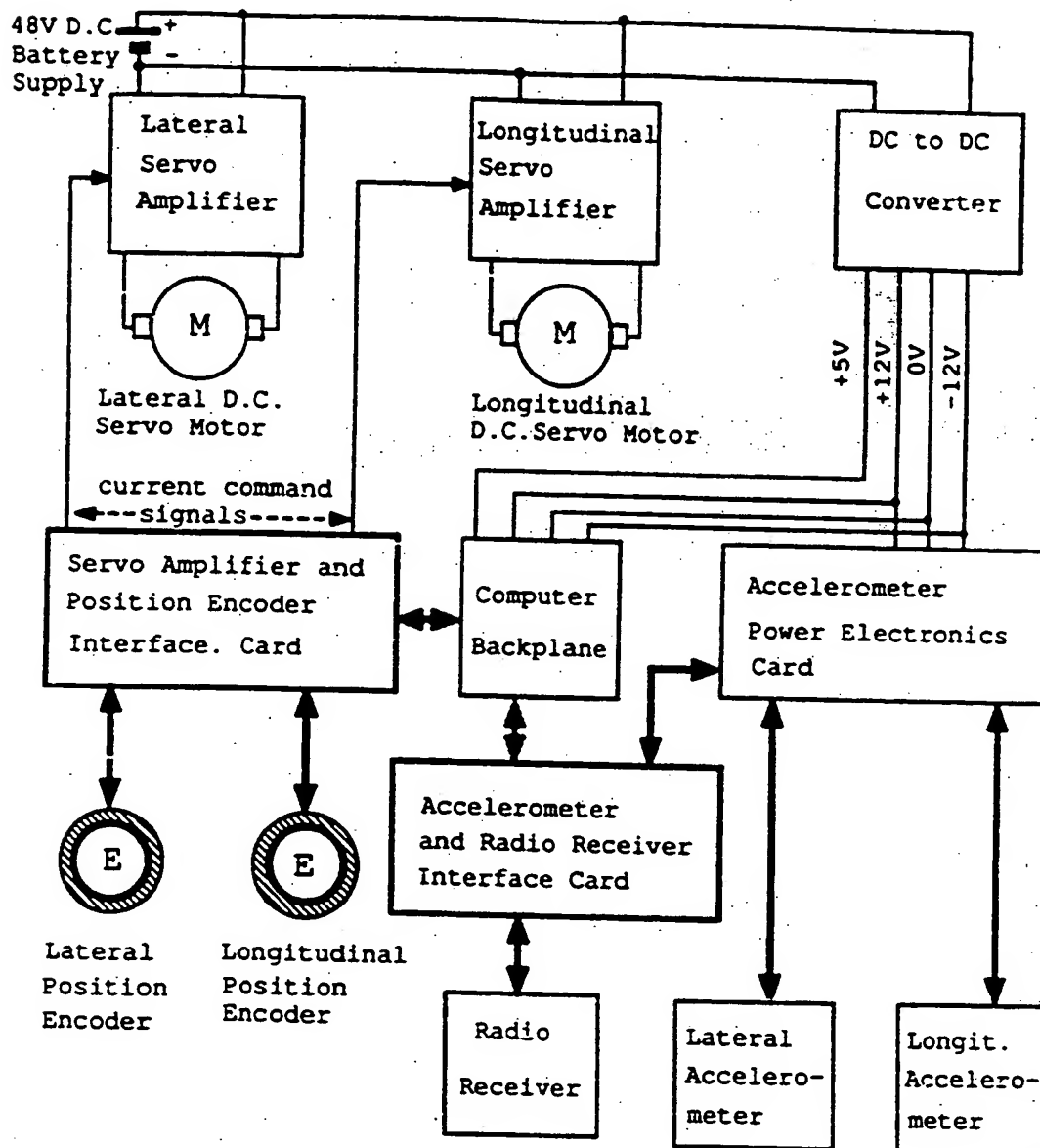


Figure J.6: Electrical and Electronic Wiring Diagram

Appendix K

Gear Ratio for Maximum Wheel Acceleration

K.1 Introduction

The unicycle wheel is driven by a direct current motor mounted on the frame. A gear and belt drive system is used to increase the motor torque. If the frame is falling forward or backward away from vertical, it will be advantageous to apply maximum acceleration of the wheel to reposition the wheel axle directly below the frame's center of mass. This appendix will show how the optimal gear ratio is calculated to allow maximum acceleration of the wheel.

K.2 Optimal gear ratio for wheel drive system

A schematic diagram of the wheel drive system is shown in Figure K.1.

The gear drive system has the constraint equation:

$$\omega = n(\Omega - \dot{\theta}) \quad (\text{K.1})$$

Assuming no slip at the ground contact point of the wheel, the second constraint equation is:

$$\dot{x} = r_w \Omega \quad (\text{K.2})$$

The rotational and translational kinetic energy elements of the system are:

Wheel:

$$T_R^W = \frac{1}{2} I_2^W \Omega^2 \quad (\text{K.3})$$

$$T_T^W = \frac{1}{2} m_W \dot{x}^2 \quad (\text{K.4})$$

Frame:

$$T_R^F = \frac{1}{2} I_2^F \dot{\theta}^2 \quad (\text{K.5})$$

$$T_T^F = \frac{1}{2} m_F (\dot{x} + r_F \dot{\theta})^2 \quad (\text{K.6})$$

Motor rotor:

$$T_R^R = \frac{1}{2} I_2^R (\omega + \dot{\theta})^2 \quad (\text{K.7})$$

The potential energy of the system is:

$$V = m_F r_F g \cos \theta \quad (\text{K.8})$$

The Lagrangian is then:

$$\begin{aligned} L &= T_{tot} - V_{tot} \\ &= \frac{1}{2} [I_2^W \Omega^2 + m_W \dot{x}^2 + I_2^F \dot{\theta}^2 + m_F (\dot{x} + r_F \dot{\theta})^2 \\ &\quad + I_2^R (\omega + \dot{\theta})^2] - m_F r_F g \cos \theta \end{aligned} \quad (\text{K.9})$$

Let the derivatives of the generalized coordinates of the system be:

$$\begin{aligned} q_1 &= \bar{\Omega} ; \dot{q}_1 = \Omega \\ q_2 &= x ; \dot{q}_2 = \dot{x} \\ q_3 &= \theta ; \dot{q}_3 = \dot{\theta} \\ q_4 &= \bar{\omega} ; \dot{q}_4 = \omega \end{aligned} \quad (\text{K.10})$$

208 APPENDIX K. GEAR RATIO FOR MAXIMUM WHEEL ACCELERATION

The two nonholonomic constraint equations K.1 and K.2 are augmented to Lagrange's equation to give:

$$\frac{d}{dt} \left(\frac{\partial L}{\partial \dot{q}_i} \right) - \frac{\partial L}{\partial (q_i)} = \sum_{j=1}^2 \lambda_j a_{ji} + Q_i \quad (\text{K.11})$$

(for $i = 1, 2, 3, 4$)

where Q_i is a generalized force. Friction forces will be neglected for the purposes of this derivation.

$$a_{ji} \equiv \frac{\partial \phi_j}{\partial (q_i)} \quad (\text{K.12})$$

(for $j = 1, 2$)

where ϕ_j are the constraint equations of the system.

$$\phi_1 = \omega + n(\theta - \Omega) = 0 \quad (\text{K.13})$$

$$\phi_2 = \dot{x} - r_W \Omega = 0 \quad (\text{K.14})$$

Rewritten in differential form:

$$1.d\omega + n(d\theta - d\Omega) = 0 \quad (\text{K.15})$$

$$1.d\dot{x} - r_W d\Omega = 0 \quad (\text{K.16})$$

We can readily identify the a_{ji} coefficients:

$$\begin{aligned} a_{11} &= -n & a_{12} &= 0 & a_{13} &= n & a_{14} &= 1 \\ a_{21} &= r_W & a_{22} &= 1 & a_{23} &= 0 & a_{24} &= 0 \end{aligned} \quad (\text{K.17})$$

Apply Lagrange's equations for each generalized coordinate:

1. $q_1 = \Omega$:

$$I_2^W \dot{\Omega} = -\lambda_1 n - \lambda_2 r_W \quad (\text{K.18})$$

2. $q_2 = x$:

$$(m_W + m_F)\ddot{x} + m_F r_F \ddot{\theta} = \lambda_2 \quad (\text{K.19})$$

3. $q_3 = \theta$:

$$(I_2^F + m_F r_F^2 + I_2^R) \ddot{\theta} + m_F r_F \ddot{z} + I_2^R \dot{\omega} - m_F r_F g \sin \theta = n \lambda_1 - Q_R \quad (K.20)$$

4. $q_4 = \bar{\omega}$:

$$I_2^R \ddot{\theta} + I_2^R \dot{\omega} = \lambda_1 + Q_R \quad (K.21)$$

where Q_R is the motor rotor torque.

Eliminate the two Lagrange multipliers to yield the two dynamic equations of motion for the system:

$$\begin{aligned} & [I_2^F + m_F r_F(r_W + r_F) + I_2^R] \ddot{\theta} + [m_W r_W + m_F(r_W + r_F)] \ddot{z} \\ & + I_2^R \dot{\omega} + I_2^W \dot{\Omega} - m_F r_F g \sin \theta = -Q_R \end{aligned} \quad (K.22)$$

$$(n I_2^R + m_F r_F r_W) \ddot{\theta} + n I_2^R \dot{\omega} + I_2^W \dot{\Omega} + (m_W + m_F) r_W \ddot{z} = n Q_R \quad (K.23)$$

Use the constraint equations to eliminate the ω and z variables:

$$\begin{aligned} & [I_2^F + m_F r_F(r_W + r_F) + (1-n)I_2^R] \ddot{\theta} \\ & + [I_2^W + m_W r_W^2 + m_F r_W(r_W + r_F) + n I_2^R] \dot{\Omega} - m_F r_F g \sin \theta = -Q_R \end{aligned} \quad (K.24)$$

$$[n(1-n)I_2^R + m_F r_F r_W] \ddot{\theta} + [I_2^W + n^2 I_2^R + (m_W + m_F) r_W^2] \dot{\Omega} = n Q_R \quad (K.25)$$

Subtract equation K.25 from K.24

$$\begin{aligned} & [I_2^F + m_F r_F^2 + (n-1)^2 I_2^R] \ddot{\theta} + [n(1-n)I_2^R + m_F r_F r_W] \dot{\Omega} \\ & = m_F r_F g \sin \theta - (n+1) Q_R \end{aligned} \quad (K.26)$$

210 APPENDIX K. GEAR RATIO FOR MAXIMUM WHEEL ACCELERATION

Notice that equation K.25 and K.26 compare well to the longitudinal dynamic equations of motion if the reflected rotor moments of inertia are taken into account.

Now proceed to calculate the optimal gear ratio for maximum wheel acceleration:

Eliminate $\bar{\theta}$ between equation K.25 and K.26:

Define:

$$A = n(1-n)I_2^R + m_F r_F r_W \quad (K.27)$$

$$B = I_2^W + n^2 I_2^R + (m_W + m_F) r_W^2 \quad (K.28)$$

$$C = I_2^F + m_F r_F^2 + (n-1)^2 I_2^R \quad (K.29)$$

$$D = m_F r_F g \sin \theta \quad (K.30)$$

$$\dot{\Omega} = \frac{[n(C+A)+A]Q_R - AD}{BC - A^2} \quad (K.31)$$

We want the maximum wheel acceleration as a function of the gear ratio, n and since the frame will be nominally vertical, $\theta = 0$ and therefore $D=0$.

We can set :

$$\frac{d\dot{\Omega}}{dn} = \frac{d}{dn} \left[\frac{n(C+A)+A}{BC+A^2} \right] Q_R = 0 \quad (K.32)$$

and solve for the optimal gear ratio n_{opt} analytically.

The gear ratio used in the mechanical design may not necessarily be exactly the same as the optimal gear ratio calculated above. It is therefore more useful to use equation K.31 to plot the curve of $\frac{\dot{\Omega}}{Q_R}$ as a function of the gear ratio, n , in order to see the effect of nonoptimal gear ratios used in practice.

Equations K.28 through K.30 can be readily extended to include the mass and inertia properties of the turntable on top of the frame:

$$\bar{A} = n(1-n)I_2^R + (m_F r_F + m_T r_T) r_W$$

$$\bar{B} = I_2^W + n^2 I_2^R + (m_W + m_F + m_T) r_W^2$$

$$\bar{C} = I_2^F + m_F r_F^2 + I_2^T + m_T r_T^2 + (n-1)^2 I_2^R$$

The measured mechanical parameters for the unicycle from Appendix M and the CTRL-C program lgtnopt.ctr is used to generate the curve of Figure K.2.

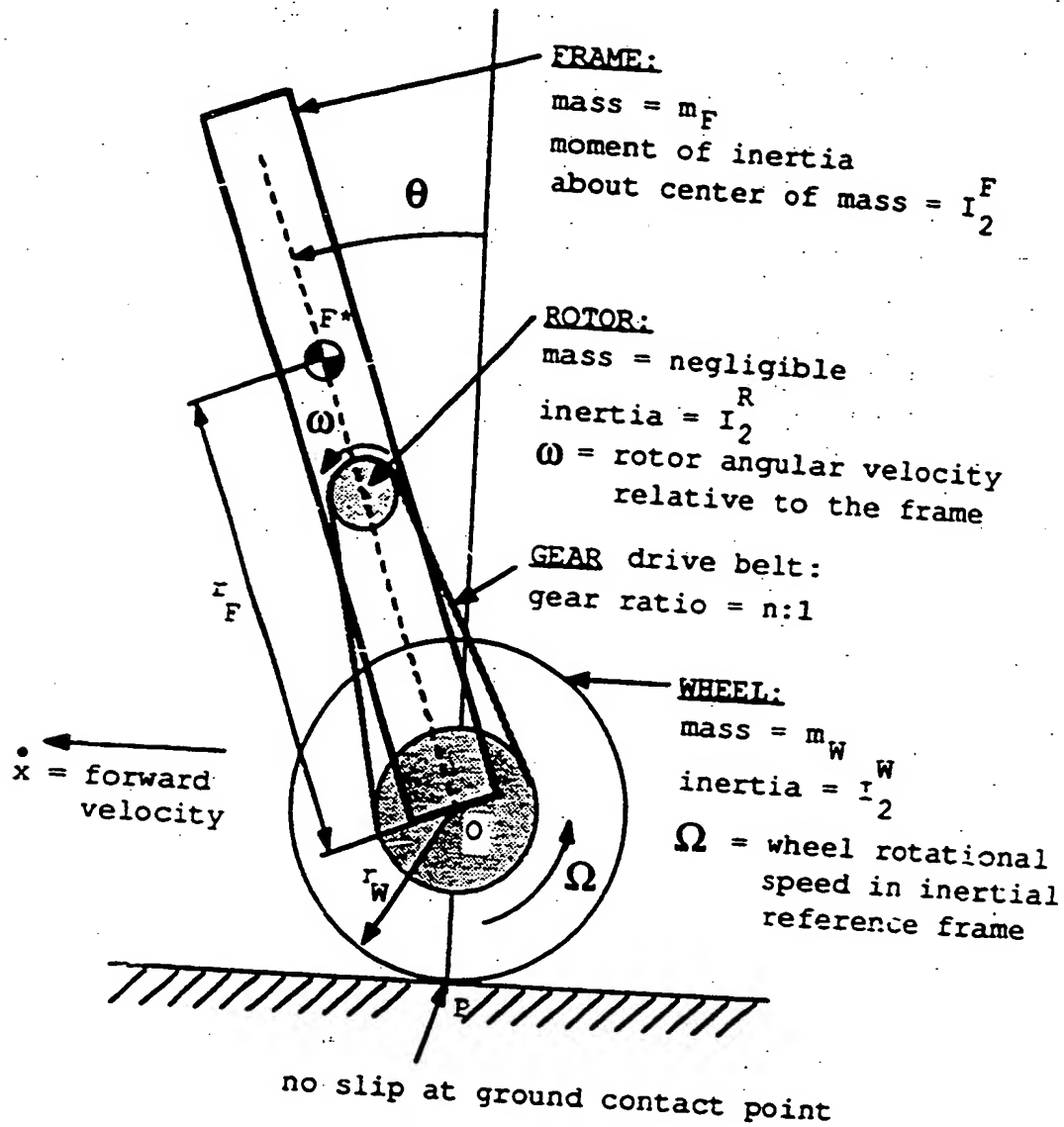


Figure K.1: Wheel Drive System

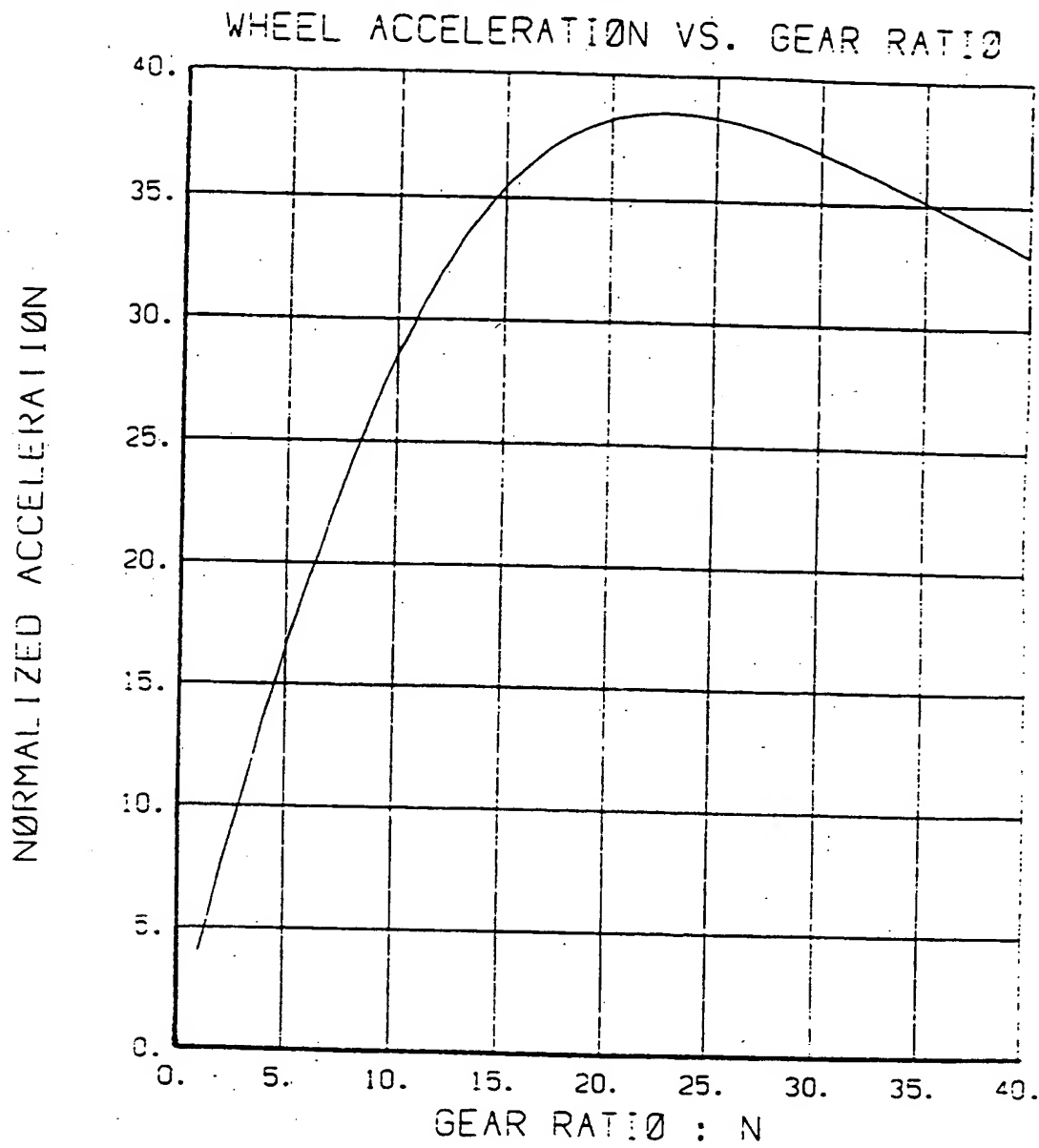


Figure K.2: Normalized Wheel Acceleration as a Function of the Wheel Drive System Gear Ratio

Appendix L

Unicycle Mechanical Design

L.1 Introduction

One of the goals of this research is to compare the performance of a computer stabilized one wheeled robot to that of a person riding a unicycle. The mechanical design of the unicycle should therefore approximately emulate a human riding a unicycle.

A person uses four major motions to balance on a unicycle. The longitudinal stabilization is largely obtained through the torques exerted on the pedals of the wheel and to a lesser extent by the forward backward leaning motion of the rider's torso. The simplified mechanical robot emulates the pedal control action only by a direct current motor driving the wheel through a reduction gear system. Lateral stabilization is obtained through sideways leaning of the rider's body and by twisting his torso with the arms partially extended. During the twisting action, the rider uses the inertia of the upper part of his body to rapidly steer the wheel of the unicycle into the direction into which the unicycle is falling. In this way the lateral component of the ground reaction force on the wheel is used to upright the falling unicycle. It was shown in Appendix F that the twisting motion is much more effective than the sideways leaning motion for lateral stabilization of the

unicycle. The rotary battery pack on top of the unicycle robot is used to simulate the twisting motion of a human rider's torso. It should be noted that although the battery pack is designed to allow full 360 degree rotations, it will not be used as a control moment gyro for stabilizing the unicycle.

The mass, inertias and length dimensions of the unicycle robot were selected to be similar to those of a teenage child riding an actual unicycle. This will enable interesting comparisons between the computer stabilized and human stabilized unicycles without the need of scaling the time constants of the dynamic system.

The unicycle robot consists of three major parts:

1. The wheel drive system (Figure L.1)
2. Frame and electronics system: This is the middle section of the robot and consists of a frame which connects the wheel drive system to the turntable drive system. The on board microprocessor, servo amplifiers and other electronic components are mounted to the frame.
3. The turntable drive system (Figure L.2)

All of the more complex parts of the unicycle robot were manufactured out of Aluminum (Al 6061 - T6) using a numerically coded milling machine.

Full scale drawings prepared on the Hewlett-Packard "HPDRAFT" system are available on floppy disc at the Computer Aided Design Facility of the Design Division, Department of Mechanical Engineering, Stanford University. The Pascal code for programming the MATSUURA milling machine is also available at the same facility.

L.2 Effect of center of mass height

Here, we simplify the unicycle model to consist of a wheel and a frame only. We neglect friction effects and assume that a direct drive torque motor has its rotor on the wheel axle and its stator connected to the frame.

The longitudinal system dynamic equations can be obtained from equations N.1 and N.2 by letting $I_2^T = m_T = r_T = f_W = 0$. We will be investigating the control torque required to cause a constant wheel acceleration. Since we are interested in performance near the state where the frame is stabilized vertically, θ can also be set equal to zero in equation N.1.

$$(I_2^F + m_F r_F^2) \ddot{\theta} + m_F r_F r_W \ddot{\Omega} = -Q_W \quad (L.1)$$

$$m_F r_F r_W \ddot{\theta} + [I_2^W + (m_W + m_F) r_W^2] \ddot{\Omega} = Q_W \quad (L.2)$$

Eliminate $\ddot{\theta}$:

$$\begin{aligned} \frac{Q_W}{\ddot{\Omega}} &= \frac{[I_2^F + m_F r_F^2][I_2^W + (m_W + m_F) r_W^2] - (m_F r_F r_W)^2}{I_2^F + m_F r_F (r_W + r_F)} \\ &= \frac{I_2^F [I_2^W + (m_W + m_F) r_W^2] + [I_2^W + m_W r_W^2] m_F r_F^2}{m_F r_F^2 + m_F r_W r_F + I_2^F} \end{aligned} \quad (L.3)$$

The expression on the right hand side can be viewed as the effective inertia that has to be accelerated by the wheel torque motor.

Figure L.3 shows how the effective moment of inertia decreases as the center of mass of the frame is placed at increasing heights above the wheel axle.

Letting $r_F = 0$ in equation L.3 gives the maximum effective inertia, which is the case where the frame center of mass is at the height of the wheel axle:

$$I_{max} = I_2^W + (m_W + m_F) r_W^2 \quad (L.4)$$

Letting $r_F \rightarrow \infty$ the minimum effective inertia is obtained:

$$I_{min} = I_2^W + m_W r_W^2 \quad (L.5)$$

It is therefore concluded that the mechanical design should place the center of mass of the frame as high above the wheel axle as possible for ease of stabilization. The side support frames of the wheel drive system were manufactured on a numerical milling machine and lightened out to leave a rib structure with minimal weight around the lower sections. The heavy drive motors were mounted as high on the structure as was practical. The turntable drive system which contains the lead-acid batteries is mounted at the top of the robot. Although the frame structural design was made as light as possible, it was designed strong enough so that structural flexibility effects need not be a consideration during the control system design.

L.3 Design of the gear drive systems

A precision cable and polyurethane chain drive system from BERG Inc. was selected for the gear drive systems. These chain and sprocket components require no lubrication and have small backlash effects at reasonable cost. It also facilitates gear ratio adjustment at any stage of the unicycle robots life cycle without the need for mechanical redesign.

Bearings are supplied on gear shafts to reduce friction. The bearings are mounted in bearing blocks whose positions can be adjusted. In this way the drive belt tensions can be adjusted to minimize backlash in the drive systems.

Appendices G and K show that optimal gear ratios can be selected for the wheel drive and turntable drive systems. The optimal turntable gear ratio is selected to yield maximum yaw acceleration of the frame, since this is the action that will be utilized to stabilize the unicycle laterally. The wheel gear ratio is selected to

APPENDIX L. UNICYCLE MECHANICAL DESIGN

yield maximum wheel acceleration about its axle, since this is how longitudinal instability will be controlled.

For the mechanical parameters measured and shown in Appendix M, a practical gear ratio for the wheel drive system is 24 : 1 and 60 : 1 for the turntable drive system.

1/5 SCALE DIMENSIONS in INCHES

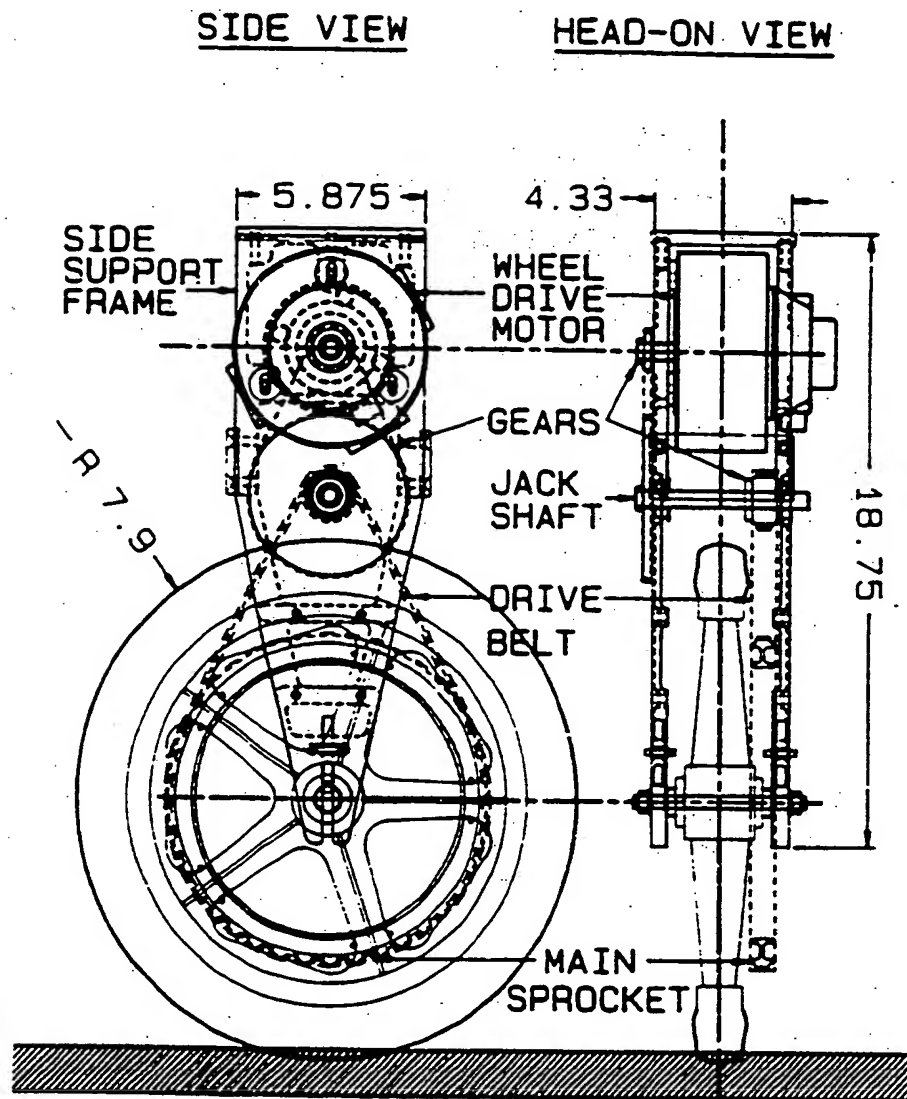


Figure L.1: Wheel Drive System

1/5 SCALE

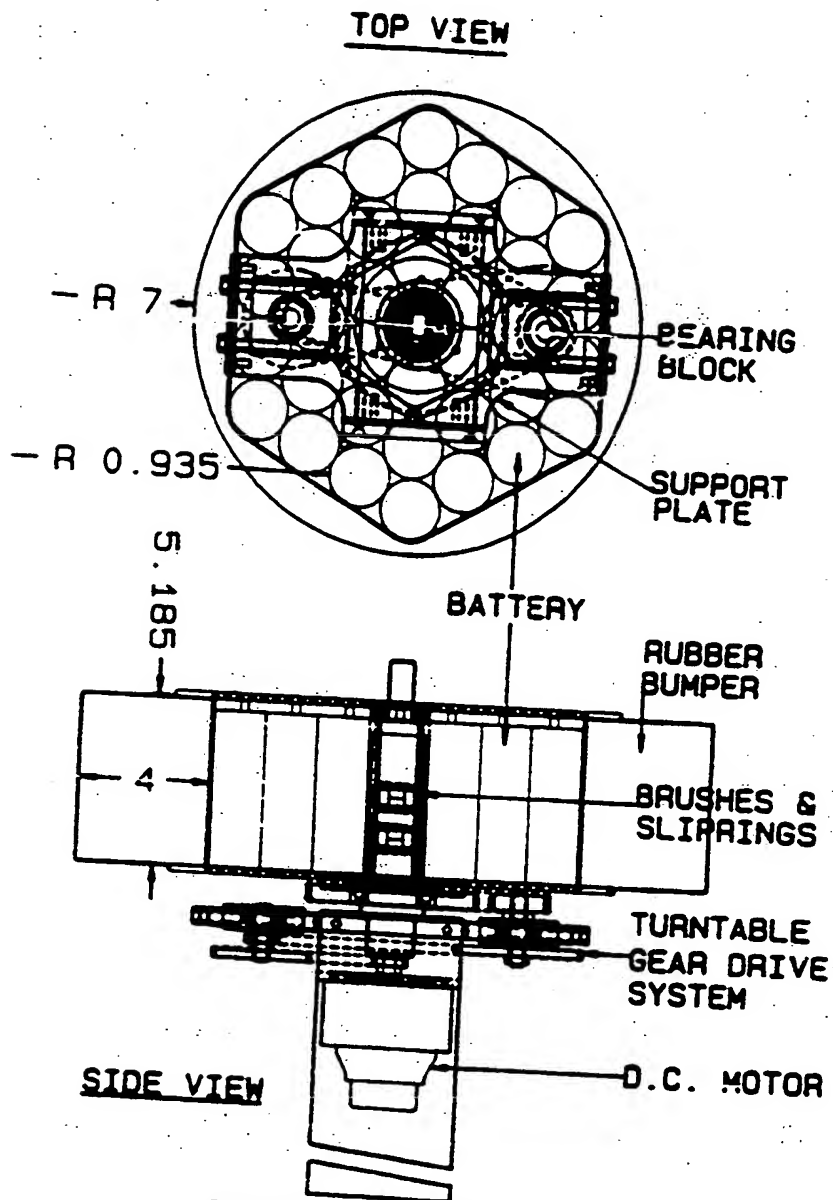
APPENDIX L. UNICYCLE MECHANICAL DESIGN
DIMENSIONS in INCHES

Figure L.2: Turntable Drive System

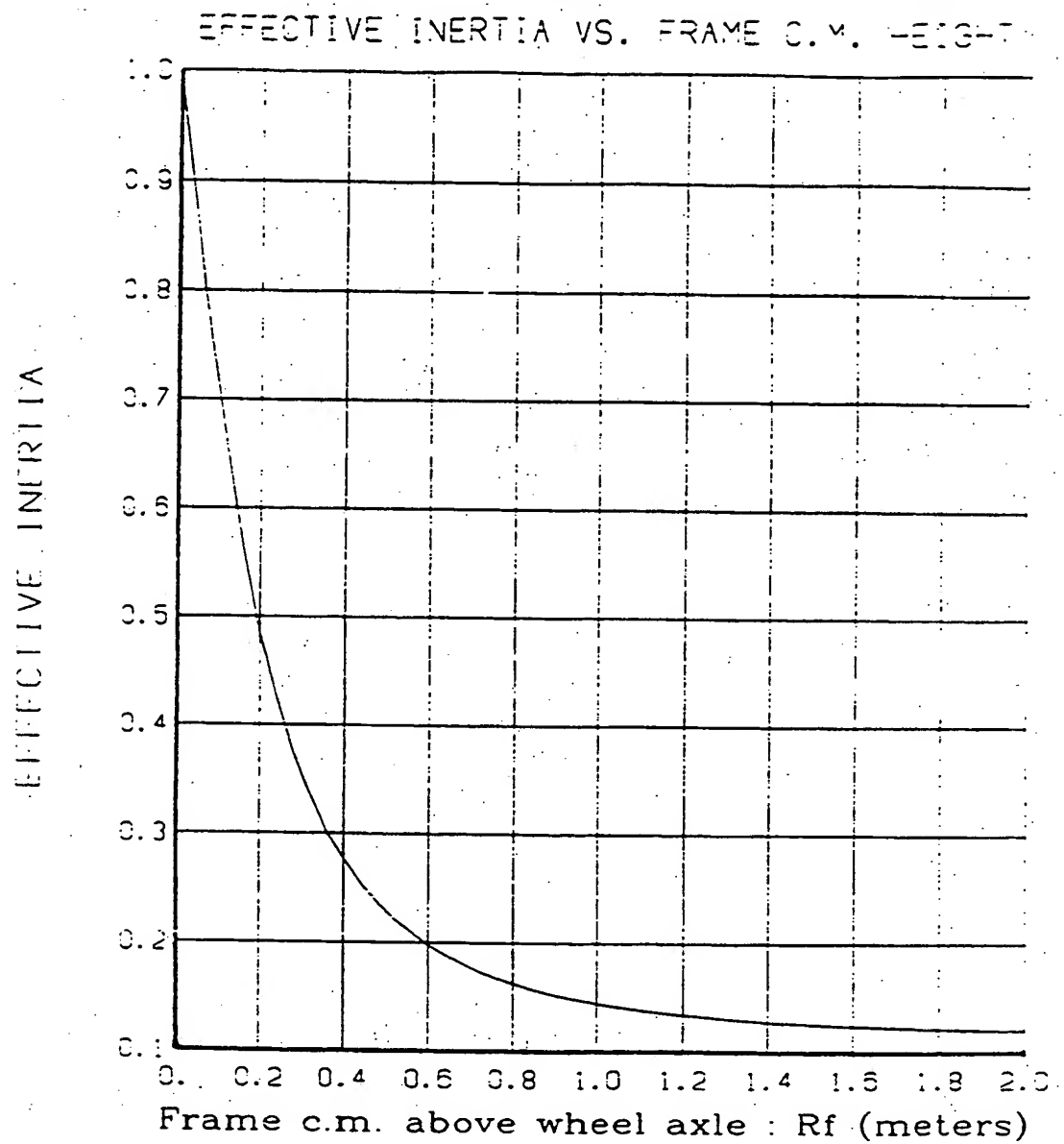


Figure L3: Effective Longitudinal System Moment of Inertia as a Function of the Height of the Frame Center of Mass above the Wheel Axle

Appendix M

Mechanical Parameter Measurements

M.1 Inertia measurement method

The moments of inertia of the wheel, frame and turntable about their mass centers were measured by means of the trifilar pendulum method. Since the objects are relatively symmetric, the cross products of inertia were assumed to be negligibly small and the three principal moments of inertia were determined for each part.

The equation relating oscillation period of the pendulum to the moment of inertia of the object is derived below. For practical reasons we used a trifilar pendulum to perform the experiments, but we will derive the equations for a bifilar pendulum for simplicity, since the results are the same. The oscillation amplitude of the pendulum is kept small enough to validate small angle approximations for the angles θ and γ shown in Figure M.1.

Vertical force balance:

$$2T \cos \gamma \cong 2T = mg \quad (\text{M.1})$$

Torque balance:

$$-2Tr \sin \gamma \cong -2Tr\gamma = I\ddot{\theta} \quad (\text{M.2})$$

From geometry:

$$r\theta \cong l\gamma \Rightarrow \ddot{\theta} \cong \frac{l}{r}\ddot{\gamma} \quad (\text{M.3})$$

From equation M.1 to M.3

$$\ddot{\gamma} + \frac{mgr^2}{Il}\gamma = 0 \quad (\text{M.4})$$

The solution of this differential equation is a sinusoidal function with an oscillation frequency of :

$$\omega_n = \sqrt{\frac{mgr^2}{Il}} = \frac{2\pi}{\tau} \quad (\text{M.5})$$

where τ is the period of the oscillation. With the mass of the object and the local gravity constant known, as well as the two lengths l and r , the moment of inertia is :

$$I = \frac{g}{l} \left(\frac{r}{2\pi} \right)^2 m\tau^2 \quad (\text{M.6})$$

M.2 Center of mass measurement method

The center of mass for each object was determined by finding the locations where each object would balance when placed on a narrow beam.

M.3 Friction measurements

M.3.1 Longitudinal system friction coefficients

The friction in the drive chains and at the contact point between the wheel and the ground are nonlinear functions of the rotational speeds. For simplicity it is assumed that the wheel drive system consists of a Coulomb friction and a viscous friction component. An approximate value for the viscous friction was obtained by closing a velocity feedback loop by means of the tachometer mounted on the

APPENDIX M. MECHANICAL PARAMETER MEASUREMENTS

wheel drive motor and commanding various constant speeds in the vicinity of the nominal wheel speed. The average torque over 100 samples was calculated for each speed. A linear regression of these data points with the torque values on the abscissa and the wheel speeds on the ordinate yields a straight line whose slope gives the viscous friction. The value is recorded in the table of the next section.

The Coulomb friction in the wheel drive system was determined by swinging the upside down unicycle with the wheel rigidly clamped to a suspended beam. It can be shown that the envelope of a free oscillation decays linearly for a system with Coulomb friction only:

From equation N.1 and the upside down unicycle and no applied torque:

$$I_0 \ddot{\theta} = -f_w \dot{\theta} - mgl\theta - f_c \operatorname{sgn}(\dot{\theta}) \quad (\text{M.7})$$

where:

$$I_0 = I_2^F + m_F r_F^2 + I_2^T + m_T r_T^2 + n^2 I_2^R \quad (\text{M.8})$$

$$mgl = (m_F r_F + m_T r_T)g \quad (\text{M.9})$$

$$f_c = \text{coulomb friction measured in N} \cdot \text{m}$$

Since $f_c \gg f_w \dot{\theta}$ equation M.7 can be simplified to

$$\ddot{\theta} + \frac{mgl}{I_0} \theta = -\frac{f_c}{I_0} \operatorname{sgn}(\dot{\theta}) = \pm \frac{f_c}{I_0} \quad (\text{M.10})$$

Laplace transform:

$$s^2 \Theta - s\theta_0 - \dot{\theta}_0 + \frac{mgl}{I_0} \Theta = \pm \frac{f_c}{I_0} \cdot \frac{1}{s} \quad (\text{M.11})$$

where θ_0 and $\dot{\theta}_0$ is the initial angle and velocity of the free oscillation. The experiment will be performed with $\dot{\theta}_0 = 0$ and $\theta_0 \neq 0$.

$$\Theta(s) = \frac{s\theta_0}{s^2 + \omega_n^2} \pm \frac{\frac{f_c}{I_0}}{s(s^2 + \omega_n^2)} \quad (\text{M.12})$$

where

$$w_n^2 = \frac{mgl}{I_0} \quad (\text{M.13})$$

The inverse Laplace transform of equation M.12 yields

$$\theta(t) = \left(\theta_0 \mp \frac{f_c}{mgl} \right) \cos w_n t \pm \frac{f_c}{mgl} \quad (\text{M.14})$$

The amplitude of above time response decays linearly with $\frac{4f_c}{mgl}$ during every complete sinusoidal cycle which provides a means of obtaining the Coulomb friction, f_c , from experimental data.

In the present unicycle configuration where we actually measure $\dot{\theta}(t)$, equation M.14 can be differentiated to yield

$$\dot{\theta}(t) = \left(\pm \frac{f_c}{mgl} - \theta_0 \right) w_n \sin w_n t \quad (\text{M.15})$$

In this case the amplitude of the $\dot{\theta}(t)$ response decays with

$$\Delta \dot{\theta} = \frac{4f_c}{mgl} \cdot w_n \quad (\text{M.16})$$

during each cycle.

Notice that the undamped natural frequency w_n can also be determined from the experimental data since the period of the oscillation is

$$\tau = \frac{1}{w_n} = \frac{I_0}{mgl} \quad (\text{M.17})$$

Figure M.2 shows a plot of the experimental data. By means of equation M.16 above, it is calculated that the Coulomb friction for the wheel drive system is

$$f_c = 1.84 \quad \text{N} \cdot \text{m} \quad (\text{M.18})$$

and the undamped natural frequency is

$$\begin{aligned} w_n &= 3.63 \quad \text{rad/sec} \\ &= 0.58 \quad \text{hz} \end{aligned} \quad (\text{M.19})$$

M.3.2 Lateral system friction measurements

The turntable friction is measured by closing a velocity feedback loop on the turntable speed. The position encoder mounted on the turntable drive motor shaft is used to obtain the speed of the turntable relative to the frame. Various constant speeds around zero are commanded while the frame is constrained in movement and the average torque over 100 samples is calculated. When these data points are plotted with the wheelspeeds on the ordinate and a straight line is fitted through these data points, the slope of this line yields the viscous friction and the intercept with the vertical axis gives the Coulomb friction present in the turntable drive system.

The friction between the ground and the rubber tire is not only very nonlinear, but also varies with the type of the terrain that the unicycle is traversing. An estimation of the ground friction during yaw motions was obtained by a similar procedure as described above, but in this case the turntable instead of the frame was constrained from turning.

M.4 Measured mechanical parameters**Wheel:**

$$m_W = 2.109 \text{ kg}$$

$$r_W = 0.195 \text{ m}$$

$$I_1^W = I_3^W = 0.01888 \text{ kg} \cdot \text{m}^2$$

$$I_2^W = 0.03716 \text{ kg} \cdot \text{m}^2$$

$$f_W = 0.047 \text{ N} \cdot \text{m per r/s}$$

$$f_G = 0.0245 \text{ N} \cdot \text{m per r/s}$$

Frame:

$$m_F = 23.18 \text{ kg}$$

$$r_F = 0.451 \text{ m}$$

$$I_1^F = 1.3514 \text{ kg} \cdot \text{m}^2$$

$$I_2^F = 1.5121 \text{ kg} \cdot \text{m}^2$$

$$I_3^F = 0.3635 \text{ kg} \cdot \text{m}^2$$

APPENDIX M. MECHANICAL PARAMETER MEASUREMENTS

Turntable:

$$m_T = 24.09 \text{ kg}$$

$$r_T = 0.797 \text{ m}$$

$$I_1^T = I_2^T = 0.2928 \text{ kg} \cdot \text{m}^2$$

$$I_3^T = 0.5028 \text{ kg} \cdot \text{m}^2$$

$$f_T = 0.0786 \text{ N} \cdot \text{m per r/s}$$

Lateral accelerometer height above wheel axle:

$$r_{S3} = 0.186 \text{ m}$$

Longitudinal accelerometer height above wheel axle:

$$r_{R3} = 0.635 \text{ m}$$

M.5 D.C. motor and gear drive system parameters

Longitudinal System:

Motor Rotor Inertia:

$$I_2^R = 4.52 \times 10^{-4} \text{ kg} \cdot \text{m}^2$$

M.5. D.C.MOTOR AND GEAR DRIVE SYSTEM PARAMETERS

229

Motor Torque Constant:

$$K_T^{LGT} = 6.3 \times 10^{-2} \text{ N} \cdot \text{m} / \text{A}$$

Lateral System:

Motor Rotor Inertia:

$$J_3^R = 4.377 \times 10^{-5} \text{ kg} \cdot \text{m}^2$$

Motor Torque Constant:

$$K_T^{LAT} = 3.3 \times 10^{-2} \text{ N} \cdot \text{m} / \text{A}$$

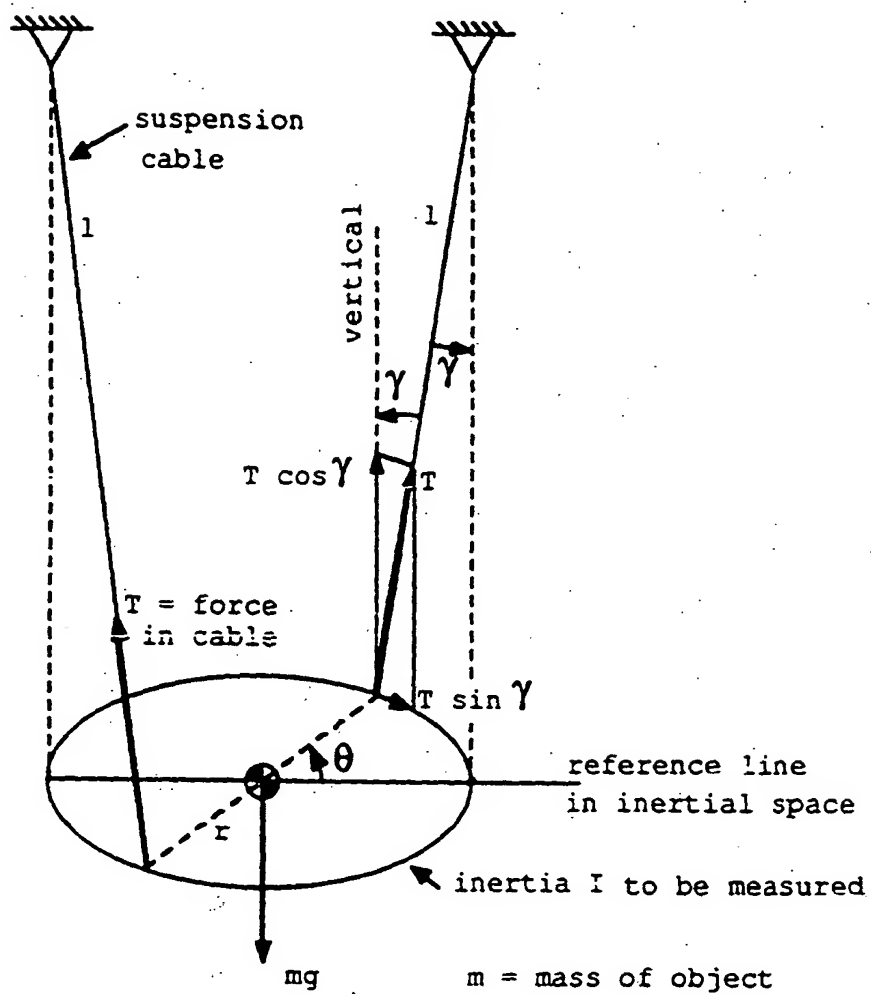


Figure M.1: Schematic Diagram of a Bifilar Pendulum for Measuring the Moment of Inertia of an Object

COULOMB FRICTION EXPERIMENT

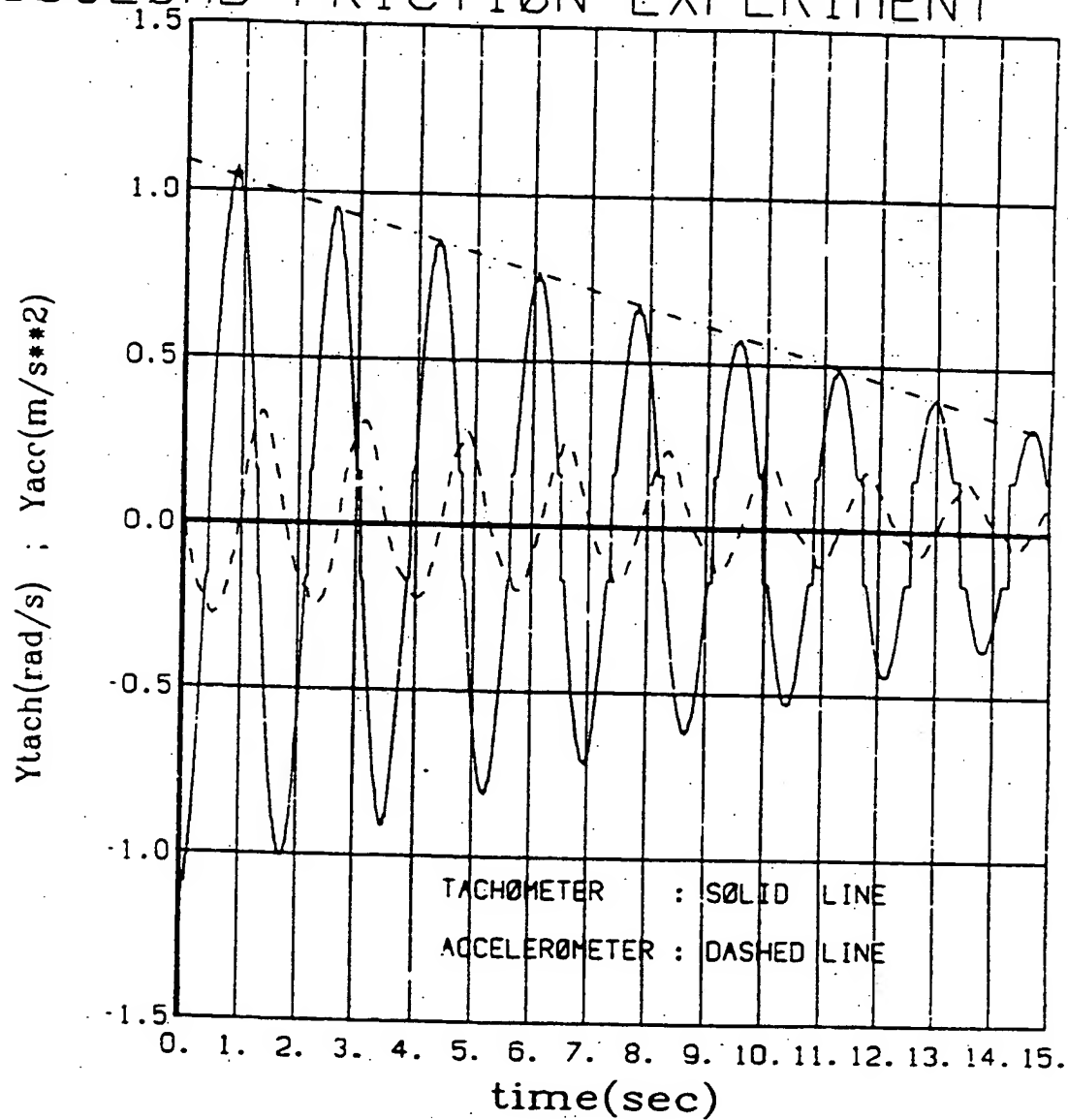


Figure M.2: Tachometer and Accelerometer Responses during Free Oscillation of the Upside Down Unicycle

Appendix N

Continuous Time Longitudinal Control System

N.1 Longitudinal equations of motion

The longitudinal equations of motion can be found from derivations in Appendices A, B and C. The following assumptions are made to decouple these equations from the lateral system dynamic equations:

1. The nominal turntable angular rotation speed $\eta_0 = 0$.
2. The unicycle frame is symmetric about a lengthwise centerline. This implies that $r_1 = r_2 = 0$.

With these assumptions, the longitudinal dynamic equations of motion from equations A.94 and A.95 simplify to:

$$\begin{aligned} & [I_2^F + m_F r_F^2 + I_2^T + m_T r_T^2] \ddot{\theta} + (m_F r_F + m_T r_T) r_W \dot{\Omega} \\ & = f_W (\Omega_0 + \Omega - \dot{\theta}) + (m_F r_F + m_T r_T) g \theta - Q_W \end{aligned} \quad (N.1)$$

$$\begin{aligned} & [m_T r_T + m_F r_F] r_W \ddot{\theta} + [I_2^W + (m_W + m_F + m_T) r_W^2] \ddot{\Omega} \\ & = f_W (\dot{\theta} - \Omega_0 - \Omega) + Q_W \end{aligned} \quad (N.2)$$

The derivations in Appendix A assume that the wheel is driven by a torque Q_W applied directly to the axle. The robot that was constructed uses a gear drive system to drive the wheel. The inertia of the d.c. motor should be reflected to the wheel as indicated by the dynamic equations K.25 and K.26 for the geared drive system for the wheel. The modified dynamic equations of motion that include the finite motor rotor inertia I_2^R are:

$$\begin{aligned} & [I_2^F + m_F r_F^2 + I_2^T + m_T r_T^2 + (n-1)^2 I_2^R] \ddot{\theta} + [(m_F r_F + m_T r_T) r_W + n(n-1) I_2^R] \dot{\Omega} \\ & = f_W (\Omega_0 + \Omega - \dot{\theta}) + (m_F r_F + m_T r_T) g \theta - Q_W \end{aligned} \quad (N.3)$$

$$\begin{aligned} & [(m_T r_T + m_F r_F) r_W + n(n-1) I_2^R] \ddot{\theta} + [I_2^W + (m_W + m_F + m_T) r_W^2 + n^2 I_2^R] \dot{\Omega} \\ & = f_W (\dot{\theta} - \Omega_0 - \Omega) + Q_W \end{aligned} \quad (N.4)$$

The constant wheel speed term, Ω_0 , does not affect the longitudinal system dynamics other than causing a constant torque loss due to friction. In practice these friction losses will be compensated for by increasing the commanded torque to the drive motors by the required constant value. Ω_0 is therefore ignored in the design of the longitudinal feedback control system.

Rewriting these equations into state space representation, they become:

$$\begin{bmatrix} I_{11} & I_{12} & 0 \\ I_{21} & I_{22} & 0 \\ 0 & 0 & 1 \end{bmatrix} \begin{bmatrix} \ddot{\theta} \\ \dot{\Omega} \\ \dot{\theta} \end{bmatrix} = \begin{bmatrix} -f_W & f_W & J_{13} \\ f_W & -f_W & 0 \\ 1 & 0 & 0 \end{bmatrix} \begin{bmatrix} \dot{\theta} \\ \Omega \\ \theta \end{bmatrix} + \begin{bmatrix} -1 \\ 1 \\ 0 \end{bmatrix} Q_W \quad (N.5)$$

Where:

$$I_{11} = I_2^F + m_F r_F^2 + I_2^T + m_T r_T^2 + (n-1)^2 I_2^R \quad (N.6)$$

$$I_{12} = I_{21} = (m_F r_F + m_T r_T) r_W + n(n-1) I_2^R \quad (N.7)$$

$$I_{22} = I_2^W + (m_W + m_F + m_T) r_W^2 + n^2 I_2^R \quad (N.8)$$

$$J_{13} = (m_F r_F + m_T r_T) g \quad (N.9)$$

234 APPENDIX N. CONTINUOUS TIME LONGITUDINAL CONTROL SYSTEM

Multiplication of equation N.5 by the inverse of the first matrix containing the inertia terms, yields the standard state space form of the system of dynamic equations:

$$\dot{\mathbf{x}} = \mathbf{F}\mathbf{x} + \mathbf{G}u \quad (\text{N.10})$$

where $u = Q_w$ and $\mathbf{x} = [\dot{\theta}, \Omega, \theta]^T$.

N.2 Longitudinal sensors

A tachometer and an accelerometer are used as the longitudinal sensors.

The tachometer is mounted directly on the rotor shaft of the wheel drive motor. It is actually a digital position encoder, but angular velocity information is extracted from this sensor by means of the electronic circuitry described in Appendix I. If it is assumed that the wheel gear drive system has negligible elasticity and backlash, the tachometer on the motor shaft reads:

$$\omega_{LGT} = n_{LGT}(\Omega_0 + \Omega - \dot{\theta}) \quad (\text{N.11})$$

where n_{LGT} is the known wheel drive system gear ratio, Ω_0 is the constant nominal wheel speed and is typically much larger than the wheel perturbation velocity Ω and the frame pitch rate $\dot{\theta}$. Since Ω_0 is known, a measurement consisting of a combination of the two states Ω and $\dot{\theta}$ can be reconstructed in the microprocessor software:

$$y_t = \Omega - \dot{\theta} \quad (\text{N.12})$$

The accelerometer design is described in Appendix H. It is mounted on the unicycle frame, with its acceleration sensitive axis in the direction of the forward motion of the unicycle. With the accelerometer mounted at a height r_{R3} above the wheel axle, it measures a combination of the acceleration due to the pitch of the frame and the forward acceleration of the wheel of the unicycle. As shown in

Figure N.1, the signal measured by the accelerometer is proportional to the servo pendulum control torque:

$$Q_{N(LGT)} = k_a[g\theta - (r_W\dot{\Omega} + r_{R3}\ddot{\theta})] \quad (N.13)$$

The pitch acceleration of the frame and the wheel acceleration are from equation N.5:

$$\ddot{\theta} = F_{11}\dot{\theta} + F_{12}\dot{\Omega} + F_{13}\theta + G_1Q_W \quad (N.14)$$

$$\ddot{\Omega} = F_{21}\dot{\theta} + F_{22}\dot{\Omega} + F_{23}\theta + G_2Q_W \quad (N.15)$$

By scaling in the microprocessor software and by using equations N.14 and N.15, the accelerometer measurement can be rewritten in terms of the states and control input:

$$\begin{aligned} y_a &= g\theta - r_W\dot{\Omega} - r_{R3}\ddot{\theta} \\ &= -(r_{R3}F_{11} + r_W F_{21})\dot{\theta} - (r_{R3}F_{12} + r_W F_{22})\dot{\Omega} \\ &\quad + (g - r_{R3}F_{13} - r_W F_{23})\theta - (r_{R3}G_1 + r_W G_2)Q_W \end{aligned} \quad (N.16)$$

N.3 Longitudinal system characteristics

The CTRL-C program 'lgchar.ctr' is used to calculate the longitudinal system characteristics.

The results presented in section N.3.1 show the state transition matrix and the input and output matrices for the system with measured mechanical parameters as listed in Appendix M. The eigenvalues calculated show a pair of poles on the real axis on either side of the imaginary axis. These are due to the pitch instability of the frame of the unicycle. The third pole is the rigid body mode which is slightly shifted from the origin due to the wheel friction.

236 APPENDIX N. CONTINUOUS TIME LONGITUDINAL CONTROL SYSTEM

The controllability matrix (marked CTR in the print-out) shows that all three modes are controllable with the wheel torque, Q_w . All modes are also observable from the tachometer and accelerometer measurements. The residue matrix shows how much of each mode is present in the tachometer and accelerometer measurements.

The program also calculates open-loop transfer functions as shown below. A frequency response (Figure N.2) of the transfer function from the wheel torque to the pitch angle, shows that the open-loop bandwidth of the longitudinal system is approximately 0.75 Hz.

N.3.1 Longit. system characteristics calculation

```
UCTCS/LOGCHAR.CTR

LONGITUDINAL SYSTEM CHARACTERISTICS

*****

LONGITUDINAL STATES : THETA.DOT; OMEGA; THETA

CONTROL INPUT : WHEEL MOTOR TORQUE (QW)

MEASUREMENTS : TACHOMETER; ACCELEROMETER

UNITS : METERS, RADIANS, SECONDS

RR3      .

0.6350

PLOT      .
```

N.3. LONGITUDINAL SYSTEM CHARACTERISTICS

237

-0.0333	0.0333	54.5447
0.1138	-0.1138	-151.2607
1.0000	0.	0.

GLGT -

-0.7075
2.4216
0.

RLGT -

-1.0000	1.0000	0.
-0.0011	0.0011	4.6700

RLGT -

0.
-0.0230

EIGVAL -

-0.0216
7.3232
-7.4486

EIGVEC -

0.0000	-0.3620	-0.3592
1.0000	1.0000	1.0000
-0.0006	-0.0494	0.0482

CONTROLLABILITY, OBSERVABILITY AND RESIDUE MATRICES :

CTR -

0.4597

238 APPENDIX N. CONTINUOUS TIME LONGITUDINAL CONTROL SYSTEM

0.9659

0.9961

OBS -

1.0000 1.3620 1.3592

-0.0018 -0.2294 0.2267

RESIDU -

0.4597 1.3156 1.3539

-0.0008 -0.2216 0.2258

TRANSFER FUNCTION FROM WHEEL DRIVE TORQUE TO ~~YACCELERATION MEASUREMENT~~

GAIN -

3.1291

ZEROS -

2.8309

-2.8309

POLES -

-7.4406

7.3232

-0.0216

TRANSFER FUNCTION FROM WHEEL DRIVE TORQUE TO ACCELEROMETER MEASUREMENT

GAIN -

-0.0230

ZEROS -

$$-0.0000 + 9.44571$$

$$-0.0000 - 9.44571$$

$$0.0000 + 0. \quad 1$$

POLES =

$$-7.4486$$

$$7.3232$$

$$-0.0216$$

N.3.2 Experimental confirmation transfer functions

Before a control system for the longitudinal stabilization can be designed, experiments should be performed to verify that the actual plant transfer functions correspond to the theoretical model. The unstable longitudinal dynamics are difficult to identify in an openloop configuration. The unicycle was therefore suspended upside down with the wheel clamped to a beam. Although this configuration cannot provide information on the influence of the wheel dynamics in the system, it can be used to confirm certain parameters of the longitudinal system.

The theoretical model for the upside down unicycle configuration is

$$I_0 \ddot{\theta} = -f_w \dot{\theta} - f_c \operatorname{sgn}(\dot{\theta}) - mgl\theta + Q_w \quad (\text{N.17})$$

where

$$\begin{aligned} I_0 &= I_2^F + m_F r_F^2 + I_2^T + m_T r_T^2 + n^2 I_2^R \\ mgl &= (m_F r_F + m_T r_T)g \end{aligned} \quad (\text{N.18})$$

Apart from Coulomb friction, f_c , the belt and sprocket wheel drive system also has other nonlinearities like backlash and torque variations due to the imperfect gear system. A tight velocity feedback loop was therefore closed first to enhance the system linearity:

240 APPENDIX N. CONTINUOUS TIME LONGITUDINAL CONTROL SYSTEM

$$Q_W = -k_T(\dot{\theta} - y_c) \quad (N.19)$$

so that the closed loop system becomes

$$I_0 \ddot{\theta} = -f_W \dot{\theta} - f_c \operatorname{sgn}(\dot{\theta}) - k_T \dot{\theta} - mgl\theta + k_T y_c \quad (N.20)$$

If the velocity feedback gain is large enough the feedback torque will completely dominate the plant friction effects, so that the transfer function can be approximated by

$$I_0 \ddot{\theta} = -k_T \dot{\theta} - mgl\theta + k_T y_c \quad (N.21)$$

Henceforth the tachometer speed command, y_c , can be considered as the new longitudinal system control input. The Laplace transform of this equation gives

$$\frac{\Theta(s)}{y_c(s)} = \frac{k_T}{I_0 s^2 + k_T s + mgl} \quad (N.22)$$

The state space representation of the continuous time longitudinal system is therefore

$$\begin{bmatrix} \ddot{\theta} \\ \dot{\theta} \end{bmatrix} = \begin{bmatrix} -\frac{k_T}{I_0} & -\frac{mgl}{I_0} \\ 1 & 0 \end{bmatrix} \begin{bmatrix} \dot{\theta} \\ \theta \end{bmatrix} + \begin{bmatrix} \frac{k_T}{I_0} \\ 0 \end{bmatrix} y_c \quad (N.23)$$

The accelerometer sensor measures the specific force on the frame at a distance r_{R3} from the wheel axle:

$$y_a = r_{R3} \ddot{\theta} + g\theta \quad (N.24)$$

so that the closed loop system transfer function to accelerometer measurement is

$$\frac{y_a(s)}{y_c(s)} = \frac{k_T(r_{R3}s^2 + g)}{I_0 s^2 + k_T s + mgl} \quad (N.25)$$

The frequency response of this transfer function have the following characteristics which can be verified experimentally:

- The low frequency gain is $\frac{k_T g}{mgl}$.
- The high frequency gain is $\frac{k_T r_{R3}}{I_0}$.
- The zeros are at $\omega_z = \pm \sqrt{\frac{g}{r_{R3}}}$ so that the plant should have zero gain at this frequency.

- The undamped natural frequency of the poles are at $\omega_p = \pm \sqrt{\frac{mg}{b}}$. The relative positions of ω_p and ω_s on the frequency axis will be evident from the phase behavior of the experimental results.

The proportional tachometer feedback compensator was implemented as a digital control system in the on board microprocessor of the unicycle. A fast sampling frequency of 100 hz was selected and a computational delay of 1.2 ms between the sampling instant and the moment the control command is issued, was measured. This delay, T_d , was included in the plant model by means of a first order Padé approximation:

$$\begin{aligned} \frac{\bar{u}(s)}{u(s)} &= e^{-T_d s} = \frac{e^{-\frac{T_d}{2}s}}{e^{\frac{T_d}{2}s}} \\ &\cong \frac{1 - \frac{T_d}{2}s}{1 + \frac{T_d}{2}s} = -\frac{s - \frac{2}{T_d}}{s + \frac{2}{T_d}} \end{aligned} \quad (N.26)$$

To include the delay in the state space model, an additional state, x_d , is defined. Equation N.26 in the time domain then becomes

$$\begin{aligned} \dot{x}_d &= \frac{2}{T_d}(u - x_d) \\ \bar{u} &= 2x_d - u \end{aligned} \quad (N.27)$$

The original plant $\dot{x} = Fx + G\bar{u}$ of equation N.23, is therefore modified to include the transportation delay:

$$\begin{bmatrix} \dot{x} \\ \dot{x}_d \end{bmatrix} = \begin{bmatrix} F & 2G \\ 2 & -\frac{2}{T_d} \end{bmatrix} \begin{bmatrix} x \\ x_d \end{bmatrix} + \begin{bmatrix} -G \\ \frac{2}{T_d} \end{bmatrix} u \quad (N.28)$$

A listing of a CTRL-C program that calculates the discrete time system matrices for equation N.28 as well as the transfer function from the tachometer speed input command to the measured accelerometer output is shown in the next section.

Sinusoidal tachometer speed commands were generated in the on board computer of the unicycle and used to excite the system. The accelerometer output signal was

242 APPENDIX N. CONTINUOUS TIME LONGITUDINAL CONTROL SYSTEM

recorded and a typical input-output time response is shown in Figure N.3. Notice that some distortion in the accelerometer signal occurs at the instants when the sign of the acceleration changes. This is probably caused by backlash in the drive system, which cannot be corrected by feedback since the tachometer is mounted on the drive motor and not directly to the wheel.

Figure N.4 shows the theoretical frequency response with the measured data points indicated with squares. The sharp decrease in the gain between 0.6 and 0.7 hz confirms that the transfer function zeros are near the theoretical location of 0.63 hz. The fact that the phase first decreases below zero degrees and then has a positive discontinuity indicates that the undamped natural frequency of the complex pole pair is at a lower frequency (theoretically 0.58 hz) than the zeros. The measured low and high frequency gains are within 2 dB of the expected theoretical values. The discrepancies between the measured and theoretical frequency responses are attributed to the following factors:

- The electronic interface used to extract angular velocity information from the position encoder on the wheel drive motor (Appendix I) was designed to provide accurate wheel speed information in the vicinity of the nominal wheel speed of 3 rad/sec. In the frequency response identification experiments with the wheel clamped to the suspending beam, the maximum value of the sinusoidal speed command was only 0.05 rad/sec so that the resolution of the velocity information available to the controller, is suboptimal.
- Characteristics of the belt drive system like backlash and elasticity have been ignored in the linear theoretical model. Although it is assumed that the control torque dominates the friction effects in the drive system, it is reasonable to expect that at low speeds, frictional characteristics can be worse and include stiction effects when the speed becomes zero at the apexes of the pendulum swings.

In spite of these reservations, satisfactory agreement between the experimental

data and theoretical predictions has been obtained. The conclusion is drawn that the theoretical model for the upside down pendulum is acceptable. Since the unicycle parts with major weights and inertias as well as the complete wheel drive system have been included in the experiment, it is assumed that the model for the vertical unicycle on its wheel is also valid for small pitch motions.

N.3.3 Upside down unicycle transfer functions

ucycld/pend.ctr

LOT UPSIDE DOWN UCYC WITH PADE APPROX FOR TIME DELAY

LONGITUDINAL STATES : THETA.DOT; OMEGA; THETA; ID

CONTROL INPUT : WHEEL MOTOR TORQUE (QU)

MEASUREMENTS : TACHOMETER; ACCELEROMETER

UNITS : METERS, RADIAN, SECONDS

TSAMPLTACH -

0.0100

TDELATTACH -

0.0012

***** CONTINUOUS TIME SYSTEM MATRICES *****

PLGT -

1.0d+03 *

244 APPENDIX N. CONTINUOUS TIME LONGITUDINAL CONTROL SYSTEM

-0.0000	-0.0132	-0.0001
0.0010	0.	0.
0.	0.	-1.7094

GLGT -

1.0d+03 •

0.0000

0.

1.7004

HLGT -

-1.0000	0.	0.
---------	----	----

0.0014	-1.4440	0.
--------	---------	----

HLGT -

0.

0.0288

***** DISCRETE TIME SYSTEM MATRICES *****

PHI -

0.9993	-0.1317	-0.0001
--------	---------	---------

0.0100	0.9993	-0.0000
--------	--------	---------

0.	0.	0.0000
----	----	--------

GAM -

-0.0004

-0.0000

1.0000

***** PLANT TRANSFER FUNCTIONS *****

N.3. LONGITUDINAL SYSTEM CHARACTERISTICS

245

TRANSFER FUNCTION FROM WHEEL DRIVE TORQUE TO TACHMETER MEASUREMENT

TACHZEROS -

-0.1326

1.0000

TACHEPOLES -

0.0000 + 0. 1

0.9993 + 0.03631

0.9993 - 0.03631

TACHGAIN -

3.99844-04

TRANSFER FUNCTION FROM WHEEL DRIVE TORQUE TO ACCELEROMETER MEASUREMENT

ACCEZEROS -

-0.0000 + 0. 1

0.9993 + 0.03931

0.9993 - 0.03931

ACCEPOLES -

0.0000 + 0. 1

0.9993 + 0.03631

0.9993 - 0.03631

ACCGAIN -

0.0288

***** TACHMETER FEEDBACK LOOP PARAMETERS (INNER LOOP) *****

246 APPENDIX N. CONTINUOUS TIME LONGITUDINAL CONTROL SYSTEM

TACH LOOP PROPORTIONAL FEEDBACK COMPENSATOR GAIN=KT

KT

25.0

CLOSED TACHOMETER LOOP GAIN, ZEROS AND POLES : $TACC(S)/TACHEND(S)$

TACHLOOPZE =

$0.9993 + 0.03931$

$0.9993 - 0.03931$

$-0.0000 + 0. 1$

TACHLOOPPO =

$0.9937 + 0.03581$

$0.9937 - 0.03581$

$0.0013 + 0. 1$

TACHLOOPGA =

0.7190

N.4 Longitudinal control system design

The feedback control system design is performed in three steps:

1. Assume that all states are available to the feedback controller and design the optimal feedback gains for a linear quadratic regulator.
2. Design an optimal linear quadratic estimator to estimate all the lateral states from the tachometer and accelerometer measurements.
3. Discretize the continuous time design so that it can be implemented as a digital control system in the microprocessor on the unicycle.

A block diagram of the feedback control system is shown in Figure N.5. x is the state vector $[\dot{\theta} \ \Omega \ \theta]^T$ and u is the control input torque, Q_w . The measured output vector, y_M , is the tachometer and accelerometer signals. It was decided that the reference input, r , to the regulator should be a commanded perturbation of the wheel angular velocity, Ω_w . This will enable increasing and decreasing of the unicycle forward speed by external commands. The regulator also features integral error control to provide zero error to step input commands and improved rejection of constant disturbances on the plant.

N.4.1 Optimal continuous time regulator design

If it is assumed that all the plant states are available to the controller, an optimal linear quadratic regulator can be designed to minimize the cost function:

$$J = \frac{1}{2} \int_0^{\infty} (x^T A x + u^T B u) dt \quad (N.29)$$

where A and B are diagonal matrices whose diagonal elements are the weights on the states and control input.

It was decided to introduce feedback of the integral of the error in the wheel speed. This will ensure good control of the unicycle forward speed and rejection of constant disturbance inputs on the plant. This introduces an extra state, e , and from the block diagram in Figure N.5 the closed loop system matrices are:

$$\begin{aligned} \begin{bmatrix} \dot{e} \\ \dot{x} \end{bmatrix} &= \begin{bmatrix} 0 & H \\ 0 & F \end{bmatrix} \begin{bmatrix} e \\ x \end{bmatrix} + \begin{bmatrix} 0 \\ G \end{bmatrix} u + \begin{bmatrix} -1 \\ 0 \end{bmatrix} r \\ u &= -[C_e \ C] \begin{bmatrix} e \\ x \end{bmatrix} \end{aligned} \quad (N.30)$$

where $H = [0 \ 1 \ 0]$ for integral error feedback of the wheel speed Ω .

A CTRL-C program 'lgtlqg.ctr' is used to calculate the optimal feedback gains for specified weighting matrices A and B . A print-out of the results of the program is

248 APPENDIX N. CONTINUOUS TIME LONGITUDINAL CONTROL SYSTEM

shown in section N.6.1. The diagonals of the weighting matrices are called ADIAG and BDIAG in the print-out and the feedback gains are CERR and CLGT for the integral error and state feedback gains respectively.

For analysis of the closed loop system, equation N.30 can be rewritten as:

$$\begin{bmatrix} \dot{e} \\ \dot{x} \end{bmatrix} = \begin{bmatrix} 0 & H \\ -GC_0 & F - GC \end{bmatrix} \begin{bmatrix} e \\ x \end{bmatrix} + \begin{bmatrix} -1 \\ 0 \end{bmatrix} \Omega_c \quad (N.31)$$

$$\Omega = [0 \ 0 \ 1 \ 0] \begin{bmatrix} e \\ x \end{bmatrix} \quad (N.32)$$

If the state weighting matrix places a penalty, a , on the error in the wheel speed only, and the control, u , is weighted by $b = 1$, a locus of the closed loop poles as a function of $\frac{a}{b}$ can be calculated. These closed loop pole locations for values of $\frac{a}{b}$ ranging from 0 to 10 000 are plotted in Figure N.6. This is essentially a symmetric rootlocus plot. The low frequency branches of the loci approach the location of the zero and the reflected non minimum phase zero of $\frac{\Omega}{\Omega_c}$ as $\frac{a}{b}$ approaches infinity. This constitutes an inherent bandwidth limitation for the unicycle longitudinal closed loop dynamics with a regulator designed by the technique of minimizing a linear quadratic cost function.

For practical reasons the value of $\frac{a}{b}$ should not be too large, because the state feedback gains would be so large that signal saturations in the controller may occur. A choice of $\frac{a}{b} = 30$ gives moderate gains and an acceptably fast closed loop response.

Figure N.7 shows the time response of the closed loop system for a step command to increase the wheel speed by 1 r/s.

The frequency response plot of Figure N.8 shows that the closed loop longitudinal

system has a bandwidth of approximately 0.3Hz.

N.5 Process and measurement noise models

In order to evaluate the performance of various compensators, a model of the process and measurement noise is required. The plant model is modified to include these random disturbance effects:

$$\dot{z} = Fz + Gu + G_n w \quad (\text{N.33})$$

$$y_m = Mz + v \quad (\text{N.34})$$

where:

w is a random disturbance vector, with spectral density matrix Q

v is a random measurement noise vector, with spectral density matrix R .

The complete statistical nature of these random noise signals is rarely known in practice. Since we can usually rely on the inherent band limitation present in most control systems, it is convenient to assume that $w(t)$ and $v(t)$ are independent white noise processes. We now proceed to estimate the ratios of the spectral densities.

Let

R_t = spectral density of the tachometer measurement noise in units of rad^2/s .

R_a = spectral density of the accelerometer measurement noise in units of m^2/s^3 .

From practical experience with the accelerometers and tachometers that were constructed, the ratio of the measurement spectral densities is estimated as

$$\frac{R_t}{R_a} = \frac{0.05}{0.1} \text{ rad}^2 \text{s}^2 / \text{m}^2 \quad (\text{N.35})$$

The principal source of process noise in the plant is the vibrations of the unicycle

caused by the roughness of the terrain over which the wheel travels.

It is assumed that process noise enters the plant with the same input distribution matrix as the control torque, i.e. $G_n = G$. In the absence of the exact knowledge of the statistical nature of the process noise, it is assumed that the spectral density of Q is much larger than the measurement noise spectral densities. A choice of $\frac{Q}{R_T}$, which places the estimator poles in the same s -plane region as the regulator poles is (see Section N.6.1).

$$\frac{Q}{R_T} = 20 \text{ N}^2 \text{m}^2 \text{s}^2 \quad (\text{N.36})$$

For the numerical simulations in the sections that follow, it will be necessary to approximate the continuous time purely random gauss-markov processes (with the spectral densities Q and R given) by discrete time gauss-markov sequences (with covariance matrices QD and RD). Chapter 11 of reference [Bryson 2] shows that a good approximation of the continuous random process would be a discrete gaussian random sequence with a correlation time T_c which is short compared to the characteristic time constants of the plant, and a covariance (QD) determined from:

$$Q(t) \cong 2 \cdot T_c \cdot QD \quad (\text{N.37})$$

likewise

$$R_t(t) \cong 2 \cdot T_c \cdot RD_t \quad (\text{N.38})$$

$$R_a(t) \cong 2 \cdot T_c \cdot RD_a \quad (\text{N.39})$$

The shortest characteristic time in the longitudinal system is about 0.125 sec (from the inverted pendulum poles at $s \cong \pm 8 \text{ rad/s}$). A noise correlation time of $T_c = 0.01 \text{ sec}$ is therefore assumed, and taken to be the same for all 3 noise sources.

Even though only the ratios of the various spectral densities are considered during an LQG estimator design, we need to estimate particular values for these quantities that can be used in time response simulations. From equation N.16 and the actual values of the coefficients of the states, we see that the accelerometer measurement

$$y_a \cong g\theta \quad (\text{N.40})$$

If we assume that the spectral densities of the random noises are reasonably uniform from 0 hz to the control bandwidth, we can approximate the noise covariance by the square of the standard deviation of the signal, eg.

$$RD_a \cong \sigma_a^2 \quad (\text{N.41})$$

Figure N.7 shows that the maximum pitch angle during a typical maneuver is 1 degree. The maximum acceleration is then (from equation N.40):

$$(y_a)_{\max} \cong 0.1 \text{ m/s}^2 \quad (\text{N.42})$$

Assume that $(\sigma_a)_{\max}$ is approximately 10% of $(y_a)_{\max}$, then

$$\sigma_a = 0.01 \text{ m/s}^2 \quad (\text{N.43})$$

$$RD_a = (.01)^2 = 1 \times 10^{-4} \text{ m}^2/\text{s}^4 \quad (\text{N.44})$$

From equations N.37 to N.39 the tachometer measurement noise covariance and standard deviation is

$$RD_t = 5 \times 10^{-5} \text{ rad}^2/\text{s}^2 \quad (\text{N.45})$$

$$\sigma_t = \sqrt{RD_t} = 7.07 \times 10^{-3} \text{ rad/s} \quad (\text{N.46})$$

and the process noise covariance and standard deviation is

$$QD = 1 \times 10^{-3} \text{ N}^2\text{m}^2 \quad (\text{N.47})$$

$$\sigma_p = \sqrt{QD} = 3.16 \times 10^{-2} \text{ Nm} \quad (\text{N.48})$$

The computer language CTRL-C has a function that generates a random number with normal distribution (0 mean and standard deviation of 1.0) every time it is

called. Simulation of the noise signals will therefore be performed by using a time step equal to the 0.01 sec correlation time and then scaling the random number with the square root of the appropriate covariance.

N.6 Optimal continuous time estimator design

A linear quadratic estimator can be designed to estimate all the states of the longitudinal system from the accelerometer and tachometer measurements, provided that we have some knowledge of the degree of uncertainty in the measurements and of the degree of intensity of the random disturbances on the plant. The plant model is modified to include the random disturbance effects on the plant and measurements:

$$\begin{aligned}\dot{x} &= Fx + Gu + G_n w \\ y_m &= Mx + v\end{aligned}\tag{N.49}$$

where:

x is the state vector

w is a random disturbance vector

y_m is a vector of the measured quantities

v is a random measurement noise vector.

Assume that $w(t)$ and $v(t)$ are independent white noise processes with spectral density matrices Q and R , respectively. A Kalman-Bucy filter, [Kalman] with filter gains L , can then be designed for the optimal estimate of the state vector, \hat{x} , given by

$$\dot{\hat{x}} = F_0 \hat{x} + G_0 u + L(y_m - M\hat{x})\tag{N.50}$$

Ideally the plant model used in the estimator would have the same parameters as the actual plant, i.e. $F_0 = F$ and $G_0 = G$.

The complete statistical nature of the random plant disturbance vector, w , and the process noise input matrix, G_n , is rarely known in practice. By the lack of any better approximations, the process noise input matrix is assumed to be the same as the control input matrix, i.e. $G_n = G$. w is then a scalar white noise process, whose spectral density, Q , will be selected upon inspection of the symmetric root locus of the estimator poles.

The spectral densities of the random noise in the tachometer and accelerometer measurements can be determined with frequency spectrum analysing instruments. If we assume that the spectral densities are reasonably uniform from 0 hz to the control bandwidth, we only need to concern ourselves with the ratio of the two measurement noise spectral densities during the estimator design.

The paper by Bryson and Hall in [Leonides] give the Euler-Lagrange equations for the optimal filter problem as:

$$\begin{bmatrix} \dot{x} \\ \dot{\lambda} \end{bmatrix} = \begin{bmatrix} F & -G_n Q G_n^T \\ -M^T R^{-1} M & -F^T \end{bmatrix} \begin{bmatrix} x \\ \lambda \end{bmatrix} + \begin{bmatrix} 0 \\ M^T R^{-1} \end{bmatrix} y_m \quad (\text{N.51})$$

$$w = -Q G_n^T \lambda \quad (\text{N.52})$$

If we take the Laplace transform of the above three equations, and eliminate $x(s)$ and $\lambda(s)$ we obtain the symmetric rootlocus characteristic equation (SRCE)

$$\left| I + Q Z^T(-s) R^{-1} Z(s) \right| = 0 \quad (\text{N.53})$$

where:

$$Z(s) = \frac{y_m(s)}{w(s)} = \begin{bmatrix} Z_t(s) \\ Z_a(s) \end{bmatrix} = M(sI - F)^{-1} G_n \quad (\text{N.54})$$

254 APPENDIX N. CONTINUOUS TIME LONGITUDINAL CONTROL SYSTEM

and $Z_t(s)$ and $Z_a(s)$ are the transfer functions from the process noise input to tachometer and accelerometer measurements respectively.

If the two measurement noise processes are uncorrelated, equation N.53 can be rewritten as

$$1 + Q \left[\frac{Z_t(-s)Z_t(s)}{R_t} + \frac{Z_a(-s)Z_a(s)}{R_a} \right] = 0 \quad (\text{N.55})$$

If we let $Z_t(s) = \frac{N_t(s)}{D(s)}$ we can rewrite N.55 as

$$-\frac{R_t}{Q} = \frac{N_t(-s)N_t(s) + \frac{R_t}{R_a}N_a(-s)N_a(s)}{D(-s)D(s)} \quad (\text{N.56})$$

The zeros of the symmetric root locus equation above are a function of the ratio of the measurement noise spectral densities. They are called the compromise zeros because they are located somewhere between the zeros of $Z_t(s)$ and $Z_a(s)$. The form of the locus of the compromise zeros as a function of $\frac{R_t(s)}{R_a(s)}$ is shown in Figure N.9.

The CTRL-C program 'lgtlqest' is used to calculate the compromise zeros and estimator poles as functions of R_t , R_a and Q . The results of this program are listed in the next section.

The process noise spectral density (Q_{LGT} in the print-out) was then chosen so that the low frequency estimator poles were in the same range as the low frequency regulator poles.

The Kalman filter gain matrix, L , of equation N.50 is indicated under ESTGAINS in the print-out.

The matrix equations that constitute the complete longitudinal system with a full

order estimator and feedback of the integral error and estimated states can be summarized as:

$$\dot{\hat{x}} = F\hat{x} + Gu + G_n w \quad (\text{N.57})$$

$$y_m = M\hat{x} + v \quad (\text{N.58})$$

$$\dot{e} = H\hat{x} - r \quad (\text{N.59})$$

$$\dot{e} = -C_e e - C\hat{x} \quad (\text{N.60})$$

$$\dot{\hat{x}} = F_0\hat{x} + G_0u + L(y_m - M\hat{x}) \quad (\text{N.61})$$

The interconnection of all these equations is shown in the longitudinal system blockdiagram of Figure N.5. These equations can be represented in matrix form for analysis and simulation purposes:

$$\begin{bmatrix} \dot{\hat{x}} \\ \dot{e} \\ \dot{\hat{x}} \end{bmatrix} = \begin{bmatrix} F & -GC_e & -GC \\ 0 & 0 & H \\ LM & -G_0C_e & F_0 - G_0C - LM \end{bmatrix} \begin{bmatrix} \hat{x} \\ e \\ \hat{x} \end{bmatrix} + \begin{bmatrix} 0 \\ -1 \\ 0 \end{bmatrix} r + \begin{bmatrix} G_n & 0 \\ 0 & 0 \\ 0 & L \end{bmatrix} \begin{bmatrix} w \\ v \end{bmatrix} \quad (\text{N.62})$$

The eigenvalues of the system matrix above are the same as the eigenvalues of the regulator and the estimator if $F_0 = F$, and $G_0 = G$. If the initial estimate of the state vector is the same as the initial state vector, the step response of this system will be the same as the response for the full state feedback system of Figure N.7. An example of the response when $\theta(0) = 0.1$ rad, but the initial estimate $\hat{\theta}(0) = 0$ rad is shown in Figure N.10. It can be seen that large excursions of the plant states occur initially because the control commands are issued based on the wrong estimates of the plant states. As the LQG estimator improves its estimates of the plant states, the wheel speed approaches the commanded value of $\Omega_c = 0$ and the frame is held vertical ($\theta(0) = 0$ rad).

The performance of the closed loop system in the presence of measurement and process noise was evaluated. The plot of Figure N.11 is generated with the initial

256 APPENDIX N. CONTINUOUS TIME LONGITUDINAL CONTROL SYSTEM

state estimate the same as the initial plant state and noise inputs as described in section N.5.

N.6.1 LQE gain calculation program

UCTCS/LGTLOG.CTR

ANALOG LONGITUDINAL CONTROL SYSTEM WITH FULL ORDER LQ ESTIMATOR

.....

LONGITUDINAL STATES : THETA.DOT; OMEGA; THETA

CONTROL INPUT : WHEEL MOTOR TORQUE (QV)

MEASUREMENTS : TACHOMETER; ACCELEROMETER

UNITS : METERS, RADIANS, SECONDS

***** CONTINUOUS TIME PLANT MATRICES *****

PLGT -

-0.0333 0.0333 54.5447

0.113C -0.1138 -151.2607

1.0000 0. 0.

GLGT -

-0.7075

2.4216

0.

GNOISELGT -

-0.7075

N.6. OPTIMAL CONTINUOUS TIME ESTIMATOR DESIGN

257

2.4216

0.

HLGT -

-1.0000	1.0000	0.
-0.0011	0.0011	4.6700

HLGT -

0.

-0.0230

***** MATRICES FOR INTEGRAL ERROR FEEDBACK CONTROL *****

EXTENDED STATE VECTOR IS : OMEGA.ERR; THETA.DOT; OMEGA; THETA

FINT -

0.	0.	1.0000	0.
0.	-0.0333	0.0333	54.5447
0.	0.1138	-0.1138	-151.2607
0.	1.0000	0.	0.

GINT -

0.

-0.7075

2.4216

0.

***** REGULATOR DESIGN *****

COST FUNCTION WEIGHTING FACTORS ON STATES AND CONTROL :

ADJAG -

258 APPENDIX N. CONTINUOUS TIME LONGITUDINAL CONTROL SYSTEM

30.0 0. 0. 0.

BDIAG -

1.0

OPTIMAL INTEGRAL ERROR AND STATE FEEDBACK GAINS :

CERR -

-5.4772

CLGT -

-47.6924 -6.8830 -228.2964

REGPOLES -

-1.2208 - 1.0005i

-1.2208 + 1.0005i

-7.3891 + 0.7295i

-7.3891 - 0.7295i

***** ESTIMATOR DESIGN *****

PROCESS AND MEASUREMENT NOISE SPECTRAL DENSITIES :

QLGT -

1.0

RLGT -

0.0500 0.

0. 0.1000

1PER FM. ZEROS FROM PROCESS NOISE INPUT TO TACHOMETER & ACCELEROMETER OUTPUTS :

N.6. OPTIMAL CONTINUOUS TIME ESTIMATOR DESIGN

259

TACZEROS -

2.8309

-2.8309

ACCZEROS -

-0.0000 + 9.4457i

-0.0000 - 9.4457i

0.0000 + 0. i

PLANTPOLES -

-7.4486

7.3232

-0.0216

COMPROMIZE ZEROS FOR SYMMERIC ROOTLOCUS OF ESTIMATOR :

CONPRZEROS -

192.0571

-192.0571

3.0991

2.5927

-3.0991

-2.5927

OPTIMAL ESTIMATOR GAINS AND ESTIMATOR POLES :

ESTGAINS -

-6.3092 0.6621

15.7493 -1.0452

-0.7363 0.1181

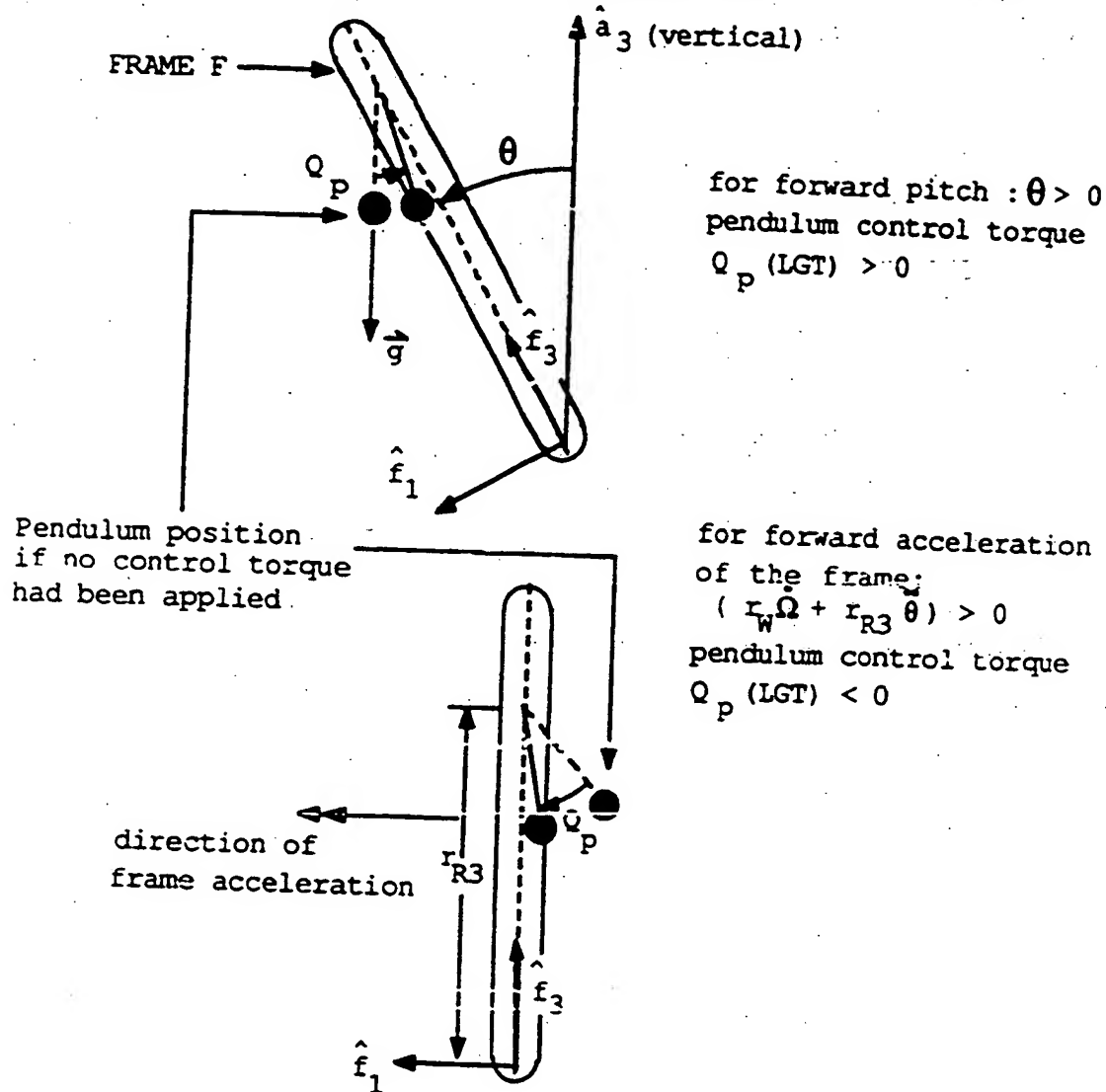
260 APPENDIX N. CONTINUOUS TIME LONGITUDINAL CONTROL SYSTEM

ESTPOLES -

-1.5374 - 0.0000i

-1.4218 + 0.0000i

-16.8260 - 0.0000i



The output signal from the servo accelerometer is proportional to the total pendulum control torque: $Q_p \text{ (LGT)} = k_a [g\theta - (r_w \dot{\Omega} + r_{R3} \ddot{\theta})]$

Figure N.1: Longitudinal Accelerometer Measurement

262 APPENDIX N. CONTINUOUS TIME LONGITUDINAL CONTROL SYSTEM

LONGITUDINAL PLANT OPENLOOP FREQUENCY RESPONSE

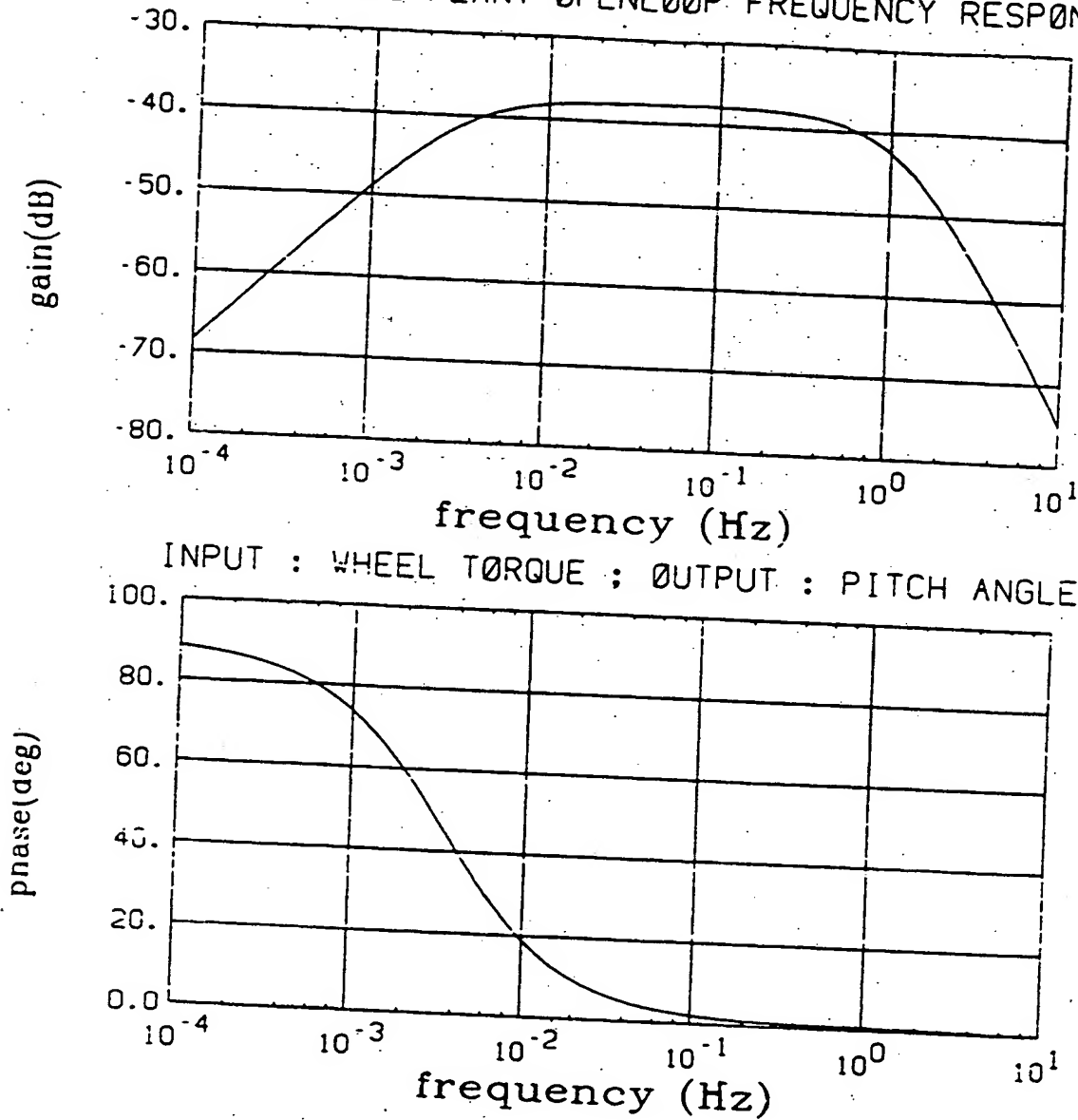


Figure N.2: Openloop Frequency Response of $\frac{\theta(s)}{Q_w(s)}$

INPUT FREQUENCY = 0.2 HERTZ

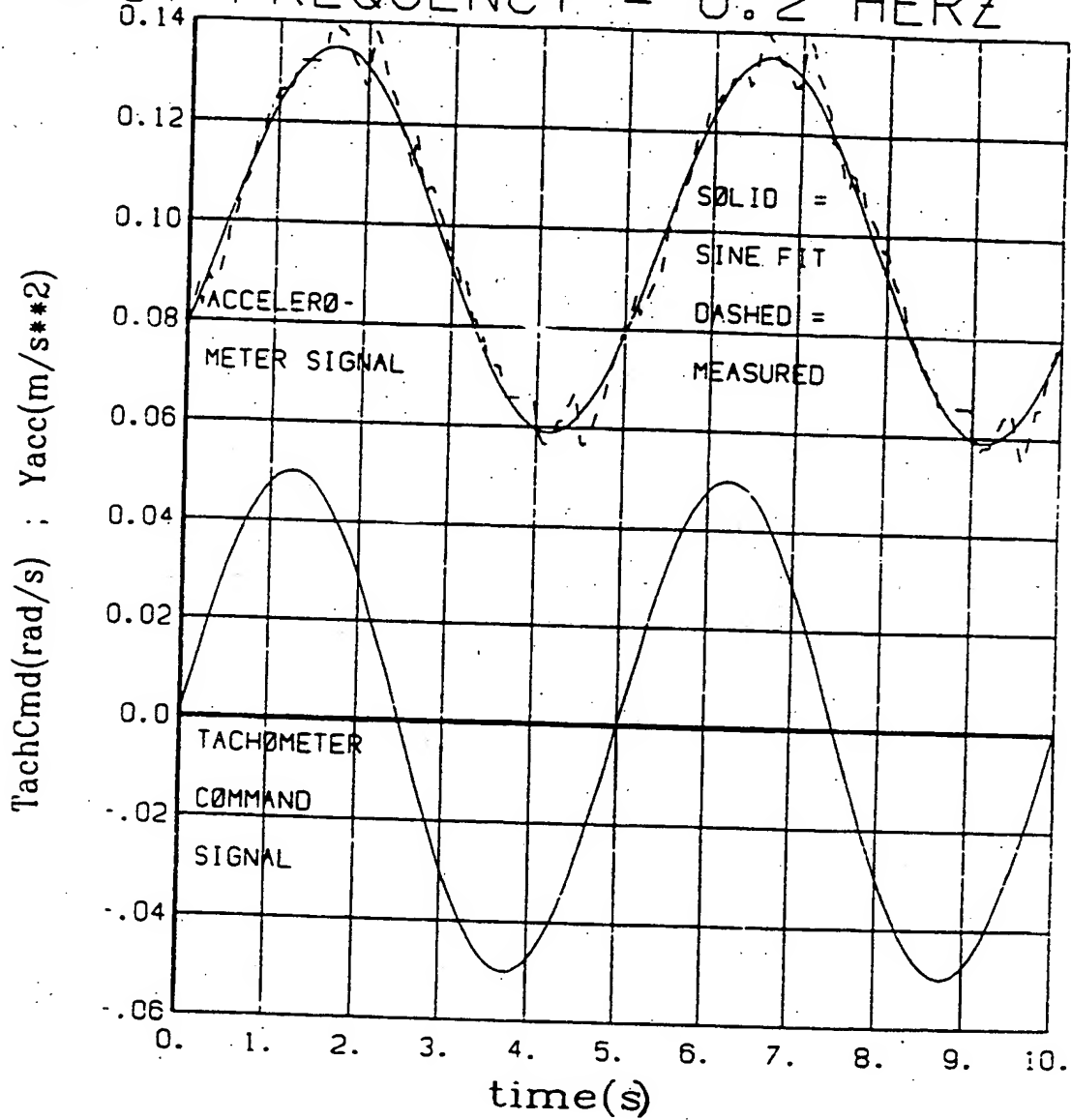
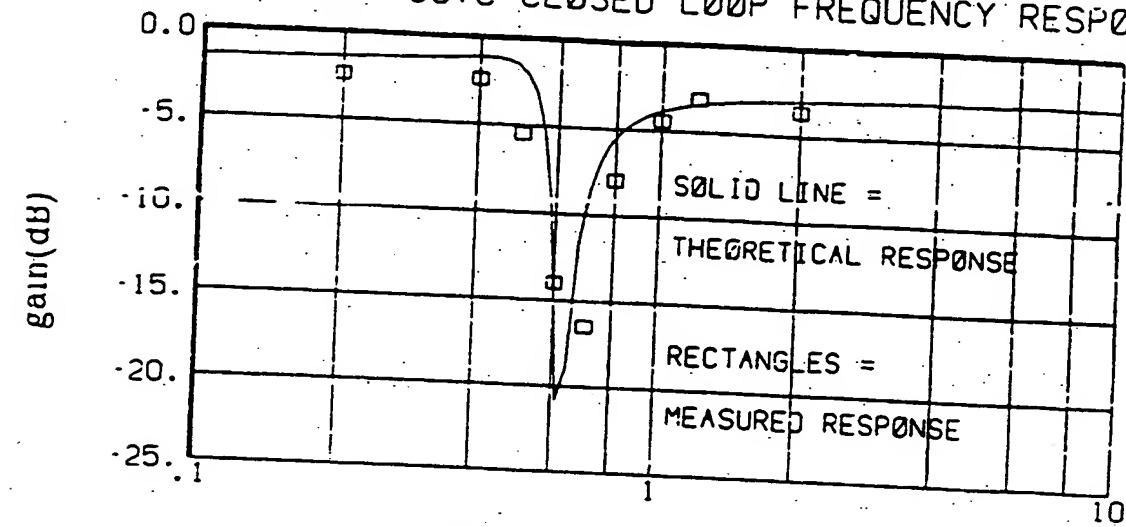


Figure N.3: Typical Time Response During a Transfer Function Identification Test

264 APPENDIX N. CONTINUOUS TIME LONGITUDINAL CONTROL SYSTEM

UPSIDE DOWN UCYC CLOSED LOOP FREQUENCY RESPONSE



frequency (Hz)

INPUT : TACH CMD ; OUTPUT : YACCEL

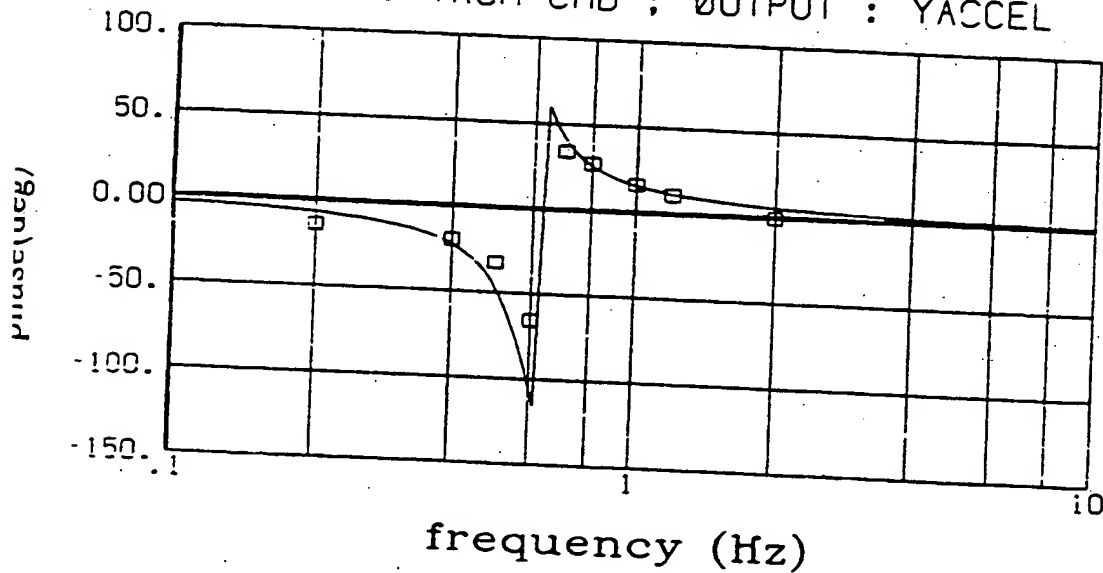


Figure N.4: Theoretical and Measured Frequency Responses for the Upside Down Uni-cycle

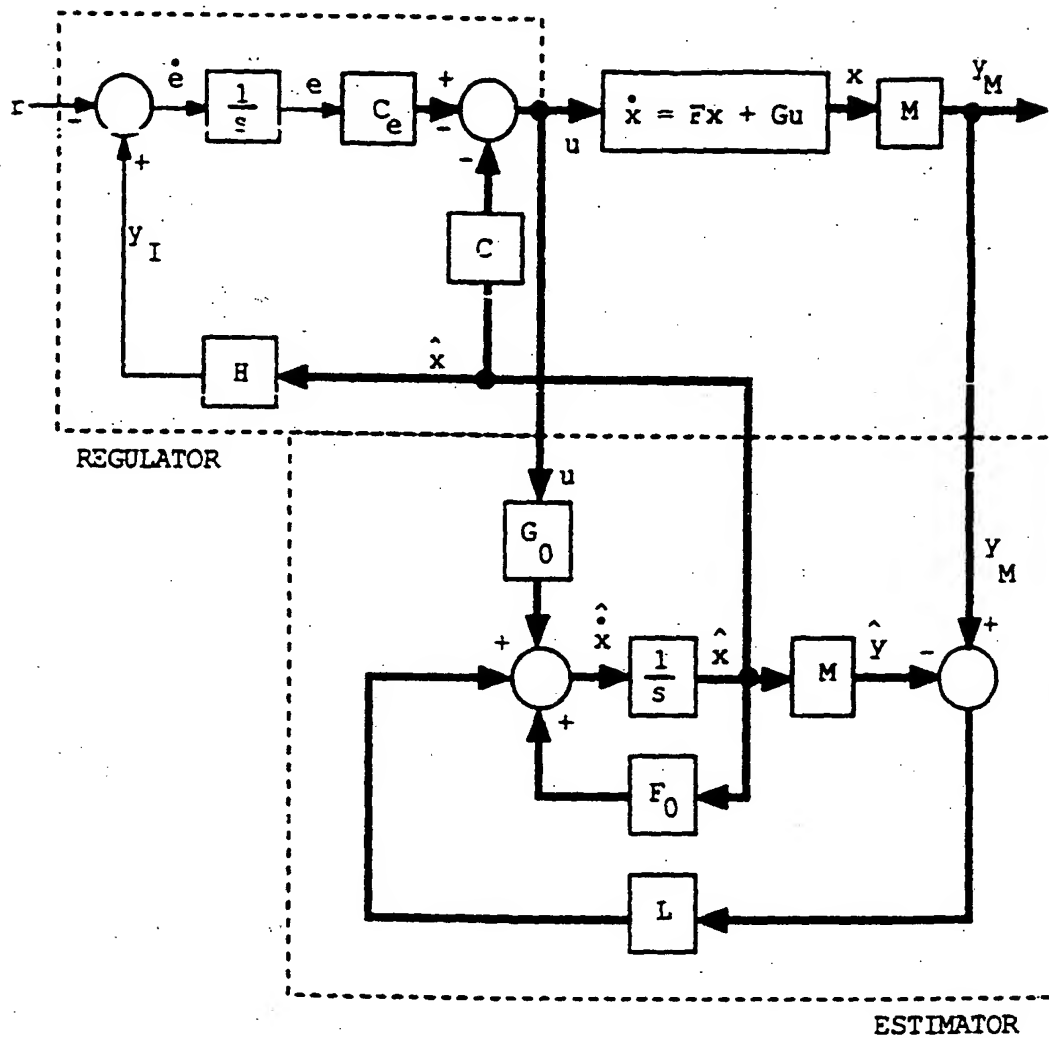


Figure N.5: General Feedback Control System Blockdiagram

SYMMETRIC ROOT LOCUS OF LONGIT. SYSTEM

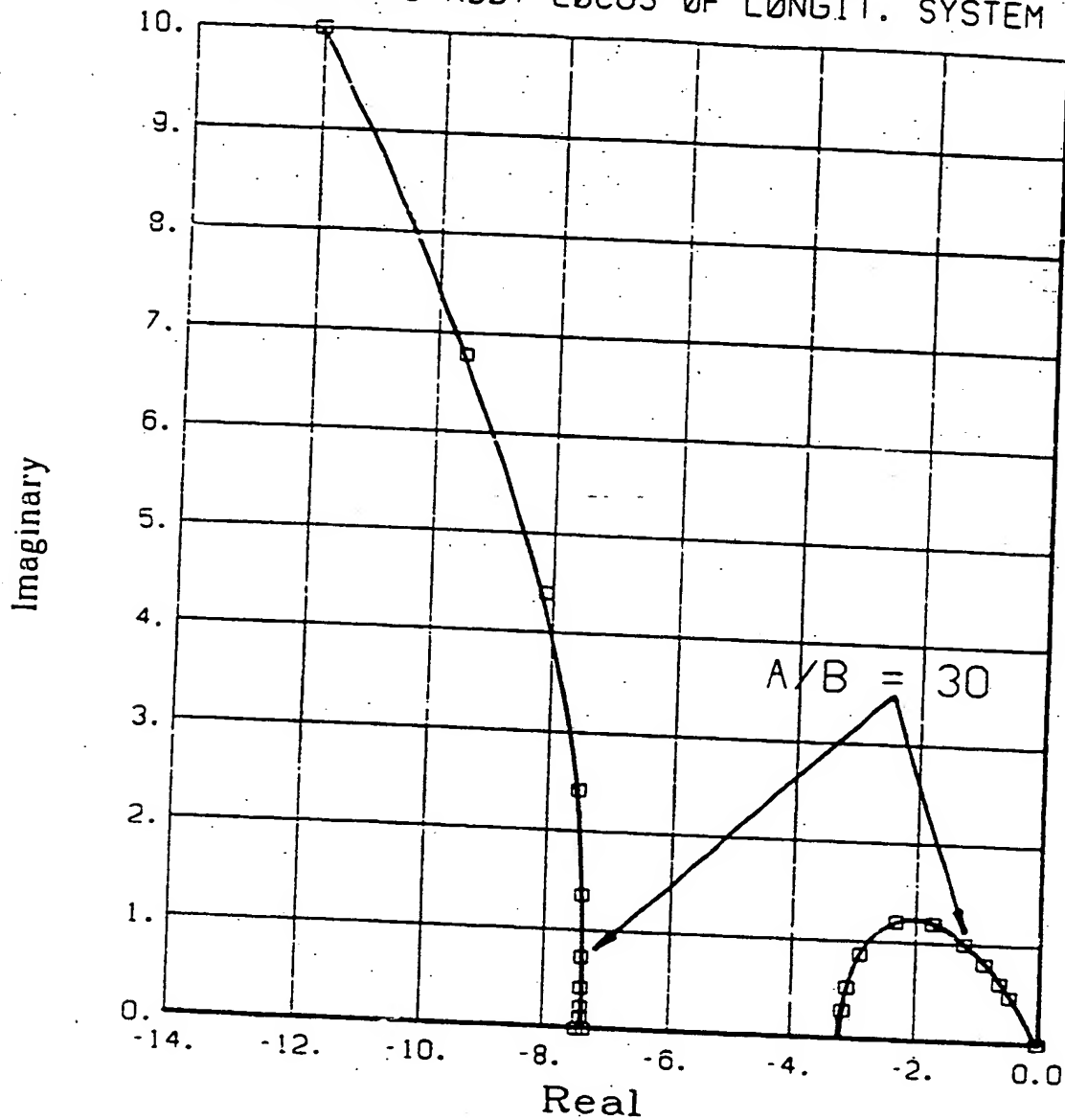


Figure N.5: Symmetric Rootlocus of the Longitudinal Closed Loop System for values of $\frac{A}{B}$ ranging from 0 to 10 000

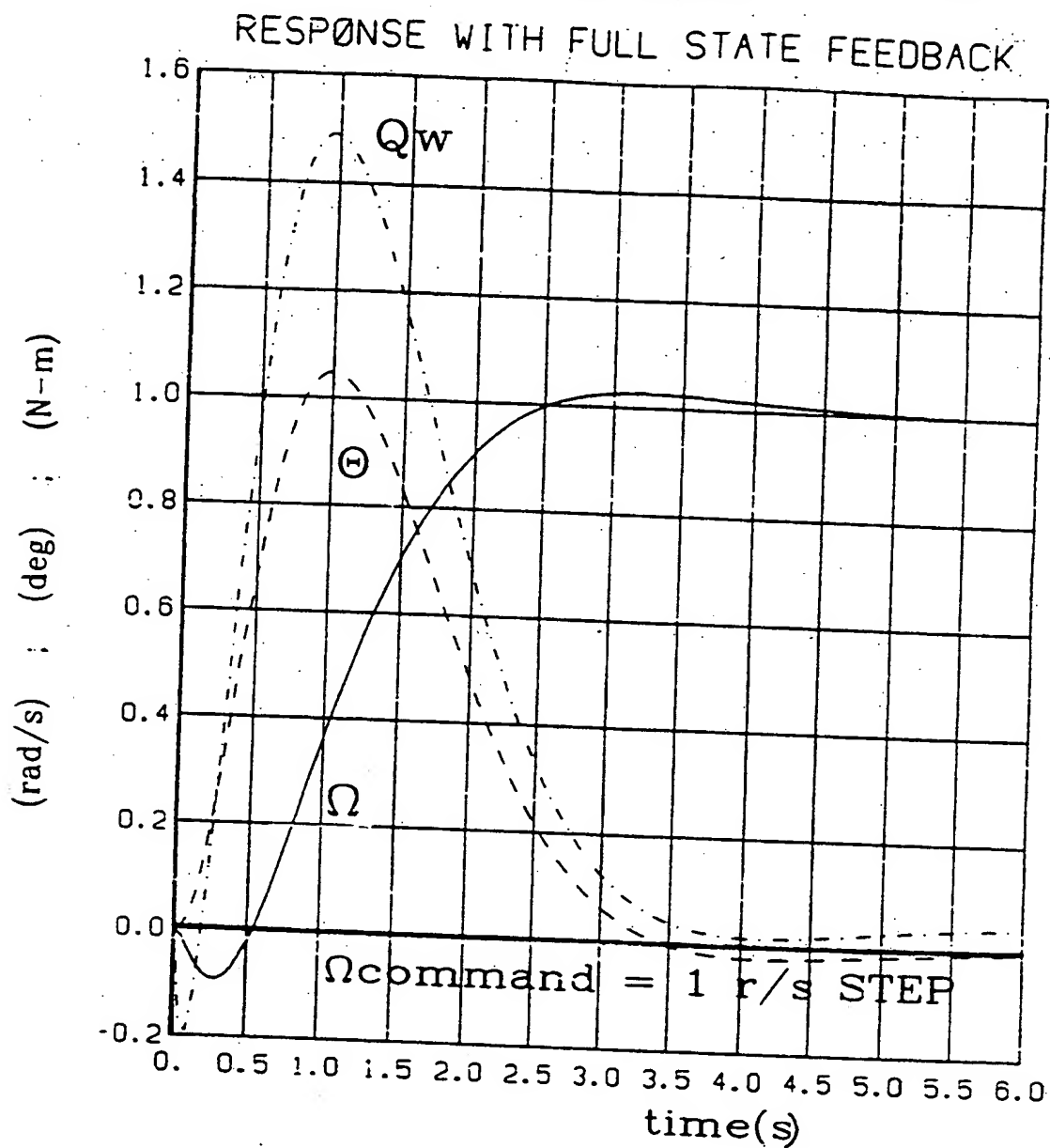


Figure N.7: Step Response of the Longitudinal Closed Loop System with Full State Feedback

268 APPENDIX N. CONTINUOUS TIME LONGITUDINAL CONTROL SYSTEM

FREQ. RESPONSE WITH FULL STATE FEEDBACK

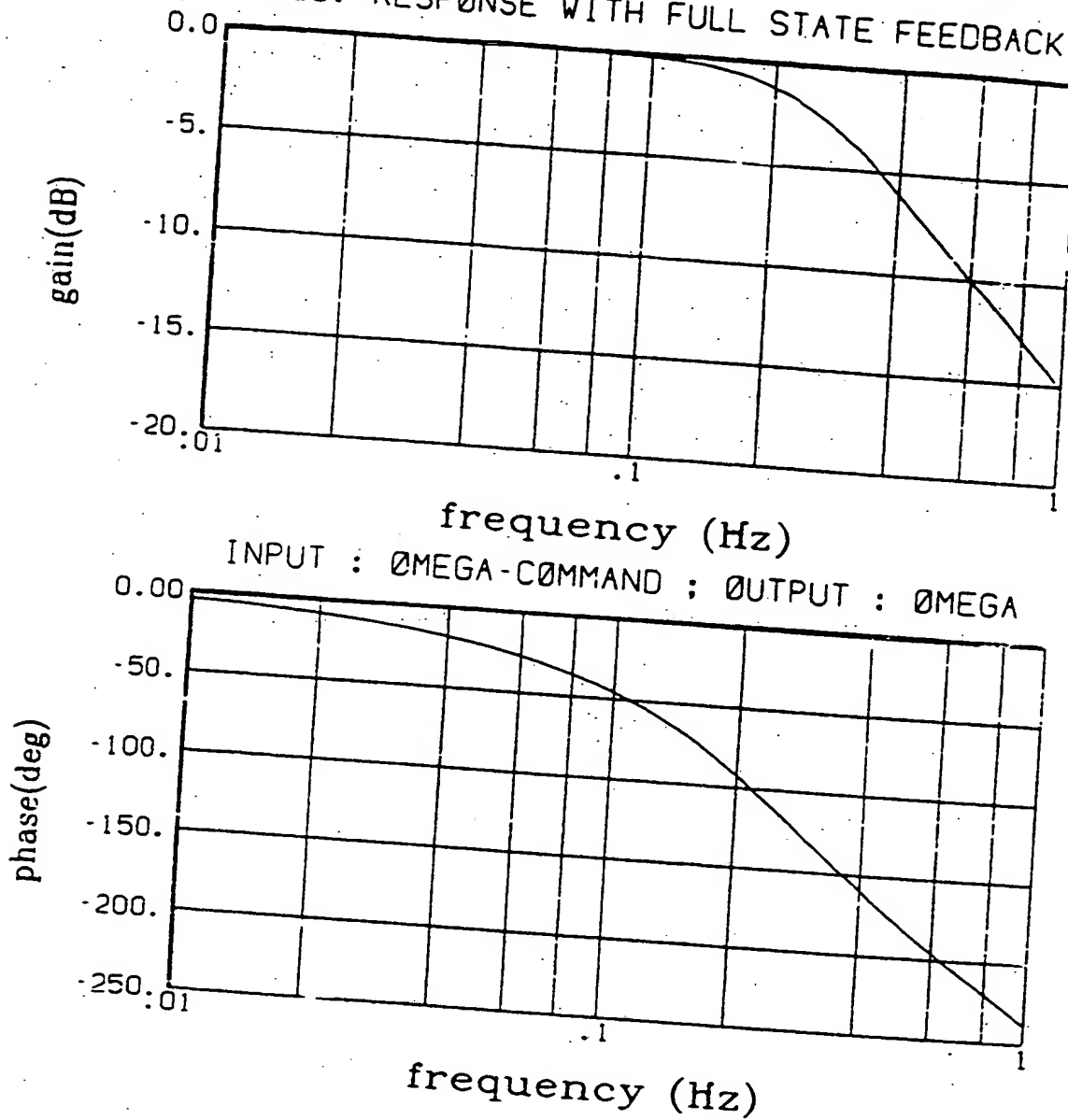


Figure N.8: Frequency Response of the Longitudinal Closed Loop System with Full State Feedback

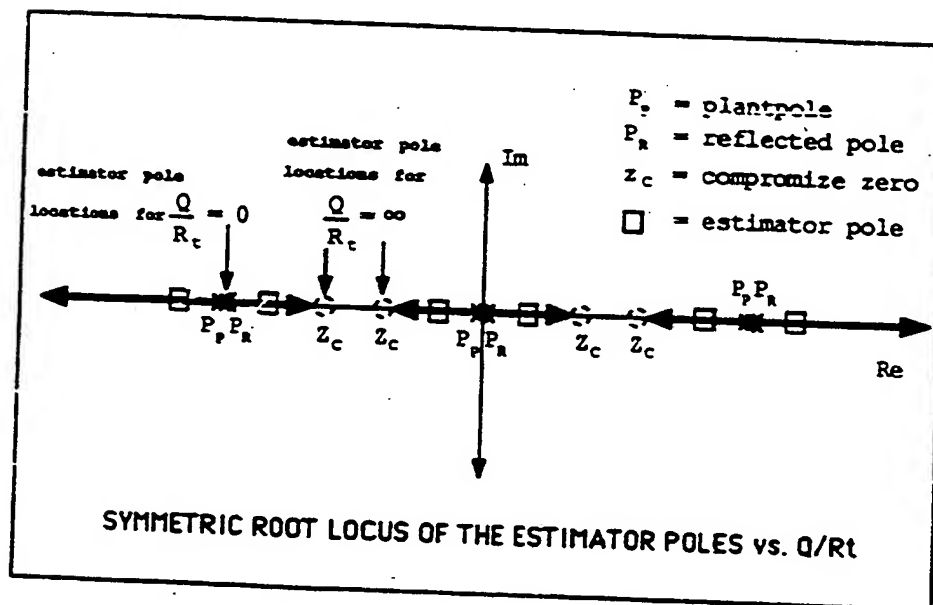
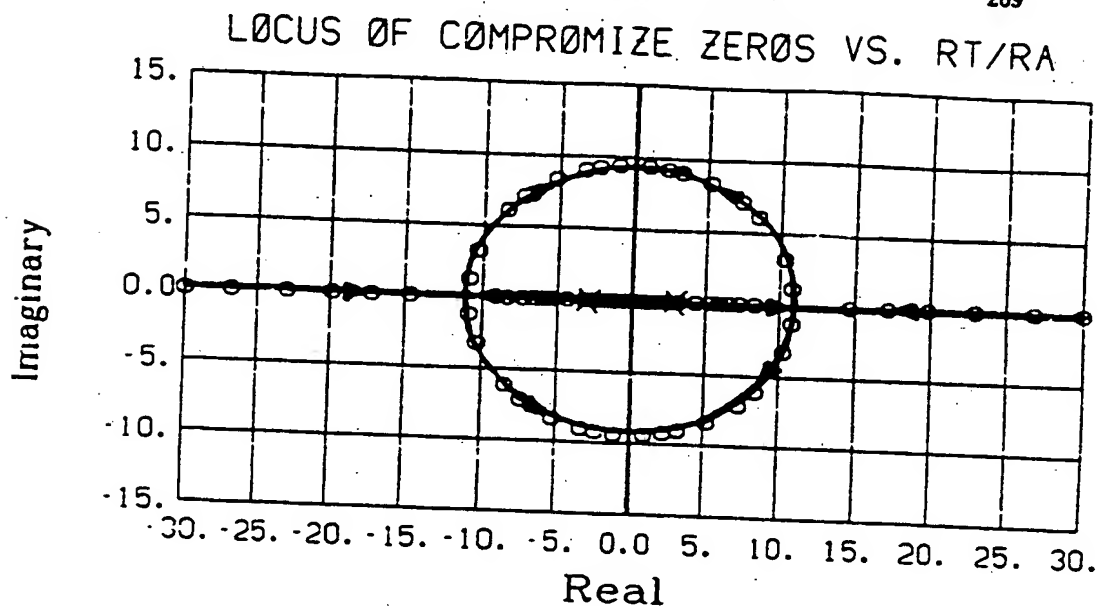


Figure N.9: Symmetric Root Loci of the Compromise Zeros and Estimator Poles

RESPONSE WITH FULL ORDER ESTIMATOR

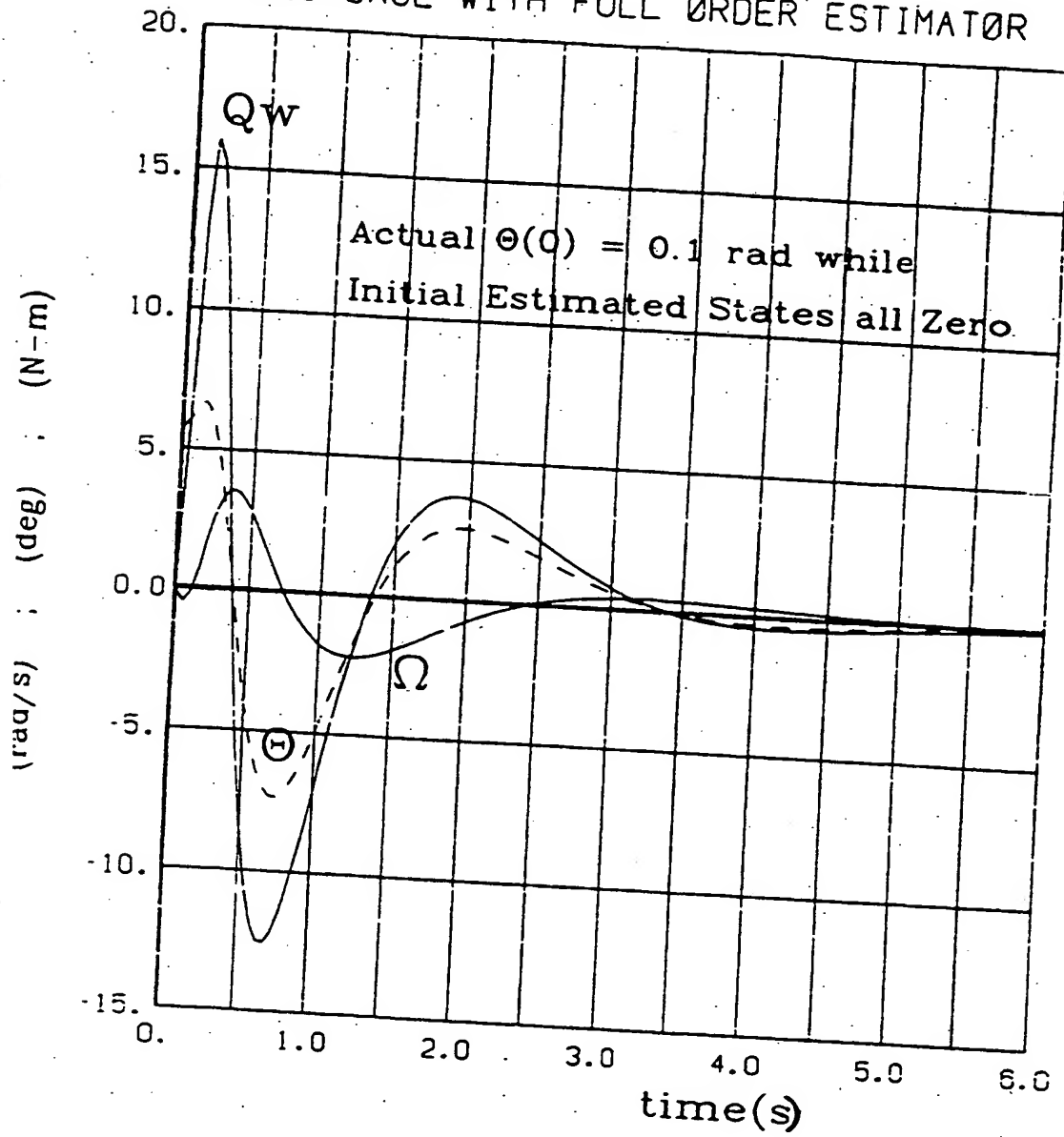


Figure N.10: Response of the Longitudinal System with a Full Order Estimator with $\theta(0) = 0.1$ rad

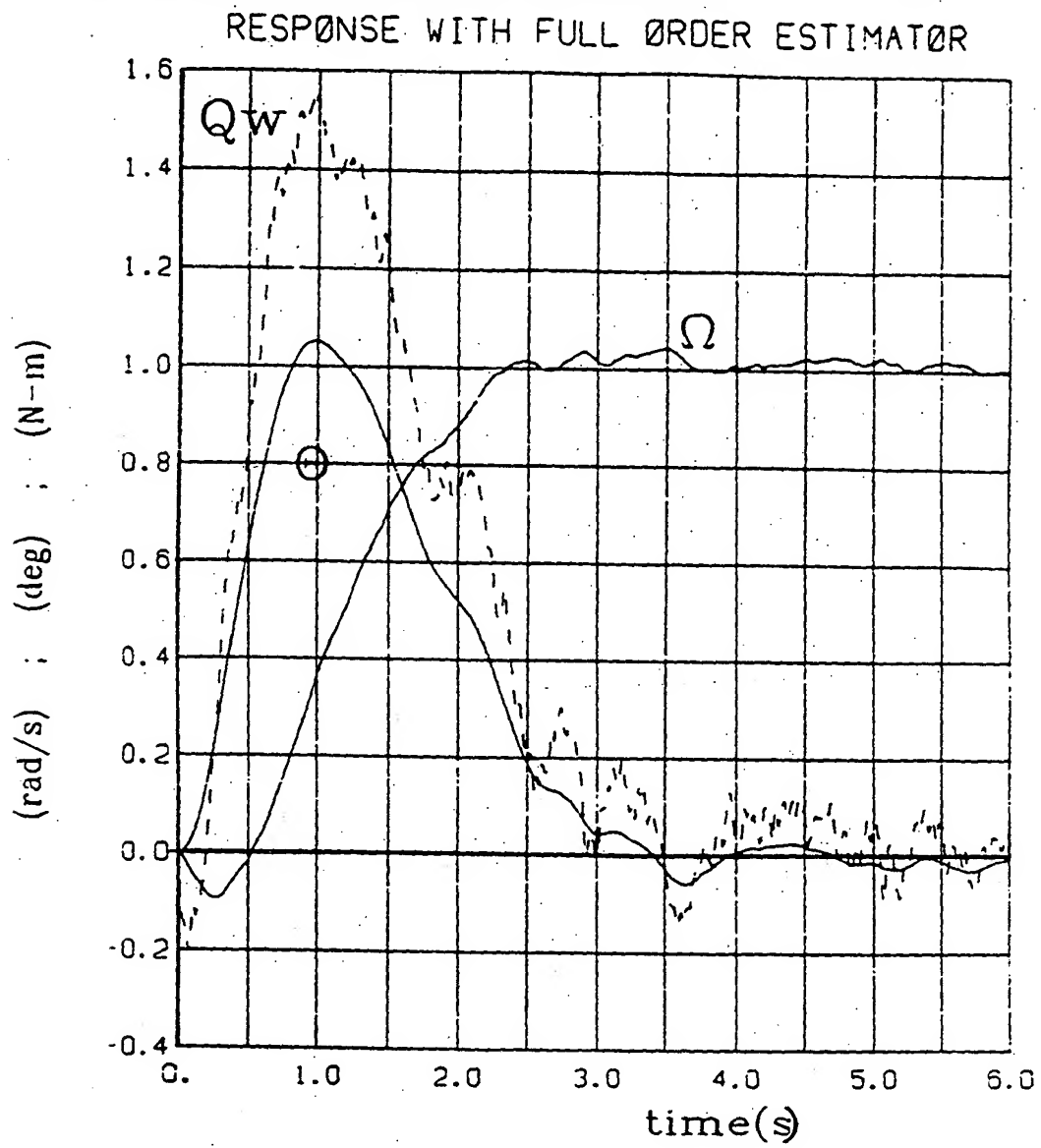


Figure N.11: Step Response of the Closed Loop System with a Full Order Estimator and Measurements Corrupted by Noise

Appendix O

Discrete Time Longitudinal Control System

O.1 Sampling rate selection

The continuous time compensator designed in the previous section must be discretized for implementation as a digital control system in the on-board computer of the unicycle. The selection of the best sample rate for the digital computer is a compromise among many factors. First of all, the sample period must be long enough to allow all the control calculations for the longitudinal and lateral control systems to be completed. The sampling theorem states that in order to reconstruct an unknown band-limited continuous signal from samples of that signal, the sample rate f_s must be at least twice as high as the highest frequency contained in the unknown signal. We can consider the input signal to a digital controller to have a spectral content up to the system's closed loop bandwidth, f_c . The longitudinal closed loop system has a bandwidth of less than 0.5 Hz, so that the fundamental lower bound on the sampling frequency should be approximately 1 Hz. In order to have acceptable tracking effectiveness of the reference input command, good regulation during random disturbance inputs and rejection of errors due to measurement noise, it is customary to use sampling rates of at least an

order of magnitude greater than this value. (Refer to chapter 10 in [Franklin]). Experiments with the microprocessor mounted on the unicycle have shown that all the control system calculations can be done in less than 25 milliseconds. A sampling frequency of 40 Hz is therefore chosen, i.e.

$$T_{\text{sample}} = 0.025 \text{ sec.} \quad (0.1)$$

We can associate a pure transportation delay of approximately one half of a sample period with the sample and zero-order-hold (ZOH) device which converts the analog plant signals for input to the microprocessor.

$$G_{\text{ZOH}}(s) = e^{-\frac{sT}{2}}$$

where s is the Laplace operator.

The phase shift added to the openloop system due to the sampling process is calculated, because it can decrease the phase margin of stability significantly if the sample rate is too low. At the closed loop bandwidth (f_{BW}) of approximately 0.5 Hz, the phase lag due to the ZOH is

$$\begin{aligned} \phi_{\text{ZOH}} &= \frac{\omega_{BW} T_{\text{sample}}}{2} \\ &= \pi \frac{f_{BW}}{f_{\text{sample}}} = 2.25 \text{ degrees} \end{aligned}$$

This small phase lag should not have a serious effect on the system stability.

0.2 Equivalent discrete LQG compensator

0.2.1 Discrete time regulator

A discrete time regulator with integral error feedback of the wheel speed, Ω , can be designed by first discretizing the continuous time plant matrices of equation N.30, using the sample time T , defined in the previous section:

$$\begin{bmatrix} e(k+1) \\ x(k+1) \end{bmatrix} = \begin{bmatrix} 1 & H_e \\ 0 & \Phi \end{bmatrix} \begin{bmatrix} e(k) \\ x(k) \end{bmatrix} + \begin{bmatrix} \Gamma_e \\ \Gamma \end{bmatrix} u(k) + \begin{bmatrix} \Gamma_r \\ 0 \end{bmatrix} r(k) \quad (0.2)$$

where $x(k) = [\theta(k) \ \Omega(k) \ \theta(k)]^T$

and $r(k)$ is the reference input.

The measured outputs are

$$y_m(k) = Mx(k) + Nu(k) \quad (0.3)$$

Simplify equation 0.2 to:

$$x_I(k+1) = \Phi_I x_I(k) + \Gamma_I u(k) + \Gamma_{I,r} r(k) \quad (0.4)$$

where $x_I(k) = [e(k) \ \theta(k) \ \Omega(k) \ \theta(k)]^T$

The continuous time cost function of equation N.29 can also be converted to an equivalent digital performance index as described in Appendix D of reference [Bryson 1].

Given the continuous time performance index

$$J = \frac{1}{2} \int_0^\infty (x_I^T A x_I + u^T B u) dt \quad (0.5)$$

the CTRL-C program 'lgtdlq.ctr' uses the algorithm by Van Loan [Van Loan] to calculate the weighting matrices in the discrete time performance index below, which will produce the discrete closed loop system whose performance is the same as that of the original continuous time system.

$$J_D = \sum_{k=0}^{\infty} [x_I^T(k) \bar{u}^T(k)] \begin{bmatrix} AD & ND \\ ND^T & BD \end{bmatrix} \begin{bmatrix} x_I(k) \\ u(k) \end{bmatrix} \quad (0.6)$$

The QZ algorithm in CTRL-C does not currently support the cross terms ND in the cost function above, but if we transform the system in equation 0.4 to

$$x_I(k+1) = (\Phi_I - \Gamma_I B D^{-1} \cdot ND^T) x_I(k) + \Gamma_I \bar{u}(k) \quad (0.7)$$

$$\bar{u}(k) = u(k) + B D^{-1} \cdot ND^T x_I(k) = -\bar{C} x_I(k) \quad (0.8)$$

the cost function of equation 0.6 becomes

$$\bar{J}_D = \sum_{k=0}^{\infty} x_I^T(k) (AD - ND \cdot B D^{-1} \cdot ND^T) x_I(k) + \bar{u}^T(k) B D \bar{u}(k) \quad (0.9)$$

We can now use the standard QZ algorithm to solve for the regulator feedback gains \bar{C} of the system of equation 0.7 and modified cost function of equation 0.9. The desired feedback gain for the regulator $u(k) = -C_I x_I(k)$ is then from equation 0.8:

$$C_I = \bar{C} - BD^{-1}ND^T \quad (0.10)$$

A print-out of the results of this program is shown in section 0.2.3. The optimal feedback control law, with all states available, is:

$$u(k) = -C_e e(k) - C \begin{bmatrix} \dot{\theta}(k) \\ \Omega(k) \\ \theta(k) \end{bmatrix} \quad (0.11)$$

A pole mapping of the continuous time regulator poles of section N.6.1 by means of the z-transformation, $z = e^{sT}$, confirms the locations of the equivalent discrete time design's regulator poles as indicated in the print-out listed in section 0.2.3. The step response of the discrete plant shown in Figure 0.2 is also the same as the continuous system step response of Figure N.7.

0.2.2 Discrete time estimator

A discrete equivalent of the continuous time estimator of section N.6 is designed to estimate the plant states from the two sampled data measurements of the tachometer and accelerometer signals.

The spectral densities of the process and measurement noise inputs, Q and R of the continuous time system must be converted to covariance matrices QD and RD for the digital estimator. Appendix D of reference [Bryson 1] shows that QD can be found using duality of the regulator performance index design conversion.

The measurement noise input $v_d(t)$ to the discrete time estimator is a sample of the random white noise input $v(t)$ of equation N.49. For the discrete time system

we should rather model $v(t)$ as colored noise with a variance V and a correlation time T_c that is small compared to the shortest time constant of the plant. $v(t)$ could be generated by the first order system

$$T_c \dot{v}(t) + v(t) = n(t) \quad (O.12)$$

where $n(t)$ is a white noise process with spectral density

$$R = 2VT_c \quad (O.13)$$

If we discretize the shaping filter of equation O.12 with the sample period of T_s , we have

$$v_d(k+1) = e^{-\frac{T_s}{T_c}} v_d(k) + n_d(k) \quad (O.14)$$

and the variance of the purely random sequence $n_d(k)$ is

$$RD = V \left[1 - e^{-\frac{T_s}{T_c}} \right] \quad (O.15)$$

as derived in reference [Bryson 1].

If V is eliminated between equations O.13 and O.15,

$$RD = \frac{\left[1 - e^{-\frac{T_s}{T_c}} \right]}{2T_c} \cdot R \quad (O.16)$$

The elements of the RD matrix were therefore chosen proportional to the elements of the given spectral density matrix, R , as a function of the correlation time T_c and the sampling period T_s . The choice of values for T_c and T_s was motivated in sections N.5 and O.1 respectively.

A print-out of the discrete time matrices is given in the next section. It shows the optimal closed loop estimator eigenvalues and the Kalman filter gains, L , where

$$\hat{x}(k+1) = \Phi \hat{x}(k) + \Gamma u(k) \quad (O.17)$$

$$\hat{x}(k) = \hat{x}(k) + L[y_m(k) - M\hat{x}(k) - Nu(k)] \quad (O.18)$$

0.2. EQUIVALENT DISCRETE LQG COMPENSATOR

277

Equation 0.17 is known as the time update of the Kalman filter and equation 0.18 is called the measurement update. Substitution of 0.17 into 0.18 gives the prediction estimator equation

$$\bar{x}(k+1) = \Phi[I - LM]\bar{x}(k) + \Phi Ly_m(k) + [\Gamma - \Phi LN]u(k) \quad (0.19)$$

The optimal prediction estimator poles are therefore given by the eigenvalues of $\Phi[I - LM]$.

The integral error state which is shown as part of the plant system of equations 0.4 is actually part of the compensator.

Therefore let

$$e(k+1) = e(k) + H_e \bar{x}(k) + \Gamma_e u(k) + \Gamma_r r(k) \quad (0.20)$$

where

$$H_e = \Phi_I(1, 2:4) \quad (0.21)$$

$$\Gamma_e = \Gamma_I(1) \quad (0.22)$$

The regulator feedback law is

$$u(k) = -C_e e(k) - C \bar{x}(k) \quad (0.23)$$

Equations 0.19, 0.20 and 0.23 can now be combined to form the compensator system matrices

$$\begin{bmatrix} e(k+1) \\ \bar{x}(k+1) \end{bmatrix} = \begin{bmatrix} 1 - \Gamma_e C_e & H_e - \Gamma_e C \\ (\Phi LN - \Gamma)C_e & \Phi[I - LM] + [\Phi LN - \Gamma]C \end{bmatrix} \begin{bmatrix} e(k) \\ \bar{x}(k) \end{bmatrix} + \begin{bmatrix} 0 \\ \Phi L \end{bmatrix} y_m(k) + \begin{bmatrix} \Gamma_r \\ 0 \end{bmatrix} r(k) \quad (0.24)$$

$$u(k) = -[C_e \ C] \begin{bmatrix} e(k) \\ \bar{x}(k) \end{bmatrix} \quad (0.25)$$

A block diagram of the discrete time closed loop system is shown in Figure 0.1. The closed loop system matrices are obtained by using the plant equation $z(k+1)$

$= \Phi x(k) + \Gamma u(k)$ and eliminating $u(k)$ and $y_m(k)$ from this equation and the compensator equations:

$$\begin{bmatrix} x(k+1) \\ e(k+1) \\ \tilde{x}(k+1) \end{bmatrix} = \begin{bmatrix} \Phi & -\Gamma C_e & -\Gamma C \\ 0 & 1 - \Gamma_e C_e & H_e - \Gamma_e C \\ \Phi LM & -\Gamma C_e & \Phi[I - LM] - \Gamma C \end{bmatrix} \begin{bmatrix} x(k) \\ e(k) \\ \tilde{x}(k) \end{bmatrix} + \begin{bmatrix} 0 \\ \Gamma_r \\ 0 \end{bmatrix} r(k) \quad (O.26)$$

If the initial estimate of the state vector is the same as the initial plant state vector, the step response of this system will be the same as the response for the full state feedback system of Figure O.2. An example of the response when $\theta(0) = 0.1$ rad, but the initial estimate $\hat{\theta}(1) = 0$ rad is shown in Figure O.3. It can be seen that large excursions of the plant states occur initially because the control commands are issued based on the wrong estimates of the plant states. As the LQG estimator improves its estimates of the plant states, the wheel speed approaches the commanded value of $\Omega_c = 0$ and the frame is held vertical ($\theta = 0$ rad).

O.2.3 Optimal regulator and estimator gains

DISCRETE LONGITUDINAL LQG DESIGN

LONGITUDINAL STATES : THETA.DOT; OMEGA; THETA

CONTROL INPUT : WHEEL MOTOR TORQUE (QV)

MEASUREMENTS : TACHOMETER, ACCELEROMETER

0.2. EQUIVALENT DISCRETE LQG COMPENSATOR

279

UNITS : METERS, RADIANS, SECONDS

***** CONTINUOUS TIME SYSTEM MATRICES *****

FLGT -

-0.0333 0.0333 54.5447

0.1138 -0.1138 -151.2607

1.0000 0. 0.

GLGT -

-0.7075

2.4216

0.

GNOISE -

-0.7075

2.4216

0.

HLGT -

-1.0000 1.0000 0.

-0.0011 0.0011 4.6700

HLGT -

0.

-0.0230

***** CONTINUOUS TIME SYSTEM MATRICES WITH INTEGRAL ERROR FB *****

EXTENDED STATE VECTOR IS : OMEGA.ERR; THETA.DOT; OMEGA; THETA

280 APPENDIX O. DISCRETE TIME LONGITUDINAL CONTROL SYSTEM

FINT -

0.	0.	1.0000	0.
0.	-0.0333	0.0333	54.5447
0.	0.1138	-0.1138	-151.2607
0.	1.0000	0.	0.

GINT -

0.
-0.7075
2.4216
0.

GREFINT -

-1.0
0.
0.
0.

• WEIGHTING FACTORS FOR OPTIMAL CONTINUOUS TIME REGULATOR •

ADTAG -

30.0 0. 0. 0.

BDTAG -

1.0

• PROCESS AND MEAS. SPECTRAL DENSITIES FOR CONTINUOUS SYSTEM •

QLGT -

1.0

0.2. EQUIVALENT DISCRETE LQG COMPENSATOR

281

RLGT -

0.0500 0.
0. 0.1000

***** DISCRETE TIME SYSTEM MATRICES *****

TSAMPLE -

0.0250

PHI -

1.0162 0.0008 1.3692
-0.0445 0.9971 -3.7957
0.0251 0.0000 1.0171

GAMMA -

-0.0178
0.0607
-0.0002

• DISCRETE TIME SYSTEM MATRICES WITH INTEGRAL ERROR FEEDBACK •

PHINT -

1.0000 -0.0004 0.0250 -0.0473
0. 1.0162 0.0008 1.3692
0. -0.0445 0.9971 -3.7957
0. 0.0251 0.0000 1.0171

GAININT -

0.0008
-0.0178
0.0607

282 APPENDIX O. DISCRETE TIME LONGITUDINAL CONTROL SYSTEM

-0.0002

GAREFINT -

-0.0250

0.

0.

0.

• DISCRETE OPTIMAL REGULATOR COST FUNCTION WEIGHTING MATRICES •

AD -

0.7500	-0.0001	0.0094	-0.0118
-0.0001	0.0000	-0.0000	0.0000
0.0094	-0.0000	0.0002	-0.0002
-0.0118	0.0000	-0.0002	0.0003

BD -

1.04-03 •

0.1893

-0.0000

0.0035

-0.0054

BD -

0.0250

• DISCRETE REGULATOR FEEDBACK GAINS FOR ERROR AND STATES •

CERR -

-4.4247

0.2. EQUIVALENT DISCRETE LQG COMPENSATOR

283

CLGT

-41.0670 -5.6284 -201.8878

• DISCRETE REGULATOR POLES •

REGPOLES

0.8312 + 0.01521i

0.8312 - 0.01521i

0.9696 + 0.02431i

0.9696 - 0.02431i

• DISCRETE SYSTEM PARAMETERS AND NOISE COVARIANCE MATRICES •

QD

0.0126 -0.0431 0.0002

-0.0431 0.1474 -0.0005

0.0002 -0.0005 0.0000

RD

2.5000 0.

0. 5.0000

• CURRENT ESTIMATOR GAIN MATRIX •

LLGT

-0.1155 0.0126

0.2900 -0.0193

-0.0138 0.0023

• PREDICTION ESTIMATOR GAIN MATRIX : LPRED=PHI•LLGT •

LPRED

APPENDIX O. DISCRETE TIME LONGITUDINAL CONTROL SYSTEM

-0.1360 0.0160

0.3465 -0.0286

-0.0169 0.0027

• PREDICTION ESTIMATOR POLES •

ESTPOLES -

0.6780 + 0.0000i

0.8922 - 0.0000i

0.9654 + 0.0000i

• CLOSED LOOP SYSTEM POLES •

SYSPOLES -

0.6780 - 0.0000i

0.8312 + 0.0152i

0.8312 - 0.0152i

0.8922 + 0.0000i

0.9654 - 0.0000i

0.9696 - 0.0243i

0.9696 + 0.0243i

***** COMPENSATOR MATRICES *****

ACOMP -

1.0034 0.0308 0.0292 0.1056

-0.0769 0.1663 0.0389 -2.2157

0.2657 2.7681 0.9887 8.4615

-0.0007 0.0017 0.0160 0.9723

BCOMP -

0.2. EQUIVALENT DISCRETE LQG COMPENSATOR

285

0.	0.	-0.0250
-0.1360	0.0160	0.
0.3465	-0.0286	0.
-0.0169	0.0027	0.

CCOMP

4.4247	41.0670	5.6284	201.8878
--------	---------	--------	----------

DCOMP

0.	0.	0.
----	----	----

MODAL FORM OF COMPENSATOR :

COMPENSATOR INPUTS : [YIACH(K) YACC(K) REF(K)]

COMPENSATOR OUTPUT : QU(K) = WHEEL TORQUE

AMODAL

-0.0564	-0.0000	0.0000	0.0000
0.0000	0.9314	0.0000	0.0000
0.0000	0.0000	1.0011	0.
0.0000	-0.0000	0.0000	1.2545

BMODAL

4.6483	-0.5677	0.6521
0.0806	-0.0061	-0.0008
0.2574	-0.0476	-0.2435
-1.2481	0.2868	-0.0448

CMODAL

-1.1031	-2.1475	-0.0305	1.3899
---------	---------	---------	--------

APPENDIX O. DISCRETE TIME LONGITUDINAL CONTROL SYSTEM

DPRDAL -

0. 0. 0.

SYSPOLESN -

 $0.6780 + 0. i$ $0.8312 + 0.0152i$ $0.8312 - 0.0152i$ $0.8922 - 0.0000i$ $0.9654 + 0. i$ $0.9696 + 0.0243i$ $0.9696 - 0.0243i$

NOMINAL WHEEL SPEED DURING STEADY STATE :

OMEGA0 -

3.0

STEADY STATE VALUES OF ESTIMATOR STATES $\hat{x}_i(1)$ THROUGH $\hat{x}_i(4)$: \hat{x}_i -

13.3487

3.4915

-38.7489

15.2396

STEADY STATE VALUE OF CONTROL TORQUE:

QV -

0.141

0.3 Modal decomposition of LQG compensator

The number of numerical calculations can be significantly reduced if the compensator of equations 0.24 and 0.25 is transformed to modal form. Implementing the compensator in this form is also numerically less sensitive.

Rewrite the compensator as

$$x_c(k+1) = A_c x_c(k) + B_c \begin{bmatrix} y_m(k) \\ r(k) \end{bmatrix} \quad (0.27)$$

$$u(k) = C_c x_c(k) + D_c \begin{bmatrix} y_m(k) \\ r(k) \end{bmatrix} \quad (0.28)$$

where

$$B_c = \begin{bmatrix} 0 & -1 \\ \Phi L & 0 \end{bmatrix} = [B_y \quad B_r] \quad (0.29)$$

Let the modal coordinate state vector be $\xi(k)$, then

$$x(k) = T\xi(k) \Rightarrow \xi(k) = T^{-1}x(k) \quad (0.30)$$

where T is a non-singular transformation matrix, whose columns are the right eigenvectors of A_c above.

With this transformation applied to equations 0.27 and 0.28 the modal form of the compensator becomes

$$\xi(k+1) = A_m \xi(k) + B_m \begin{bmatrix} y_m(k) \\ r(k) \end{bmatrix} \quad (0.31)$$

$$u(k) = C_m \xi(k) + D_m \begin{bmatrix} y_m(k) \\ r(k) \end{bmatrix} \quad (0.32)$$

where

$$\begin{aligned} A_m &= T^{-1}A_cT \\ B_m &= T^{-1}B_c \\ C_m &= C_cT \\ D_m &= D_c \end{aligned} \quad (0.33)$$

A_m is a diagonal matrix if A_c has no repeated eigenvalues. The values of the compensator matrices in modal form are listed at the end of Section 0.2.3.

Notice that since $D_m = 0$,

$$u(k) = C_m \xi(k) \quad (0.34)$$

The closed loop system with the compensator in modal form then becomes

$$\begin{bmatrix} x(k+1) \\ \xi(k+1) \end{bmatrix} = \begin{bmatrix} \phi & \Gamma C_m \\ B_r M & A_m + B_r N C_m \end{bmatrix} \begin{bmatrix} x(k) \\ \xi(k) \end{bmatrix} + \begin{bmatrix} 0 \\ B_r \end{bmatrix} r(k) \quad (0.35)$$

The compensator is implemented in the on-board microprocessor of the unicycle, using the FORTH [Mach2] programming language. Since calculation of the control torque command takes up approximately 25% of the sampling period, a prediction compensator is implemented to calculate the correct control command at the next sampling instant, based on measurements at the present sampling instant. The algorithm is summarized below:

- At the sampling instant, issue the control torque command $u(k)$ that was calculated during the previous sampling period, to the wheel drive motor.
- Read the sensors to obtain $y_m(k)$ and $r(k)$.
- Update the compensator states by using equation 0.31:

$$\xi(k+1) = A_m \xi(k) + B_m \begin{bmatrix} y_m(k) \\ r(k) \end{bmatrix}$$

- Calculate the control command for the next sampling instant, $u(k+1)$, by using equation 0.32:

$$u(k+1) = C_m \xi(k+1)$$

- Wait for the next sampling instant and then repeat the loop.

In order to start the longitudinal system with minimum transients in the control torque the best estimate for the initial values of the estimator states should be used. The unicycle is first brought up to the nominal speed Ω_0 by using feedback of the tachometer signal only. No attempt is made to stabilize the unicycle during this phase, and the operator holds the unicycle as vertical as possible during the speed-up phase. The plant model simplifies to a first order system

$$[I_2^W + (m_W + m_F + m_T)r_W^2]\dot{\Omega} + f_W\Omega = Q_W \quad (0.36)$$

with the coefficients as defined in Appendix M. A PID compensator with integral error feedback control was designed, with the transfer function

$$Q_W(z) = K_t \frac{z - z_t}{z - 1} [\Omega_{cmd}(z) - \Omega(z)] \quad (0.37)$$

$K_t = 16$ and $z_t = 0.9$ gives a good time response of the longitudinal system during the phase where the wheel speed is accelerated to the nominal operating speed.

The initial values for the plant and estimator states when the nominal operating speed is reached, can be calculated from equation 0.35 by noticing that in this steadystate condition

$$\begin{bmatrix} x_0 \\ \xi_0 \end{bmatrix} = \begin{bmatrix} x(k+1) \\ \xi(k+1) \end{bmatrix} = \begin{bmatrix} x(k) \\ \xi(k) \end{bmatrix} \quad \text{and} \quad r(k) = \Omega_0 \quad (0.38)$$

so that

$$\begin{bmatrix} x_0 \\ \xi_0 \end{bmatrix} = \left[I - \begin{bmatrix} \Phi & \Gamma C_m \\ B_y M & A_m + B_y N C_m \end{bmatrix} \right]^{-1} \begin{bmatrix} 0 \\ B_r \end{bmatrix} \Omega_0 \quad (0.39)$$

whence we find ξ_0 that should be used to initialize the compensator states in the on-board computer.

A listing of the FORTH code that implements the longitudinal control algorithm is shown in Appendix P.

O.4 Pole-zero compensator with accelerometer sensor

Control systems designed by successive loop closure techniques not only produce compensators of low order, but usually have better robustness to plant variations than LQG designs.

We will use the same sampling period as for the LQG design. The CTRL-C program 'lgt dtach' is used to design the controller and a listing of the program is shown in the next section. The on board microprocessor on the unicycle takes a finite time, T_{delay} , to complete all the calculations for the compensator. This delay is incorporated in the plant model as a pure transportation lag by means of a first order Padé approximation before the plant is discretized. Section N.3.2 describes how this adds an additional state to the plant state space model.

The first loop closure in the compensator design is a proportional feedback of the tachometer signal. Figure O.4 shows the rootlocus of the tachometer feedback loop as a function of the feedback gain K_t . We would like to select K_t as large as possible since this would decrease the nonlinear effects of stiction, Coulomb friction and friction variations due to the eccentricities in the gears of the wheel drive system. Figure O.4 also shows that there is an upper limit on the magnitude of K_t because the damping in the tachometer feedback loop can become unacceptably low.

The accelerometer feedback loop is closed next. Since an unstable pole is present, a compensation pole is placed close to it outside of the unit circle. A compensation zero is also placed just inside the unit circle to draw the rootlocus into the stable region of the z -plane as shown in Figure 0.5. Notice that there is a range of loop gain values, K_a , for which the closed loop system is stable. The lower bound on K_a is determined by the gain for which the low frequency locus enters the unit circle and the upper bound by when the high frequency part of the locus leaves the stability region. Without careful compensator design it can happen that the damping on the low frequency closed loop poles is not yet sufficient before the damping on the high frequency poles become unacceptably low. The final design of the compensator was obtained through iteration and inspection of the closed loop step response.

In order to simulate the time response of the closed loop system the compensator was modeled as shown in the block diagram of Figure 0.6. The block diagram shows a first order compensator in the tachometer loop for greater generality, but it can be changed to a proportional feedback controller by letting $p_t = z_t = 0$.

The plant equations are

$$x(k+1) = \Phi x(k) + \Gamma u(k) \quad (0.40)$$

$$y_m(k) = Mx(k) + Nu(k) \quad (0.41)$$

where $y_m(k)$ is the measured tachometer, $y_t(k)$, and accelerometer, $y_a(k)$.

The compensator matrices are

$$\begin{bmatrix} z_t(k+1) \\ z_a(k+1) \end{bmatrix} = \begin{bmatrix} p_t & K_a(p_a - z_a) \\ 0 & p_a \end{bmatrix} \begin{bmatrix} z_t(k) \\ z_a(k) \end{bmatrix} + \begin{bmatrix} -1 & -K_a \\ 0 & -1 \end{bmatrix} \begin{bmatrix} y_r(k) \\ y_a(k) \end{bmatrix} + \begin{bmatrix} K_r K_a \\ K_r \end{bmatrix} r(k) \quad (0.42)$$

or

$$\hat{z}(k+1) = A_c \hat{z}(k) + B_c y_m(k) + R_c r(k) \quad (O.43)$$

$$u(k) = \begin{bmatrix} K_t(p_t - z_t) & K_t K_a(p_a - z_a) \end{bmatrix} \begin{bmatrix} z_t(k) \\ z_a(k) \end{bmatrix} + \begin{bmatrix} -K_t & -K_t K_a \end{bmatrix} \begin{bmatrix} y_t(k) \\ y_a(k) \end{bmatrix} + [K_t K_a K_r] r(k) \quad (O.44)$$

or

$$u(k) = C_c \hat{z}(k) + D_c y_m(k) + S_c r(k) \quad (O.45)$$

The value of K_r is selected so that the transfer function from $r(k)$ to $\delta_a(k)$ is unity in steady state:

$$\begin{aligned} \lim_{z \rightarrow 1} \frac{\delta_a(k)}{r(k)} &= \lim_{z \rightarrow 1} K_r K_a \frac{z - z_a}{z - p_a} \\ &= K_r K_a \frac{1 - z_a}{1 - p_a} = 1 \end{aligned} \quad (O.46)$$

so that K_r must be

$$K_r = \frac{1}{K_a} \cdot \frac{1 - p_a}{1 - z_a} \quad (O.47)$$

We can now combine the plant equations 0.40 and 0.41 with the compensator equations 0.43 and 0.45 to obtain the closed loop system equations:

$$\begin{bmatrix} z(k+1) \\ \hat{z}(k+1) \end{bmatrix} = \begin{bmatrix} \Phi + \Gamma D_c J M & \Gamma(C_c + D_c J N C_c) \\ B_c J M & A_c + B_c J N C_c \end{bmatrix} \begin{bmatrix} z(k) \\ \hat{z}(k) \end{bmatrix} + \begin{bmatrix} \Gamma(S_c + D_c J N S_c) \\ R_c + B_c J N S_c \end{bmatrix} r(k) \quad (O.48)$$

where

$$J = [I - N D_c]^{-1} \quad (O.49)$$

Figure 0.7 shows a step response for a 1 r/s command in wheel speed. Figure 0.8 shows the loop gain and phase versus frequency of the longitudinal system.

0.4. POLE-ZERO COMPENSATOR WITH ACCELEROMETER SENSOR 293

0.4.1 Successive loop closure compensator parameters

UCTCS/LCTDTACH.CTR

LCT DISCRETE COMPENSATOR DESIGN WITH PADE APPROX FOR TIME DELAY

.....

LONGITUDINAL STATES : THETA.DOT; OMEGA; THETA; ID

CONTROL INPUT : WHEEL MOTOR TORQUE (QV)

MEASUREMENTS : TACHOMETER; ACCELEROMETER

UNITS : METERS, RADIANS, SECONDS

TSAMPLE -

0.0250

TDELAY -

0.0060

***** CONTINUOUS TIME SYSTEM MATRICES *****

PLGT -

-0.0333	0.0333	54.5447	-1.4149
0.1138	-0.1138	-151.2607	4.8433
1.0000	0.	0.	0.
0.	0.	0.	-400.0000

GLGT -

294 APPENDIX O. DISCRETE TIME LONGITUDINAL CONTROL SYSTEM

0.7075
-2.4216
0.
400.0000

HLGT

-1.0000 1.0000 0. 0.
-0.0011 0.0011 4.6700 0.

HLGT

0.
-0.0230

***** DISCRETE TIME SYSTEM MATRICES *****

PHI

1.0162 0.0008 1.3692 -0.0038
-0.0445 0.9971 -3.7967 0.0122
0.0251 0.0000 1.0171 -0.0001
0. 0. 0. 0.0000

GAM

-0.0142
0.0485
-0.0001
1.0000

***** PLANT TRANSFER FUNCTIONS *****

TRANSFER FUNCTION FROM WHEEL DRIVE TORQUE TO TACHOMETER MEASUREMENT

TACHGAIN

0.4. POLE-ZERO COMPENSATOR WITH ACCELEROMETER SENSOR

295

$$0.0627 + 0.00001$$

TACHZEROS -

$$1.0733$$

$$0.9317$$

$$-0.2488$$

TACHPOLES -

$$1.2009 - 0.00001$$

$$0.9996 + 0.00001$$

$$0.8301 - 0.00001$$

$$0.0000 + 0. \quad 1$$

TRANSFER FUNCTION FROM WHEEL DRIVE TORQUE TO ACCELEROMETER MEASUREMENT

ACCGAIN -

$$0.0230 + 0.00001$$

ACCGZEROS -

$$1.0035 + 0.23591$$

$$1.0000 - 0.00001$$

$$1.0035 - 0.23591$$

$$-0.0023 + 0. \quad 1$$

ACCPoles -

$$1.2009 - 0.00001$$

$$0.9996 + 0.00001$$

$$0.8301 - 0.00001$$

$$0.0000 + 0. \quad 1$$

TRANSFER FUNCTION FROM WHEEL DRIVE TORQUE TO WHEEL SPEED (OMEGA)

296 APPENDIX O. DISCRETE TIME LONGITUDINAL CONTROL SYSTEM

ONCGAIN =

0.0485 + 0.0000i

ONCOZCZOS =

1.0238

0.9227

-0.2488

ONCPOLES =

1.2009 - 0.0000i

0.9996 + 0.0000i

0.8301 - 0.0000i

0.0000 + 0. 1

***** TACHOMETER FEEDBACK LOOP PARAMETERS (INNER LOOP) *****

TACH LOOP PROPORTIONAL FEEDBACK COMPENSATOR GAIN-KT

KT =

15.0

CLOSED TACHOMETER LOOP GAIN, ZEROS AND POLES : TACHC(S)/TACHCND(S)

TACHLOOPZE =

1.0035 + 0.2359i

1.0000 + 0.0000i

1.0035 - 0.2359i

-0.0023 + 0. 1

TACHLOOPPO =

1.0876 + 0.0000i

0.4. POLE-ZERO COMPENSATOR WITH ACCELEROMETER SENSOR

297

0.9423 - 0.00001

0.0302 + 0.47681

0.0302 - 0.47681

TACHLOOPGA -

-0.3447

***** ACCELEROMETER FEEDBACK LOOP PARAMETERS (OUTER LOOP) *****

FIRST ORDER COMPENSATOR:

GAIN=KA; ZA=ZERO & PA=POLE

KA -

-20.0

PA -

1.0500

ZA -

0.9600

KA -

0.0625

ACCLDOPZE -

1.0838 + 0.00001

0.9600 - 0.00001

0.9227 + 0.00001

-0.2488 + 0. i

```
ACCTLOGPP0
```

```
0.9351 + 0.1625i
```

```
0.9782 + 0.0281i
```

```
0.9782 - 0.0281i
```

```
0.9351 - 0.1625i
```

```
0.0337 - 0.0000i
```

O.5 Pole-zero compensator with vertical sensor

We will use the same successive loop closure design approach as in section O.4, but this time assume that we have a sensor that measures the pitch angle, θ . The first loop closure in the compensator is feedback of the tachometer signal, with an integral error compensator consisting of a pole at $z = 1$ and a zero at $z_t = 0.75$. Figure O.9 shows the root locus of the tachometer feedback loop as a function of the loop gain K_t . The print out of the CTRL-C program that was used to design the compensator is shown in section O.5.1.

The pitch angle feedback loop is closed next, with a first order compensator where the pole is at $z = 1.03$ and the zero at $z = 0.95$. The root locus of the outer loop is shown in Figure O.10. Notice that the high frequency root locus enters the unstable region of the z -plane for high loop gains $|K_p| > 150$. This is a significant improvement over the situation with the accelerometer sensor where the high frequency root locus branches were strongly attracted by the pair of complex zeros just outside the unit circle. The enlargement of the low frequency root locus branch near $z = 1$ (Figure O.11) shows that the loop gain K_p was selected so that the closed loop poles were well damped.

The simulation of Figure O.12 shows a time response of the closed loop system to

0.5. POLE-ZERO COMPENSATOR WITH VERTICAL SENSOR

299

a unit step command in wheel speed.

0.5.1 Pitch feedback compensator calculation

UCTC7/LGDTACH.CTR

LGT DISCRETE COMPENSATOR DESIGN WITH PADE APPROX FOR TIME DELAY

.....

.....

CONTROL INPUT : WHEEL MOTOR TORQUE (QW)

MEASUREMENTS : TACHOMETER; PITCH SENSOR

UNITS : METERS, RADIANS, SECONDS

TSAMPLE =

0.0250

TDELAY =

0.0040

***** CONTINUOUS TIME SYSTEM MATRICES *****

PLGT =

-0.0333	0.0333	54.5447	-1.4149
0.1132	-0.1132	-151.2607	4.8433
1.0000	0.	0.	0.
0.	0.	0.	-500.0000

300 APPENDIX O. DISCRETE TIME LONGITUDINAL CONTROL SYSTEM

GLOT =

0.7075
-2.4216
0.
500.0000

ELGT =

-1.0 1.0 0. 0.
0. 0. 1.0 0.

ELMT =

0.
0.

***** DISCRETE TIME SYSTEM MATRICES *****

PHI =

1.0162 0.0008 1.3692 -0.0029
-0.0445 0.9971 -3.7957 0.0098
0.0251 0.0000 1.0171 -0.0001
0. 0. 0. 0.0000

GAM =

-0.0149
0.0509
-0.0002
1.0000

***** PLANT TRANSFER FUNCTIONS *****

TRANSFER FUNCTION FROM WHEEL DRIVE TORQUE TO TACHOMETER MEASUREMENT

0.5. POLE-ZERO COMPENSATOR WITH VERTICAL SENSOR

301

TACHGAIN -

0.0658

TACHZEROS -

1.0733

0.9317

-0.1895

TACHPOLES -

1.2009 - 0.00001i

0.9995 + 0.00001i

0.8301 - 0.00001i

0.0000 + 0. 1

TRANSFER FUNCTION FROM WHEEL DRIVE TORQUE TO PITCH MEASUREMENT

PITCHGAIN -

-1.56144-04

PITCHZEROS -

-1.7782

1.0000

-0.0003

PITCHPOLES -

1.2009 + 0.00001i

0.9995 + 0.00001i

0.8301 - 0.00001i

0.0000 + 0. 1

APPENDIX O. DISCRETE TIME LONGITUDINAL CONTROL SYSTEM

TRANSFER FUNCTION FROM WHEEL DRIVE TORQUE TO WHEEL SPEED (OMEGA)

OMEGAGAIN -

0.0509

OMEGAZEROS -

1.0838

0.9227

-0.1896

OMEGAPOLES -

1.2009 + 0.00001

0.9996 + 0.00001

0.8301 - 0.00001

0.0000 + 0. 1

***** TACHOMETER FEEDBACK LOOP PARAMETERS (INNER LOOP) *****

TACH LOOP PROPORTIONAL FEEDBACK COMPENSATOR GAIN-KT, ZERO-ZT, POLE-PT

KT -

15.0

ZT -

0.7500

PT -

1.0

CLOSED TACHOMETER LOOP GAIN, ZEROS AND POLES : YPITCH(S)/TACHEND(S)

O.5. POLE-ZERO COMPENSATOR WITH VERTICAL SENSOR

303

TACHLOOPZE -

-1.7782 - 0.00001

1.0000 - 0.00001

0.7500 + 0.00001

-0.0203 + 0. i

TACHLOOPPO -

0.1735 + 0.41601

1.0766 + 0.00001

0.9271 - 0.00001

0.6922 + 0.00001

0.1735 - 0.41601

TACHLOOPGA -

0.0023

***** PITCH ANGLE FEEDBACK LOOP PARAMETERS (OUTER LOOP) *****

FIRST ORDER COMPENSATOR:

GAIN-KP: ZP-ZERO & PP-POLE

KP -

-40.0

PP -

1.0300

ZP -

0.9500

304 APPENDIX O. DISCRETE TIME LONGITUDINAL CONTROL SYSTEM

IR -

0.0150

PITCHLOOPZ -

1.0838 - 0.0000i

0.9500 + 0.0000i

0.9227 - 0.0000i

0.7500 + 0.0000i

-0.1895 + 0.0000i

PITCHLOOPP -

0.3144 + 0.4736i

0.3144 - 0.4736i

0.9834 + 0.0249i

0.9834 - 0.0249i

0.8472 - 0.0000i

0.5366 + 0.0000i

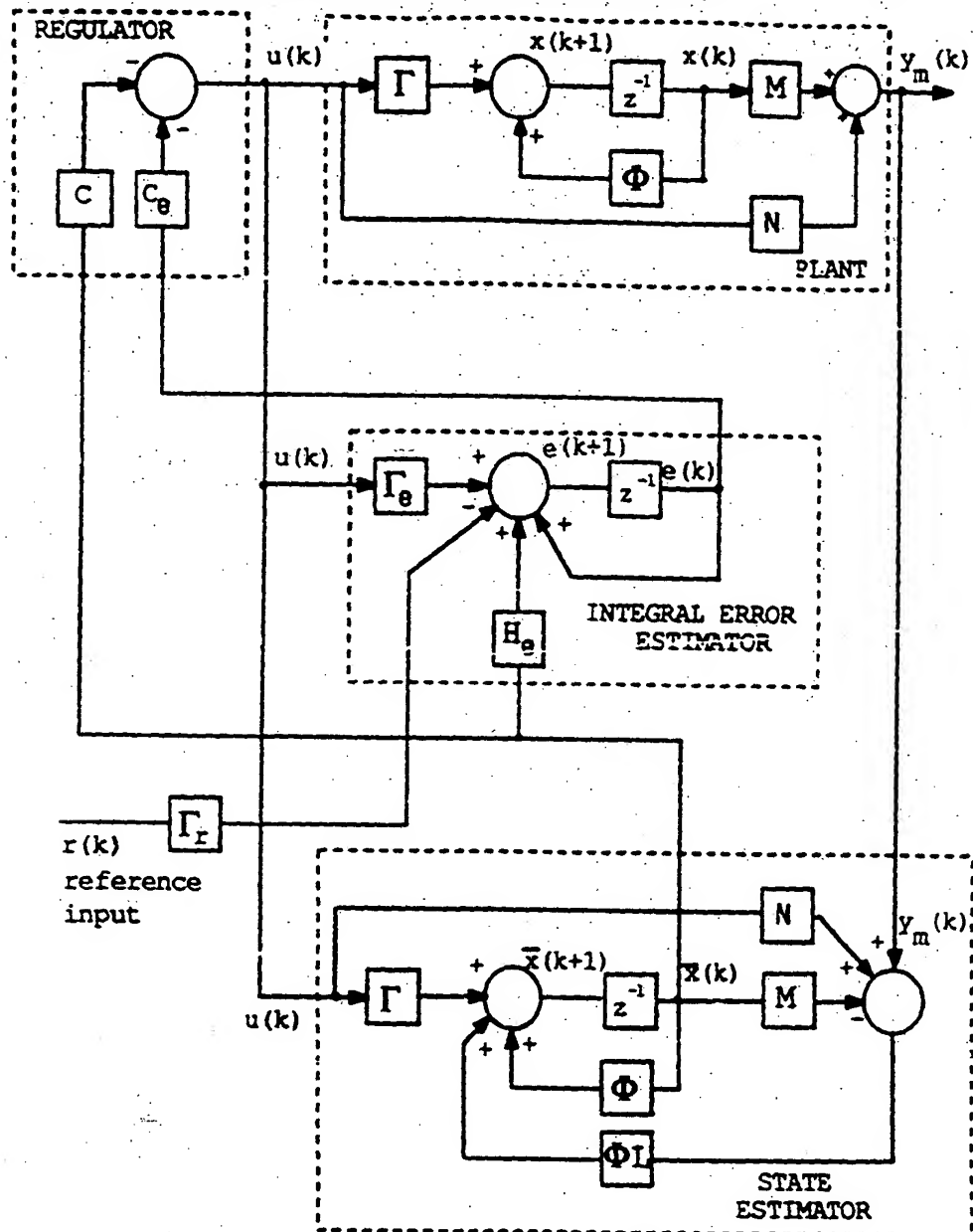


Figure 0.1: Blockdiagram of a Discrete Time LQG Compensator with Integral Error Feedback

DISCRETE SYSTEM RESPONSE WITH FULL STATE F.B.

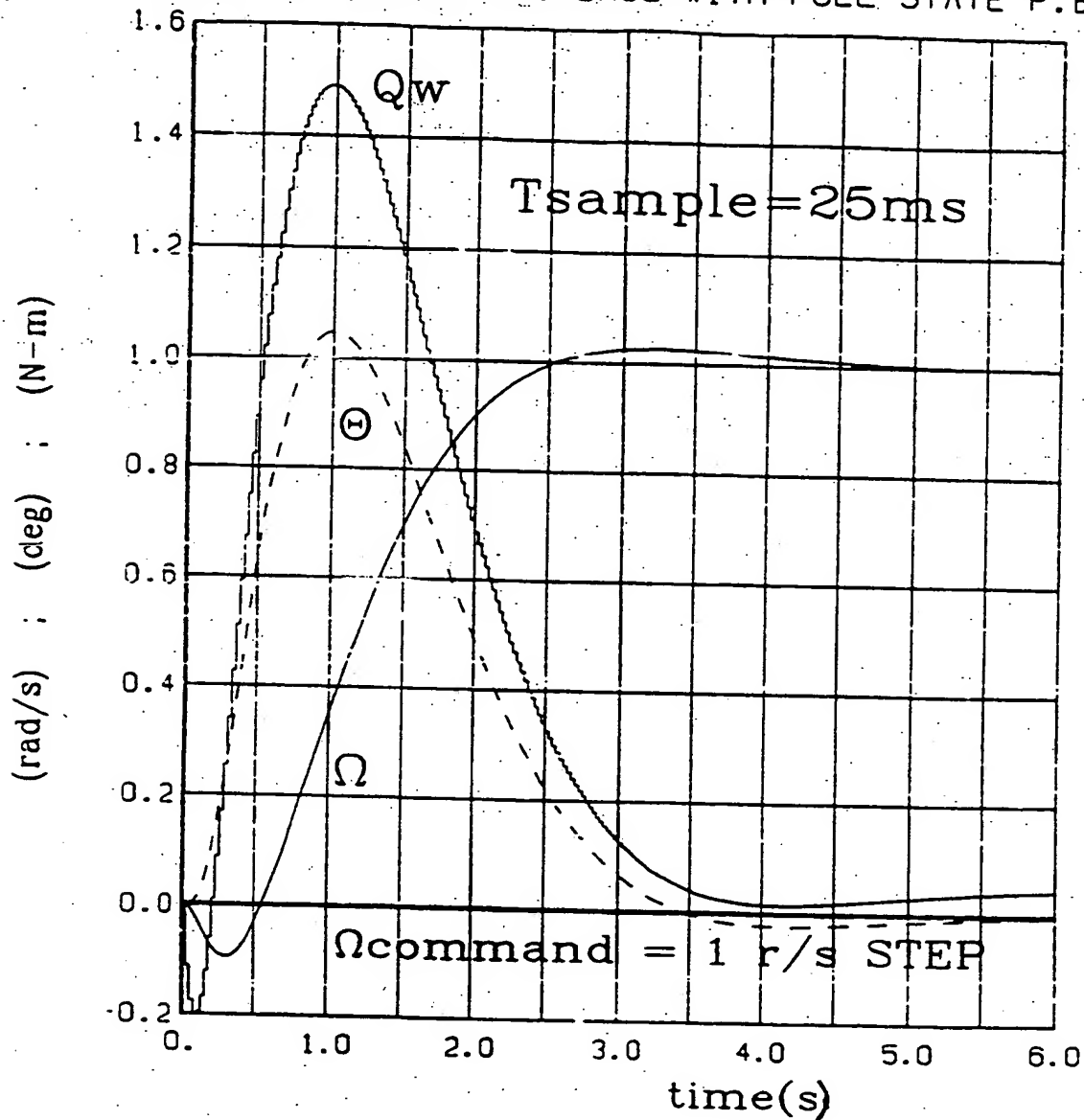


Figure O.2: Step Response of the Longitudinal Discrete Time System with Full State Feedback

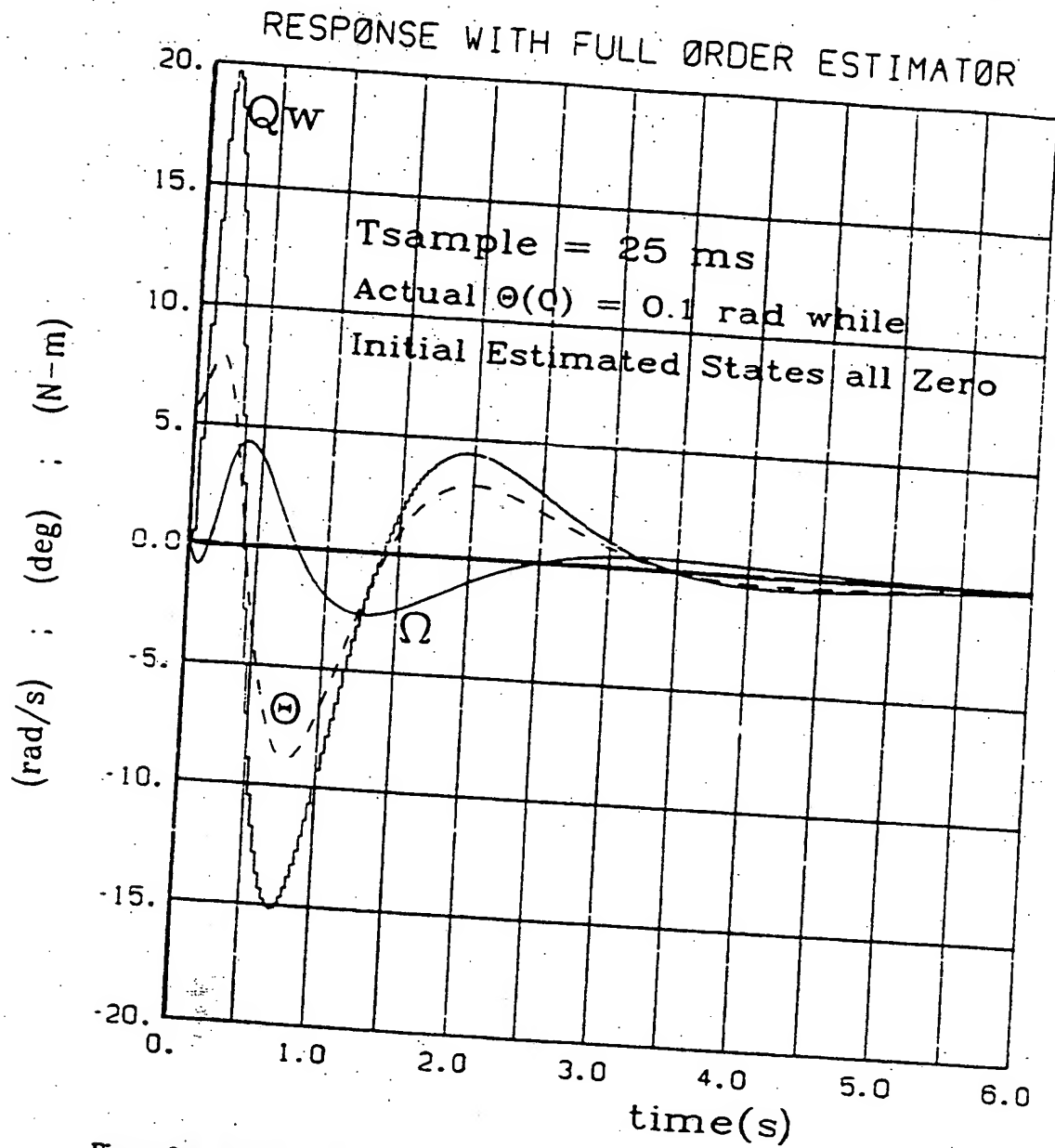


Figure 0.3: Response of the Longitudinal System with a Full Order Estimator with $\theta(0) = 0.1 \text{ rad}$, but $\dot{\theta}(0) = 0 \text{ rad/s}$

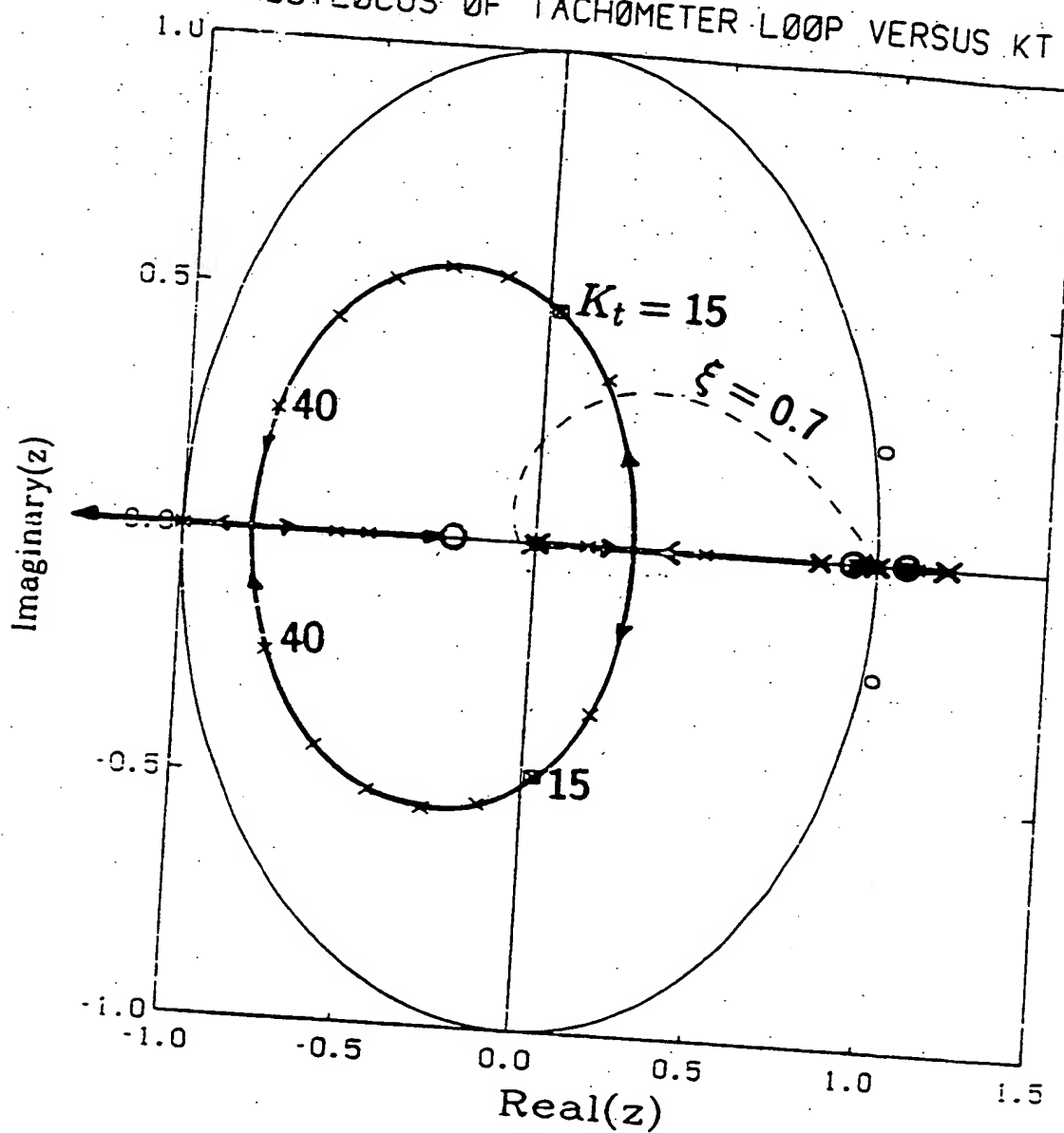
ROOTLOCUS OF TACHOMETER LOOP VERSUS K_T 

Figure O.4: Rootlocus of the Discrete Time Longitudinal Tachometer Loop with Proportional Feedback of the Tachometer Measurement

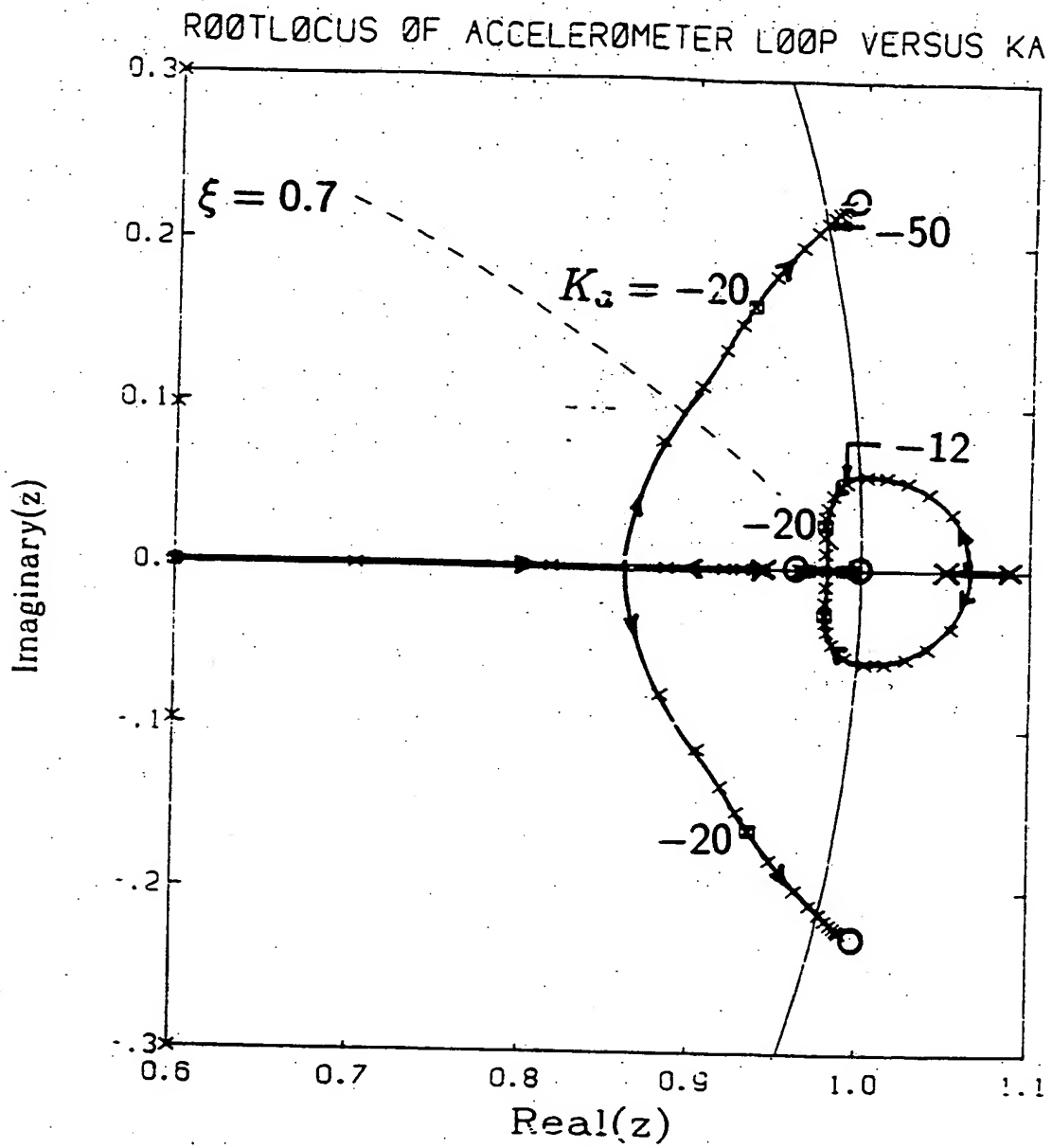


Figure 0.5: Rootlocus of the Accelerometer Loop with a First Order Pole-zero Compensator

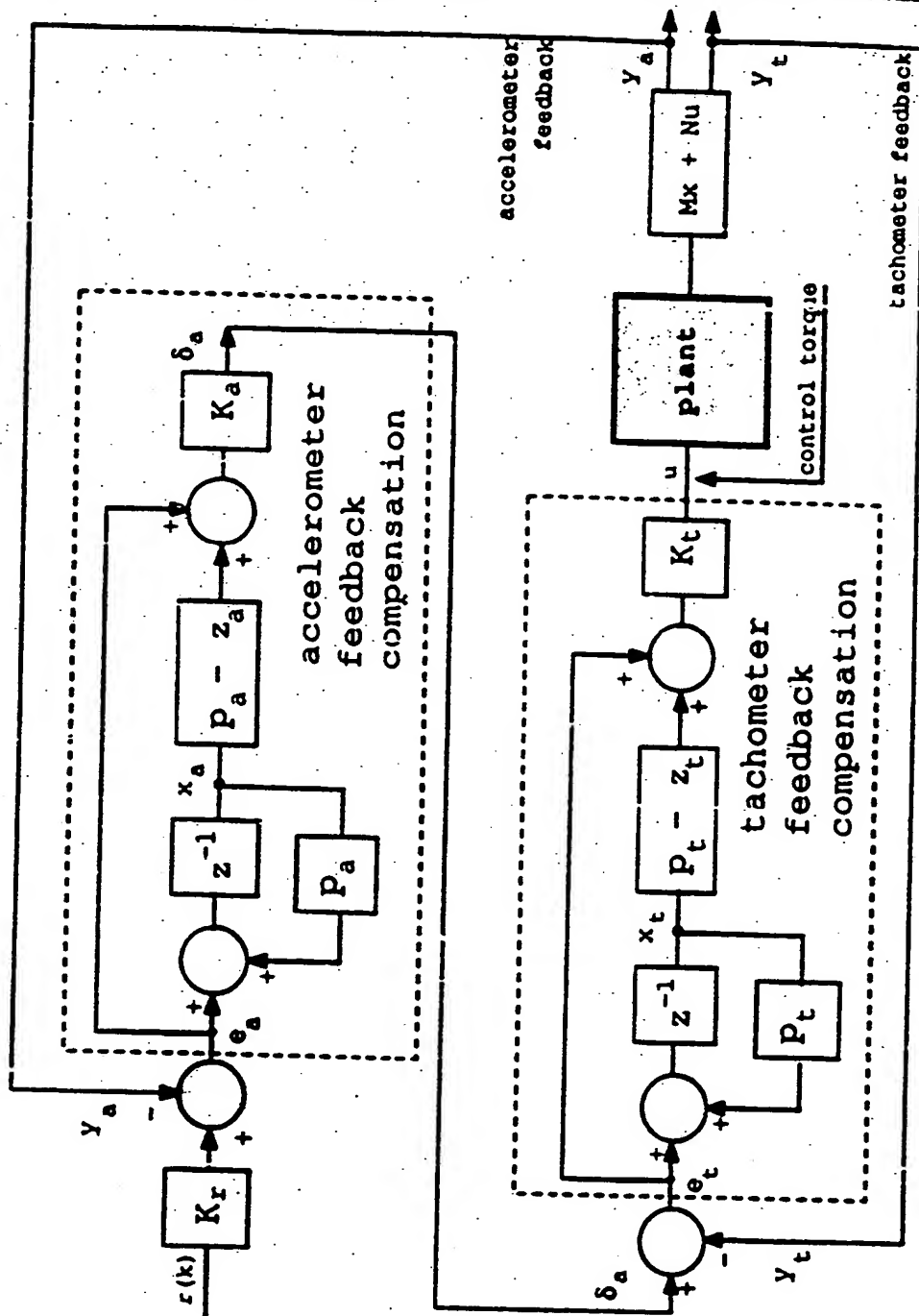


Figure O.6: Blockdiagram of the Discrete Longitudinal Successive Loop Closure Control System

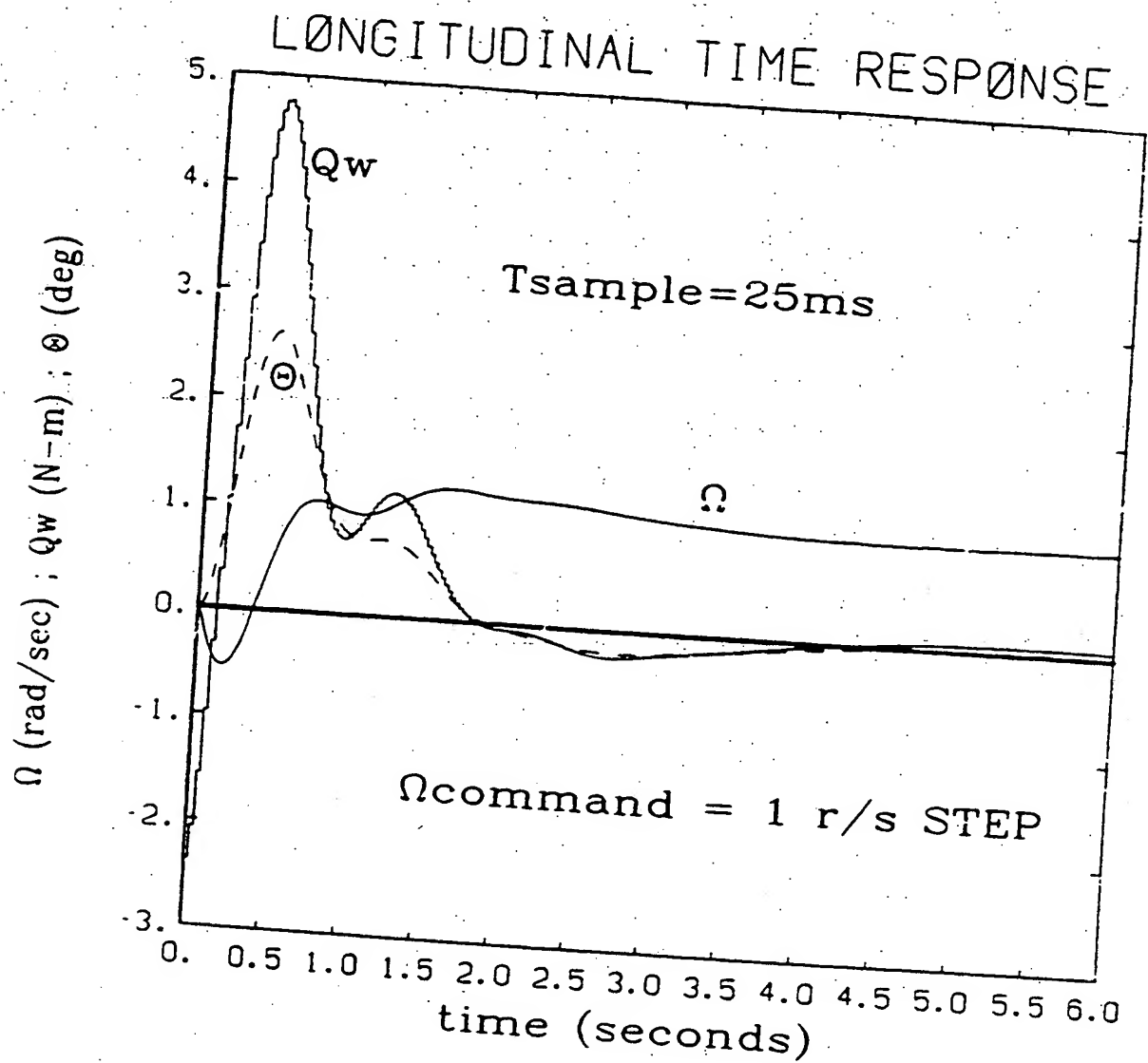


Figure 0.7: Step Response of the Longitudinal Closed Loop System Designed by Successive Loop Closure

LONGITUDINAL PLANT CLOSED LOOP FREQUENCY RESPONSE

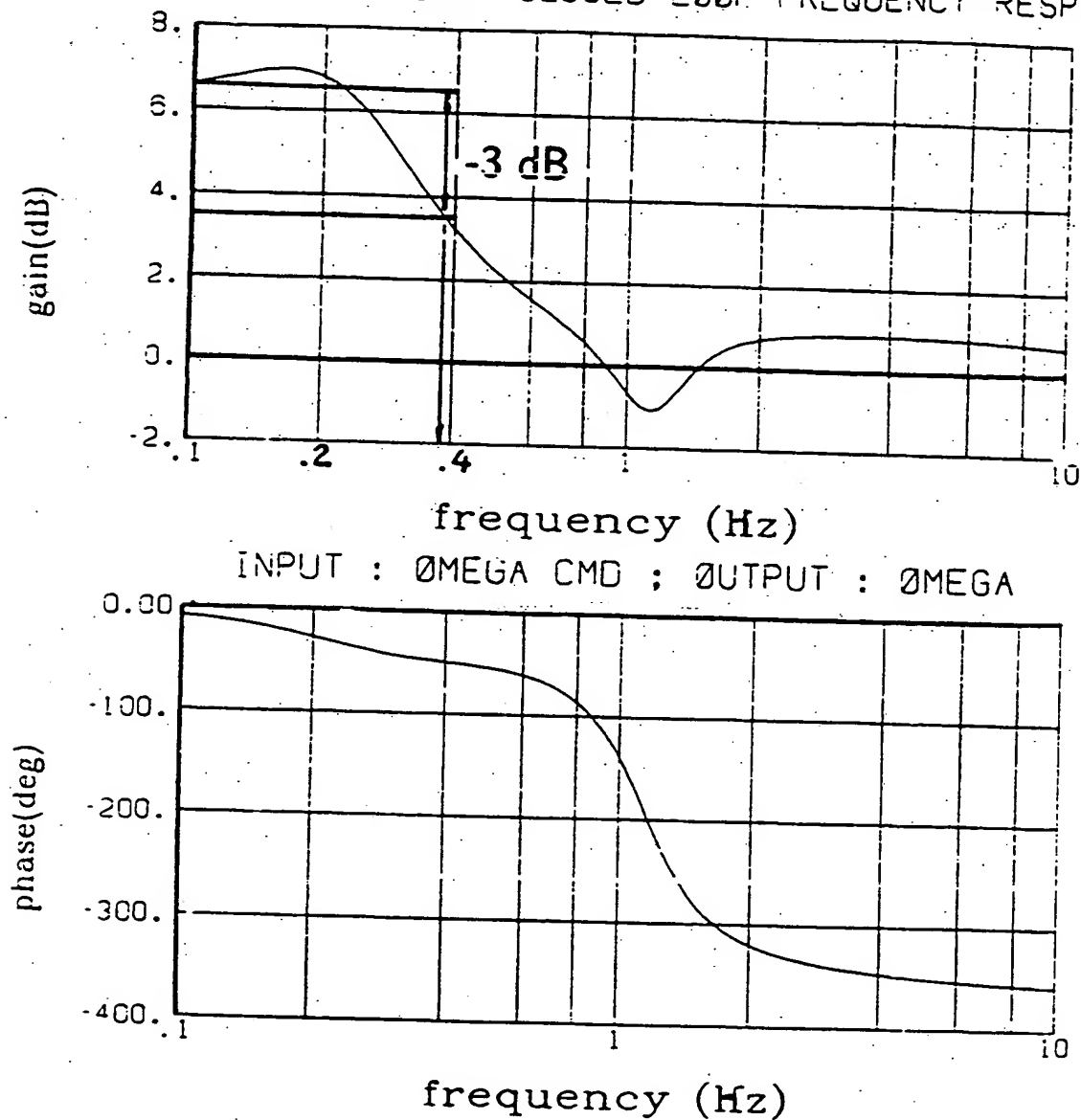


Figure O.8: Loop Gain and Phase versus Frequency of the Discrete Time Longitudinal Control System Designed by Successive Loop Closure

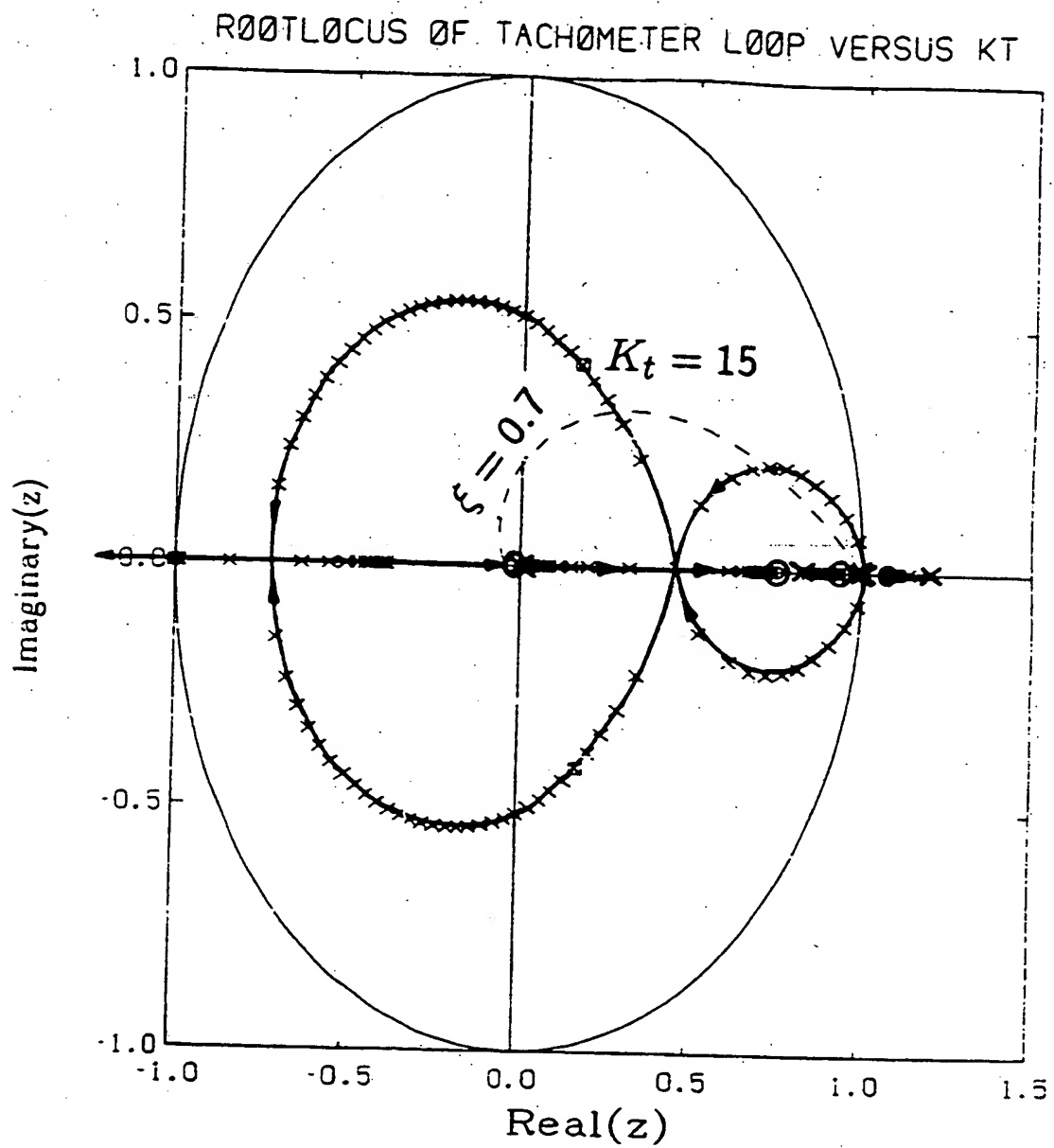


Figure 0.9: Root Locus of the Discrete Time Longitudinal Tachometer Loop with Integral Error Feedback of the Tachometer Measurement

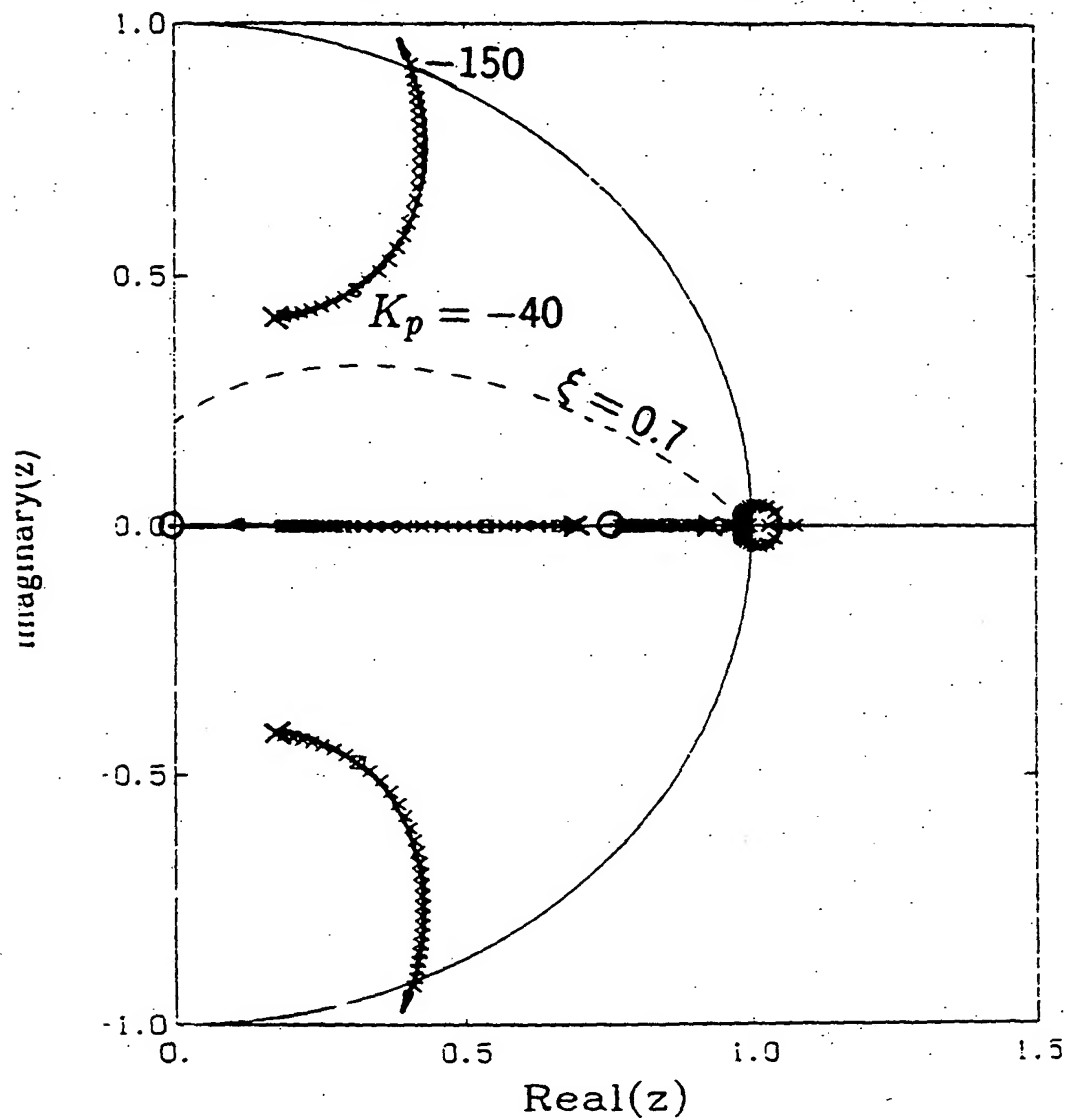
ROOTLOCUS OF PITCH F.B. LOOP VERSUS K_P 

Figure O.10: Root Locus of the Pitch Angle Feedback Loop with a First Order Compensator

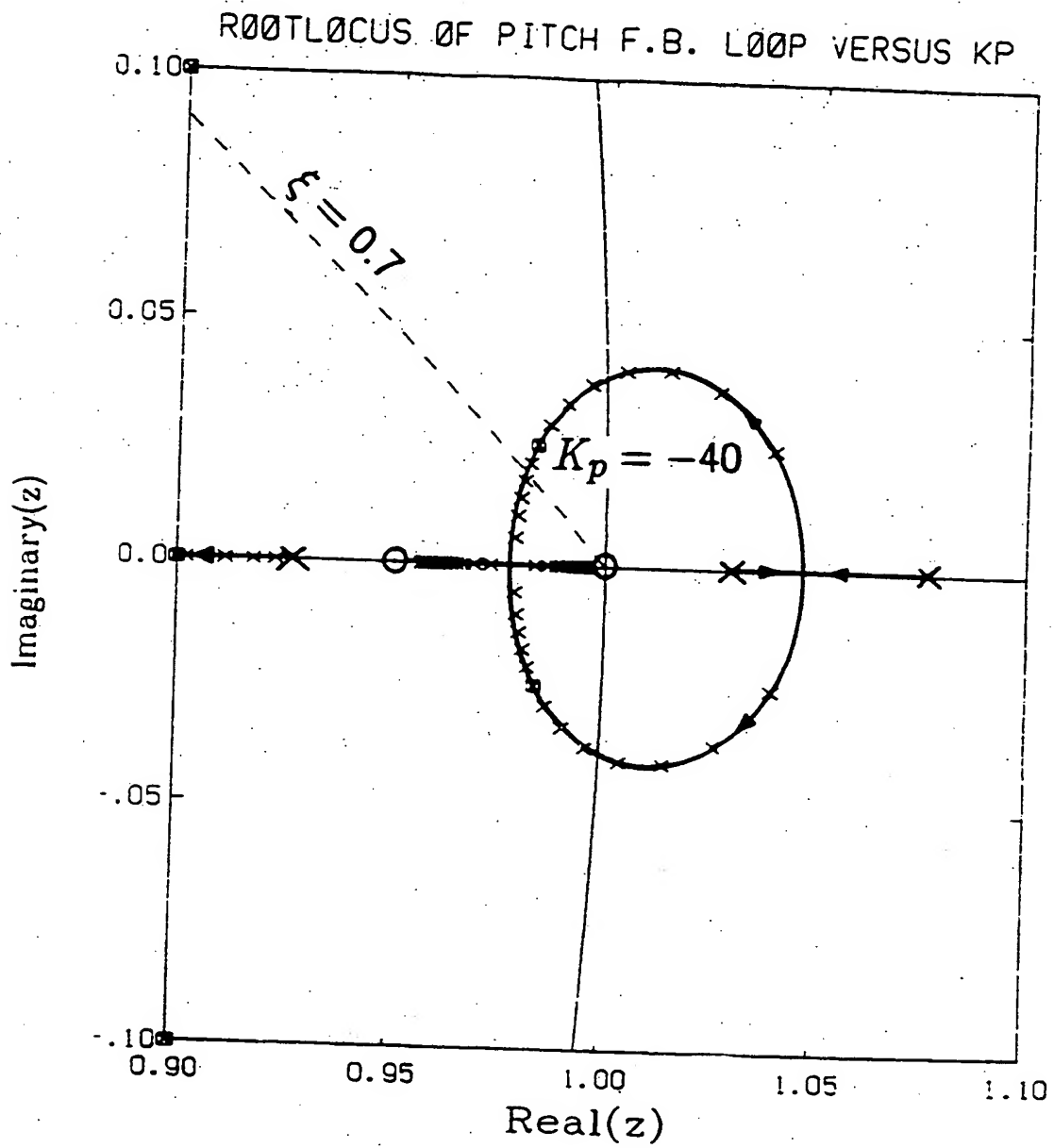


Figure 0.11: Enlargement of the Pitch Loop Root Locus in the Vicinity of $z = 1$

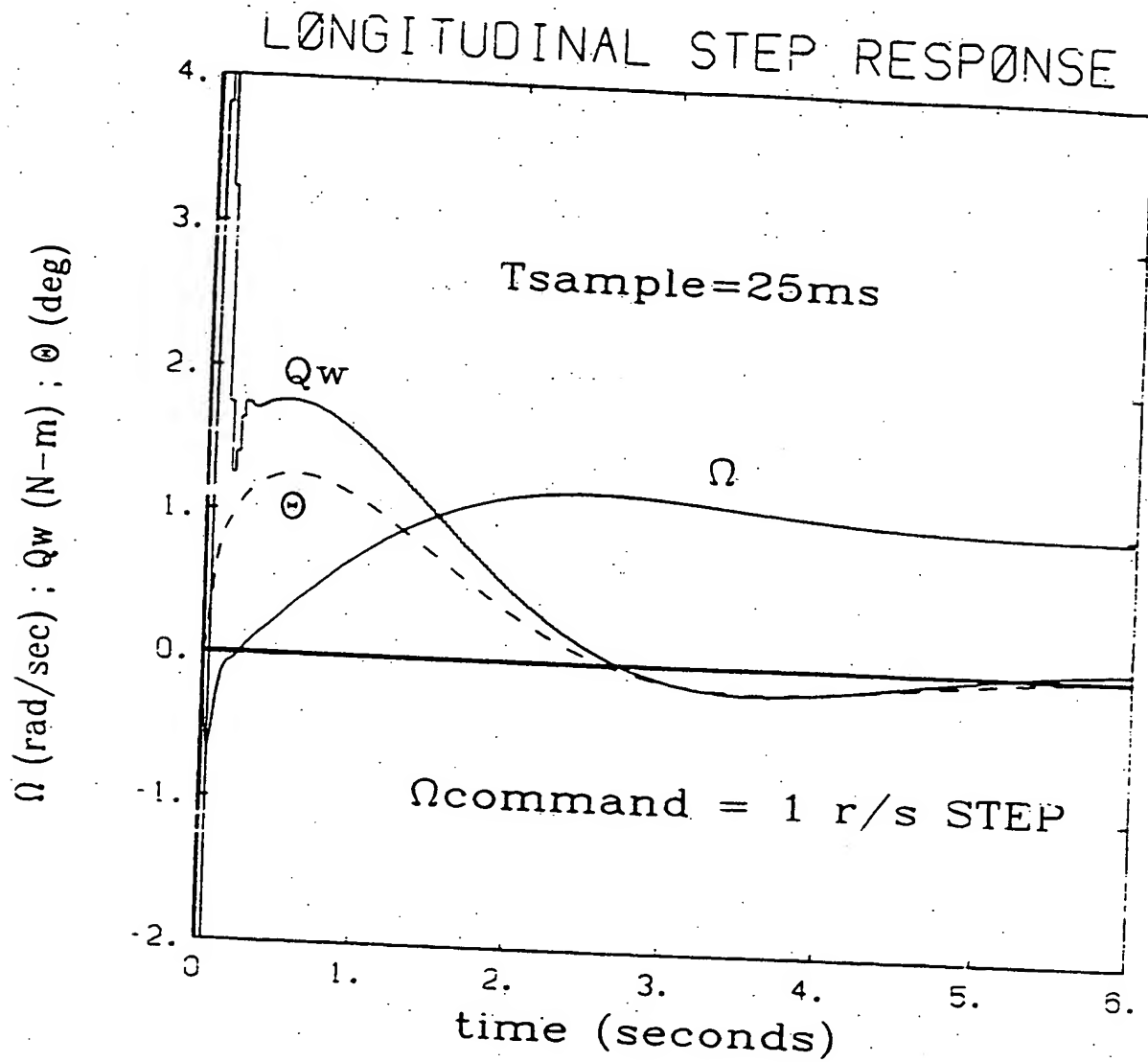


Figure O.12: Step Resonse of the Longitudinal Closed Loop System with Pitch Angle Feedback

Appendix P

FORTH Codes for Longitudinal Control

P.1 Successive Loop Closure and Accelerometer

The FORTH [Mach2] code which implements the compensator designed by successive loop closure (section 0.4) with an accelerometer sensor, is listed below. During the first 200 sample periods, the control algorithm closes the tachometer feedback loop only, to bring the wheel speed up to the nominal speed, Ω_0 . The operator tries to hold the unicycle robot as vertical as possible during this stage. Thereafter the algorithm closes the accelerometer feedback loop to start the balancing process.

All the compensator calculations are performed in fixed point arithmetic with a 64-bit word length, in order to minimize the computational delay. The tachometer measurement and control torque signals are scaled up by a factor of 10^3 and the accelerometer signal is scaled up by a factor of 10^6 in the computations in order to maintain good numerical accuracy.

APPENDIX P. FORTH CODES FOR LONGITUDINAL CONTROL

The program listing is documented with comments to explain the logic of the algorithm.

```
( ----- Longitudinal Control Turnkey Program ----- )

( Program to test ucyc9/lgtdtach controller : Tsample = 25 milliseconds )
( Tight tach feedback loop closed first )

O VERIFY !
LOAD/TARGET ( Turn echoing off during downloading )

( ***** DEFINE ADDRESSES AND CONSTANTS ***** )

HEX

800000 CONSTANT LATDACADDR ( Set LAT DAC's address )
800010 CONSTANT LGTDACADDR ( Set LGT DAC's address )
800020 CONSTANT LATENCADDR ( Set LAT Encoder's address )
800030 CONSTANT LGTEENCADDR ( Set LGT Encoder's address )

800080 CONSTANT RCCOUNTER0 ( Radio Receiver Interface )
800082 CONSTANT RCCOUNTER1 ( Counter Addresses )
800084 CONSTANT RCCOUNTER2
800086 CONSTANT RCCONTROLWORD ( Counter Controlword address )

800090 CONSTANT RCTRIGGER ( Trigger address to RESET IRQ flip-flop )

68 CONSTANT LEVEL2_IRQ ( Level2 Autovector Address )

8000D0 CONSTANT S2ADDR ( Sample & Hold's address )
8000E0 CONSTANT MUXADDR ( Multiplexer's address )
8000F0 CONSTANT ADCADDR ( Analog-to-Digital Converter's address )
```

0 CONSTANT LATACCHX (MUXCode for Lateral Accelerometer)
 1 CONSTANT LGTACCHX (MUXCode for Longitudinal Accelerometer)

 81000F CONSTANT RTCCtrlADDR (Set Real Time Clock's Ctrlword address)
 81000B CONSTANT RTCCounter1 (Set Real Time Clock's Counter 1 address)
 0 CONSTANT CHANNEL0 (Terminal task number)

DECIMAL

15 CONSTANT LGTKt (Tach loop gain)
 -20 CONSTANT LGTla (Acc loop gain)
 62500 CONSTANT LGTKr (Kv=10.6 : reference ~~input~~ gain)

 3000 CONSTANT Omega0 (1000*nominal wheel speed)

 500 CONSTANT STORELength (# of entries to be saved in STORE arrays)

 1250 CONSTANT RTCPeri0d1 (Real Time Clock Timer 1 initial count)
 (for 40 hz sampling freq)

VARIABLE LATPWM (Lateral Radio Pulse Width)
 VARIABLE LGTPWM (Longit. Radio Pulse Width)

VARIABLE TICKSAVE (Memory location to save tick count)

VARIABLE LgtEncCount (Counter for 2 wheel speeds to average)
 VARIABLE SpeedUpCount (counter for time in speed-up mode)

VARIABLE STORECount (Counts numbers stored in STORE arrays)

VARIABLE LGTCmd (LGT acceleration command *10e6)
 VARIABLE LGTTrak (LGT accelerometer compensator state*10e6)

VARIABLE Ytach3 (Tachometer measurement *10e3)
 VARIABLE Yacc6 (Accelerometer measurement * 10e6)
 VARIABLE Qx3 (Wheel Torque *10e3)

APPENDIX P. FORTH CODES FOR LONGITUDINAL CONTROL

400 1000 BACKGROUND SLAVE

400 1000 TERMINAL BOSS

(***** REAL TIME CLOCK REPROGRAMMING WORDS *****)

CODE RTCset (Sets RTC Counter 1 to sample rate)

MOVE.L DO, -(A6) (saves contents of DO on stack)

MOVE.B \$874, RTCctrlADOR (Rewrites Ctrlword for counter 1)

MOVE.W RTCperiod1, DO

MOVE.B DO, RTCcounter1 (Send low byte)

LSR.W \$8, DO

MOVE.B DO, RTCcounter1 (Send high byte)

MOVE.L (A6)+, DO (Restores original value of DO)

RTS (Return to subroutine)

END-CODE

CR . (Loaded RTCset)

ALSO MATH

FP32

FVARIABLE STORE1 STORELength 2= 2= VALLOT (Time history)

FVARIABLE STORE2 STORELength 2= 2= VALLOT (arrays 1, 2, 3)

FVARIABLE STORE3 STORELength 2= 2= VALLOT

(***** REAL TIME CLOCK READING WORDS *****)

CODE ZEROtheTICKS (-) (Zeros the tick counter register)

CLR.L (A5)

RTS

END-CODE

P.1. SUCCESSIVE LOOP CLOSURE AND ACCELEROMETER

321

```

CR .( Loaded ZEROthTICKS )

CODE TICKStoSTACK ( - n ) ( Loads tick count on top of stack )
MOVE.L (A5),-(A5) ( Current tick counter value onto stack )
RTS
END-CODE
CR .( Loaded TICKStoSTACK )

( ***** CONTROL SYSTEM ALGORITHM WORDS ***** )

: S 2048 LATDACADDR W! 2048 LGTDACADDR W! ; ( Quick motors stop )

: ?DACSATURATE ( n - n ) ( Check if DAC command Saturates )
DUP 4095 > ( check for positive saturation )
IF DROP 4095 ( drop large value & supply sat. value )
ELSE DUP 0 < ( check for negative saturation )
IF DROP 0 ( drop large value & supply sat. value )
THEN THEN : ( otherwise keep commanded DAC value )

: WAITAN ( n - ) ( S/V WAIT for n*30 microseconds )
0 DO LOOP ;

: CHECKTSAMPLE ( - f ) ( Check if sample time has expired )
TICKStoSTACK ( get tick count )
0 > ; ( sets true flag if dt >= Tsample )
CR .( Loaded CHECKTSAMPLE )

: WORK ACTIVATE ( Activate Background task )
S ( Stop all motors )

0 LGTcmd ! ( Initial LGT reference input assumed = 0 )
0 LGTtrk ! ( Initialize acc. comp. state to zero )

0 SpeedUpCount ! ( Initialize SPEED_UP counter )

0 STUNECount ! ( Initialize STUNEi counter )

```

APPENDIX P. FORTH CODES FOR LONGITUDINAL CONTROL

RTClock (Set Real Time clock to Tsample)

BEGIN

CHECKTSAMPLE (Check if sample time has expired)

IF ZEROthetics (If TRUE Reset counter to zero . . .)

(===== READ LGT TACHOMETER AND ACCELEROMETER =====)

LGTENCADDR W0 (read binary value from enc. interface)

(Bt <- top of stack)

LGTACCMUX MUXADDR W! (switch MUX to LGT accelerometer)

1 S&HADDR W! (sample analog signal)

1 WAIT4N (wait 30 microsec for S&H to settle)

0 S&HADDR W! (place S&H device in HOLD mode)

1 ADCADDR W! (Starts A to D Converter)

1 WAIT4N (buy a little time for ADC to finish)

ADCADDR W0 (reads binary value from A/D)

(Bt Ba <- top of stack)

4095 - 4884 = 10003660 + (convert to a voltage=10e6)

-31576 100000 =/ (scale by LGTACCGAIN => acc=10e6)

(Bt Ya6 <- top of stack)

DUP Yacc6 ! (save copy of accel to print later)

(Bt Ya6 <- top of stack)

SpeedUpCount @ 200 > (check if speed-up phase is over)

(===== ACCELEROMETER LOOP COMPENSATION =====)

IF (if so , add accelerometer compensation)

LGTCmd @ (get acceleration command)

LGTr = (mult. by Kr=10e6 -> 10e6 = accel. cmd)

P.1. SUCCESSIVE LOOP CLOSURE AND ACCELEROMETER

323

```

SWAP - ( subtract Ya6 to get acc. error=10e6 )
DUP ( save a copy for compensator update )
( Bt Ea6 Ea6 <- top of stack )

LGTmk 0 ( get LGT accelerometer compensator state )
( Bt Ea6 Ea6 Ia6<- top of stack )
9 100 +/- ( multiply by pa-za and add to acc. error )

LGTka 1000 +/- ( mult. by LGTka; div. by 1000 => 1000=da )
( Bt Ea6 da3 <- top of stack )

ELSE ( during speed-up do tach loop comp. only )

DROP ( drop -Ya6 from top of stack )
0 0 ( supply zeroes for Ea6 and da3 )
( Bt 0 0 <- top of stack )

( ===== TACHOMETER LOOP COMPENSATION ===== )

THEN ( do tachometer compensation loop )

Omega0 + ( wheel speed + da3 )
( Bt Ea6 sum <- top of stack )

ROT ( get binary value of the tach )
( Ea6 sum Bt <- top of stack )

DUP ( copy to determine sign later )
10471976 SWAP / ( get 1000=abs(ytach) )

SWAP 2 MOD 0= ( get sign of the wheel speed : )
IF NEGATE THEN ( 0 => even s => neg. speed )
( Ea6 sum Yt3 <- top of stack )

DUP Ytach3 ! ( save a copy to print later )
( Ea6 sum Yt3 <- top of stack )

```

APPENDIX P. FORTH CODES FOR LONGITUDINAL CONTROL

```

( get velocity error10a3 )
- ( Ea6 Et3 <- top of stack )

LGTkt * ( mult tach loop gain )
( -> 1000=Wheel torque )
( Ea6 Qw3 <- top of stack )

DUP Qw3 ! ( make a copy to print later )
( Ea6 Qw3<- top of stack )

15120 + 2048 15120 */ ( get binary command for DAC )

?DACSATURATE ( check if DAC saturates )

LGTDACADDR W! ( output torque command )
( Ea6<- top of stack )

( ***** COMPENSATOR STATE UPDATE ***** )

LGTtak * ( get LGT accelerometer compensator state )
( Vw6 Vw6 <- top of stack )

105 100 */ ( multiply by LGTpa )
+ LGTak ! ( add to the acc. error and save that(k+)) )
( stack empty <- top of stack )

1 SpeedUpCount +! ( increment speed-up counter )

( ***** STORE TIME HISTORY ***** )
STORECount @ STORELength <
IF
Qw3 @ D>F 1000. F/ ( Scale to normal units )
STORE1 STORECount @ 2* 2* + F! ( multiply index by 4 to )
( store 64 bit # )

Ytach3 @ D>F 1000. F/ ( Scale to normal units )

```

P.1. SUCCESSIVE LOOP CLOSURE AND ACCELEROMETER

325

STORE2 STORECount @ 2* 2* + P!

Yacc6 @ DF 1000000. F/ (Scale to normal units)

STORE3 STORECount @ 2* 2* + P!

1 STORECount +! (Increment the counter of 8 stored)

THEN

THEN PAUSE (Go do terminal task)

AGAIN ;

(--- BUILDING OF TERMINAL & BACKGROUND TASKS FOR TURNKEY APPLICATION ---)

: WHIP (Build and Activate Background task)

SLAVE BUILD

SLAVE WORK ;

: PKEY (Check if key was depressed)

BEGIN

PAUSE

?TERMINAL

DOP

IF

KEY DROP

THEN

UNTIL ;

: PRINT ACTIVATE (Activate Terminal task)

-1 INIT-DISK (reset all disk drives)

BEGIN

CR

." Press any key to see BACKGROUND variable "

?KEY

APPENDIX P. FORTH CODES FOR LONGITUDINAL CONTROL

```
CR ." Qv=[ "
STORELength 0 DO
  STORE1 I 2* 2* + P0
  I 9 MOD 0= IF ." .. " CR
  THEN P. ." "
  PAUSE LOOP ." ]: " CR
```

```
CR ." Ytach=[ "
STORELength 0 DO
  STORE2 I 2* 2* + P0
  I 9 MOD 0= IF ." .. " CR
  THEN P. ." "
  PAUSE LOOP ." ]: " CR
```

```
CR ." Yacc=[ "
STORELength 0 DO
  STORE3 I 2* 2* + P0
  I 9 MOD 0= IF ." .. " CR
  THEN P. ." "
  PAUSE LOOP ." ]: " CR
```

```
CR
```

```
AGAIN ;
```

```
: START
```

```
CHANNEL0 BOSS BUILD ( Initializes Terminal Task )
```

```
BOSS PRINT
```

```
WHIP ; ( Initializes Background Task )
```

```
TURKEY START ( Turn program into a TURKEY application )
```

```
CR CR CR
```

```
.( Write protect STATIC memory and reset the computer )
```

```
EOF
```

P.2 LQG Compensator with Accelerometer Sensor

The FORTH code which implements the LQG compensator (sections 0.2 and 0.3) is listed below. The algorithm has an initial phase to bring the robot up to the nominal wheel speed, Ω_0 , where after the LQG compensator is invoked to start the balancing process.

The compensator is implemented in modal form since it requires fewer arithmetic operations. Floating point arithmetic is used because of its convenience and the fact that the calculation time is not that critical due to the prediction estimator that is used.

```
( CTRL-C program : ucyc6/lgtqlqg.ctr )

( ----- Longitudinal Control Turnkey Program ----- )

( Discrete LQG compensator with integral error feedback of wheel speed )

O VERIFY !
LOAD/TARGET ( Turn echoing off during downloading )

( ===== DEFINE ADDRESSES AND CONSTANTS ===== )

HEX

800000 CONSTANT LATDACADDR ( Set LAT DAC's address )
800010 CONSTANT LGTDACADDR ( Set LGT DAC's address )
800020 CONSTANT LATENCADDR ( Set LAT Encoder's address )
```

APPENDIX P. FORTH CODES FOR LONGITUDINAL CONTROL

800030 CONSTANT LGTENCADDR (Set LGT Encoder's address)
 800080 CONSTANT RCCOUNTER0 (Radio Receiver Interface)
 800082 CONSTANT RCCOUNTER1 (Counter Addresses)
 800084 CONSTANT RCCOUNTER2
 800086 CONSTANT RCCONTROLWORD (Counter Controlword address)
 800090 CONSTANT RCTRIGGER (Trigger address to RESET IRQ flip-flop)

68 CONSTANT LEVEL2_IRQ (Level2 Autovector Address)

8000D0 CONSTANT S8ADDR (Sample & Hold's address)
 8000E0 CONSTANT MUXADDR (Multiplexer's address)
 8000F0 CONSTANT ADCADDR (Analog-to-Digital Converter's address)

0 CONSTANT LATACCHX (MUXCode for Lateral Accelerometer)
 1 CONSTANT LGTACCHX (MUXCode for Longitudinal Accelerometer)

81000F CONSTANT RTCctrlADDR (Set Real Time Clock's Ctrlword address)
 81000B CONSTANT RTCcounter1 (Set Real Time Clock's Counter 1 address)

DECIMAL

VARIABLE LATPWM (Lateral Radio Pulse Width)
 VARIABLE LGTPWM (Longit. Radio Pulse Width)

VARIABLE LATDACCHD (Commanded Lateral Current)
 VARIABLE LGTDACCHD (Commanded Longitudinal Current)

VARIABLE TICKSAVE (Memory location to save tick count)

VARIABLE LgtSBflag (SPEED_UP / BALANCE flag)
 VARIABLE LgtEncCount (Counter for 8 wheel speeds to average)
 VARIABLE SpeedUpCount (Counter for period in SPEED_UP mode)
 VARIABLE STORECount (Counts numbers stored in STORE arrays)

P.2. LQG COMPENSATOR WITH ACCELEROMETER SENSOR

329

```

VARIABLE PanicFlag ( 1 => panic ; 0 => everything OK )

240 CONSTANT STORELength ( max # of entries which in array STORE1 )
0 CONSTANT CHANNEL0

1200 CONSTANT STOPperiod1 ( Real Time Clock Timer 1 initial count ;

( NOTE : Must do Radio Initialization code BEFORE Math words are included )

( ***** RADIO RECEIVER READING WORDS ***** )

CODE RADIO_READ ( Reads Radio Receiver Channels upon IRQ )
MOVE.L D0,-(A6) ( saves contents of D0 on stack )
MOVE.L $24(A4),-(A6)
MOVE.L D6,(A3)+
MOVE.L D6,D6
MOVE.L (A6)+,D6
MOVE.B $821,RCCONTROLWORD ( Latches all counts )
MOVE.W RCCOUNTER1,D0 ( Reads LSB of Counter1 )
MOVE.B D0,LATPW ( Save temporary )
MOVE.W RCCOUNTER1,D0 ( Reads MSB of Counter1 )
LSL.W $8,D0
MOVE.B LATPW,D0 ( Get LSB )
MOVE.W D0,LATPW ( Save )
MOVE.W RCCOUNTER2,D0 ( Reads LSB of Counter2 )
MOVE.B D0,LATPW ( Save temporary )
MOVE.W RCCOUNTER2,D0 ( Reads MSB of Counter2 )
LSL.W $8,D0
MOVE.B LATPW,D0 ( Get LSB )
MOVE.W D0,LATPW ( Save )
MOVE.B $83F,RCCONTROLWORD ( Rewrites Ctrlword to 1 )
MOVE.B $0,RCCOUNTER1 ( Write LSB of initial counter1 )
MOVE.B $0,RCCOUNTER1 ( Write MSB of initial counter1 )
MOVE.B $84F,RCCONTROLWORD ( Rewrites Ctrlword to 2 )
MOVE.B $0,RCCOUNTER2 ( Write LSB of initial counter2 )
MOVE.B $0,RCCOUNTER2 ( Write MSB of initial counter2 )
MOVE.B $1,BCTRIGGER ( Reset IRQ flip-flop on Radio Int )

```

APPENDIX P. FORTH CODES FOR LONGITUDINAL CONTROL

```

MOVE.L D6,-(A6)
MOVE.L D5,D6
MOVE.L -(A3),D6
MOVE.L (A6)+,$24(A4)
MOVE.L (A6)+,CC ( Restores original value of D0 )
RTE ( Return from exception routine )

END-CODE
CR .( Loaded RADIO_READ )

: RADIO_INIT ( Initialize Radio Control Interface & Interrupt )

['] RADIO_READ ( Initialize Radio Receiver ... )
LEVEL2_IRQ ! ( ... Level 2 Autovector )

BINARY

10001111 RCONTROLWORD C! ( Set Counters 1,2 )
01001111 RCONTROLWORD C! ( for Mode 0 )

1  RCTRIGGER    C!    ( Reset IRQ flip-flop on Radio Intf )

DECIMAL ;

RADIO_INIT ( Do radio receiver interrupt initialization )

( NOTE : Must do Radio Initialization code BEFORE Math words are included )

( ***** REAL TIME CLOCK REPROGRAMMING WORDS ***** )

CODE RTCset ( Sets RT Clock Counter 1 to sample rate )
MOVE.L D0,-(A6) ( saves contents of D0 on stack )

MOVE.B $374,RTCtrlADDR ( Rewrites Ctrlword for counter 1 )

```


P.2. LQG COMPENSATOR WITH ACCELEROMETER SENSOR

331

```
MOVE.W SRTCperiod1,D0
MOVE.B D0,RTCCounter1 ( Send low byte )
LSR.W #8,D0
MOVE.B D0,RTCCounter1 ( Send high byte )

MOVE.L (A6)+,DC ( Restores original value of D0 )
RTS ( Return to subroutine )

END-CODE

CR . ( Loaded RTCCast )

ALSO MATH ( include floating point processor words )
FP32 ( set for 32 bit floating point numbers )

3. PCONSTANT Omega0 ( Nominal wheel speed )

19.8 PCONSTANT LAT10Hrtorq ( Lateral 10*Ngear*Ktorque )
15.12 PCONSTANT LGT10Hrtorq ( Longit. 10*Ngear*Ktorque )

0.35048 PCONSTANT LATACCGAIN ( LAT Accel'meter calibr constant )
-0.31576 PCONSTANT LGTACCGAIN ( LGT Accel'meter calibr constant )
( in units of m/s^2 per volt )

1. PCONSTANT LGTpt ( LGT tach comp pole )
0.9 PCONSTANT LGTzt ( LGT tach comp zero )
16. PCONSTANT LGTKt ( LGT tach comp gain )

FVARIABLE LGTcommand ( LGT command from radio receiver )
FVARIABLE LGTtach_meas ( LGT tachometer meas )
FVARIABLE LGTacc_meas ( LGT accelerometer meas )

FVARIABLE LATcommand ( LAT command from radio receiver )
FVARIABLE LATtach_meas ( LAT tachometer meas )
FVARIABLE LATacc_meas ( LAT accelerometer meas )
```

APPENDIX P. FORTH CODES FOR LONGITUDINAL CONTROL

```

FVARIABLE thetadot ( Plant theta_dot )
FVARIABLE omega ( Plant omega )
FVARIABLE theta ( Plant theta )

FVARIABLE LGTVelError ( LGT velocity error )

FVARIABLE LGTatk ( LGT tach loop compensator state )

FVARIABLE LGTchat1k ( modal compensator state )
FVARIABLE LGTchat2k ( modal compensator state )
FVARIABLE LGTchat3k ( modal compensator state )
FVARIABLE LGTchat4k ( modal compensator state )

FVARIABLE EtaSign ( Sign of Turntable speed ETA )
FVARIABLE OmegaSign ( Sign of Wheel speed OMEGA )

FVARIABLE LGTcontrolTorq ( Qcontrol = Qv of simulations )
FVARIABLE LGTTorqAverage ( Average Longit Torque = Qfric )
FVARIABLE LGTtotalTorq ( Qtotal = Qfric + Qcontrol )

FVARIABLE OmegaOAverage ( Average Wheel Speed )

FVARIABLE OmegaOAccum ( Wheel Speed Accumulator )
FVARIABLE LGTTorqAccum ( Longit Torque Accum. )

FVARIABLE STORE1 STORELength 4 * VALLOT ( Time history )
FVARIABLE STORE2 STORELength 4 * VALLOT ( arrays )
FVARIABLE STORE3 STORELength 4 * VALLOT

400 1000 BACKGROUND SLAVE
400 1000 TERMINAL BOSS

( ***** DIGITAL-TO-ANALOG CONVERTER WORDS ***** )

```

P.2. LQG COMPENSATOR WITH ACCELEROMETER SENSOR

333

```

: WAS 5000 0 DO 1000 1000 = DROP LOOP : ( General purpose S/W wait loop )

: ?DACSATURATE ( n - n ) ( Check if DAC command Saturates )
DUP 4095 > ( check for positive saturation )
IF DROP 4095 ( drop large value & supply sat. value )
ELSE DUP 0 < ( check for negative saturation )
IF DROP 0 ( drop large value & supply sat. value )
THEN THEN : ( otherwise keep commanded DAC value )

: LATDAC ( in - ) ( Get 12 bit binary <-> Qt )
LATIONKtorq P/ ( divide by 10*Ngear*Ktorque )
1. PSWAP P- 2048. P=
P>I ?DACSATURATE ( check if 0 < BINARY < 4096 )
LATDACADR W! : ( write 16 bit word to LATDAC )

: LGTDAC ( in - ) ( Get 12 bit binary <-> Qv )
PNEGATE ( so that Qv > 0 causes Omega0 > 0 )
LGTIONKtorq P/ ( divide by 10*Ngear*Ktorque )
1. PSWAP P- 2048. P=
P>I ?DACSATURATE ( check if 0 < BINARY < 4096 )
LGTDACADR W! : ( write 16 bit word to LGTDAC )
CR .( Loaded LGTDAC )

: S 0. LATDAC 0. LGTDAC : ( Quick way to stop motors )

( ***** ANALOG-TO-DIGITAL CONVERTER WORDS ***** )

: WAIT4N ( n - ) ( S/W WAIT for n*4 microseconds )
0 DO LOOP :

: MUXSWITCH ( n - ) ( switches MUX to specified input channel n )
MUXADR W!
1 WAIT4N : ( waits 4 microsec. for MUX to settle )

: SAMPLEHOLD ( - ) ( SAMPLE and HOLD command )
1 SBRADR W! ( sample analog signal )
7 WAIT4N ( waits 28 microsec. for S&H to settle )

```

APPENDIX P. FORTH CODES FOR LONGITUDINAL CONTROL

```
0 SHADDER W! ; ( place S&H device in HOLD mode )
```

```
: AD_CONVERTER ( - n ) ( Do Analog to Digital Conversion )
```

```
1 ADCADDR W! ( Starts A to D Converter )
```

```
9 WAITs ( waits 30 microsec. for ADC to finish )
```

```
ADCADDR W@ : ( Reads the digital result from the ADC )
```

```
: AtoD_CONVERT ( n - n ) ( Input Channels ; Output Digitize value )
```

```
MUXSWITCH ( Complete process for an AtoD Conversion )
```

```
SAMPLERHOLD
```

```
AD_CONVERTER ;
```

```
( ***** ACCELEROMETER READING WORDS ***** )
```

```
: RLATACC ( - fn ) ( Reads acceleration as the instrument sees it )
```

```
4095
```

```
LATACCW@ AtoD_CONVERT ( Reads binary value from A/D )
```

```
- D/F ( Converts to floating point s )
```

```
0.004884 F*
```

```
10.00356 FSWAP F- ( Get analog voltage )
```

```
LATACCGAIN F* ( Multiply by calibr. constant to get ... )
```

```
: ( real acceleration seen by the instrument )
```

```
: RLGTACC ( - fn ) ( Reads acceleration as the instrument sees it )
```

```
4095
```

```
LGTACCW@ AtoD_CONVERT ( Reads binary value from A/D )
```

```
- D/F ( Converts to floating point s )
```

```
0.004884 F*
```

```
10.00356 FSWAP F- ( Get analog voltage )
```

```
LGTACCGAIN F* ( Multiply by calibr. constant to get ... )
```

```
: ( real acceleration seen by the instrument )
```

```
CR . ( Loaded RLGTACC )
```

```
( ***** POSITION ENCODER READING WORDS ***** )
```

```

: RLATENC ( - fn ) ( Read Turntable Speed ETA )
LATENCADDR W0 ( Read number of clock pulses counted )
DUP 2 MOD 0= ( 0 => even number => negative speed )
IF -1. EtaSign P! ( 1 => odd number => positive speed )
ELSE 1. EtaSign P!
THEN D/F ( Convert encoder reading to float. point )
27.2708 PSWAP F/
EtaSign P0 P0 ; ( Turntable Speed ETA in rad/sec )

: RLCTENC ( - fn ) ( Read Wheel Speed OMEGA )
LCTENCADDR W0 ( Read number of clock pulses counted )
DUP 2 MOD 0= ( 0 => even number => negative speed )
IF -1. OmegaSign P! ( 1 => odd number => positive speed )
ELSE 1. OmegaSign P!
THEN D/F ( Convert encoder reading to float. point )
10471.9755 PSWAP F/
OmegaSign P0 P0 ; ( Wheel Speed OMEGA in rad/sec )

CR .( Loaded RLCTENC )

( ***** REAL TIME CLOCK READING WORDS ***** )

CODE ZEROtheTICKS ( - ) ( Zeroes the tick counter register )
CLR.L (A5)
RTS
END-CODE
CR .( Loaded ZEROtheTICKS )

CODE TICKStoSTACK ( - n ) ( Loads tick count on top of stack )
MOVE.L (A5),-(A6) ( Current tick counter value onto stack )
RTS
END-CODE
CR .( Loaded TICKStoSTACK )

( ***** RADIO RECEIVER READING WORDS ***** )

: RLATPWH ( - LatR/C ) ( Read Lateral radio command )

```

APPENDIX P. FORTH CODES FOR LONGITUDINAL CONTROL

```

LATPMW W0 5164 - ( Remove bias )
DP 1700. F/ : ( Scale to a value between -1 and +1 )

: RLGTPMW ( - LgtR/C ) ( Read Longit. radio command )
  LGTPMW W0 5164 - ( Remove bias )
  DP -1700. F/ : ( Scale to a value between -1 and +1 )
  CR . ( Loaded RLGTPMW )

( ===== CONTROL SYSTEM ALGORITHM WORDS ===== )

: CHECKSAMPLE ( - f ) ( Check if sample time has expired )
  TICKStoSTACK ( get tick count )
  0 > : ( sets true flag if dt >= Tsample )
  CR . ( Loaded CHECKSAMPLE )

: READ_SENSORS ( - ) ( reads radio commands, tachos & accelerometers )

  RLGTACC ( Reads Longitud. acceleration : ya )
  LGTacc_meas F! ( save the accelerometer measurement ya )

  RLATACC ( Reads lateral acceleration as seen by sensor )
  LATacc_meas F!

  RLGTENC ( Reads wheel speed - pitch rate )
  LGTtach_meas F! ( Saves longit. tach measurement yt )

  RLATENC ( Reads turntable speed relative to frame : "eta" )
  LATtach_meas F! ( Saves lateral tach measurement yt )

  RLGTPMW ( Reads command from radio receiver )
  FDRMP 0. ( Temporary no additional wheel speed commanded )
  Omega0 F+ ( Add nominal wheel speed )
  LGTcommand F! ( Saves Longit. command )

  RLATPMW ( Reads command from radio receiver )
  LATcommand F! : ( Saves Lateral command )

```

```

CR .( Loaded READ_SENSORS )

: PLANTmodel ( Plant model for simulation purposes )

( First calculate  $y(k) = Rx(k) + zn(k)$  : )
omega P0 thetadot P0 F- LGTtach_meas F! ( simulated tach meas. )

0.0011 omega P0 thetadot P0 F- P0
4.67 theta P0 P0 F+
-.023 LGTtotalTorq P0 P0 F+ ( direct feedthrough term )
LGTacc_meas F! ( simulated acc measurement )

( simulate state transitions :  $x(k+1) = PHI \cdot x(k) + GAMMA \cdot u(k)$  )
1.0162 thetadot P0 P0
0.0008 omega P0 P0 F+
1.3632 theta P0 P0 F+

-0.0178 LGTtotalTorq P0 P0 F+
( thetadot(k+1) remains on stack )

-0.0445 thetadot P0 P0
0.9971 omega P0 P0 F+
-3.7957 theta P0 P0 F+

0.0607 LGTtotalTorq P0 P0 F+
( omega(k+1) remains on stack )

0.0251 thetadot P0 P0
0.0 omega P0 P0 F+
1.0171 theta P0 P0 F+

-0.0002 LGTtotalTorq P0 P0 F+
( theta(k+1) remains on stack )

```

APPENDIX P. FORTH CODES FOR LONGITUDINAL CONTROL

```

theta    F!
omega    F!
thetadot F!

```

```

( CR ." thetadot = " thetadot F0 F. )

```

```

( CR ." omega = " omega F0 F. )

```

```

( CR ." theta = " theta F0 F. )

```

```

: GetAverageOmega0 ( - ) ( Checks if Average Omega0 ... )
  ( close to desired Omega0 )

```

```

  LgtEncCount @ D- PDUP ( number of numbers in accumulators )

```

```

  Omega0Accum F0 PSWAP F/ ( calculate average wheel speed )

```

```

  Omega0Average F! ( stores the value )

```

```

  LGTTorqAccum F0 PSWAP F/ ( calculate average friction torque )

```

```

  LGTTorqAverage F! ( stores the value )

```

```

  0. Omega0Accum F! ( Clears the accumulator )

```

```

  0. LGTTorqAccum F! ( Clears the accumulator )

```

```

  0 LgtEncCount ! ( Resets counter )

```

```

  1 SpeedUpCount +! ( increment counter )

```

```

  SpeedUpCount @ 3 > ( check if 300 sample periods have passed )

```

```

  IF 1 LgtSRflag ! ( Set flag => BALANCE routine next time )

```

```

  0 SpeedUpCount ! ( Reset counter )

```

```

  THEN ;

```

```

  CR . ( Loaded GetAverageOmega0 )

```

```

: CHECK_SPEED ( - ) ( Check if wheel speed is up to Omega0 )

```

```

  LGTtach_meas F0 ( Reads Wheel speed onto Floating Point stack )

```

```

  Omega0Accum F0 F+ Omega0Accum F! ( Accumulate Speeds )

```


P.2 LQG COMPENSATOR WITH ACCELEROMETER SENSOR

339

```

LGTtotalTorq P0 ( Reads latest commanded wheel torque )
LGTtorqAccum P0 P+ LGTtorqAccum P! ( Accumulate torques )

1 LGTEncCount +! ( Increments 8 wheel speeds stored counter )
LGTEncCount 8 100 > ( Check if enough values saved on stack )
IF GetAverageOmega0
THEN ;
CR .( Loaded CHECK_SPEED )

: SPEED_UP ( Tachometer FB compensation to speed up wheel to Omega0 )

Omega0 ( nominal wheel speed )
RLGTENC FDUP LGTtach_meas P! ( reads wheel speed and saves it )
P- LGTVelError P! ( present velocity error )

LGTpt LGTst P- LGTtrk P0 P- LGTVelError P0 P+ LGTtrk P0
FDUP LGTDAC ( Issues wheel torque command through D/A )
LGTtotalTorq P! ( Saves the control command )

LGTVelError P0 LGTpt LGTtrk P0 P- P+
LGTtrk P! ( Update tach comp state for next Tsample )

CHECK_SPEED : ( Check if wheel speed is up to Omega0 )

: LGT_CONTROL ( Calculates the LGT contr output for this sample instant )

LGTtorqAverage P0
LGTctrlTorq P0 P+ ( Add control torque to friction torque )
FDUP LGTtotalTorq P! ( save the total torque commanded )
LGTDAC ; ( Output torque command to wheel motor )
CR .( Loaded LGT_CONTROL )

: LGTCompUpdate ( Updates LGT compensator states and control ... )
( for next Tsample )

-0.0564 LGTtrk P0 P-

```

APPENDIX P. FORTH CODES FOR LONGITUDINAL CONTROL

```

4.6483 LGTtach_meas F0 F0 F+
-0.5677 LGTacc_meas F0 F0 F+
0.0521 LGTcommand F0 F0 F+
    LGTzhat1k    F!    ( store z1hat(k+1) for next Tsample )

0.9314 LGTzhat2k    F0 F0
0.0506 LGTtach_meas F0 F0 F+
-0.0051 LGTacc_meas F0 F0 F+
-0.0008 LGTcommand F0 F0 F+
    LGTzhat2k    F!    ( store z2hat(k+1) for next Tsample )

1.0011 LGTzhat3k    F0 F0
0.2574 LGTtach_meas F0 F0 F+
-0.0476 LGTacc_meas F0 F0 F+
-0.2435 LGTcommand F0 F0 F+
    LGTzhat3k    F!    ( store z3hat(k+1) for next Tsample )

1.2545 LGTzhat4k    F0 F0
-1.2481 LGTtach_meas F0 F0 F+
0.2868 LGTacc_meas F0 F0 F+
-0.0448 LGTcommand F0 F0 F+
    LGTzhat4k    F!    ( store z4hat(k+1) for next Tsample )

-1.1031 LGTzhat1k    F0 F0 ( calculate control torque ... )
-2.1475 LGTzhat2k    F0 F0 F+ ( command for next Tsample )
-0.0305 LGTzhat3k    F0 F0 F+
1.3899 LGTzhat4k    F0 F0 F+
LGTcontrolTorq F! ; ( save u(k+1) )

```

```

: CONTROL_SYSTEM ( CONTROL of lateral & longitudinal motion )

```

```

PanicFlag 0 C= ( Check the panic flag first )

```

```

IF ( If zero => no panic )

```

```

    LGTcommand F0 F0

```

```

    -0.5 F0 0.5 F0 C= ( check if -0.5 < LGTstick < 0.5 )

```

P.2. LQG COMPENSATOR WITH ACCELEROMETER SENSOR

341

```

IF 1 PanicFlag ! ( Set panic flag )
ELSE LGT_CONTROL ( Do LGT system control )
THEN
ELSE      ( Panic Mode : Command LGT torque directly from R/C )
    LGTcommand P0 LGT10Ktorq P0 LGTDAC
    THEN
        LATcommand P0      ( get Lateral Radio Command )
        LAT10Ktorq P0      ( Lat Lateral Stick control turntable torque )
        LATDAC ;           ( Output as a Current Command to Lat motor )

CR .( Loaded CONTROL_SYSTEM )

: STORETimeHistory ( Stores a time history of a variable )

STORELength STORECount 0 > ( check all data stored ? )
IF
    LGTtotalTorq P0 ( get the variable to be stored )
    STORE1 STORECount 0 2* 2* + P! ( increment index by 4 .. )
    ( to store Fl. Pt. 8 )

    LGTtach_meas P0 ( get the variable to be stored )
    STORE2 STORECount 0 2* 2* + P!

    LGTacc_meas P0 ( get the variable to be stored )
    STORE3 STORECount 0 2* 2* + P!

1 STORECount +!      ( increment index )

THEN ; ( increments array pointer )

: WORK ACTIVATE ( Activate Background task )
S ( Stop all motors )
RADIO_INIT ( Initialize Radio receiver )

0. LGTtotalTorq P! ( Initial LGT control torque = 0 )
Omega0 LGTcommand P! ( Initial LGT ref input = 0 )

```

APPENDIX P. FORTH CODES FOR LONGITUDINAL CONTROL

```

Omega0 LGTtach_meas F! ( Initial LGT tachometer meas = 0 )
0. LGTacc_meas F! ( Initial LGT accel meas = 0 )

0. LGTVelError F! ( Initial LGT velocity error = 0 )

C. thetadot F! ( Initialize plant = 1mm, states )
Omega0 omega F!
0. theta F!

0. LGTtrk F! ( Initialize SPEED_UP comp state )

13.3487 LGTxbat1k F! ( Initialize the modal ... )
3.4915 LGTxbat2k F! ( compensator states )
-38.7439 LGTxbat3k F!
15.2396 LGTxbat4k F!

0. Omega0Accum F! ( Zero wheel speed Accumulator )
0. LGTTorqAccum F! ( Zero wheel torque Accumulator )

0. LGTTorqAverage F! ( Zero friction torque )
0.141 LGTControlTorq F! ( Steady st. ctrl torque(Qe) ... )
( for Omega0 )

0 LgtEncCount ! ( Counter for 8 wheel speeds to average )
0 SpeedUpCount ! ( Counter that determines how long to SPEED_UP )
0 PanicFlag ! ( Start with no panic condition )

0 STORZCount ! ( initialize STORZ array counter )

0 LgtSBFlag ! ( Start with speed-up algorithm )

RTCset ( Set Real Time clock to Tsample )

BEGIN
CHECKTSAMPLE ( Check if sample time has expired )
IF ZEROtheTICKS ( If TRUE Reset cntr = 0 ... )

```

P.2. LQG COMPENSATOR WITH ACCELEROMETER SENSOR

343

```

LgtSBflag ← 0 ← ( Speed_up/Balance Flag = ? .. )
IF SPEED_UP ( 0 ⇒ speed up wheel )
ELSE ( 1 ⇒ do balance algorithms )

LGT_CONTROL ( calculate LGT control torque )
STOREtimeHistory ( Stores a time histories )

READ_SENSORS ( Read all the sensors simultaneously )

( PLANTmodel simulate plant model to predict states .. )
( and measurements at next sample )

LGTCompUpdate ( Update LGT comp states for next Ts )
THEN THEN PAUSE ( Go do terminal task )

AGAIN ;

( *** BUILDING OF TERMINAL & BACKGROUND TASKS FOR TURKEY APPLICATION *** )

: WHIP ( Build and Activate Background task )
SLAVE BUILD
SLAVE WORK ;

: KEY ( Check if key was depressed )
BEGIN
PAUSE
?TERMINAL
DUP
IF
KEY DROP
THEN
UNTIL ;

: PRINT ACTIVATE ( Activate Terminal task )
-1 INIT-DISK ( reset all disk drives )
BEGIN
CR

```

APPENDIX P. FORTH CODES FOR LONGITUDINAL CONTROL

```

." Press any key to see BACKGROUND variable "
?KEY
CR ." qw=[ "
STORELength 0 DO
  STORE1 I 2* 2* + P0
  I 7 MOD 0= IF ." .. " CR
  THEN P. ." "
  PAUSE LOOP

CR ." ytach=[ "
STORELength 0 DO
  STORE2 I 2* 2* + P0
  I 7 MOD 0= IF ." .. " CR
  THEN P. ." "
  PAUSE LOOP

CR ." yacc=[ "
STORELength 0 DO
  STORE3 I 2* 2* + P0
  I 7 MOD 0= IF ." .. " CR
  THEN P. ." "
  PAUSE LOOP

:AGAIN ;

: START
  CHAMELO BOSS BUILD ( Initializes Terminal Task )
  BOSS PRINT
  WHIP : ( Initializes Background Task )

  TURKEY START ( Turn program into a TURKEY application )

CR CR CR
.( Writes protect STATIC memory and reset the computer )

END

```

P.3 Successive Loop Closure and Pitch Sensor

The FORTE code which implements the compensator designed by successive loop closure (section O.5) with a pitch angle sensor, is listed below. The particular print-out is for balancing the robot at zero speed, but it can be modified to balance longitudinally, at any wheel speed by changing the Ω constant.

Fixed point arithmetic had been used and wheel speed and control torque was scaled up by a factor of 10^3 while the accelerometer was scaled up by 10^6 .

Comments in the program listing explains the operations in the algorithm.

```
( ----- Longitudinal Control Turnkey Program ----- )
```

```
( Program to test ucyc7/lgtatch controller : Tsample = 25 milliseconds )
```

```
( Tight tach feedback loop closed first with integral error control)
```

```
( Use LORET pitch angle sensor )
```

```
0 VERIFY :
```

```
LOAD/TARGET ( Turn echoing off during downloading )
```

```
( ===== DEFINE ADDRESSES AND CONSTANTS ===== )
```

```
HEX
```

```
800000 CONSTANT LATDACADR ( Set LAT DAC's address )
```

```
800010 CONSTANT LGTDACADR ( Set LGT DAC's address )
```

```
800020 CONSTANT LATENCADR ( Set LAT Encoder's address )
```

```
800030 CONSTANT LGTENCADR ( Set LGT Encoder's address )
```

APPENDIX P. FORTH CODES FOR LONGITUDINAL CONTROL

800080 CONSTANT RCCOUNTER0 (Radio Receiver Interface)
 800082 CONSTANT RCCOUNTER1 (Counter Addresses)
 800084 CONSTANT RCCOUNTER2
 800086 CONSTANT RCCONTROLWORD (Counter Controlword address)
 800090 CONSTANT RSTRIGGER (Trigger address to RESET IRQ flip-flop)
 68 CONSTANT LEVEL2_IRQ (Level2 Autovector Address)
 8000D0 CONSTANT SRHADDR (Sample & Hold's address)
 8000E0 CONSTANT MUXADDR (Multiplexer's address)
 8000F0 CONSTANT ADCADDR (Analog-to-Digital Converter's address)
 0 CONSTANT LATACCODE (MUXCode for Lateral Accelerometer)
 1 CONSTANT LGTACCODE (MUXCode for Longitudinal Accelerometer)
 81000F CONSTANT RTCCtrlADDR (Set Real Time Clock's Controlword addr.)
 81000B CONSTANT RTCCOUNTER1 (Set Real Time Clock's Counter 1 address)
 0 CONSTANT CHANNEL0 (Terminal task number)

DECIMAL

15 CONSTANT LGTKt (Tach loop gain)
 -40 CONSTANT LGTKa (Acc loop gain)
 0 CONSTANT Omega0 (nominal wheel speed*10e3)
 320 CONSTANT STORELength (data storage array STOREi length)
 1250 CONSTANT RTCperiod1 (Real Timer Clock Timer 1 initial count)
 (for 40 hz sampling freq)

VARIABLE LATPWH (Lateral Radio Pulse Width)

VARIABLE LGTPWH (Longit. Radio Pulse Width)

VARIABLE TICKSAVE (Memory location to save tick count)

VARIABLE LgtEncCount (Counter for 8 wheel speeds to average)

P.3. SUCCESSIVE LOOP CLOSURE AND PITCH SENSOR

347

VARIABLE SpeedUpCount (8 sample periods in SPEED_UP mode)

VARIABLE STORECount (Counter for 8 numbers stored)

VARIABLE LOTCmd (LOT acceleration command *10e6)

VARIABLE LOTstat (LOT tachometer compensator state *10e6)

VARIABLE LOTTrk (LOT tachometer compensator state *10e3)

VARIABLE Ttach3 (Tachometer measurement *10e3)

VARIABLE Tacc6 (Accelerometer measurement * 10e6)

VARIABLE Qw3 (Wheel Torque *10e3)

400 1000 BACKGROUND SLAVE

400 1000 TERMINAL BOSS

(***** REAL TIME CLOCK REPROGRAMMING WORDS *****)

CODE RTCset (Sets Real Time Clock Counter 1 to sample rate)

MOVE.L D0,-(A6) (saves contents of D0 on stack)

MOVE.B #\$74,RTCCtrlADDR (Rewrites Ctrlword for counter 1)

MOVE.W RTCCperiod1,D0

MOVE.B D0,RTCCcounter1 (Send low byte)

LSR.W #8,D0

MOVE.B D0,RTCCcounter1 (Send high byte)

MOVE.L (A6)+,D0 (Restores original value of D0)

RTS (Return to subroutine)

END-CODE

CR .(Loaded RTCset)

ALSO MATH

APPENDIX F. FORTH CODES FOR LONGITUDINAL CONTROL

FP32

FVARIABLE STORE1 STORELength 2* 2* VALLOT (Time history)
 FVARIABLE STORE2 STORELength 2* 2* VALLOT (storage arrays)
 FVARIABLE STORE3 STORELength 2* 2* VALLOT

(.....)

CODE ZEROthetICKS (-) (Zeros the tick counter register)

CLR.L (A5)

RTS

END-CODE

CR .(Loaded ZEROthetICKS)

CODE TICKStoSTACK (- n) (Loads tick count on top of stack)

MOVE.L (A5),-(A6) (Current tick counter value -> stack)

RTS

END-CODE

CR .(Loaded TICKStoSTACK)

(..... CONTROL SYSTEM ALGORITHM WORDS)

: S 2048 LATDACADDR W! 2048 LGTDACADDR W! ; (Quick motors stop)

: ?DACSATURATE (n - n) (Check if DAC command saturates)

DUP 4096 > (check for positive saturation)

IF DROP 4096 (drop large value & supply sat. value)

ELSE DUP 0 < (check for negative saturation)

IF DROP 0 (drop large value & supply sat. value)

THEN THEN ; (otherwise keep commanded DAC value)

: WAIT4N (n -) (S/V WAIT for n*30 microseconds)

0 DO LOOP ;

: CHECKTSAMPLE (- f) (Check if sample time has expired)

TICKStoSTACK (get tick count)

0 > ; (sets true flag if dt >= Tsample)

CR .(Loaded CHECKTSAMPLE)

P.3. SUCCESSIVE LOOP CLOSURE AND PITCH SENSOR

349

```

: WORK ACTIVATE ( Activate Background task )
S ( Stop all motors )

0 LGTCmd ! ( Initial LGT reference input assumed = 0 )
0 LGTtrk ! ( Initialize tech. comp. state to zero )
0 LGTmak ! ( Initialize acc. comp. state to zero )

0 SpeedUpCount ! ( Initialize SPEED_UP counter )

0 STORECount ! ( Initialize STOREi array entry counter )

RTClst ( Set Real Time clock to Tsample )

BEGIN

CHECKTSAMPLE ( Check if sample time has expired )
IF ZEROthetICKS ( If TRUE Reset counter to zero . . . )

( ===== READ LGT TACHOMETER AND ACCELEROMETER ===== )

LGTENCADR W0 ( read binary value from pos enc )
( Bt <- top of stack )

LGTACCHIX MIXADOR W! ( switch MIX to LGT accelerometer )
1 S8HADR W! ( sample analog signal )
1 WAIT4M ( wait 30 microsec for S8H settle )
0 S8HADR W! ( place S8H device in HOLD mode )

1 ADCADR W! ( Starts A to D Converter )
1 WAIT4M ( wait for ADC to finish )

ADCADR W0 ( reads binary value from A/D )
( Bt Bn <- top of stack )

4095 - 4884 = 10003660 + ( convert to a voltage=10e6 )
20435 1000000 =/ ( scale by LGTACCGAIN => acc=10e6 )
( Bt Ya6 <- top of stack )

```

APPENDIX P. FORTH CODES FOR LONGITUDINAL CONTROL

```

    DUP Yacc6 ! ( save copy of accel to print )
    ( Bt Yacc6 <- top of stack )

    SpeedUpCount 0 0 > ( check if speed-up phase over )

    ( ===== ACCELEROMETER LOOP COMPENSATION ===== )

    IF ( if so , add accelerometer compensation )

        LGTCmd 0 ( get acceleration command )
        5 100 */ ( mult. by Kr to get 10e6 = accel. command )
        SWAP - ( subtract Yacc6 to get acc. error=10e6 )
        DUP ( save a copy for compensator update later )
        ( Bt Ea6 Ea6 <- top of stack )

        LGTnak 0 ( get LGT accelerometer compensator state )
        ( Bt Ea6 Ea6 Yacc6 <- top of stack )
        8 100 */ + ( multiply by pa-za and add to acc. error )

        LGTKa 1000 */ ( mult. by LGTKa, div. by 1000 -> da=10e3 )
        ( Bt Ea6 da6 <- top of stack )

        ELSE ( during speed-up do tach loop compens. only )

            DROP ( drop Yacc6 from top of stack )
            0 0 ( supply zeros for Ea6 and da3 )
            ( Bt 0 0 <- top of stack )

            ( ===== TACHOMETER LOOP COMPENSATION ===== )

            THEN ( do tachometer compensation loop )

            Omega0 + ( wheel speed + da3 )
            ( Bt Ea6 sum <- top of stack )

            ROT ( get binary tach reading )

```

P.3. SUCCESSIVE LOOP CLOSURE AND PITCH SENSOR

351

```
( Ea6 sum Bt <- top of stack )

DUP ( make a copy to )
( determine sign later )
10471976 SWAP / ( get abs(ytach)=10e3 )

SWAP 2 MOD C= ( get sign of the wheel speed : )
IF NEGATE THEN ( 0 => even & => neg. speed )
( Ea6 sum Yt3 <- top of stack )

DUP Ytach3 ! ( save a copy to print later )
( Ea6 sum Yt3 <- top of stack )

( get velocity error=10e3 )
- ( Ea6 Et3 <- top of stack )

DUP ( Save copy for tach comp update )
( Ea6 Et3 Et3 <- top of stack )

LGTxrk * ( Get LGT tach compensator state )
( Ea6 Et3 Et3 Itk <- top of stack )

25 100 */ + ( multiply by pt-rt and )
( add tach error )

LGTkt * ( multiply with tach loop gain to )
( Wheel torque=10e3 )
( Ea6 Et3 Qu3 <- top of stack )

DUP Qu3 ! ( make a copy to print later )
( Ea6 Et6 Qu3 <- top of stack )

15120 + 2048 15120 */ ( get binary command for DAC )

?DACSATURATE ( check if DAC saturates )

LGTDACADDR W! ( output torque command )
```

APPENDIX P. FORTH CODES FOR LONGITUDINAL CONTROL

```

( Ea6 Et3<- top of stack )

( ===== COMPENSATOR STATE UPDATE ===== )

LGTxk @ ( get LGT tach compens state )
( Ea6 Et3 It3 <- top of stack )

100 100 */ ( multiply by LGTpt )
+ LGTxk ! ( add to the tach. error and save xhat(k+1) )
( Ea6 <- top of stack )

LGTxak @ ( get LGT accelerometer compensator state )
( Ea6 Ia6 <- top of stack )

103 100 */ ( multiply by LGTpa )
+ LGTxak ! ( add to the acc. error and save xhat(k+1) )
( stack empty <- top of stack )

1 SpeedUpCount +! ( increment speed-up counter )

( ===== STORE TIME HISTORY ===== )
STORECount @ STORELength <
IF
Qw3 @ D/F 1000. F/ ( Scale back to normal )
STORE1 STORECount @ 2* 2* + F! ( multiply index by )
( 4 to store 64 bit s )

Ytach3 @ D/F 1000. F/ ( Scale back to normal )
STORE2 STORECount @ 2* 2* + F!

Yacc6 @ D/F 1000000. F/ ( Scale back to normal )
STORE3 STORECount @ 2* 2* + F!

1 STORECount +! ( Increment s stored )

```

P.3. SUCCESSIVE LOOP CLOSURE AND PITCH SENSOR

353

THEN

THEN PAUSE (Go do terminal task)

AGAIN ;

(*** BUILDING OF TERMINAL & BACKGROUND TASKS FOR TURKEY APPLICATION ***)

: WHIP (Build and Activate Background task)

SLAVE BUILD

SLAVE WORK ;

: KEY (Check if key was depressed)

BEGIN

PAUSE

TERMINAL

DO

IF

KEY DROP

THEN

UNTIL ;

: PRINT ACTIVATE (Activate Terminal task)

-1 INIT-DISK (reset all disk drives)

BEGIN

CR

." Press any key to see BACKGROUND variable "

KEY

Ca .- Qs-["

STORELength 0 DO

STORE1 I 2= 2= + F0

I 8 MOD 0= IF ." .. " CR

THEN P. ." "

PAUSE LOOP ."]; " CR

APPENDIX P. FORTH CODES FOR LONGITUDINAL CONTROL

```
CR ." Ytach=[ "
STORELength 0 DO
  STORE2 I 2* 2* + F6
  I 8 MOD 0= IF ." .. " CR
  THEN P. " "
  PAUSE LOOP ." ]: " CR
```

```
CR ." Yacc=[ "
STORELength 0 DO
  STORE3 I 2* 2* + P6
  I 8 MOD 0= IF ." .. " CR
  THEN P. " "
  PAUSE LOOP ." ]: " CR
```

```
CR
```

```
AGAIN ;
```

```
: START
```

```
CHANNEL0 BOSS BUILD ( Initializes Terminal Task )
```

```
BOSS PRINT
```

```
WHIP : ( Initializes Background Task )
```

```
TURKEY START ( Turn program into a TURKEY application )
```

```
CR CR CR
```

```
.( Write protect STATIC memory and reset the computer )
```

```
EOF
```


Appendix Q

Lateral Control System

Q.1 Lateral equations of motion

The lateral equations of motion can be found from derivations in Appendices A, B and C. The lateral equations can be decoupled from the longitudinal equations of motion under the same conditions mentioned in section N.1.

Equations A.90, A.91 and A.92 then simplify to:

$$[I_3^W + I_3^F]\ddot{\psi} = -I_2^W \Omega_0 \dot{\phi} - f_G \dot{\psi} + f_T \eta - Q_T \quad (Q.1)$$

$$\begin{aligned} & [I_1^W + I_1^F + I_1^T + m_W r_W^2 + m_F(r_W + r_F)^2 + m_T(r_W + r_T)^2]\ddot{\phi} \\ &= [I_2^W + m_W r_W^2 + m_F r_W(r_W + r_F) + m_T r_W(r_W + r_T)]\Omega_0 \dot{\psi} \\ &+ [m_W r_W + m_F(r_W + r_F) + m_T(r_W + r_T)]g\phi \end{aligned} \quad (Q.2)$$

$$I_3^T \ddot{\psi} + I_3^T \ddot{\eta} = -f_T \eta + Q_T \quad (Q.3)$$

If the d.c. motor rotor inertia is non zero the additional terms due to the geared drive system that should be included in the lateral dynamic equations of motion

APPENDIX Q. LATERAL CONTROL SYSTEM

can be determined by inspection of equations G.13 and G.14 in Appendix G

$$\begin{aligned} & [I_3^W + I_3^F + (1-n)I_3^R]\ddot{\psi} + n(1-n)I_3^R\dot{\eta} \\ & = -I_2^W\Omega_0\dot{\phi} - f_G\dot{\psi} + f_T\eta - Q_T \end{aligned} \quad (Q.4)$$

$$[I_3^T + n^2I_3^R]\ddot{\eta} - f_T\dot{\eta} + Q_T \quad (Q.5)$$

Equations Q.2, Q.4 and Q.5 are the dynamic equations of motion of the lateral system, where I_3^R is the moment of inertia of the rotor of the turntable drive motor and n is the gear ratio of the turntable drive system.

Rewriting these equations into state space representation, they become:

$$\begin{bmatrix} 0 & I_{12} & I_{13} & 0 \\ I_{21} & 0 & 0 & 0 \\ 0 & I_{32} & I_{33} & 0 \\ 0 & 0 & 0 & 1 \end{bmatrix} \begin{bmatrix} \dot{\phi} \\ \dot{\psi} \\ \dot{\eta} \\ \dot{\phi} \end{bmatrix} = \begin{bmatrix} J_{11} & -f_G & f_T & 0 \\ 0 & J_{22} & 0 & J_{24} \\ 0 & 0 & -f_T & 0 \\ 1 & 0 & 0 & 0 \end{bmatrix} \begin{bmatrix} \phi \\ \psi \\ \eta \\ \phi \end{bmatrix} + \begin{bmatrix} -1 \\ 0 \\ 1 \\ 0 \end{bmatrix} Q_T \quad (Q.6)$$

Where:

$$I_{12} = I_3^W + I_3^F + (1-n)I_3^R \quad (Q.7)$$

$$I_{13} = n(1-n)I_3^R \quad (Q.8)$$

$$I_{21} = I_1^W + I_1^F + I_1^T + m_W r_W^2 + m_F(r_W + r_F)^2 + m_T(r_W + r_T)^2 \quad (Q.9)$$

$$I_{32} = I_3^T + nI_3^R \quad (Q.10)$$

$$I_{33} = I_3^T + n^2I_3^R \quad (Q.11)$$

$$J_{11} = -I_2^W\Omega_0 \quad (Q.12)$$

$$J_{22} = [I_2^W + m_W r_W^2 + m_F r_W(r_W + r_F) + m_T r_W(r_W + r_T)]\Omega_0 \quad (Q.13)$$

$$J_{24} = [m_W r_W + m_F(r_W + r_F) + m_T(r_W + r_T)]g \quad (Q.14)$$

Multiplication of equation Q.6 by the inverse of the first matrix containing the inertia terms, yields the standard state space form of the system of lateral dynamic

equations:

$$\dot{x} = Fx + Gu \quad (Q.15)$$

where $u = Q_T$ and $x = [\dot{\phi}, \dot{\psi}, \eta, \phi]^T$.

Q.2 Lateral sensors

A tachometer and an accelerometer are used as the lateral sensors. A roll angle sensor, for example a vertical gyro, is also considered as an alternative to the accelerometer.

The tachometer's operation is similar to that of the one in the longitudinal system, but here it is mounted on the rotor shaft of the turntable drive motor. It reads

$$\omega_{LAT} = n_{LAT} \cdot \eta \quad (Q.16)$$

where n_{LAT} is the known gear ratio of the turntable drive system. The microprocessor can scale the tachometer measurement so that the state η is measured:

$$y_t = \eta \quad (Q.17)$$

The accelerometer is mounted on the unicycle frame so that its acceleration sensitive axis is in the direction of the sideways motion of the unicycle. It is placed on the vertical centerline of the unicycle, so that it will not measure the component due to yaw acceleration.

The accelerometer is actually a pendulum with a servo feedback loop around it to change it to an accelerometer, as described in Appendix H. The output of the instrument is a signal proportional to an internal control torque. This is generated to counter the effects of specific forces on the unicycle frame at the position where the accelerometer is mounted. The component of the frame sideways acceleration can be obtained from equation A.76 and the acceleration due to gravity is $-g\phi$ for

small roll angles. Figure Q.1 shows how the sign of the accelerometer measurement is determined.

$$Q_{A(LAT)} = k_a [-(r_W + r_{S3})\ddot{\phi} + r_W \Omega_0 \dot{\phi} + g\phi] \quad (Q.18)$$

where r_{S3} is the height above the wheel axle at which the accelerometer is mounted.

From equation Q.15

$$\ddot{\phi} = F_{11}\dot{\phi} + F_{12}\phi + F_{13}\eta + F_{14}\phi + G_1 Q_T \quad (Q.19)$$

By scaling the accelerometer measurement in the microprocessor software and by substituting equations Q.19 into Q.18, the lateral acceleration measurement can be rewritten in terms of the states and control input:

$$\begin{aligned} y_a = & -(r_W + r_{S3})F_{11}\dot{\phi} + [r_W \Omega_0 - (r_W + r_{S3})F_{12}]\phi \\ & - (r_W + r_{S3})F_{13}\eta + [g - (r_W + r_{S3})F_{14}]\phi - (r_W + r_{S3})G_1 Q_T \end{aligned} \quad (Q.20)$$

The measurement obtained from an ideal roll angle sensor would be

$$y_r = \phi \quad (Q.21)$$

Q.3 Lateral system characteristics

The lateral system dynamic behaviour is a function of the nominal wheel speed Ω_0 , as can be seen from equations Q.12 and Q.13. The results presented in section Q.3.1 show the state transition input and output matrices for a typical wheel speed of 3 rad/sec. The measured mechanical parameters used in these calculations are listed in Appendix M.

Q.3. LATERAL SYSTEM CHARACTERISTICS

359

Q.3.1 Lateral system characteristics calculation

UCTC12/LATCHAR.CTR

LATERAL SYSTEM CHARACTERISTICS

.....

LATERAL STATES : PHI.DOT; PSI.DOT; ETA; PHI

CONTROL INPUT : TURNABLE MOTOR TORQUE (QT)

MEASUREMENTS : TACHOMETER; ACCELEROMETER; ROLL ANGLE SENSOR

UNITS : METERS, RADIAN, SECONDS

.....

NOMINAL WHEEL SPEED (RAD/SEC) :

OMEGA0 -

3.0

ACCELEROMETER HEIGHT (METERS) :

RS3 -

0.6500

OPENLOOP SYSTEM MATRICES:

.....

FLAT -

APPENDIX Q. LATERAL CONTROL SYSTEM

0.	0.6575	0.	10.9719
-0.2240	-0.0492	0.1212	0.
0.1718	0.0378	-0.2122	0.
1.0000	0.	0.	0.

GLAT -

0.
-1.5415
2.6999
0.

RLAT -

0.	0.	1.0000	0.
0.	0.0294	0.	0.5387
0.	0.	0.	1.0000

RLAT -

0.
0.
0.

EIGVAL -

-0.0250
-0.2384
-3.2890
3.2910

EIGVEC -

0.0015	-0.0094	1.0000	1.0000
1.0000	-0.6515	0.0713	-0.0653
0.2031	1.0000	-0.0567	0.0483

Q.3. LATERAL SYSTEM CHARACTERISTICS

361

-0.0599 0.0392 -0.3040 0.3039

CTR -

0.1828

2.6772

0.1673

-0.1425

OBS -

0.2031 1.0000 -0.0567 0.0483

-0.0028 0.0020 -0.1617 0.1618

-0.0599 0.0392 -0.3040 0.3039

RESIDU -

0.0371 2.6792 -0.0095 -0.0069

-0.0006 0.0052 -0.0271 -0.0231

-0.0110 0.1051 -0.0509 -0.0433

TRANSFER FUNCTION FROM TURNABLE DRIVE TORQUE TO TACHOMETER MEASUREMENT.

TACHEZEROS -

3.3000

-3.2998

-0.0279

TACHEPOLES -

3.2910

-3.2890

-0.2384

-0.0250

TACHEGAIN -

APPENDIX Q. LATERAL CONTROL SYSTEM

2.6999

TRANSFER FUNCTION FROM TURNTABLE DRIVE TORQUE TO ACCELEROMETER MEASUREMENT

ACCZEROS -

0.0000 + 1.0284i

0.0000 - 1.0284i

0.0000 + j. 1

ACCPLES -

3.2910

-3.2890

-0.2384

-0.0250

ACCGAIN -

-0.0454

TRANSFER FUNCTION FROM TURNTABLE DRIVE TORQUE TO ROLL ANGLE MEASUREMENT

ROLLZEROS -

0.

ROLLPOLES -

3.2910

-3.2890

-0.2384

-0.0250

ROLLGAIN -

-1.0135

Q.4 LQG control system design

In this section we will design an optimal continuous time linear quadratic gaussian compensator for the lateral system.

The unicycle yaw rate will accurately follow a reference command if the regulator uses integral error feedback of the measured plant yaw rate. This introduces an extra state, e , to the lateral system matrices:

$$\begin{bmatrix} \dot{e} \\ \dot{x} \end{bmatrix} = \begin{bmatrix} 0 & H \\ 0 & F \end{bmatrix} \begin{bmatrix} e \\ x \end{bmatrix} + \begin{bmatrix} 0 \\ G \end{bmatrix} u + \begin{bmatrix} -1 \\ 0 \end{bmatrix} r$$

$$u = -[C_e \ C] \begin{bmatrix} e \\ x \end{bmatrix} \quad (Q.22)$$

where $H = [0 \ 1 \ 0 \ 0]$

The regular gains C_i for an optimal linear quadratic regulator were calculated by minimizing the cost function:

$$J = \frac{1}{2} \int_0^{\infty} (ae^2 + bu^2) dt \quad (Q.23)$$

A CTRL-C program 'lgtlqg.ctr' was used to calculate the regulator gains and the print-out is shown in section Q.4.1. The ratio $\frac{a}{b}$ of the weighting factors were chosen so that the step response (Figure Q.2) of the closed loop system reached the commanded value in approximately 5 seconds. Figure Q.3 shows the closed loop frequency of the lateral system. The closed loop system has a bandwidth of approximately 0.3 Hz, which is comparable to that of the longitudinal system.

APPENDIX Q. LATERAL CONTROL SYSTEM

A linear quadratic gaussian estimator was designed to estimate all the lateral states from the tachometer and roll angle sensor measurement. The modified plant model that includes the random disturbance effects on the plant and measurements, is:

$$\begin{aligned}\dot{\hat{x}} &= F\hat{x} + Gu + G_n w \\ y_m &= M\hat{x} + v\end{aligned}\quad (Q.24)$$

where:

w is a random disturbance vector with spectral density Q

y_m is a vector of the measured quantities

v is a random measurement noise vector

G_n is the process noise input distribution matrix.

The complete statistical nature of the measurement noise is not known because the actual sensors have not been selected. For this reason we will assume the same spectral densities for the tachometer (R_t) and roll angle sensor (R_r) as for the longitudinal system (refer to section N.5).

$$\begin{aligned}R_t &= 0.05 \text{ rad}^2/\text{s} \\ R_r &= 0.1 \text{ m}^2/\text{s}^3\end{aligned}\quad (Q.25)$$

The process noise spectral density is also assumed to be similar to that of the longitudinal system. The noise input distribution matrix G_n is assumed to be the same as the control input distribution matrix.

$$\begin{aligned}Q &= 2 \text{ N}^2 \text{m}^2 \text{s} \\ G_n &= G\end{aligned}\quad (Q.26)$$

A Kalman-Bucy filter [Kalman] with filter gains L , can be designed to provide an optimal estimate of the state vector \hat{x} in the presence of the specified disturbance inputs. The estimator state equation is

$$\dot{\hat{x}} = F_0 \hat{x} + G_0 u + L(y_m - M\hat{x}) \quad (Q.27)$$

Q.4. LQG CONTROL SYSTEM DESIGN

365

Ideally the plant model used in the estimator would have the same parameters as the actual plant, i.e. $F_0 = F$ and $G_0 = G$.

The Kalman filter gain matrix L is shown under ESTGAINS in the print-out listed in section Q.4.1. Equations Q.22 and Q.24 can be combined to give the lateral closed loop system matrices:

$$\begin{bmatrix} \dot{z} \\ \dot{e} \\ \dot{\hat{x}} \end{bmatrix} = \begin{bmatrix} F & -GC_e & -GC \\ 0 & 0 & H \\ LM & -G_0C_e & F_0 - G_0C - LM \end{bmatrix} \begin{bmatrix} z \\ e \\ \hat{x} \end{bmatrix} + \begin{bmatrix} 0 \\ -1 \\ 0 \end{bmatrix} r + \begin{bmatrix} G_n & 0 \\ 0 & 0 \\ 0 & L \end{bmatrix} \begin{bmatrix} w \\ v \end{bmatrix} \quad (\text{Q.28})$$

The performance of the state estimator is simulated where the actual initial roll angle $\phi(0) = 2$ degrees, while the estimated roll angle is $\hat{\phi}(0) = 0$. Figure Q.4 shows that the roll error initially increases to approximately 2.4 degrees while the state estimates are improved. In the absence of noise the estimated states track the actual plant states and the roll error is reduced to zero in approximately 5 seconds.

Q.4.1 Calculation of LQG gains

UCTC12/LATLQG.CTR

CONTINUOUS TIME LATERAL CONTROL SYSTEM WITH FULL ORDER LQ ESTIMATOR

LATERAL STATES : PHI.DOT; PSI.DOT; ETA; PHI

CONTROL INPUT : TURNABLE MOTOR TORQUE (QT)

APPENDIX Q. LATERAL CONTROL SYSTEM

MEASUREMENTS : TACHOMETER; ROLL ANGLE SENSOR

UNITS : METERS, RADIANS, SECONDS

***** CONTINUOUS TIME PLANT MATRICES *****

FLAT -

0.0000	0.6575	0.0000	10.9719
-0.2240	-0.0492	0.1212	0.0000
0.1718	0.0378	-0.2122	0.0000
1.0000	0.0000	0.0000	0.0000

GLAT -

0.0000
-1.5415
2.6999
0.0000

GNOISELAT -

0.0000
-1.5415
2.6999
0.0000

RLAT -

0.0	0.0	1.0	0.0
0.0	0.0	0.0	1.0

RLAT -

0.0
0.0

Q.4. LQG CONTROL SYSTEM DESIGN

367

***** MATRICES FOR INTEGRAL ERROR FEEDBACK CONTROL *****

EXTENDED STATE VECTOR IS : PSIDOT.ERR; PHI.DOT; PSI.DOT; ETA; PHI

FINT -

0.0000	0.0000	1.0000	0.0000	0.0000
0.0000	0.0000	0.6575	0.0000	10.9719
0.0000	-0.2240	-0.0492	0.1212	0.0000
0.0000	0.1718	0.0378	-0.2122	0.0000
0.0000	1.0000	0.0000	0.0000	0.0000

GINT -

0.0000
0.0000
-1.5415
2.6999
0.0000

***** REGULATOR DESIGN *****

COST FUNCTION WEIGHTING FACTORS ON STATES AND CONTROL :

ADYAG -

5.0 0.0 0.0 0.0 0.0

BDYAG -

1.0

OPTIMAL INTEGRAL ERROR AND STATE FEEDBACK GAINS :

CEFR -

2.2361

APPENDIX Q. LATERAL CONTROL SYSTEM

CLAT -

-45.4187 -5.9571 -0.0787 -150.9253

REGGAIN -

-3.4468

REGZEROS -

-3.3124

3.3124

-0.0000

REGPOLES -

-0.0000 + 0.0000i

-1.3237 + 1.3180i

-1.3237 - 1.3180i

-3.2921 - 0.0064i

-3.2921 + 0.0064i

***** ESTIMATOR DESIGN *****

PROCESS AND MEASUREMENT NOISE SPECTRAL DENSITIES :

QLAT -

1.0

RLAT -

0.0500 0.0000

0.0000 0.1000

Q.4. LQG CONTROL SYSTEM DESIGN

369

OPTIMAL ESTIMATOR GAINS AND ESTIMATOR POLES :

ESTGAINS -

1.2390 21.7228

0.0113 -0.3044

11.8559 0.2314

0.4628 6.5832

ESTPOLES -

-0.0279 + 0.0000i

-3.3009 + 0.0417i

-3.3009 - 0.0417i

-12.0710 - 0.0000i

APPENDIX Q. LATERAL CONTROL SYSTEM

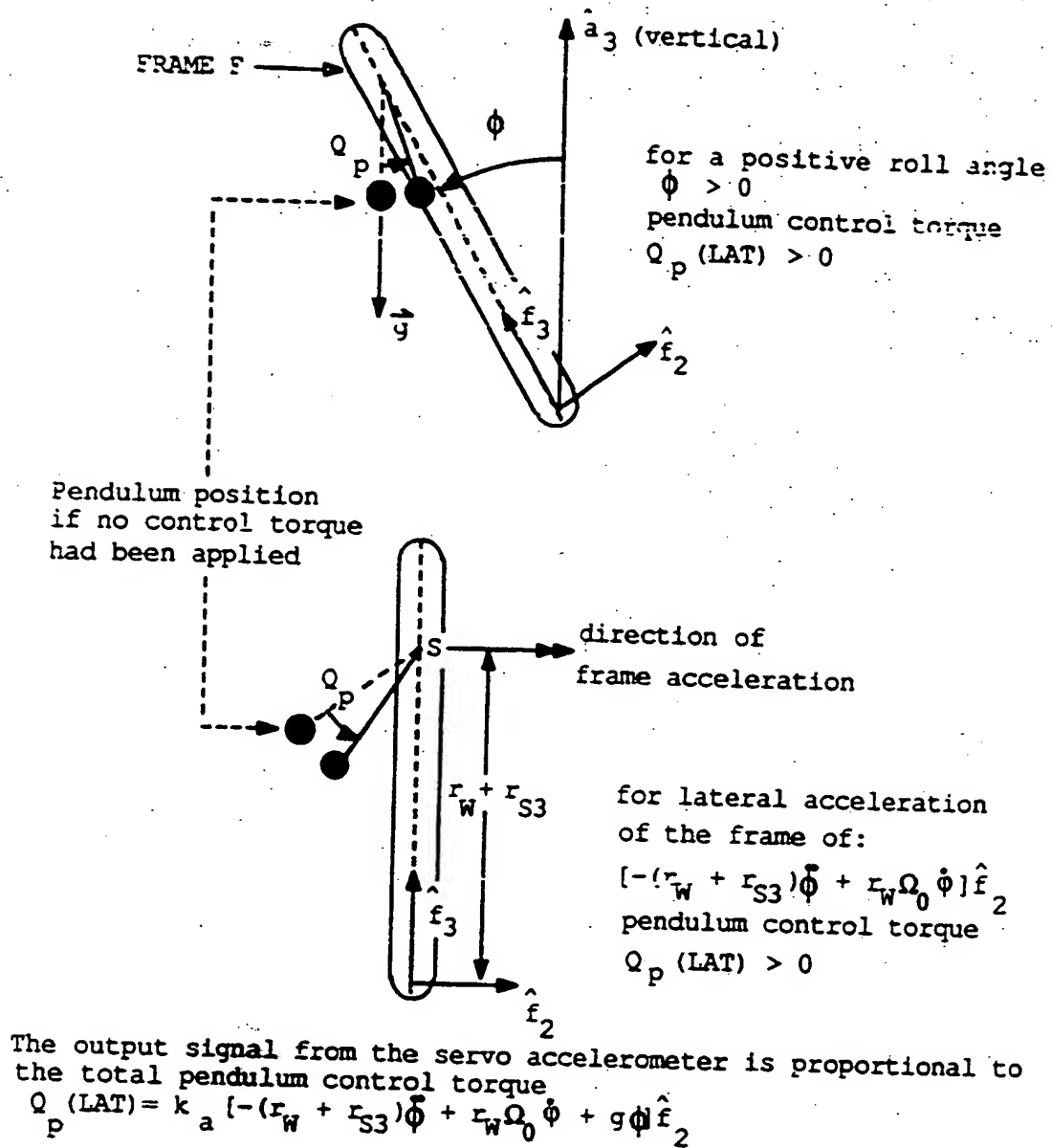


Figure Q.1: Lateral Accelerometer Measurement

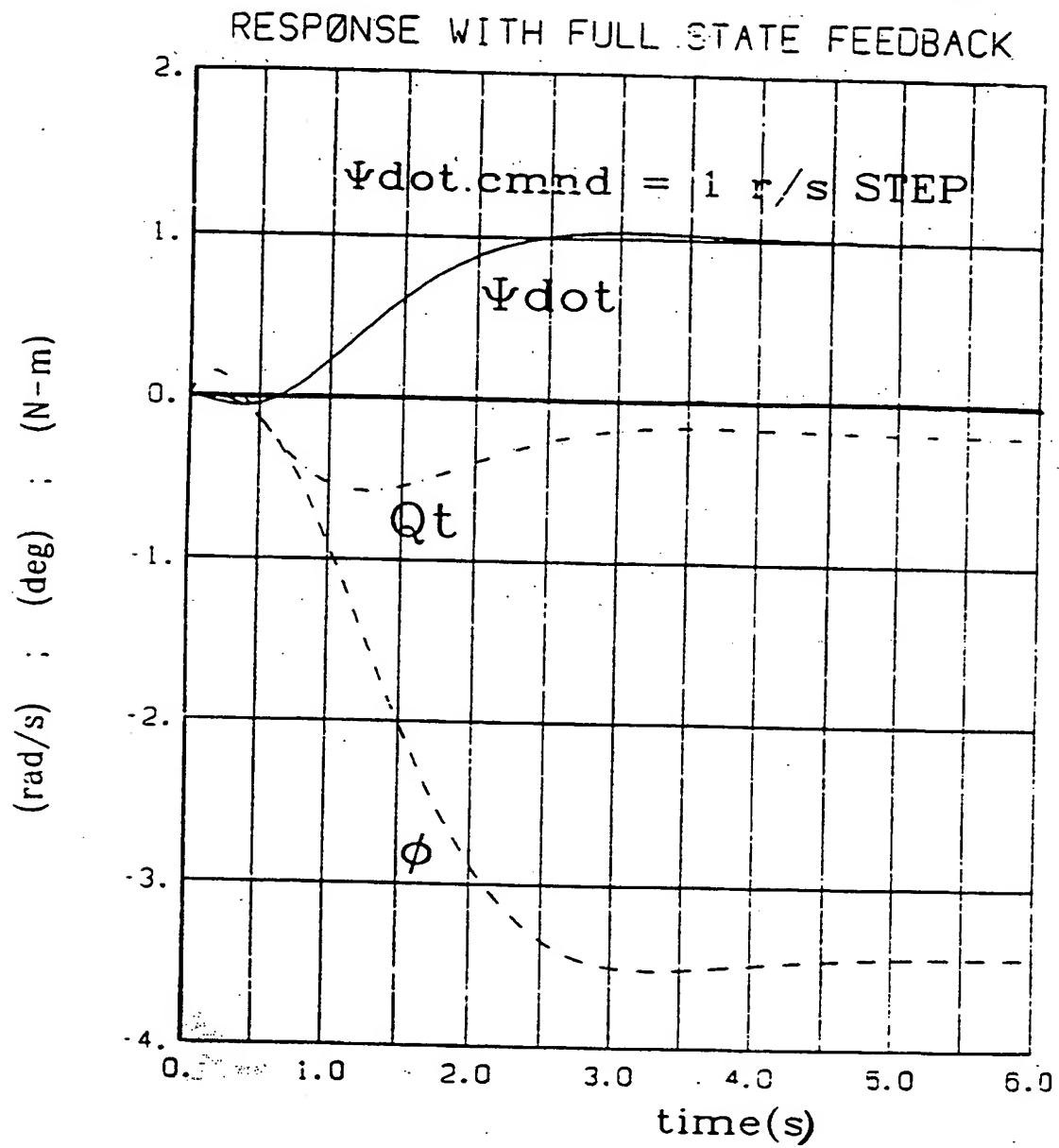


Figure Q.2: Step Response of the Lateral System with Full State Feedback

APPENDIX Q. LATERAL CONTROL SYSTEM

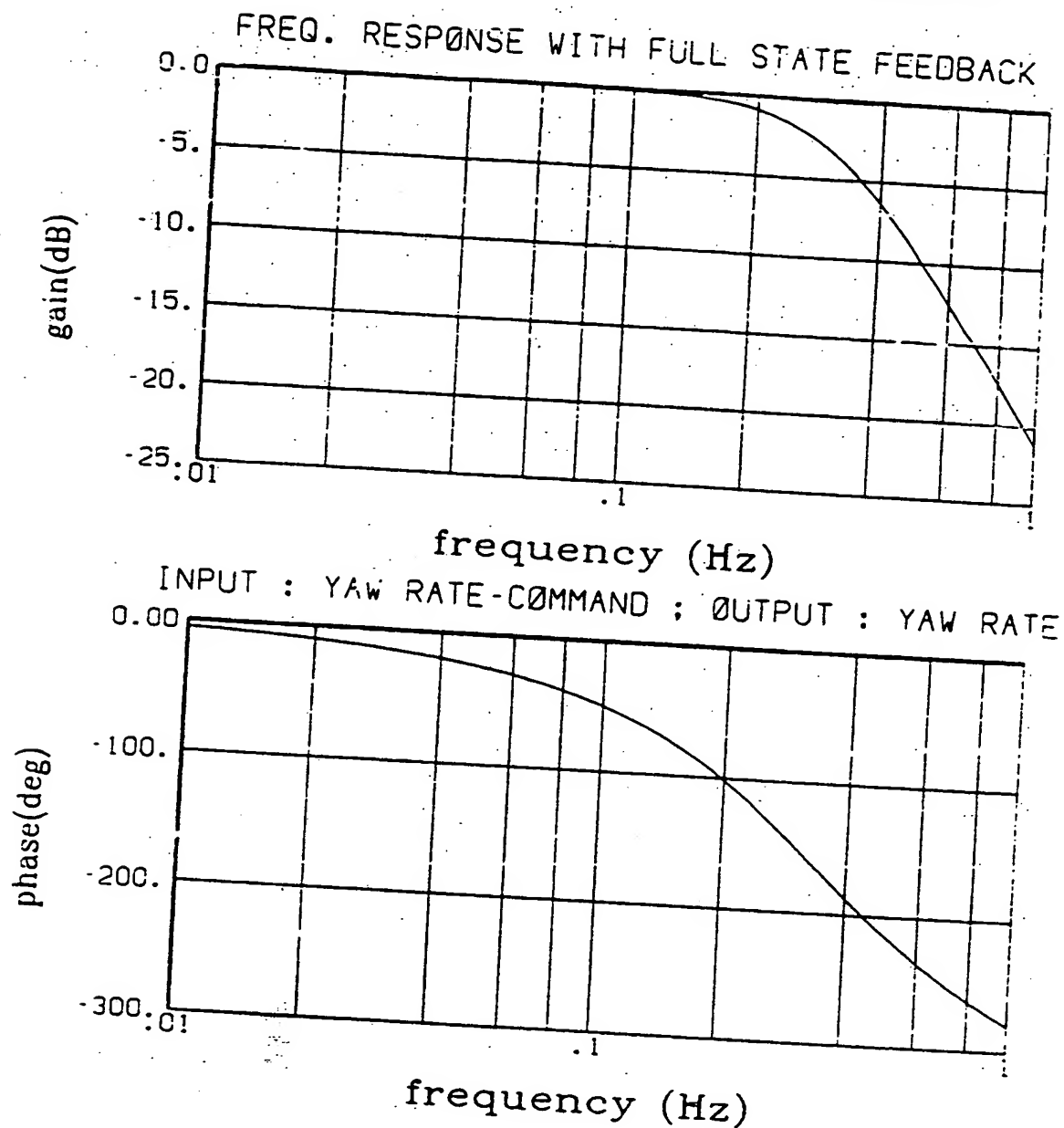


Figure Q.3: Frequency Response of the Lateral Closed Loop System with Full State Feedback

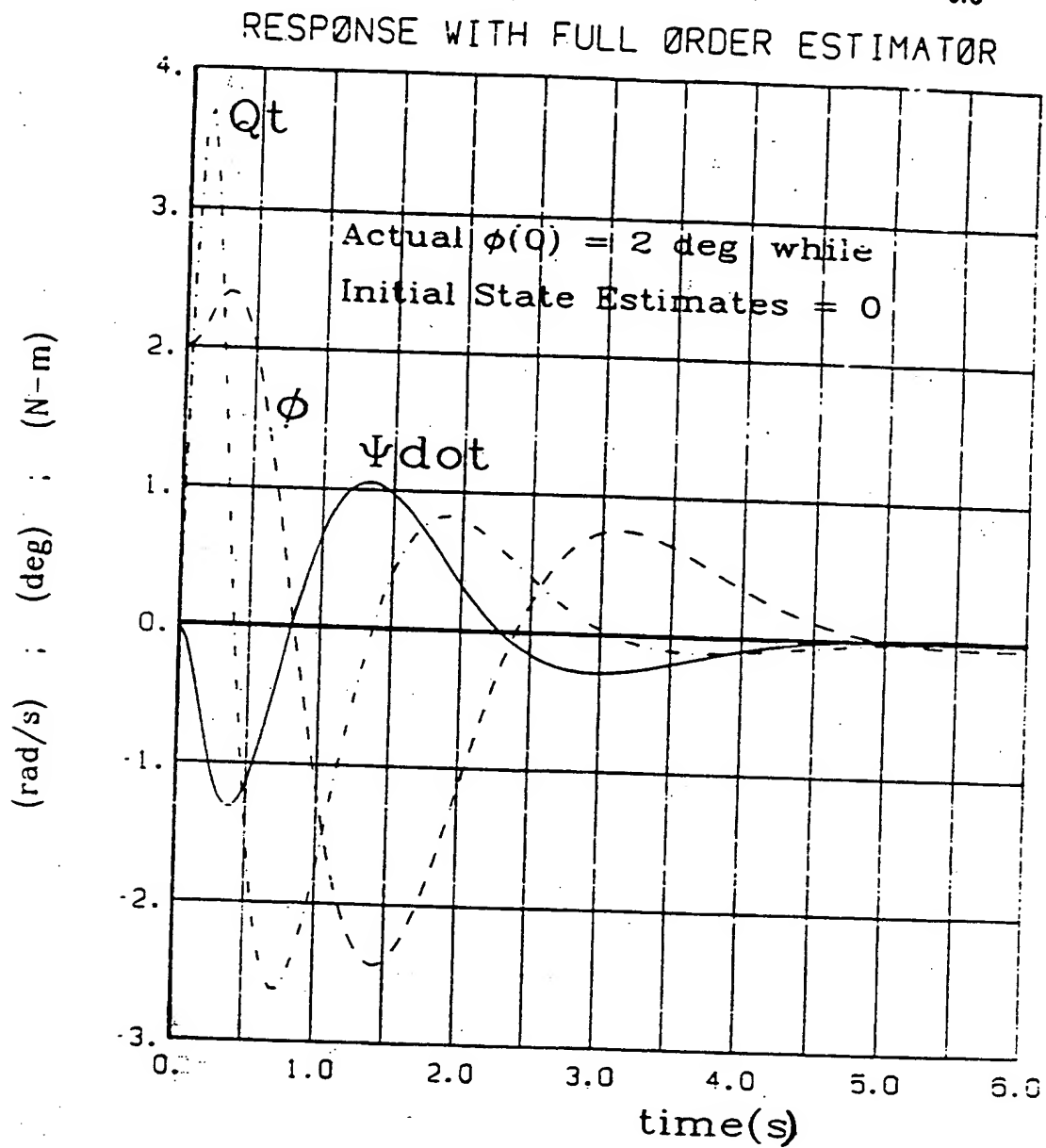


Figure Q.4: Response of the Lateral System with a Full Order Estimator and an Initial Roll Angle of 2 Degrees

Bibliography

- [Borah] Borah, L. Young, L.R. and Curry, R.E., *Sensory Mechanism Modeling*, Air Force Human Resources Laboratory report AFHRL-TR-77-70, October 1977.
- [Bryson 1] Bryson, A. E., *Control of Spacecraft and Aircraft*, Department of Aeronautics and Astronautics, Stanford University, 1987. Lecture notes pending publication.
- [Bryson 2] Bryson, A. E. and Ho Y.- C., *Applied Optimal Control*, Hemisphere Publishing Corp., Washington D.C., 1975.
- [Bryson 3] Bryson, A. E. *Discussions with and notes from the author's thesis advisor*, Stanford, 1987.
- [Capek] Capek, Karel, *R.U.R.*, English Translation by Paul Selver, S.French, New York, 1923.
- [Doyle 1] Doyle J. C., "Guaranteed Margins for LQG Regulators", IEEE Transactions for Automatic Control, volume AC-23, pp 756 - 757, 1978.
- [Doyle 2] Doyle J. C., "Robustness with Observers", IEEE Transactions for Automatic Control, volume 24, No.4, pp 607 - 611, August 1978.
- [Franklin] Franklin, G. F. and Powell, J. D., *Digital Control of Dynamic Systems*, Addison Wesley, Massachusetts, 1980.
- [Galil Motion] Galil, *ESA Series Users Manual*, Galil Motion Control, 1054 Elwell Ct, Palo Alto, CA 94303.

- [Greenwood] Greenwood, D.T., *Principles of Dynamics*, Prentice-Hall, Englewood Cliffs, 1965.
- [Higdon] Higdon, Donald T., *Automatic Control of Inherently Unstable Systems with Bounded Control Inputs*, Stanford University Thesis, Stanford, December 1963.
- [Iguchi] Iguchi, Nobuhiro, *Unicycle Robot for Rough Terrain*, paper in Japanese presented at the First Conference of the Robotics Society of Japan, December 8 - 12, 1983.
- [Infranor] Infranor, Inc., *MAVILOR Motor Catalog*, Infranor Incorporated, P.O.Box 1307, Naugatuck, Connecticut 06770.
- [Kalman] Kalman, R. E. and Bucy R., *New Results in Linear Filtering and Prediction*, Vol 83D, Trans. ASME, Jour. Basic Engr., 1961.
- [Kayton] Kayton, M. and Fried, W.R. (Ed.), *Avionics Navigation Systems*, John Wiley and Sons, New York, 1969.
- [Leonides] Leonides, C.T., *Control and Dynamic Systems*, Vol 16, Academic Press, 1980.
- [Mach2] Palo Alto Shipping Company, *MACH 2 Multitasking Forth Development System for 68000/68020 Target Systems*, Users-Manual, Palo Alto, 1986.
- [Nashner] Nashner, Lewis M., *A Rate Gyro Autopilot for a Motorbike*, MIT Thesis, Cambridge, January 1967.
- [Ogata] Ogata, K., *Modern Control Engineering*, Prentice-Hall Inc., Englewood Cliffs, N.J., 1970.
- [Ormsby] Ormsby, C.C and Young, L.R., *Integration of Semicircular Canal and Otolith Information for Multisensory Orientation Stimuli*, *Mathematical Biosciences* Vol 34, pp 1 - 21, 1977.
- [Oxford Dictionary] Oxford English Dictionary, *The Compact Edition of the Oxford English Dictionary*, Oxford University Press, Oxford, 1971.
-

- [Pars] Pars, L.A., *Analytical Dynamics*, John Wiley and Sons, New York, 1965.
- [Raibert] Raibert, Marc H., *Legged Robots that Balance*, MIT Press, Cambridge, 1986.
- [Rosenberg] Rosenberg, R.M., *Analytical Dynamics of Discrete Systems*, Plenum Press, New York, 1977.
- [Schaefer] Schaefer, John F., *On the Bounded Control of Some Unstable Mechanical Systems*, Stanford University Thesis, Stanford, April 1965.
- [Van Loan] Van Loan, C.F., *IEEE Transactions*, Volume AC - 23., June 1970.
- [Van Zytveld] Van Zytveld, Paul J., *A Method for the Automatic Stabilization of an unmanned Bicycle*, Stanford University Thesis, Stanford, June 1975.
- [Whittaker] Whittaker, E.T., *Analytical Dynamics of Particles and Rigid Bodies*, Cambridge University Press, Cambridge, 1961.
- [Wrigley] Wrigley, W., Hollister, W.M., and Denhard, W.G., *Gyroscopic Theory, Design, and Instrumentation*, M.I.T. Press, Cambridge, Mass and London, 1969.